The University of New South Wales

SCHOOL OF CIVIL ENGINEERING

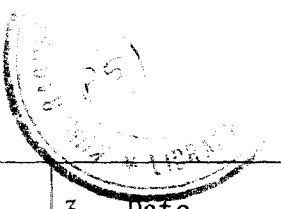

BIBLIOGRAPHIC DATA SHEET P-51

1. UNICIV Report No. R-203	2. ISBN85841 172 5	3. Date January, 1983.

4. Title and Subtitle

FORCES IN THE VICINITY OF EDGE COLUMNS IN FLAT PLATE FLOORS (Volume 1 - Tests on R. C. Models)

5. Author(s)

B. V. Rangan, Associate Professor
A. S. Hall, Emeritus Professor
) School of Civil Engineering, University of New South Wales, Kensington, N.S.W., Australia.

6. Keywords : Building codes; columns (supports); concrete slabs; connections; flat concrete slabs; moments; reinforced concrete; shear failure; shear strength; torsion.

7. Abstract

The report describes tests on half-sized models of edge panels of a reinforced concrete flat plate floor. In all five models were tested. The first model contained a floor beam and a spandrel beam. The second model contained a spandrel beam and the remaining three models did not. The primary purpose of these tests was to investigate the distribution of forces around an edge column.

Measured slab moments and shears along the face of the spandrel showed what proportion of the total panel moment entered the column directly as bending and how much as torsion in the spandrel. The proportion of shear on each face was also deduced. Both the observed behaviour and the measured forces indicated that failure originated as a torsion-shear failure in the spandrel. Expressions are derived for the torsion and shear in the spandrel and also for the capacity of the spandrel to resist these. Emphasis is placed on adequate torsion steel in the spandrel in order to prevent what has hitherto been called a punching shear failure at an edge column.

Based on these tests, a simple method for the design of slab steel in edge panels is also suggested.

8. Number of pages 240	9. Price A$20 (Special issue price).

FORCES IN THE VICINITY OF EDGE COLUMNS IN FLAT PLATE FLOORS

(Volume 1 - tests on R.C. models)

by

B.V. Rangan and A.S. Hall

UNICIV Report No R-203

PREFACE

This is a report of an investigation into the stresses in a reinforced concrete flat plate floor slab in the vicinity of an edge column. Five half-scale models were tested. Each comprised two complete panels at the edge of a building. The first model contained a floor beam and a spandrel beam. The second model contained only a spandrel beam, and this was omitted in models 3, 4 and 5. In the early models, steel strains were measured only in the region around the test column, but in later models more extensive instrumentation was employed.

From the results expressions were derived which indicate the manner in which moment and shear are transferred between the slab and the column. The expressions show how much of the total panel moment is transferred in bending and how much in torsion in the spandrels. Other expressions indicate how the shear is divided among the three faces of the column. From the later tests some indication was obtained as to how the total panel static moment M_o is divided between the end moments and the mid-span moment. One of the main findings is that there can be very considerable redistribution of moments throughout the slab as loading progresses. In view of this, very detailed analysis of the slab during design seems unjustified. It is suggested that design rules much simpler than those used at present would be quite adequate.

Various subsidiary tests are described in the report.

The report itself comprises two volumes. Volume 1 contains a description of the apparatus, a description of the tests and a comprehensive summary of the test results. There is a discussion of these results and conclusions.

Volume 2 contains two appendices. Appendix A gives design details of the models while appendix B contains all the raw laboratory data - strain gauge readings etc. Volume 2 is not for general circulation but will be supplied to interested readers on request.

CONTENTS

ACKNOWLEDGEMENTS

The authors wish to express their appreciation of the financial support of the Australian Research Grants Committee, without which the work could not have been carried out. The tests themselves were carried out under the direct supervision of Mr. David Sade and the success of the experiments is due largely to his careful work during the construction of the models and their testing.

The models were quite substantial (each weighed about 10 tonnes) and their manufacture and testing entailed considerable work. For this the authors thank the laboratory staff of the Structures Laboratory at the University of New South Wales, Kensington, Australia.

NOTATION

A_ℓ	=	total area of longitudinal steel
A_o	=	area of the rectangle defined by the longitudinal bars in the corners of the hoops
A_w	=	cross-sectional area of the bar from which the hoops are made
b	=	width of spandrel beam
c_1, c_2	=	side dimensions of column (Fig. 6.1)
D	=	overall depth of spandrel beam
E_c, E_s	=	modulii of elasticity of concrete and steel, respectively
F'_c	=	compressive strength of concrete
$f_{\ell y}$, f_{wy}	=	yield strengths of longitudinal steel and hoop steel, respectively
ℓ_{n_1}	=	clear distance between the edge column and the first interior column of the building
ℓ_{n_2}	=	clear distance between the adjacent edge columns of the building
ℓ_n	=	smaller of ℓ_{n_1} and ℓ_{n_2}
M_A (or M_B)	=	total moment at the inner edge of the spandrel A (or spandrel B), and extending across the width of the test panel (Fig. 6.1)
M	=	either M_A or M_B, as appropriate
M_{BS}, M_{SS}	=	moments which occur within the beam strip and the slab strip, respectively
M_M	=	total moment at midspan, and extending across the width of the test panel
M_o	=	total static moment = $\frac{1}{2}(M_A + M_B) + M_M$
M_{sp}	=	bending moment in the spandrel
m_y	=	calculated yield moment per unit width of the slab
s	=	spacing of hoops
t	=	thickness of slab
T_{sp}	=	twisting moment in the spandrel at the column face
T_u	=	ultimate twisting moment in the spandrel at the column face
u_o	=	perimeter of the area A_o

V_A (or V_B) = total shear force at the inner edge of spandrel A (or spandrel B), and extending across the width of the test panel (Fig. 6.1)

V = either V_A or V_B, as appropriate

V_{BS}, V_{SS} = shears which occur within the beam strip and the slab strip, respectively

V_{sp} = shear force in the spandrel at the column face

V_u = ultimate shear force in the spandrel at the column face

W_{sp} = weight of the spandrel beam or strip, plus the live load acting thereon

x_o, y_o = width and depth, respectively, of the rectangle making the area A_o

Z = a parameter

α = M_{BS}/M

β = V_{BS}/V

λ = effective width of slab parameter

ϕ = strength reduction factor

Chapter 1

GENERAL BACKGROUND

1.1 THE PROBLEM

In monolithic buildings constructed of reinforced concrete, the transfer of forces between a floor and its supporting columns has given rise to a great deal of research. Where floor beams are present, the problem is now fairly well understood. Where beams are not used, many questions still remain. The term flat slabs is usually used for floors with a drop panel. This panel complicates the analysis but strengthens the critical region. In flat plates, the absence of a drop panel enhances the architectural value of the structure but weakens the critical region which is subjected to maximum moments and shears. At edge columns, where considerable unbalanced moment has to be transferred in addition to shear, the problem is worse than at an interior column.

In view of the serious nature of the problem, it is all the more unfortunate that the nature of the transfer mechanism is not well understood and knowledge of the forces involved is incomplete and confused.

1.2 CODES OF PRACTICE

First, we look briefly at the information offered by Codes of Practice.

The total shear to be transferred can be calculated with reasonable accuracy from the floor area tributary to the particular column. Although the bending moments have an influence on the distribution of shear, this effect is minor from a practical point of view.

The ACI Code 318-77 and AS1480 (1982) offer two methods of estimating the total moment to be transferred: (i) The Equivalent Frame Method, and (ii) The Direct Design Method. In the first method an elastic analysis is carried out on a two-dimensional frame which comprises a 'slice' of the real building one panel wide and centred on a line of columns. The calculation of member properties (stiffness values) for this analysis is specified with considerable precision. These are all based on overall dimensions and thus presumably apply to the uncracked state. On

the other hand these Codes give no guidance in regard to the calculation of 'fixed-end moments' which constitute the major part of the final result.

The Direct Design Method specifies coefficients for slab moments. The method is quite specific and the validity of the coefficients can only be assessed against experimental values, which are scarce.

So much for the determination of the shear and moment to be transferred. There remains appropriate design for these forces. The shear is transferred partly at the 'front' face of the column and partly at the spandrel faces. AS1480 assumes that the shear on each face is proportional to the width of the face. However there is no experimental evidence for or against this assumption.

The unbalanced moment similarly has to be apportioned between the three faces. Here the Code embraces two methods which give widely different values. Specifically, an equation is quoted which is based on very early work by Di Stasio and Van Buren (1960). Research since then has indicated that this approach is not valid but it is still quoted in the Code. On the other hand, the Code makes use of the 'Equivalent Column' concept. This is based on work by Corley and Jirsa (1970) and by adopting the end result of this work, the Code presumably endorses the underlying arguments. These arguments, however, lead to a value for the spandrel torsion which is markedly different from that predicted by the Di Stasio and Van Buren formula. Thus, although the Code requires that spandrels "shall be designed for such torsion as shall occur" it provides conflicting information as to how such torsion shall be calculated.

In summary, these Codes provide two alternative methods of calculating the shear and moment which have to be transferred between a slab and an edge column. They specify that the slab (and spandrel beam if any) shall be suitably designed but only vague guidance as to how this shall be done.

The CEB Model Code (1978) in general makes similar recommendations.

1.3 PREVIOUS RESEARCH

Many studies, both theoretical and experimental, have been conducted into the question of transfer of shear and moment between a flat plate and a column. The majority of these studies have been concerned with interior columns, where the symmetry of the structure, if not the loading somewhat simplifies the problem. The conditions at an edge or corner column are not only more difficult to investigate, but by their very nature are those that cause more concern to the designer. Some studies of edge columns have nevertheless been carried out.

The salient problems before the investigator can be summarized as:

(a) when a total shear V and a total unbalanced moment M are to be transferred between a slab and a column, how do the various faces of the slab-column joint (the 'front' face and the two spandrel faces) share in the transfer process? and

(b) what is the strength of each face, i.e. what is the ability of the slab at each face to resist the type of action to which it is subjected? This question involves a knowledge of the mechanism of failure.

All investigations both theoretical and experimental, including the present one, deal not with the whole building, but with a localized portion in the vicinity of the joint under review. In relation to the first question above, the problem then arises that the manner of loading the localized model must be such as to ensure that the distribution of shear and moment to the various faces of the joint is the same as that in the complete building. The more localized the region selected for modelling, the less likely is this condition to be satisfied. On the other hand, larger regions may require smaller scale models, and scale effects may then become a problem.

In regard to the second question referred to above, that of determining the slab resistance at the various sides, the question of localized modelling may not appear to present such difficulties. However, the findings of the present investigation will show (see Chapter 7) that certain deformational restraints offered by the

surrounding building have an effect of several hundred per cent on the failure strength of the slab element in torsion. The possibility of this has been recognized in the ACI-ASCE Committee 426 report (1974) but in fact the extent of the models in previous research is such that the restraining effect was probably absent.

In view of these observations it is not intended here to examine other research programmes in detail but some general comments will be made. The value of the contributions made by these researches is fully acknowledged but it is nevertheless relevant to point out some shortcomings.

In regard to theoretical studies, the assumption of a straight line shear stress variation as a basis in the early work of Di Stasio and Van Buren (1960) and of Moe (1961) reflects a misconception of the action of torsion which was commonly held in those days. It was then thought that torsion was transmitted through a beam by some field of shear stresses on the cross-section. This idea was carried over to torsion effects in a slab, although the shear stress field adopted in the work quoted is unrealistically simple. It is now known that any shear stress field such as occurs in St. Venant torsion in homogeneous materials exists in reinforced concrete beams only at very low loads. Beyond cracking, the mechanism of torsion transfer is completely different. These early theories must therefore be abandoned in the same way that the early torsion theories have been superseded.

The use of an elastic theory of plates by Mast (1970) and Long (1973) to examine the distribution of the forces between the various faces of the slab-column joint could quite possibly yield results which are valid in the uncracked structure. Results will show (see Chapter 7) that there is a considerable redistribution after cracking.

More recently beam analogy theories have been advanced by Hawkins and Corley (1971) and by Islam and Park (1976). These theories are concerned with strength aspects on the different faces rather than with the distribution of the transferred forces between the faces. The theory originally proposed by Hawkins and Corley (1971) considered the joint in terms of individual beams framing into the column on the four or three sides for interior

and edge joints respectively. Expressions for the strength of each of these beam elements in shear-torsion or shear-moment as appropriate were developed. It was then assumed that failure occurs when these ultimate capacities are realised on two (for an edge column) adjacent beam sections.

A drawback to this proposal was that it resulted in a large number of equations which made its application difficult in practice. Islam and Park (1976) used a similar approach but made certain simplifying assumptions which rendered the results somewhat more readily applicable.

Basically these beam analogy theories are attractive, and in concept they are supported by the present investigation. It is not surprising that in developing expressions for the strength of the slab, the influence of slab restraint on the shear-torsion capacity of the spandrel elements was not taken into account in the works quoted, although this would considerably modify the result. In corresponding experimental work (Hawkins and Mitchell (1979) and Hawkins (1979)) the extent of the models also caused the elimination of the in-plane restraining forces and thus the experiments appeared to confirm the theory.

More doubtful is the assumption that re-distribution of the shears and moments is possible between beam elements and that the strength capacities of two adjacent elements may be added to predict the joint capacity. Upon cracking, re-distribution does take place of course. However, the above assumption assumes in effect considerable ductility in the various elements. It is a typical plastic collapse assumption, and might well be applied where bending moments are concerned. Shear failures are notoriously brittle and the assumption of a re-distribution of forces which would permit the addition of the strengths of the various elements seems hardly applicable.

These are criticisms of detail. The general model of failure represented by these theories is much easier to accept than previous proposals.

Experimental studies by Hansen and Hansen (1968), by Hawkins (1979), by Stamenkovic and Chapman (1974) and by Kaushi and Yoshizaki (1979), were carried out on models which consisted of a single column together with an adjacent area of slab. Such models would

provide no guarantee that the distribution of forces between the faces corresponded to that in the complete structure. In-plane forces would also be largely absent in such models.

The models used by Long, Cleland and Kirk (1978) contained 2 columns, an edge column and a first interior column, together with a slab of one panel width centred about the column line and extending 1½ bays onward from the edge of the building. These more extensive models may have given a superior result in regard to the force distribution around the edge column. Lack of restraint parallel to the edge would almost certainly have resulted in a low prediction of strength.

Islam and Park (1976) carried out tests to determine the efficiency of various types of shear reinforcement. These were employed on interior columns but their tests are of interest in that the results are consistent with the findings of the present investigation. It will be shown in Chapter 7 that failure at an edge column is essentially a torsion-shear failure. In view of this it is not surprising that Islam and Park found that closed stirrups are the most efficient form of shear reinforcement (when compared to bent-up bars and shear heads) as far as the strength and the ductility of slab-column connections are concerned. These findings in themselves are a clear indication of torsion failure.

Mention must also be made of previous research carried out at the University of New South Wales by Faulkes et al (1973), Fraser (1974), French et al (1975) and Fraser (1976). Some of this work was aimed at (i) acquiring a general understanding of the problems involved in flat plate floor design, (ii) developing methods of analysis quite distinct from those in use at present, and (iii) examining carry-over effects, i.e. the influence of loads on the slab moments at locations remote from their point of application. This last item was of particular importance in the design of the present tests.

Chapter 2

OBJECTIVES OF THE RESEARCH

Having regard to the above background, certain objectives were enumerated before the research was commenced. The majority of these objectives were concerned with the behaviour of the structure under uniformly distributed vertical loading.

(a) Of the total shear transferred between a flat plate and an edge column, what proportion acts at the 'front' face, and how much on the two spandrel faces?

(b) Similarly, of the total moment, how much is transmitted by direct bending and how much by torsion on the spandrel faces? It was not originally intended to check whether the value of the total moment given by either of the Code methods is valid, although it was necessary that the *distribution* of the moments between the faces should be correctly modelled.

(c) How are the shears and moments on the various faces transmitted to the column, i.e. what is the mechanism of transfer?

If these questions could be answered, a reasonably clear picture would result of the stress conditions on each of the three faces of the edge column. In view of these objectives, attention was focused initially on the region of the floor in the immediate neighbourhood of a typical edge column, which will be referred to in this report as the *test column* or *column A*. Clearly, it was necessary to provide boundary conditions to the test specimen such that the distribution of internal actions in the model approximated closely to those which would occur if the whole building were involved.

This problem of boundary conditions will be discussed in Chapter 3. As a result of such considerations it was eventually considered necessary to include the whole of the floor panel on each side of the column. The model was oriented so that the eastern edge represented the edge of the building (Fig. 2.1). The model thus extended as far as the columns C and D to the south and north of column A and as far as the first interior columns (columns F, B and E). The area enclosed by the dashed line in Fig. 2.1 was regarded as the test area, the function of the remainder being to provide adequate boundary conditions.

As testing proceeded it was realised that because the model was more extensive than originally planned it was possible to obtain additional information. Hence, in some of the later models other objectives were included.

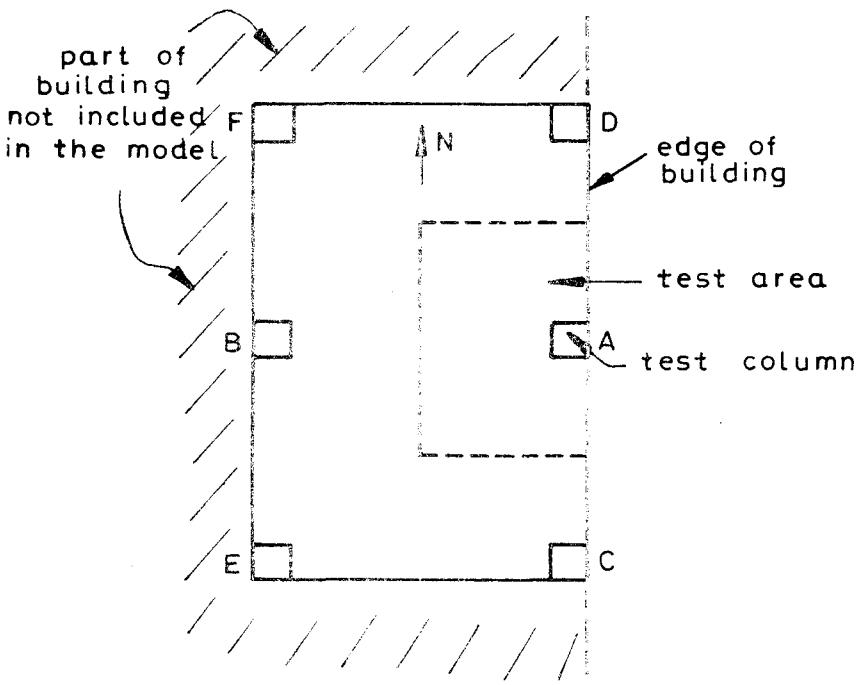

Fig. 2.1 Model selected for Investigation.

(d) To measure the total mid-span moment, M_M, midway between columns A and B.

(e) To measure the total end moment, M_I, transferred to column B by the floor panel AB.

(f) With the values obtained from (b), (d) and (e), to investigate the whole distribution of the total static moment M_o.

(g) To determine joint stiffness values and carry-over factors for the uncracked and the cracked structure by applying a couple to 'joint' A and measuring the rotation of A and the reactive moment at B.

Chapter 3

DESIGN OF THE TESTS

The study of work done by other people on related problems served to emphasize the importance of providing realistic boundary conditions. If a small region of the real building could be modelled, the size of the model could be relatively large - even full size.

The smallest feasible region would be that portion of the floor extending from the test column to a perimeter defined by the line of contraflexure. Some tests have used such a model. The downward loads on such a model are the distributed load on the floor segment itself and the shear along the contraflexure line. A difficulty arises in the determination of the distribution of the shear, which represents in effect the load coming in from the region outside the model. Such a determination partly presumes the results of the investigation. Moreover, the application of the shears so calculated would be experimentally difficult. An even more serious objection is that the position of the contraflexure line in the real floor shifts during the course of loading and cracking. Thus to arbitrarily keep the position constant would largely nullify the tests.

A slightly larger model which was considered, extended to the mid-span lines shown dashed in Fig. 2.1. The northern and southern boundaries of such a model would have zero slope by symmetry. The experimental provision of zero slope is difficult although it has been attempted by Long et al (1978). Because we are investigating an edge panel, symmetry is absent in the other direction. Hence the western boundary of such a model could not be located; and probably this boundary is the most significant.

It was therefore decided that the model should extend to the line of columns surrounding the test column, i.e. to columns C E B F D in Fig. 2.1. Computer investigations by Fraser (1974) have shown that, in the elastic range, loads applied to the panels outside this region have little influence on actions around column A. It is reasonable to assume that after cracking the effects would be even less. Along the artificial boundaries of the model, i.e. the northern, western and southern boundaries, some stiffening

would be provided to simulate in part the stiffness which in the real building would be provided by the adjacent panels. It was not possible to simulate both the torsional and flexural stiffness. Finally, it was decided that if possible tests would be carried out to check that the boundary conditions were adequate. In fact, as will be described later, moments and shears were applied to the boundaries of some models and it was shown that the influence of these at column A was small.

With two complete panels of a building included in the model, it was not possible to have a full scale representation. The overall dimensions of the model were determined as 3800 x 5700 mm. These dimensions depended mainly on the removal of the model from the test rig after testing. The models would thus be approximately half the size of a normal building. However, in designing the models the small (half-size) building was designed directly according to Code rules. The two-panel region of the building so designed was then taken to be the model, the artificial boundaries being slightly modified as mentioned above and as discussed more fully in Chapter 6.

The model floor was to be supported by six concrete columns built integral with the floor slab. The height of these stub columns will be discussed in Chapter 6. The complete model therefore had the appearance of a six-legged table.

Although the research was concerned primarily with flat plates, we had doubts about the possibility of measuring twisting moments and shears in the various strips of slab, especially the spandrel strip. We therefore decided to commence with a model containing beams, as we considered that the measurement of internal actions in beams would be rather easier. The comparison of behaviour of a floor containing beams with one without beams would also be of value.

The first model contained a spandrel beam and a floor beam running from column A to column B. The second model was similar but without the floor beam. This was a fairly typical flat plate floor, which is usually designed with a spandrel beam. The third model had no spandrel beam. Decisions about subsequent models were made after the first three had been made and tested. In fact

the fourth and fifth models were similar in shape to the third (no beams). The fifth, and last, model had a wider column at A in order to investigate the effect of the width, c_2, on the variables being measured. More details of the individual models will be given in Chapter 6.

Clearly the strongest model would be the first, with the beams. This would enable the capacity of the testing frame to be checked. It would also provide a test for the numerous instrumentation techniques some of which were of a novel nature. If necessary, these could be modified before the later, more significant, tests were undertaken.

Each model was to be tested by applying uniformly distributed load, simulated by 16 point loads on each panel. The quantities discussed in Chapter 2 were to be measured for a series of loads. In particular, attention would be paid to the change in behaviour and in the distribution of the stress field as cracking progressed.

It was also intended to apply a couple to joint A (junction of the slab with column A) and measure the corresponding rotation. Tests of the boundary conditions were to be made if possible by applying moments to the artificial boundaries.

Chapter 4

EQUIPMENT AND INSTRUMENTATION

4.1 THE REACTION FRAME

The models were built and tested on the Department's strong floor. The first necessity was the design and construction of a reaction frame. The frame comprised two portal frames, one centred over each panel of the model, and braced together for stability (Fig. 4.1).

Each portal carried a single hydraulic jack centred over the floor panel. The load from this jack was distributed equally to sixteen pressure points on the slab. It was intended initially to design the floors for a live load of 4 kN/m^2. The dead load of a floor was estimated as 2.4 kN/m^2. Hence at design ultimate load it would be necessary to apply a load of 1.8 w_L + 0.5 w_D = 8.4 kN/m^2 to the structure. Each panel was approximately 10 m^2 in area, so a jack force of about 84 kN was called for in order to reach design ultimate load. However, in a highly redundant structure such as a floor, the collapse load is certain to be higher than the design ultimate load. For this reason it was decided to use a 200 kN jack on each slab. This provided a margin of almost 2.5 times the ultimate load for which the model would be designed according to the Code.

Each portal was designed so that the height of the cross-beam could be varied, the maximum height being governed by the overhead crane.

The feet of each portal were held down by the bolts of the strong floor. The anchorage attachment (see Fig. 4.2) was designed in such a way that the two portals could be moved further apart or nearer together in case it should be found necessary to vary the dimensions of the models. In fact this facility was not used.

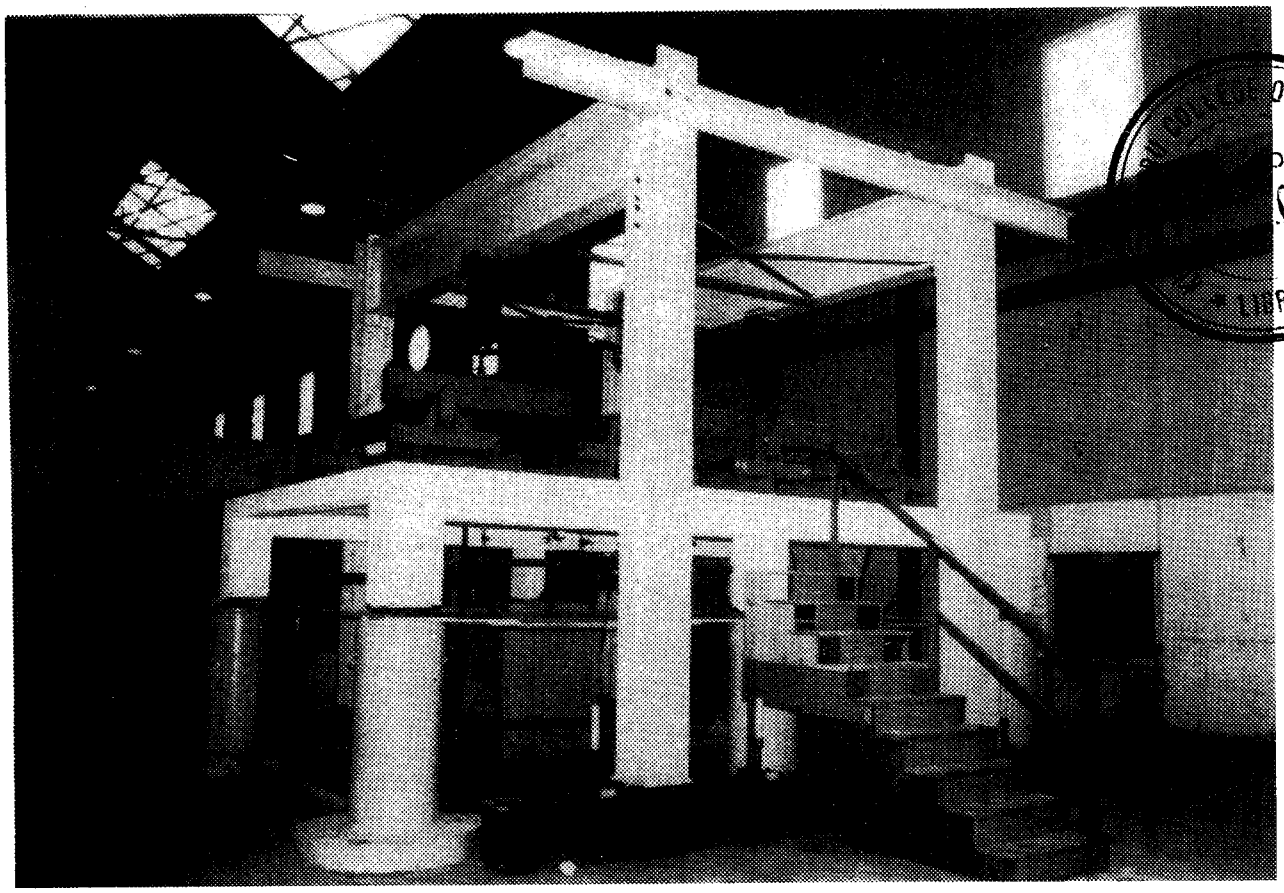

Fig. 4·1 Reaction Frame

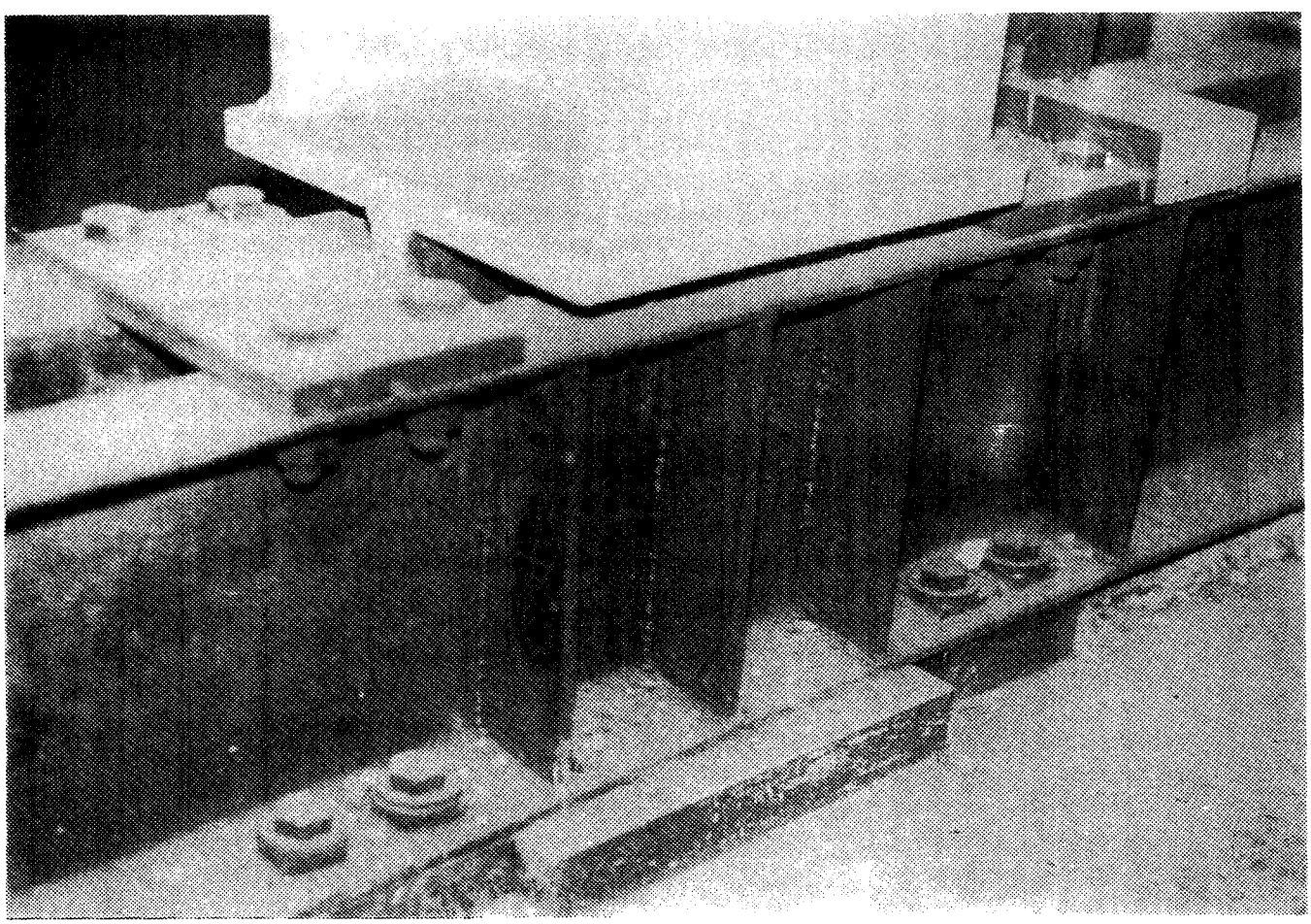

Fig. 4·2 Detail of Anchorage

4.2 SUPPORT PEDESTALS

In order to provide ease of access to the underside of the model it was decided to sit the model up on six pedestals, one for each of the peripheral model stub columns. The pedestal for the test column, A, will be described in Section 4.4. The other five pedestals were simple concrete cylinders 500 mm diameter and 1050 mm high. This height together with the stub columns would enable people to stand beneath the model floor. A greater height would have created problems with the top of the reaction frame fouling the overhead crane.

It was necessary to tie the tops of the pedestals together in order to resist the outward horizontal thrusts from the model columns. It was an essential boundary condition that no relative horizontal movement should take place between the feet of the model columns. The column shears were therefore estimated and the ties between the pedestals were made large enough to resist these forces without appreciable extension. The steel ties were 50 x 20 mm cross-section.

4.3 BALL SUPPORTS

Each of the model stub columns was terminated at what was considered to be a contraflexure point in the real building. They were therefore provided with a moment-free support. The five supports other than at column A were remote from the test area, and these columns were therefore provided with simple ball supports in spherical seats (see Figs. 4.3 and 4.4). It was recognized that with the loads involved - perhaps 40 kN at the corner columns - friction on the balls could generate some moment, but it was considered that at these remote locations these moments would have little effect on the stresses at A.

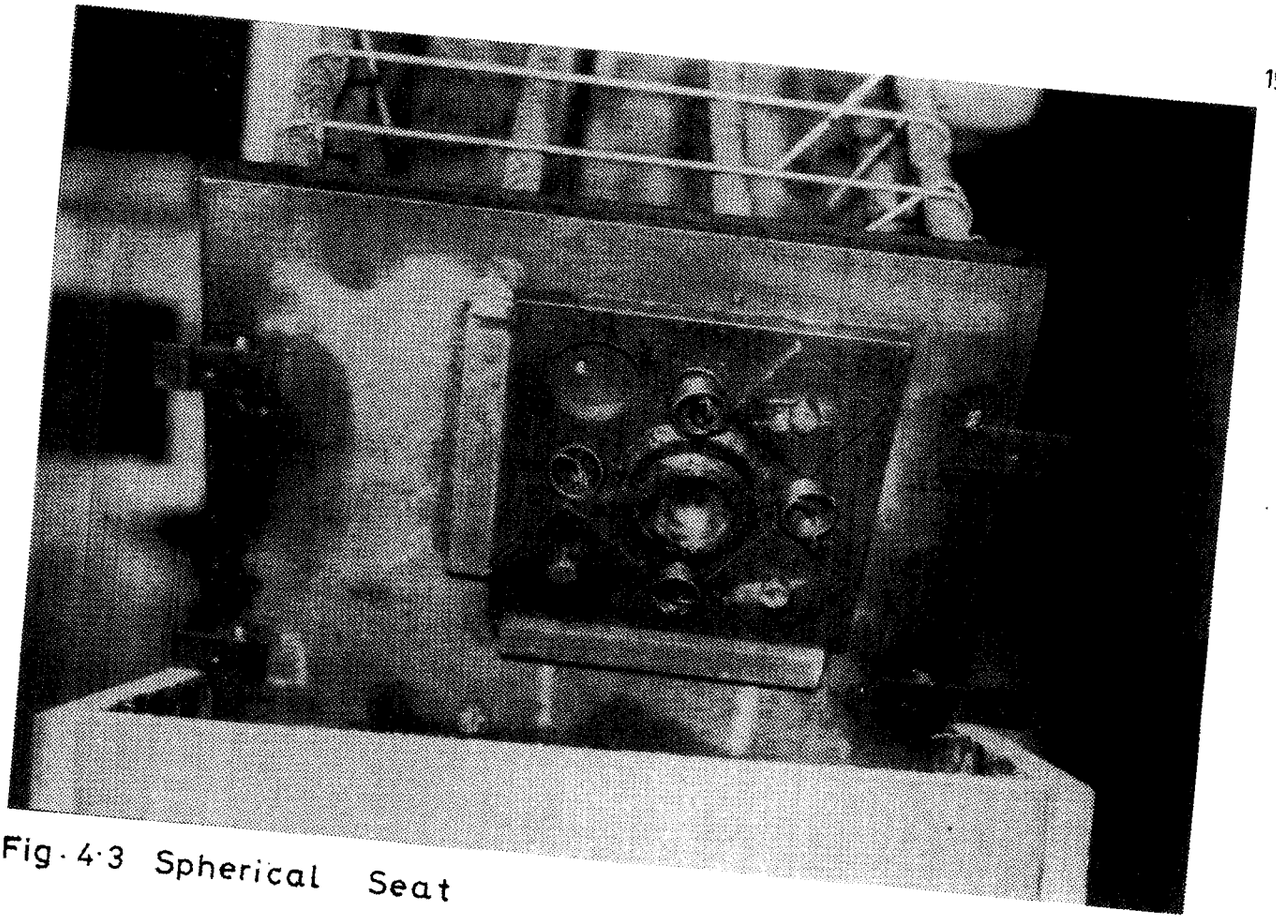

Fig. 4·3 Spherical Seat

Fig. 4·4 Ball Support

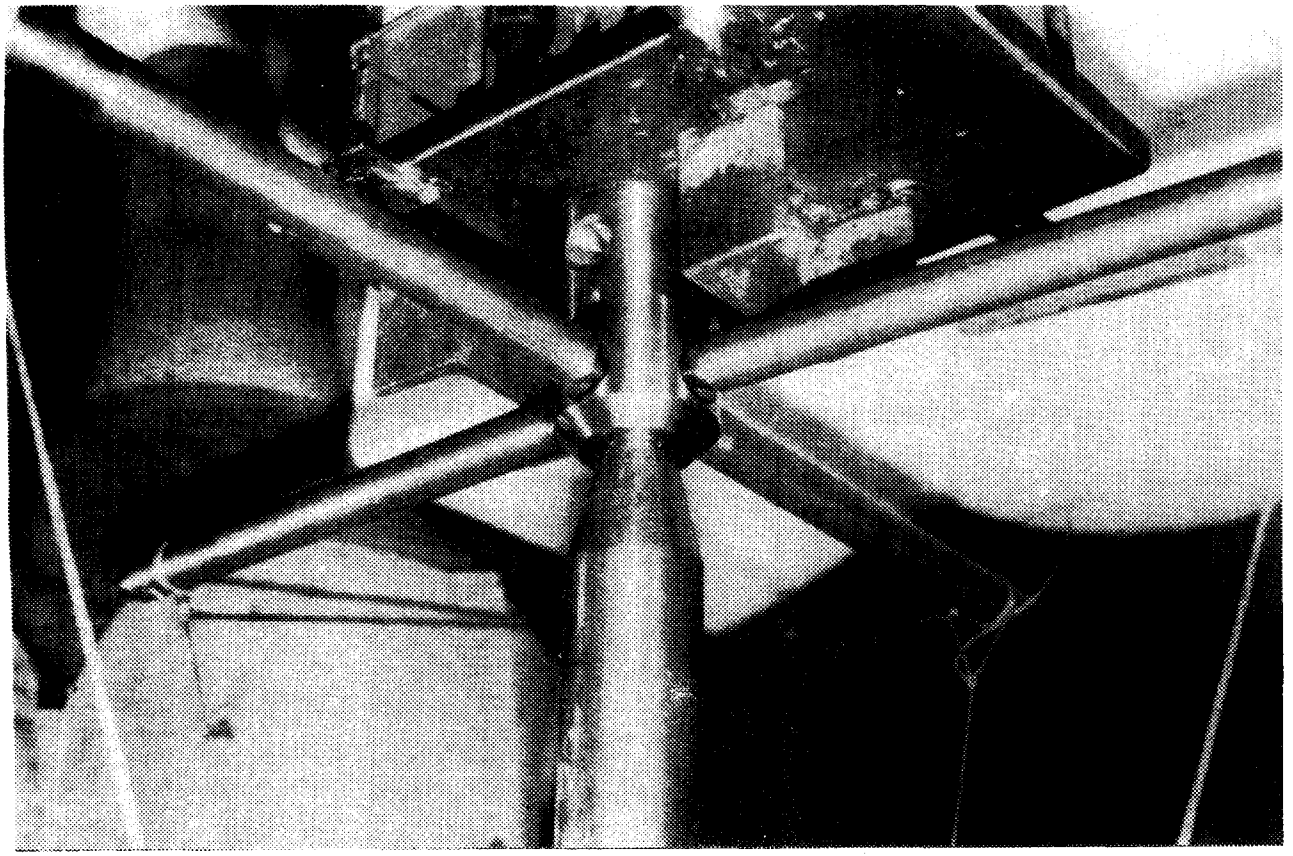

Fig. 4·5 Steel Boss

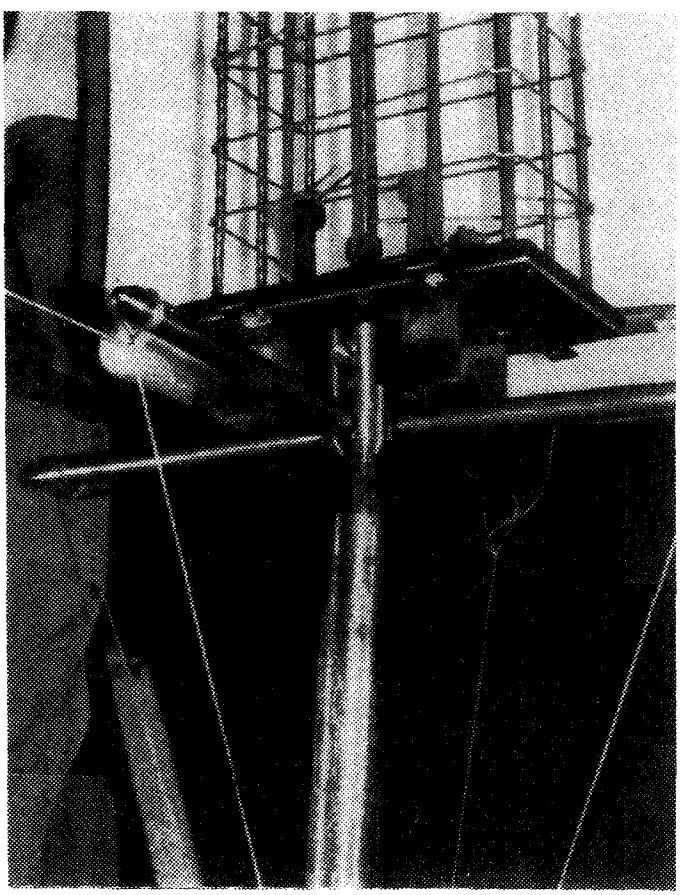

Fig 4 6 Rocker Arms

The balls were 35 mm diameter. The upper spherical seats were welded to the steel base plates of the model columns. The lower spherical seats were welded to plates cast into the pedestals. It was necessary to provide for the horizontal thrust from the stub columns. The same thrust also called for extra deep spherical seats, since it was calculated that otherwise the balls might jump from the seats.

4.4 ROCKER SUPPORTS AT COLUMN A

The provision of a moment free support at column A presented a much more serious problem. It was intended to measure the x, y, z components of force at the support of column A and to use these values to compute the bending moment at the top of the column and the total shear around the column periphery. The presence of any un-measured moment at the support would invalidate the whole experiment. The boundary condition itself also called for a moment free support. Even if any frictional moment at the support could be measured, a different moment at different load levels would correspond to a changing boundary condition.

Support mechanisms used by other investigators were studied, but it was decided not to use any of these. Instead, rockers were used rather than a ball to eliminate moment. To the base plate of column A a steel boss was fixed (Fig. 4.5) in which were five indentations. In these indentations rested five rocker arms with pointed ends, four in the horizontal plane and one vertically downward (Fig. 4.6). The remote ends of these rocker arms rested against similar seatings which were rigidly attached to an immovable pedestal (Figs. 4.7, 4.8).

The steel boss was screwed into the column base plate so that it could be recovered after the test and re-used.

The four horizontal rockers in the north, east, south and west directions were 230 mm long and 25 mm diameter. The vertical rocker was 860 mm long and 55 mm diameter. The ends of these rockers were not pointed but were rounded off to spherical ends about 8 mm diameter. This was much smaller than the diameter of the indentations in the boss so that at small loads, the boss was supported on 5 point supports. The crushing which would occur at

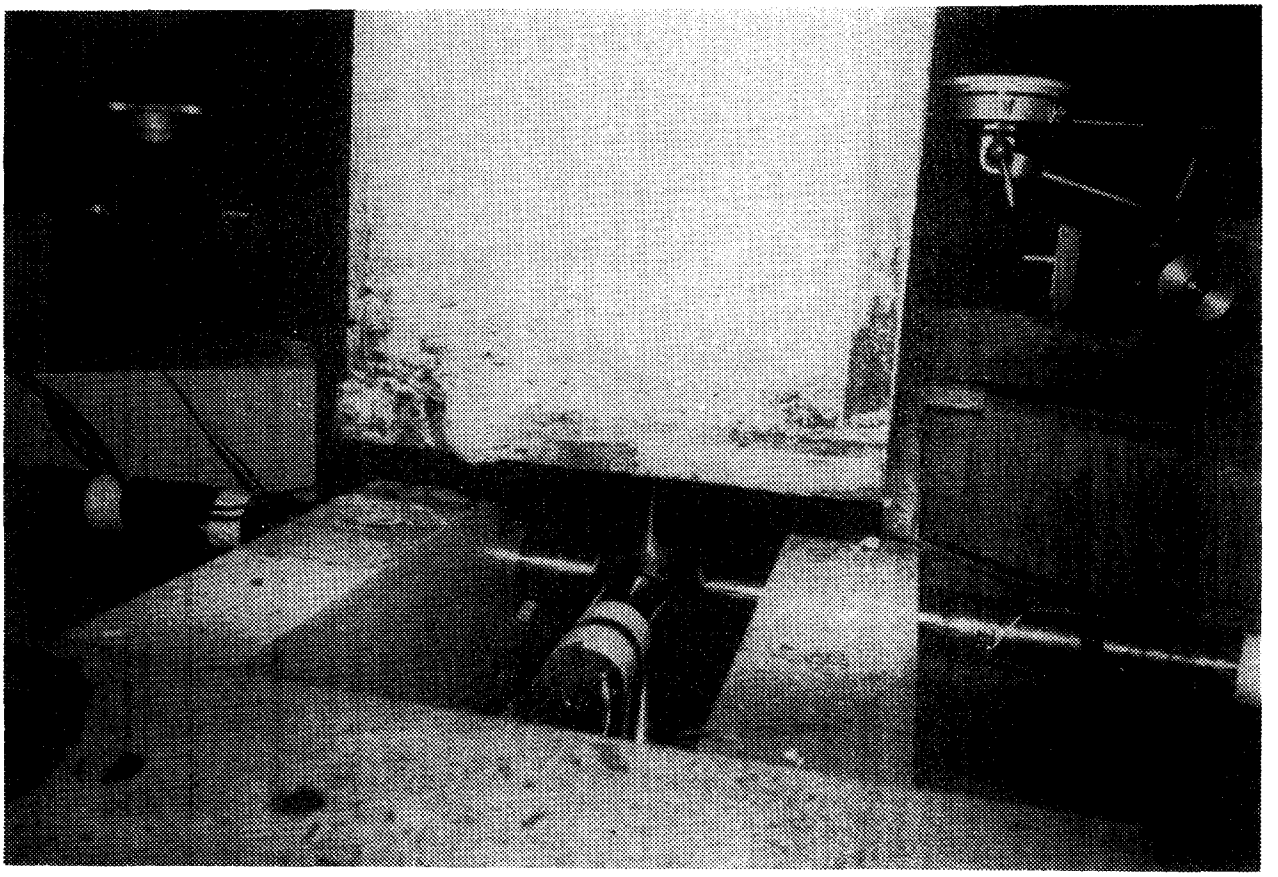

Fig. 4·7 Rocker Arms Inside Pedestal

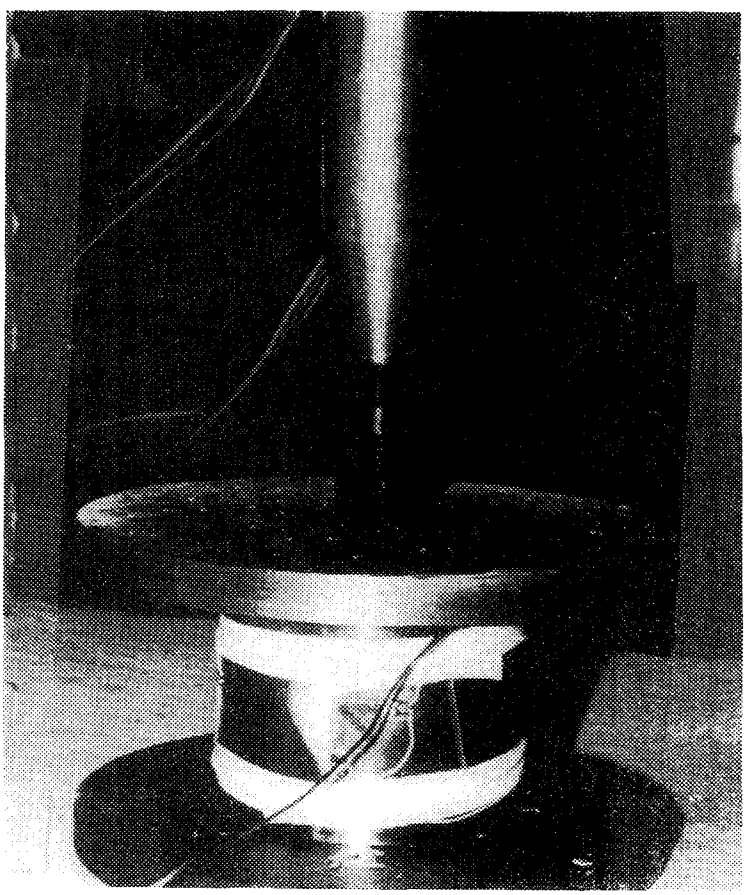

Fig. 4·8 Seat at Bottom of Vertical Rocker Arm

higher loads might permit some moment to be generated but it was estimated that the magnitude would be acceptably small.

The support pedestal had to be designed to accept the reactions from the five rocker arms. It was a hollow rectangular box with openings at the sides to permit access to the lower end of the vertical rocker. A steel frame was cast integral with the top of the pedestal and this frame supported the horizontal rocker arms. The emphasis here was on rigidity rather than strength. It was important that the supports of the rockers, particularly the E and W rockers, should not move relative to one another or to the other pedestal supports. The N and S rockers were less critical since, by the symmetry of the model the forces in these should be close to zero. The rocker seatings attached to the pedestal were all screwed to allow adjustment. Thus the horizontal rockers could be made finger tight or they could be given a pre-determined compressive force if desired.

Each rocker had strain gauges attached to it so that during a test its compressive force could be directly measured. The rockers became known as load cells and will be referred to as *load cells* hereafter and in the results. The output from these load cells were measured by a Peekel multichannel strain measuring instrument. The vertical load cell gave directly the vertical column force at A. The difference between the E and W load cells gave the E-W shear in the column. The difference between the N and S cells gave the N-S shear and this was always very close to zero.

The support worked excellently. Forces at the column A support were easy to measure. There was some evidence of the accuracy in the good agreement in those cases where cross-checks were possible with other measurements.

The form of the support also made it simple to perform stiffness tests wherein it was required to apply a moment to joint A. For this purpose the W load cell (for example) could be slackened off and a pre-selected force applied from the east by tightening up the support seating of the E load cell. The application of the required moment occupied only a few seconds.

4.5 LOAD DISTRIBUTION SYSTEM

Each panel of the model was loaded basically by a single 200 kN hydraulic jack. To simulate uniformly distributed loading, the load from this jack had to be distributed, through a series of simply supported beams to 16 regularly spaced loading pads.

The general assembly is shown in Fig. 4.9. All the beams were fabricated from steel box sections. The top beam, 254 mm x 152 mm and wall thickness 9.5 mm, carried a spherical seating to receive the jack load. This was supported by two beams 203 mm x 102 mm and wall thickness 9.5 mm. These again were supported by four beams 127 mm x 76 mm, wall thickness 6.3 mm, and finally there were eight beams 127 mm x 51 mm and wall thickness 4.9 mm.

All the support points consisted of knife edge supports (Fig. 4.10). It was considered that the length of the knife edge supports might provide insufficient stability when the system was under heavy load especially as the deflection of the slab would lead to some tilting of the system. On the other hand, any devices which inhibited freedom of articulation at the supports, while aiding stability would tend to destroy the simply supported nature of the assembly and might thus lead to non-uniform distribution at the final load points. As a compromise, each end of each beam was embraced between two vertical fins welded to the beam below. There was a small gap between the fins and the beam they embraced, the gap being filled with foam rubber (Fig. 4.9). The beam could thus tilt slightly, the resistance of the foam rubber being negligible. If the tilt became appreciable, the beam would be firmly resisted by the fins. No difficulty was experienced with the system until near the end of the last test.

The lowest eight beams were supported on the test slab through special pads (Fig. 4.11a). It was necessary to spread the load slightly at each support to avoid the possibility of punching shear. Also a small inclination of the under side of the pad, due to the slope of the floor slab under load, had to be accommodated.

The pads were manufactured by Dotmar Products Ltd., Sydney, specially for this purpose. Some details of the 100 mm x 100 mm pad are shown in Fig. 4.11b. The special plastic plate and the teflon coating allowed some relative movement between the concrete slab and the loading beam.

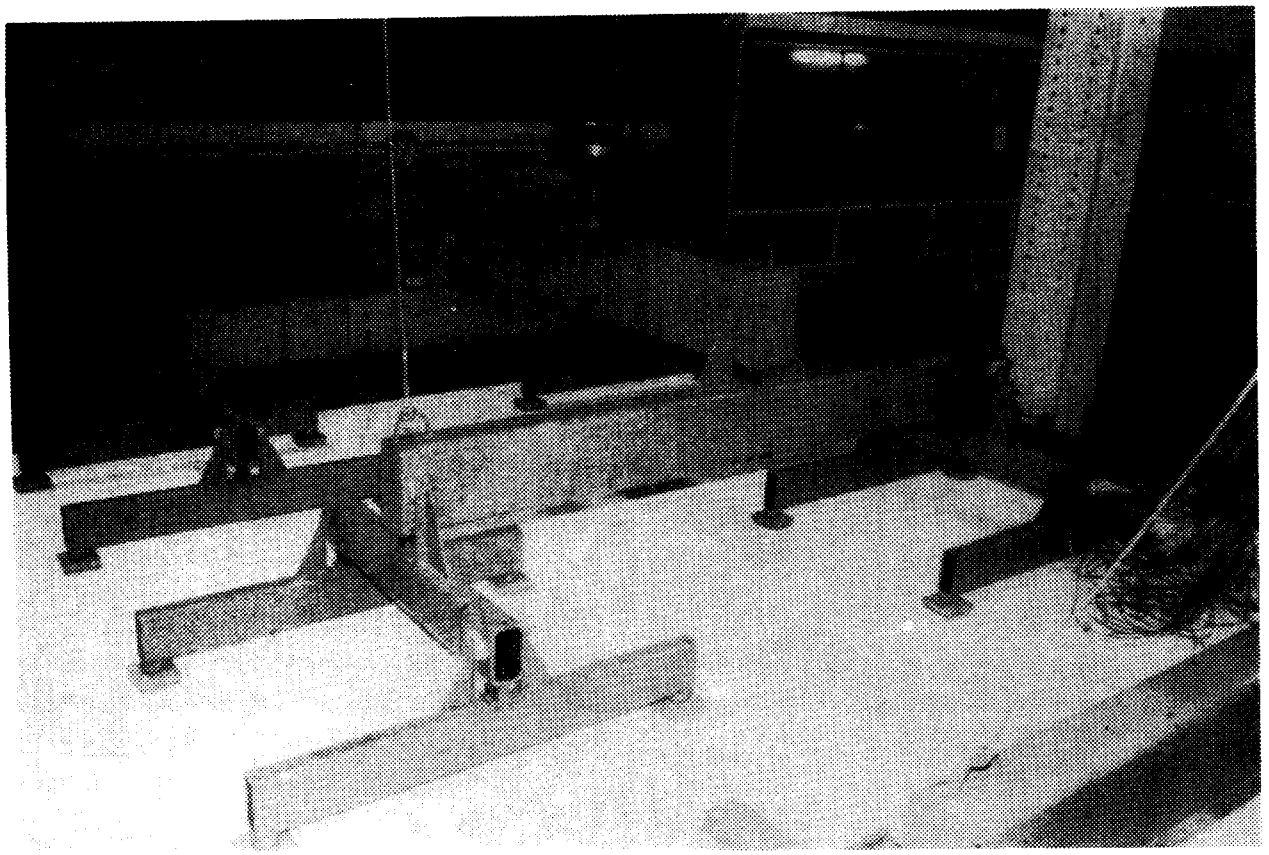

Fig. 4·9 Load Distribution System

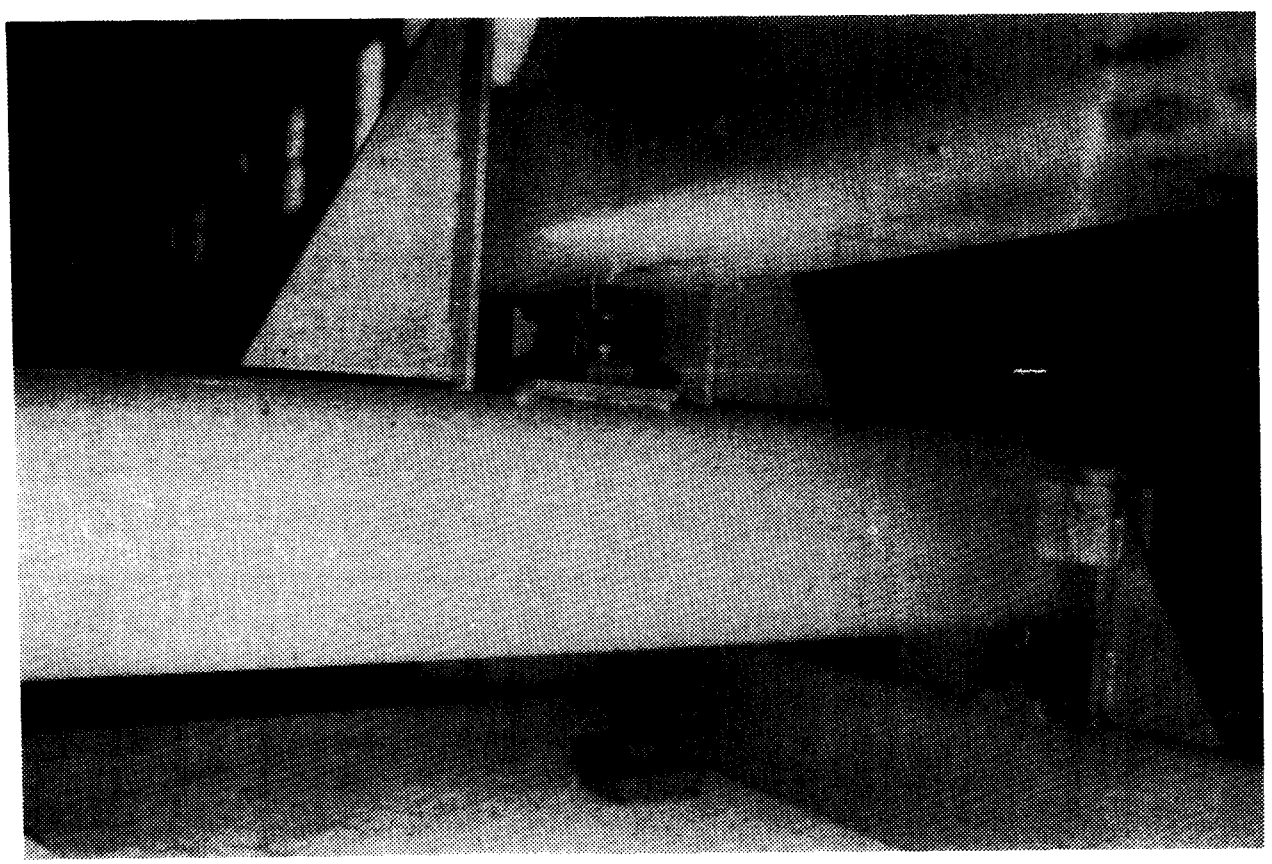

Fig. 4 10 Knife Edge Supports

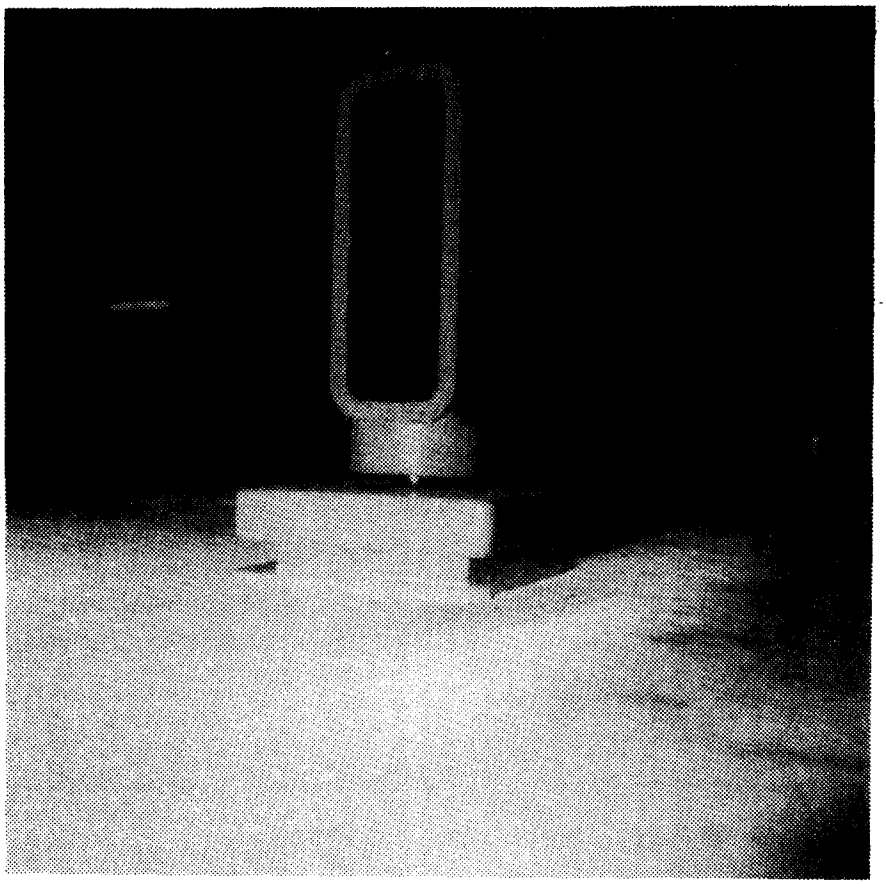

Fig. 4·11(a) Special Loading Pad

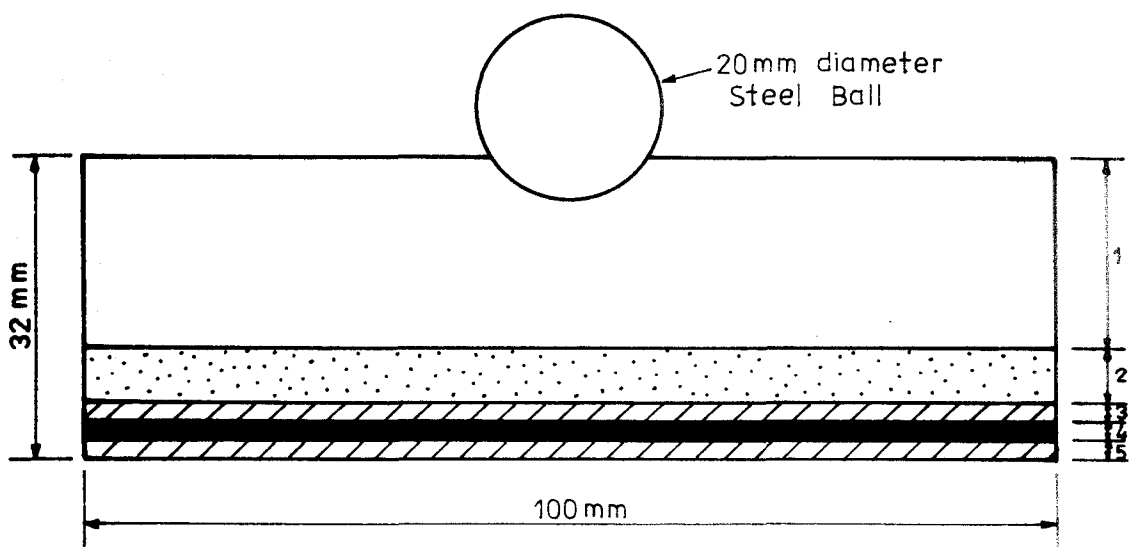

1. = 20mm Steel Plate, 2 = 6mm Natural Rubber
3. = 2mm Steel Plate, 4 = 2mm Teflon (Hostaflon)
5. = 2mm Special Plastic Plate

Fig. 4·11(b) Details of Loading Pad

4.6 MEASUREMENT OF STRAINS IN REINFORCEMENT

A primary objective was to determine, for any given load, the total negative moment, M_A, at the face of column A across a complete panel width between the centrelines of the panels on each side of A. The distribution of this moment was also quite important. The total moment could be obtained from the forces at the base of column A, which would be measured by the load cells. The distribution of this moment called for strain gauges on all the top reinforcement entering the face of the spandrel within the test region.

If the distribution of this moment M_A could be measured fairly accurately, then the portion of M_A entering the column on the western (or inner) face directly as bending moment would be known, and the remainder would represent the twisting moments in the spandrels.

It was decided also to strain gauge the longitudinal steel in the spandrels at several points. Interpretation of these strains would be obscured by the fact that the spandrel carried a combination of bending, torsion and shear. It was hoped that previous and continuing research on the torsion problem might assist.

The total shear around column A would be given directly by the vertical load cell at the base of column A. The determination of how this was distributed between the western face and the two spandrel faces presented a serious difficulty. Strains at several locations along the east-west reinforcement opposite column A were taken. It was thought that this might lead to a bending moment diagram along the floor beam AB of model 1 which, by differentiation, would lead to the shear force in this beam. Rather surprisingly, the accuracy of measurement proved sufficient for this purpose.

The planning just described led to the strain gauge layout for model 1 which contained a spandrel beam and a floor beam along the line AB. Analysis of the results of the first test indicated the desirability of measuring the total mid-span moment, M_m, and its transverse distribution. This was done in model 2 by gauges on the bottom steel at mid-span.

Further minor modifications became desirable as the tests progressed. A description of these changes for each model is given in Chapter 6 and complete details of the location of every strain gauge for each model are given in Appendix A.

In effect, the strain gauges on the reinforcement, together with the load cells at the base of column A, provided information about the internal actions within the structure.

The strain gauges had a resistance of 120 ohms and a gauge length of 20 mm. The outputs of eighty of the strain gauges were measured by a Hewlett-Packard Data Aquisition System (Model 3052A), see Fig. 4.12. The outputs from the remaining gauges were measured by a manually operated Huggenberger Bridge through a switch box. The H.P. Scanner (Model 3495A) had a switching time of less than 10 milli seconds. The H.P. data-logger was operated by a Calculator (9825A) which was programmed to scan the gauges, subtract initial readings, and print the actual strains on paper tape for each load stage.

4.7 MEASUREMENT OF DEFORMATIONS

In addition to measuring the internal actions it was decided that certain deformations should be monitored. The principal deformations were the slopes and twists along the spandrel beam. It was hoped that these might be related to the twisting and bending moments in the spandrels. It was decided also to measure slopes along the floor beam AB (twists would be zero by symmetry) and the deflections at salient points of the slab panels were also measured. These deflections would be correlated with various theories which have been proposed for the calculation of slab deflections.

4.7.1 *Laser Beam*

Various methods were considered for the measurement of angular rotations. One of these was the use of a laser beam. Along the spandrel it was necessary to measure both slopes and twists. It was therefore decided to mount the laser vertically at the required station. The light beam was intercepted by graph paper mounted horizontally about 2 m above the model (Fig. 4.13). By reading the x and y displacements of the light spot on the graph

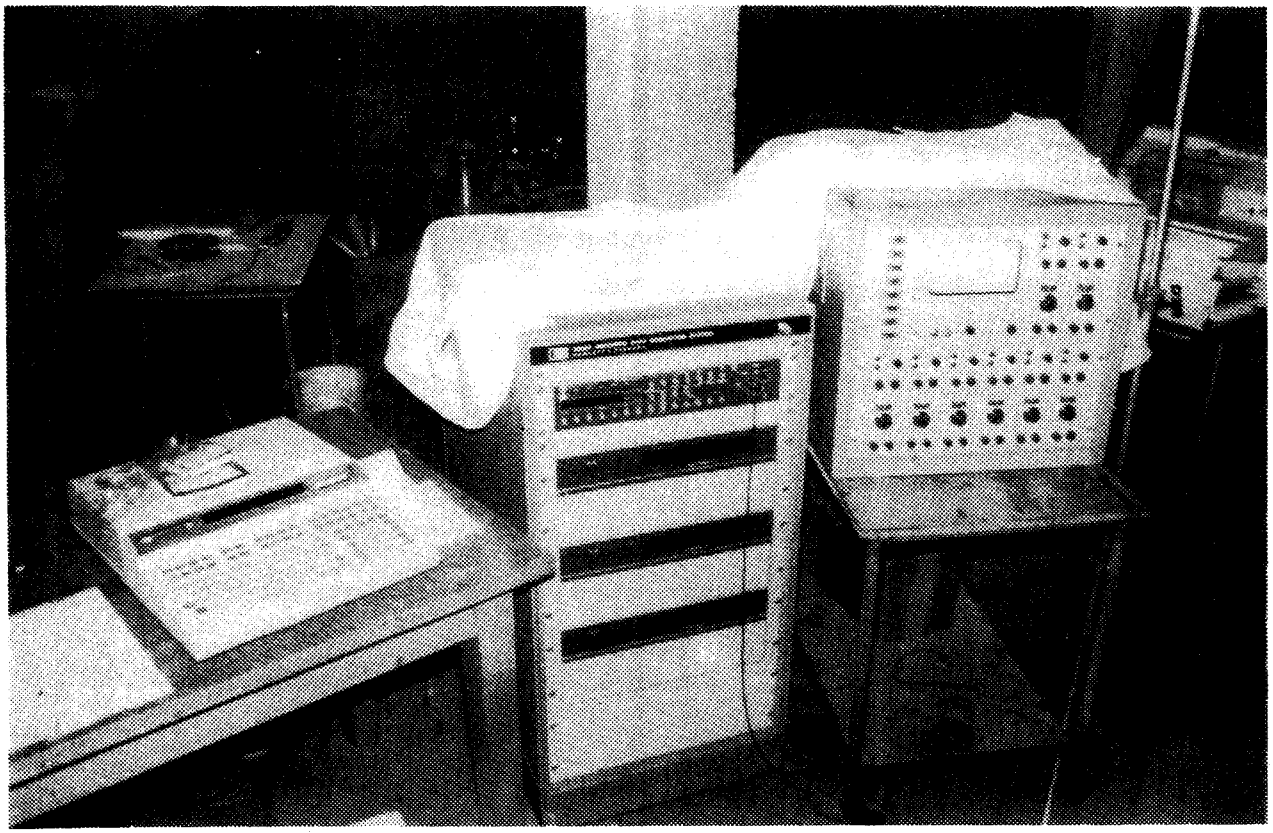

Fig. 4·12 Data Acquisition System

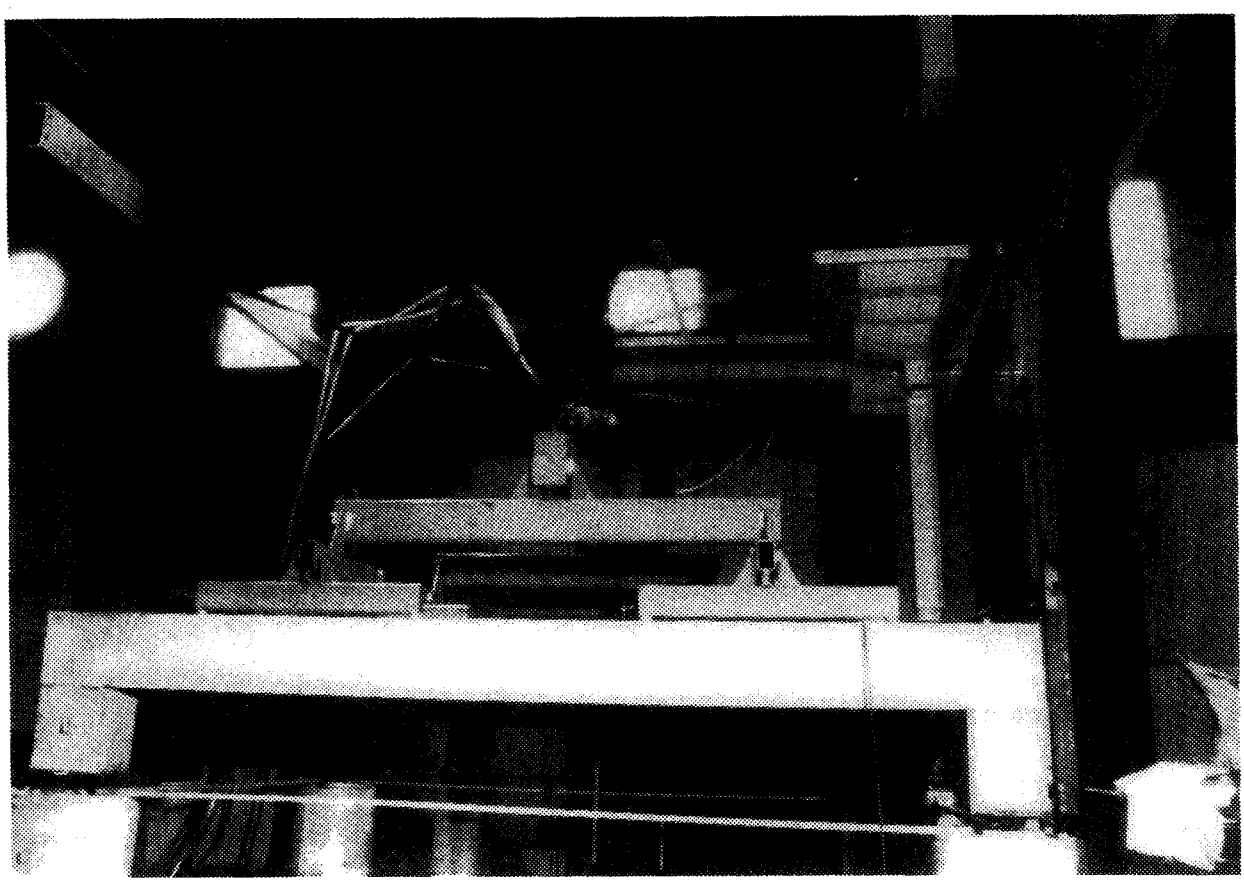

Fig 4 13 Laser Beam & Graph Paper - Genera. View

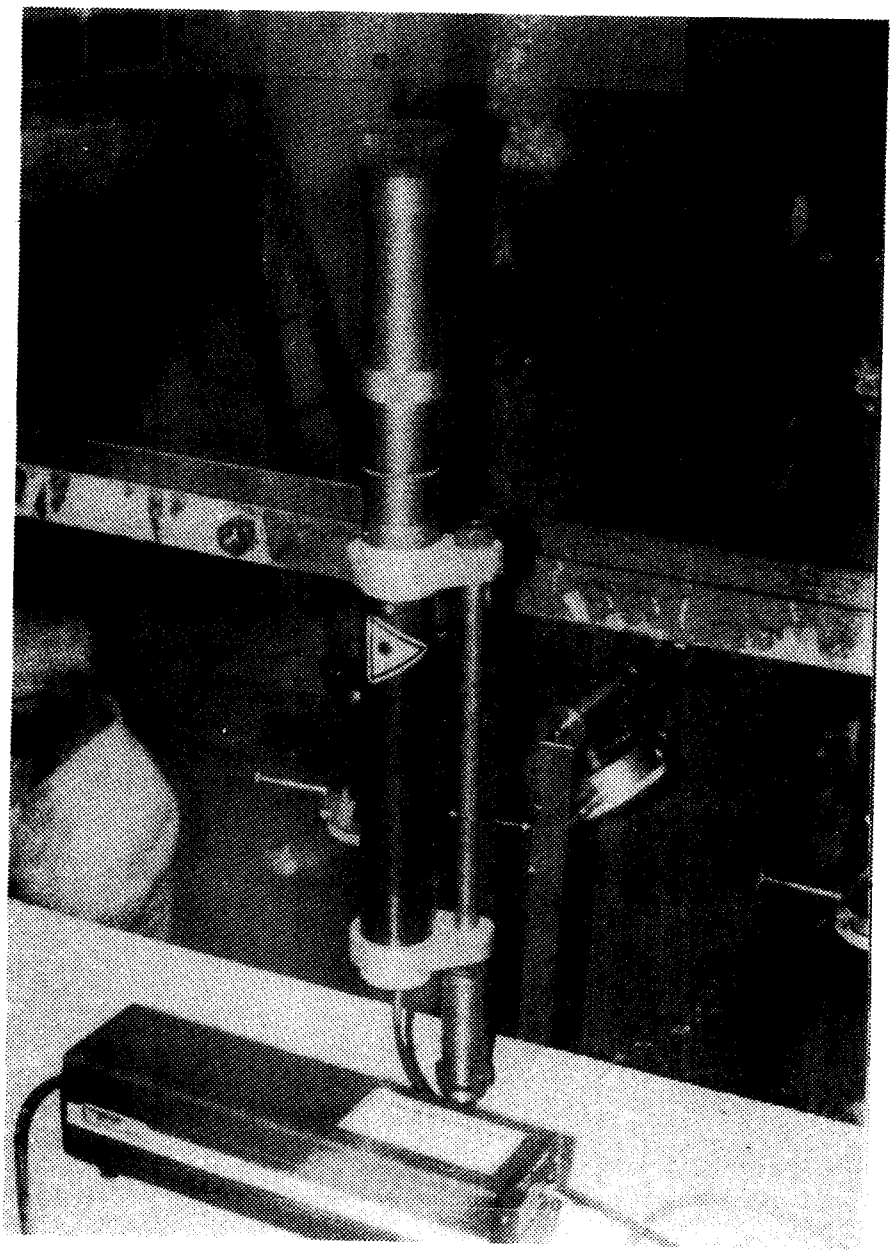

Fig. 4·14 Brass Fitting Attached to Laser

paper, both the angle of twist and the slope could be calculated. The laser was mounted in such a way that the axis of the light ray passed through the axis of the spandrel beam. In this way the vertical deflection of the spandrel under load would not affect the readings.

It was decided to measure rotations at column A as well as three points along spandrel AC (south), three points along spandrel AD (north) and three points along the floor beam AB (west), making 10 stations altogether. It was too expensive to employ 10 separate lasers, particularly as the effectiveness of the method was not known. Hence one laser was mounted successively at each of the 10 stations. That is to say, at each load stage during the test, the laser beam was mounted first at station 1 and the x and y positions of the light spot recorded. The laser was then moved to station 2 and so on.

It was essential that the mounting of the laser should be exactly reproducible. For instance, if the laser should be demounted from a given station and then replaced at the same station then, provided no model deformations had occurred in the meantime, it was essential that the light beam should return to exactly the same position as before. This was achieved by attaching a slightly tapered socket to the laser (Fig. 4.14). This fitted over correspondingly tapered mandrel at the 10 measuring stations (Fig. 4.15). In case the light beam was not co-axial with the laser housing, a small pin on the male fitting engaged with a slot in the female fitting to ensure that the laser housing returned to the same orientation. Before the testing of the first model, numerous checks were made and these proved that the errors involved in remounting the laser were insignificant compared with anticipated movements due to model deformation.

Some difficulty was experienced in concentrating the laser beam sufficiently so that the light spot on the graph paper could be accurately read. Eventually, readings correct to about 0.5 mm were obtained. With the graph paper at 2 m from the model, this represented a possible angular error of $0.5/2000 = 2.5 \times 10^{-4}$ radian.

Although the laser method of measurement was quite accurate it proved to be unnecessarily time consuming and was therefore used only on the first model.

4.7.2 *Dial Gauges for Slopes and Twists*

As an alternative to the laser method, angular deformations along the spandrel were also measured by means of dial gauges. At intervals of approximately 450 mm along the spandrel a piece of 25 x 25 x 3 angle was attached vertically to the face of the model so that it projected above and below the spandrel beam (Fig. 4.16). Bearing against each angle were four dial gauges. One at the top and one at the bottom were oriented in an east-west direction to measure the angle of twist. One at the top and one at the bottom were oriented north-south to measure the slope. The dial gauges were attached by magnetic bases to a rigid steel framework mounted on the strong floor and independent of the model.

In models 1 and 2 the angles were attached to the spandrel beam by araldite. In later models an 8 mm bolt was cast into the concrete at each measuring station. The angles could then be bolted on to the model after the formwork was stripped. Both methods were quite satisfactory but bolting was simpler.

There were seven measuring stations, one at column A and three each side - hence 28 dial gauges. It was found that the accuracy provided by these gauges was more than was necessary. The reading of these gauges was both quicker and less complicated than the use of the laser. In consequence the laser method was discontinued after the first model. Although it would have been possible to measure slopes along the line AB it was decided that this was unnecessary.

4.7.3 *Dial Gauges for Deflections*

In addition to the gauges mentioned in 4.7.2, other gauges were mounted below the model for measuring vertical deflections under load. In model 1 only two such gauges were used, one under the centre of each panel of the model. In later models a greater number were employed so that more information could be obtained about the general pattern of deflections. The number and location of these gauges for each model are all recorded in Appendix A.

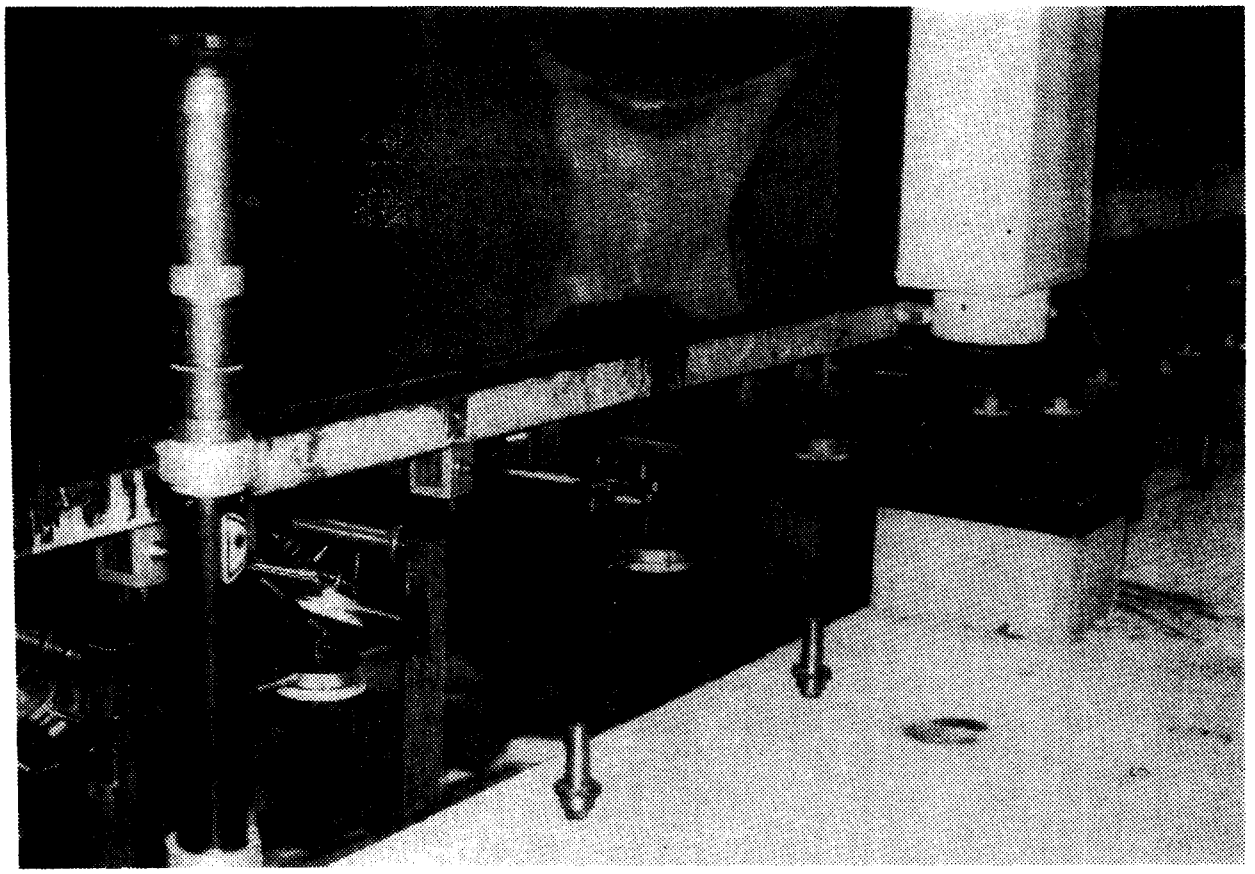

Fig. 4-15 Tapered Mandrel at Several Measuring Stations

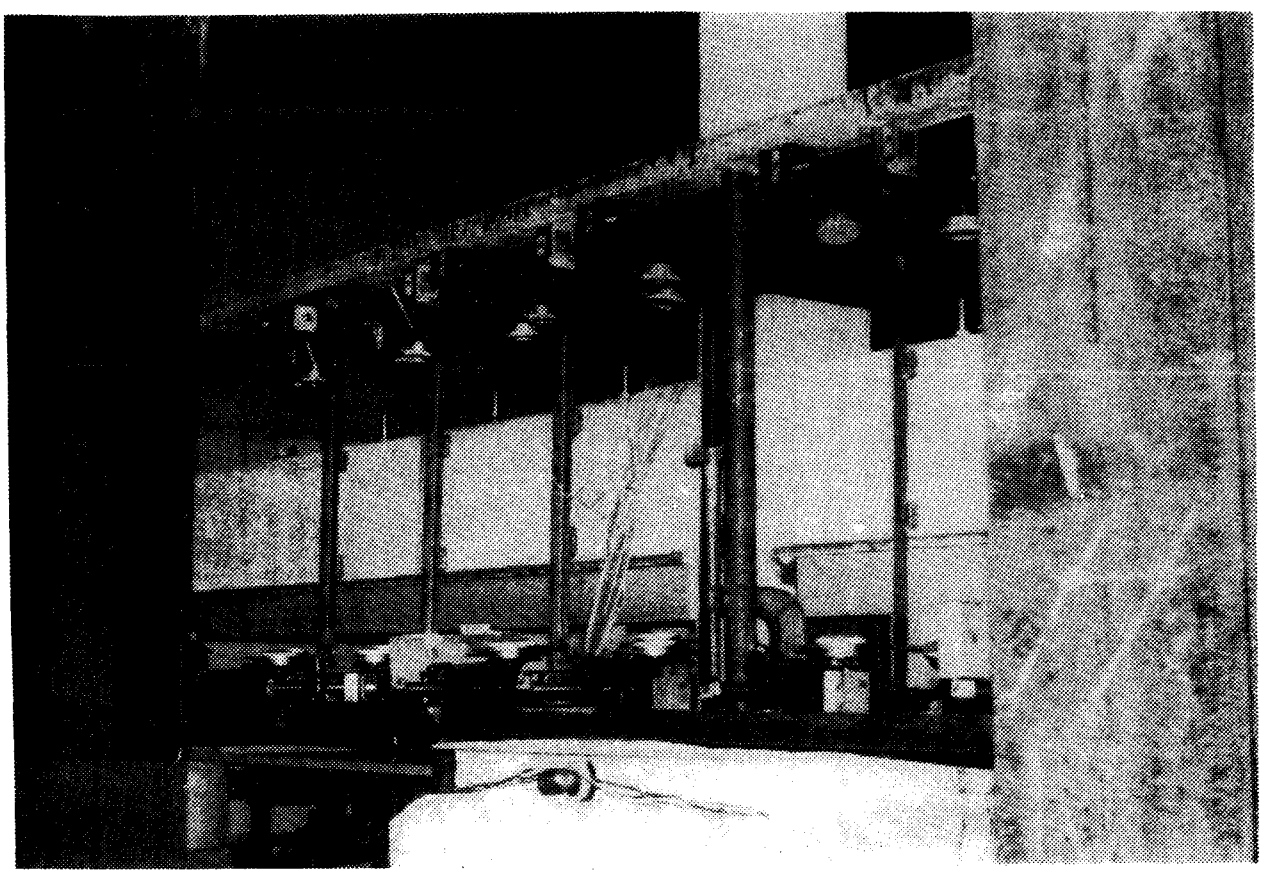

Fig. 4-16 Angles and Dial Gauges

Chapter 5

CONSTRUCTION AND TESTING - GENERAL

5.1 FORMWORK

The formwork (Fig. 5.1) was constructed from 18 mm resin-bonded plywood. In general this was fabricated in such a way that it could be re-used. It was supported on steel Acrow props and extendable beams.

To resist the outward pressure of the wet concrete the slab formwork was surrounded by 100 x 50 x 4 mm steel channels. Similarly the column forms were strapped near the base by 50 x 50 x 4 mm steel angles (Fig. 5.2).

To achieve the desired accuracy - especially in regard to the depth of the slab it was found necessary to tie the slab formwork down to the supporting beams. When the formwork was in place levels were taken round the outside of the formwork and adjustments were made until the outer wall was level to within 1 mm. This governed the top surface of the concrete. Levels were then taken on the slab soffit formwork to ensure that this was 100 mm lower than the upper surface. Adjustments were made by wedging from below. It was here that the tying down became necessary.

5.2 COLUMN BASES

The base of each column was formed by an 18 mm thick steel plate. To the upper side of this plate the main column bars were welded (Fig. 5.3). To the lower face was attached the spherical seat (Fig. 5.4). The spherical seat was first bolted to the base plate through slotted holes to permit minor adjustment. After adjustments had been made the seating was tack welded. The tack welding could later be cut and the bolts removed so that the seating could be re-used. New base plates were cut for each model.

Four lugs tack welded to the base plate supported the timber column formwork and simplified the formwork assembly.

At column A, instead of a spherical seating a steel boss was attached to the underside of the base plate. This boss had five indentations into which rested rocker arms as described in Section 4.4. The boss was screwed into the base plate and precautions were taken to prevent unscrewing during the test. In models 4 and 5, column B also had a base plate similar to the one at A.

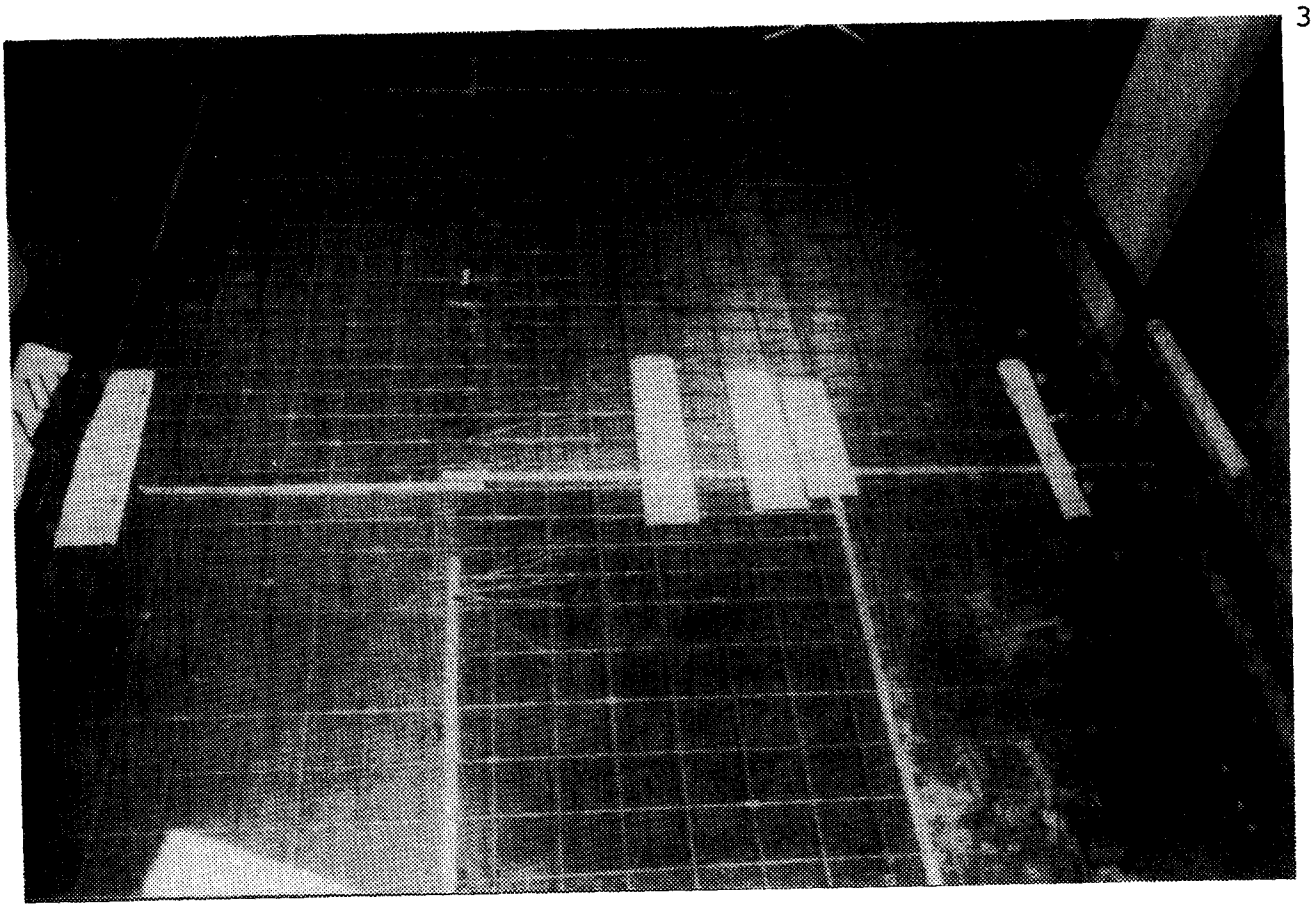

Fig. 5·1 (a) General View of Formwork from above

Fig 5·1 (b) General View of Formwork from below

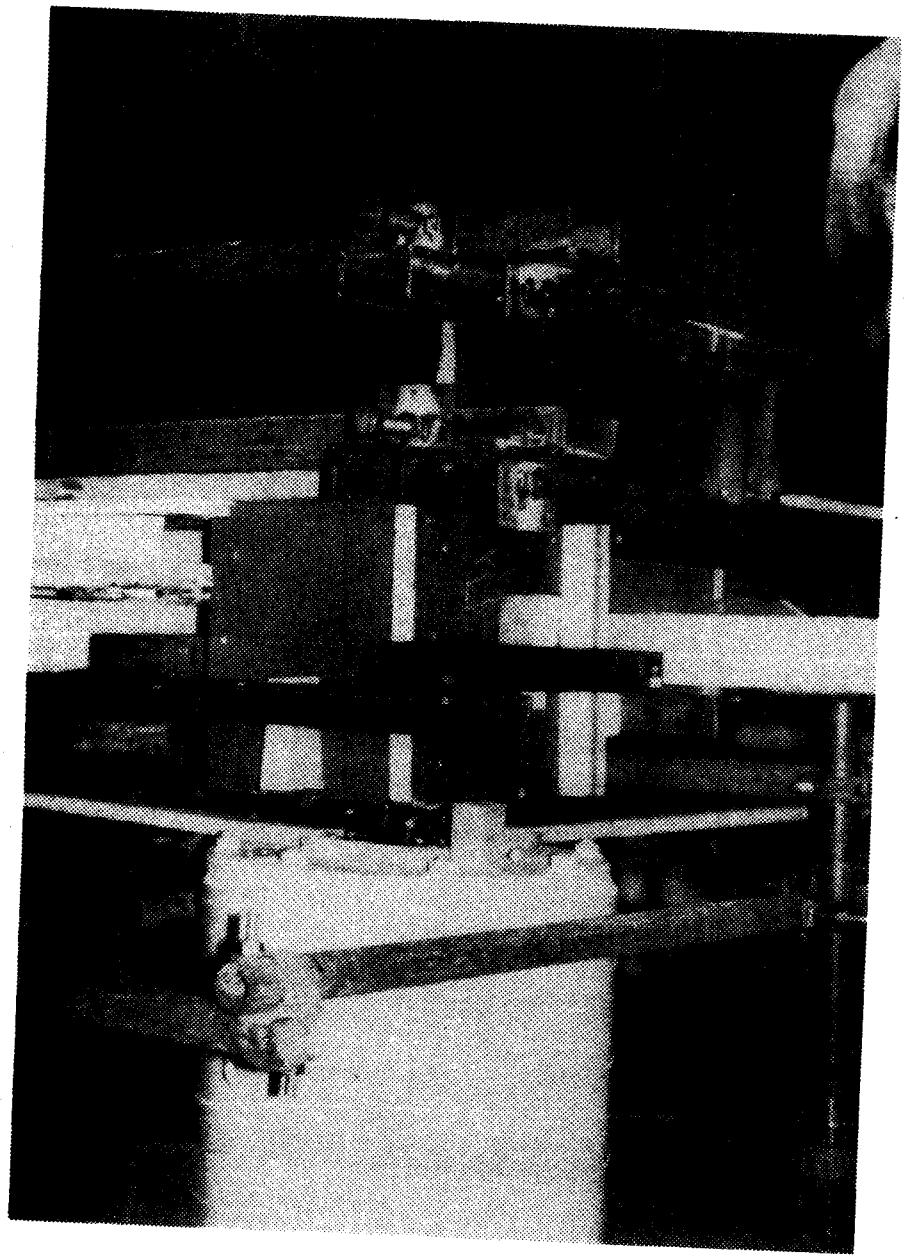

Fig. 5.2 View of Formwork at a corner

Fig. 5·3 Upper side of Column Base

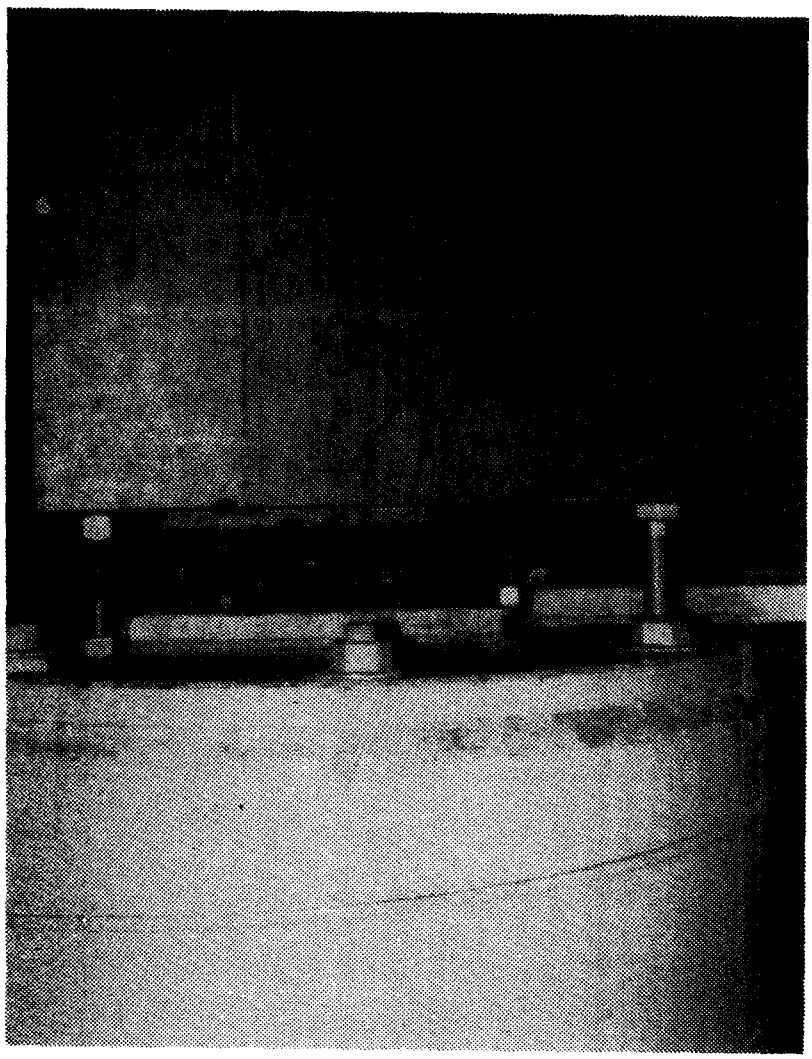

Fig 5 4 Lower Face of Column Base

5.3 ATTACHMENT OF STRAIN GAUGES

The strain gauges were attached to the surface of the reinforcing bars using the following procedure: The bar surface was first cleared, lightly sand-papered and then washed with acetone. A cyanoacrylate adhesive brand-named 'Alteco-Ace' was used to fix the strain gauge on the clean bar surface. Special terminals were also attached using the same adhesive near each strain gauge. The leads from the strain gauge were attached to the special terminals which in turn were connected to shielded lead wires. The entire region containing the strain gauge and the terminals was moisture-proofed using one coat of polyurethane called 'M-Coat' and one layer of araldite epoxy. The above procedure was highly successful and less than five per cent of the gauges installed failed.

In the first model, the shielded wire leads from the strain gauges were taken out vertically through the upper surface of the slab. This caused a minimum of weakening of the slab by virtue of the wires buried in the concrete. On the other hand great care was needed to see that the leads did not emerge from the slab surface where a loading pad was to be situated. It was found during testing that the leads interfered with walking about on the slab.

In the second model the leads were taken out through the edge of the slab. This resulted in a considerable length of wire being buried in the concrete. Also the leads emerged from the slab at rather widely scattered locations.

In the remaining models the leads were taken out through the soffit of the slab. This was found to be the most satisfactory method.

Before the concrete was cast, the position of each strain gauge was measured and recorded with reference to a three-dimensional system of co-ordinate axes (see Chapter 6).

5.4 CASTING AND CURING

Commercial ready-mixed concrete of specified strength was used for each model. One of the top beams of the testing frame

had to be removed to allow access for the dump bucket to the central part of the model.

5.5 CONNECTION OF LEADS TO STRAIN MEASURING EQUIPMENT

After the formwork had been stripped, the strain gauges were checked by means of a multi-meter. The leads were then connected to the measuring equipment. This connection presented a number of problems which were solved sequentially in the earlier models. Only by Model 4 was a really satisfactory system developed. It will therefore be worthwhile to discuss this in some detail.

The majority of the problems encountered could be associated with the connecting medium that serves to channel measured data through the loop consisting of the measuring instruments - strain gauges - and back to the data acquisition system. Since the instrumentation is very sensitive, and the actual measured signals are small in magnitude, it is most important that the electrical impulses representing experimental data will be free from any interference, internal or external. This necessitated the introduction of a simple, but reliable system for connection which also had the following characteristics:

(a) Ease of gauge identification.
(b) Simple grounding of wires and instruments.
(c) Reliable way of checking for breaks or short circuits in the loops.
(d) Easy variation of gauge to measuring channel connection if required.
(e) An arrangement of wires capable of carrying a large volume of information.
(f) A re-usable and quickly erected set up.

The experience gained from the first three models showed that using a single wire from each gauge to the instrumentation led to confused maze of wires, making it difficult, if not impossible to 'debug' any faults. As was previously mentioned, the grounding of the wires is of great significance and it was very difficult to achieve good grounding with such a large number of connectors. Another problem was the time required for the setting up of the final connection of the wires to the instrumentation; especially when

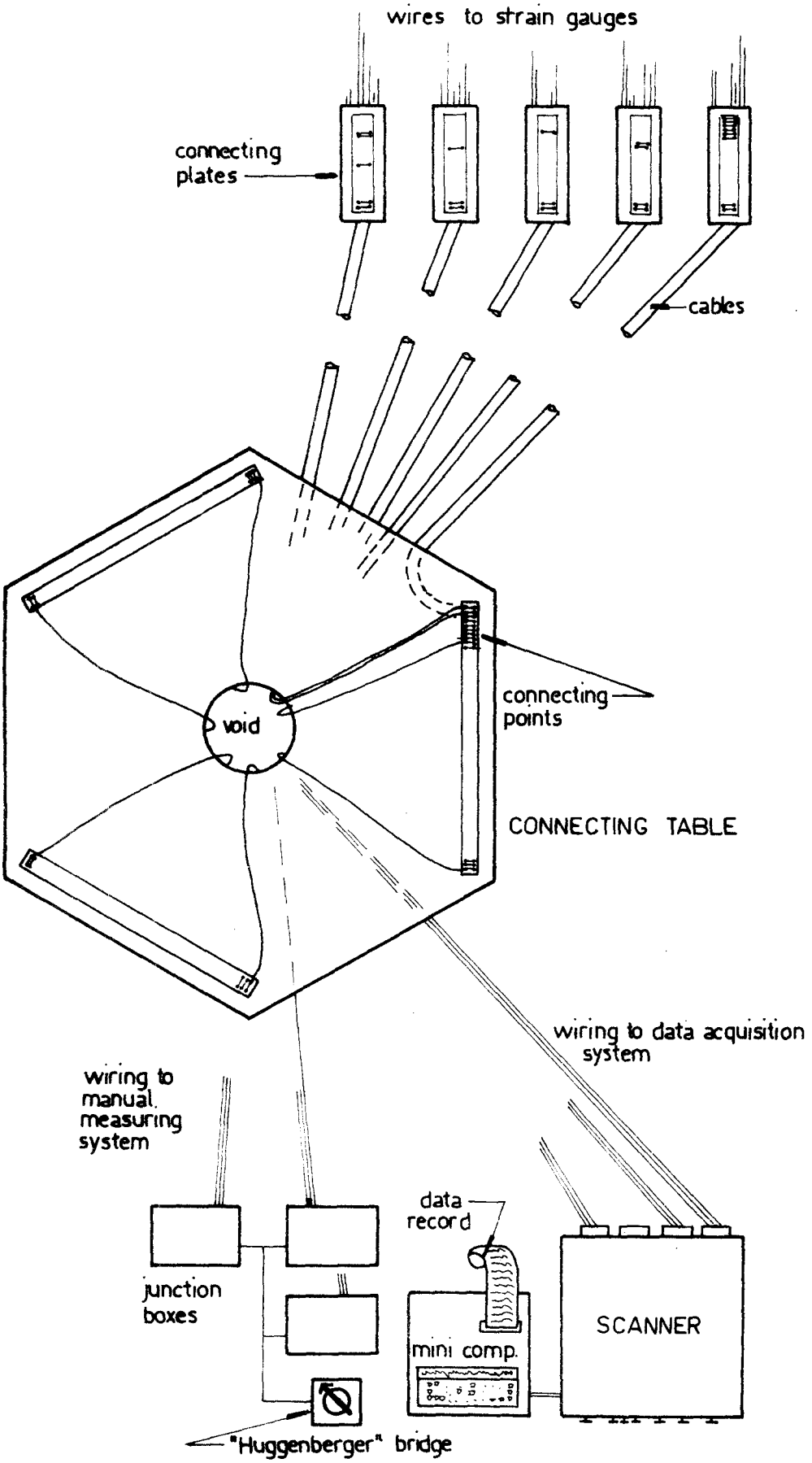

5.5 SCHEMATIC DIAGRAM SHOWING WIRING OF INSTRUMENTATION (models 4 & 5)

the monitoring equipment was not generally available until just prior to the commencement of the experiment. It is worth mentioning that after each of the early experiments considerable quantities of wire were lost and wasted due to the untangling of over 100 wires.

The solution to these problems was found by creating a permanent connector which served as a station between the gauges and the instrumentation. This connector took the form of a table with a large number of labelled built-in solderable connecting points. Cables, each containing 27 pairs of colour coded wires in bundles, led to the underside of the model from this table. These cables ended, near the model, on special plates themselves having solderable points for connection of the strain gauges in the model. Only the relatively short individual cables connecting the strain gauges with the plates were wasted in each experiment. The table, which was placed in close proximity to the data acquisition system, was connected to the removable plugs of the instrumentation and to other measuring devices by labelled wires soldered to its points.

The solderable points on the table, as well as on the special plates, were numbered the same way as the wires, so the identification of any specific gauge was easily obtainable. Also the continuity of the wires, gauge characteristics, etc., could always be checked with this set up at practically any place using the exposed soldered points. Therefore, the tracing of loose connections or gauge failure could be quickly and easily ascertained.

The set up is shown diagrammatically in Fig. 5.5. The system was independent of this particular research and it could be used in other experiments requiring the measurement of large numbers of gauges having multiple connections between model and instrumentation.

The actual 'plugging in' of the system can be left to the final stages of the preparation of the experiment, thus enabling more flexible sharing of the main equipment by various users.

The system proved itself in models 4 and 5, allowing for a shorter turn around between experiments, and practically trouble free connections and reduced number of gauges lost.

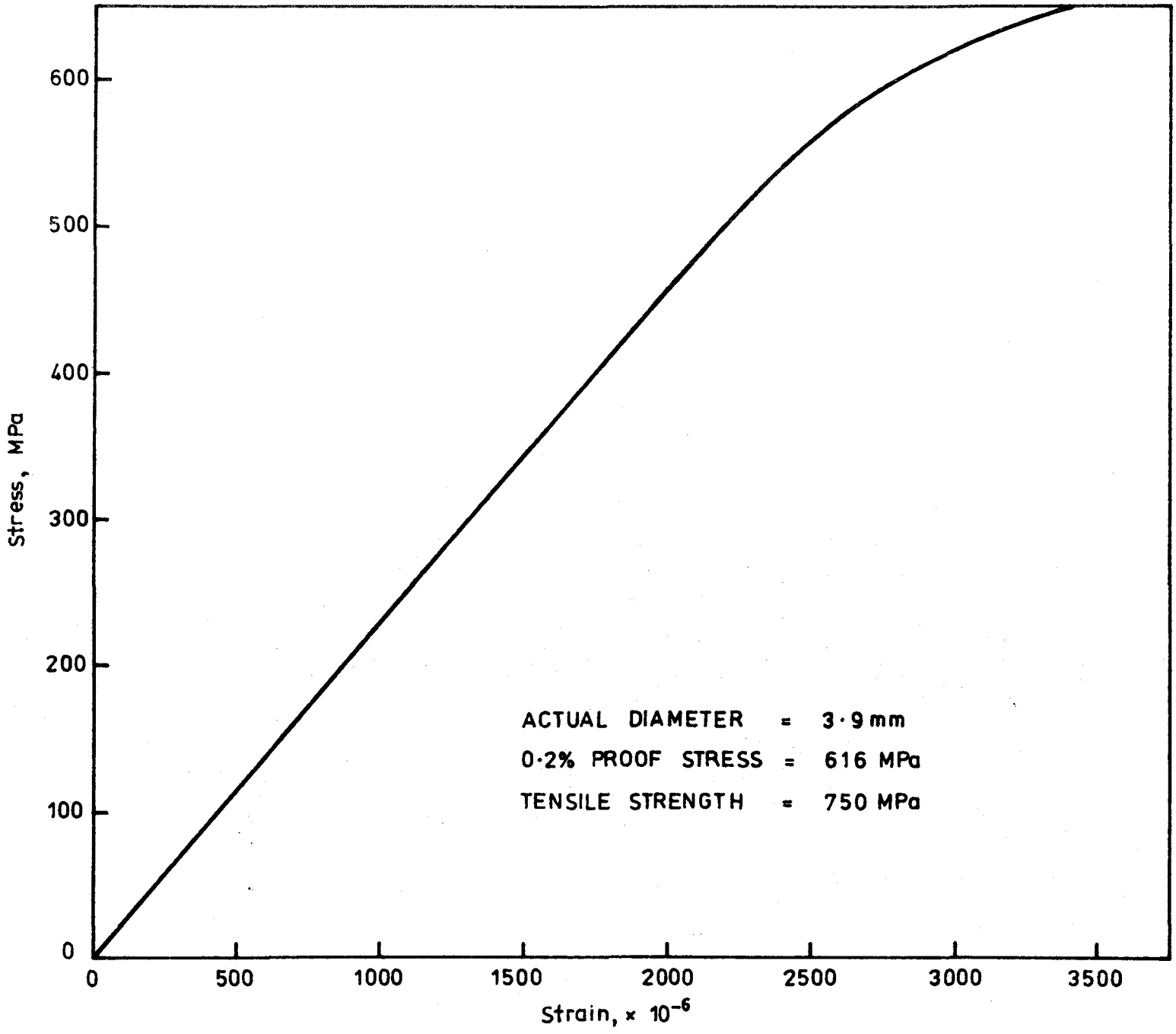

Fig. 5·6: Stress-Strain Curve for C4 Bar

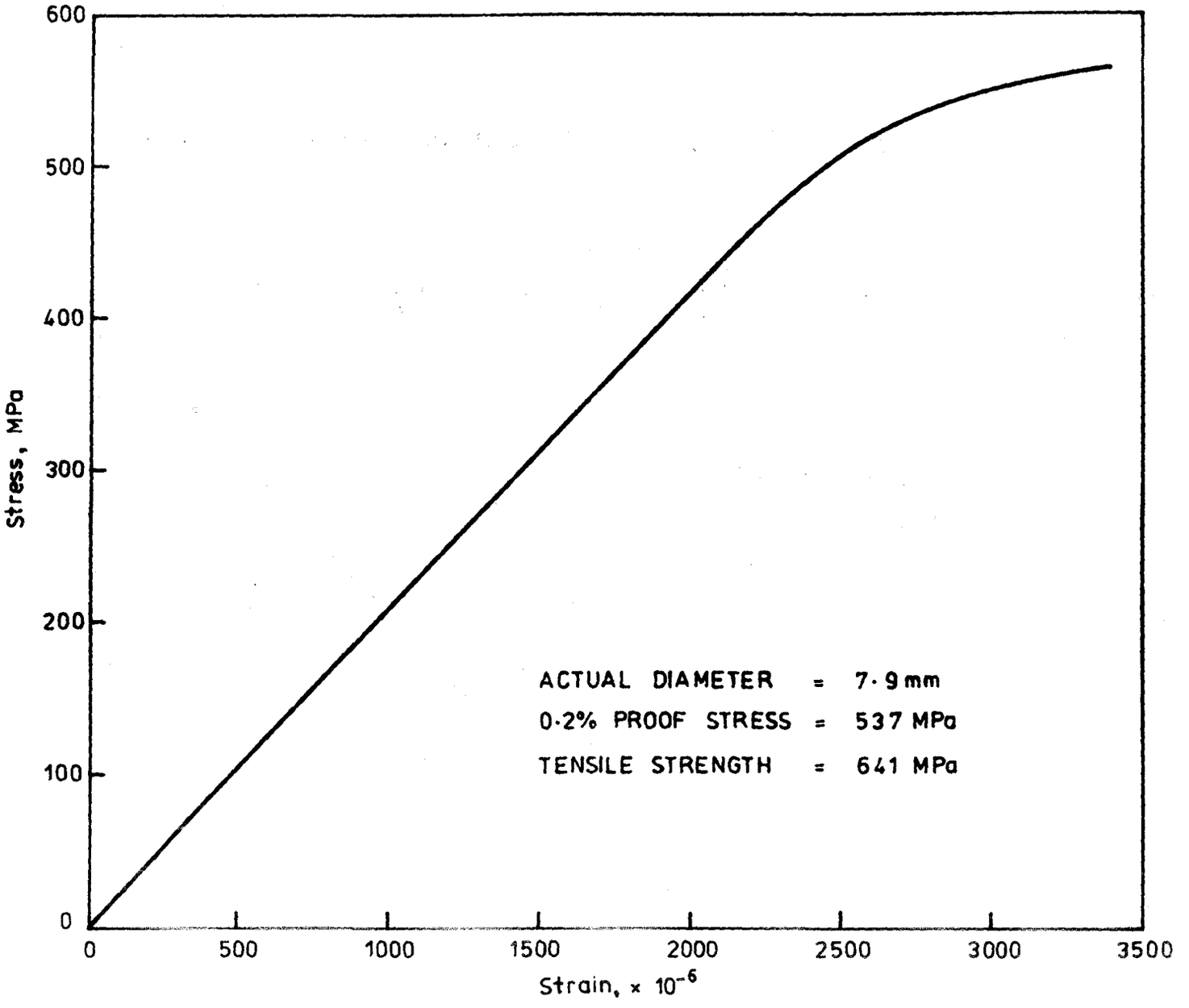

Fig. 5·8: Stress-Strain Curve for C8 Bar

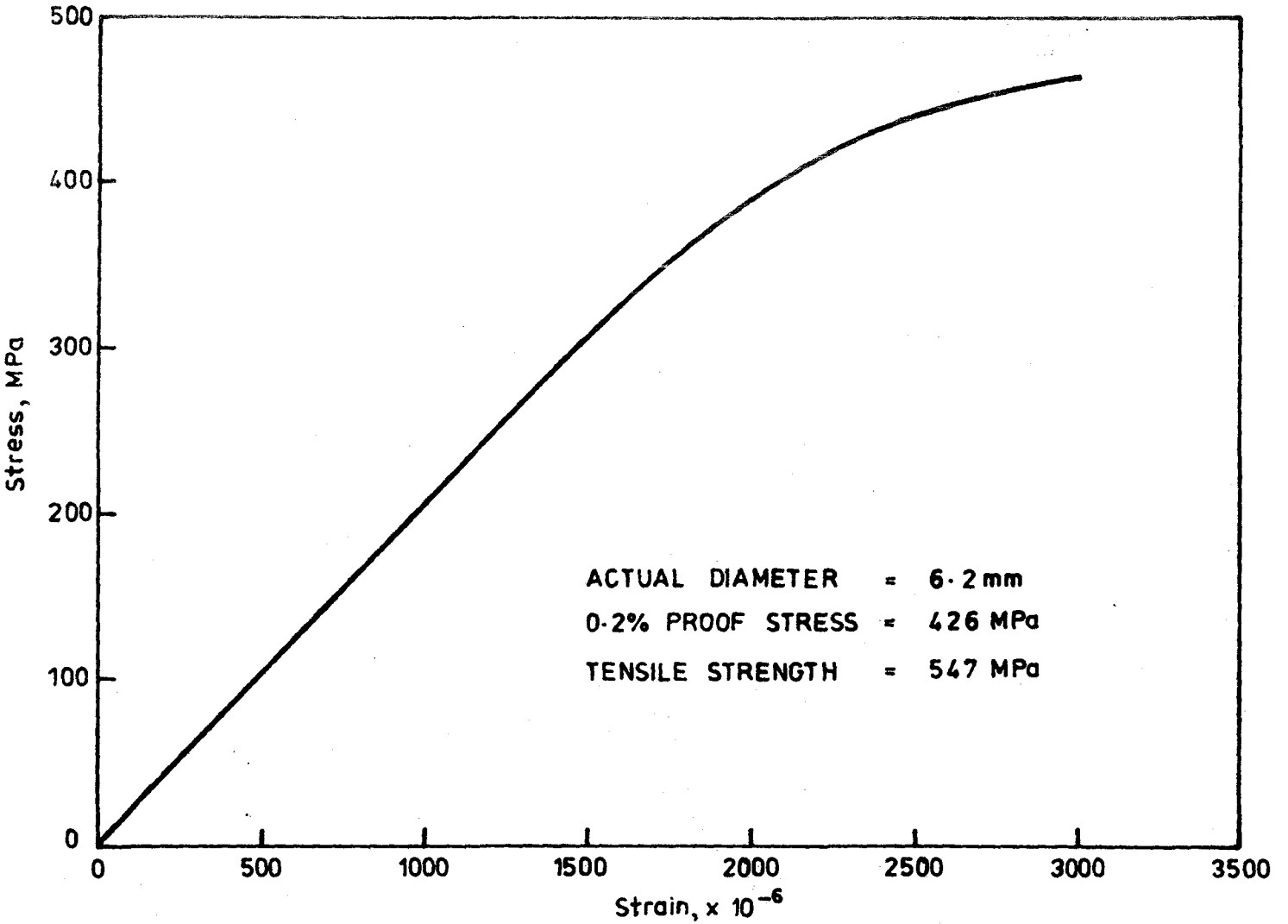

Fig. 5·7: Stress-Strain Curve for C6 Bar

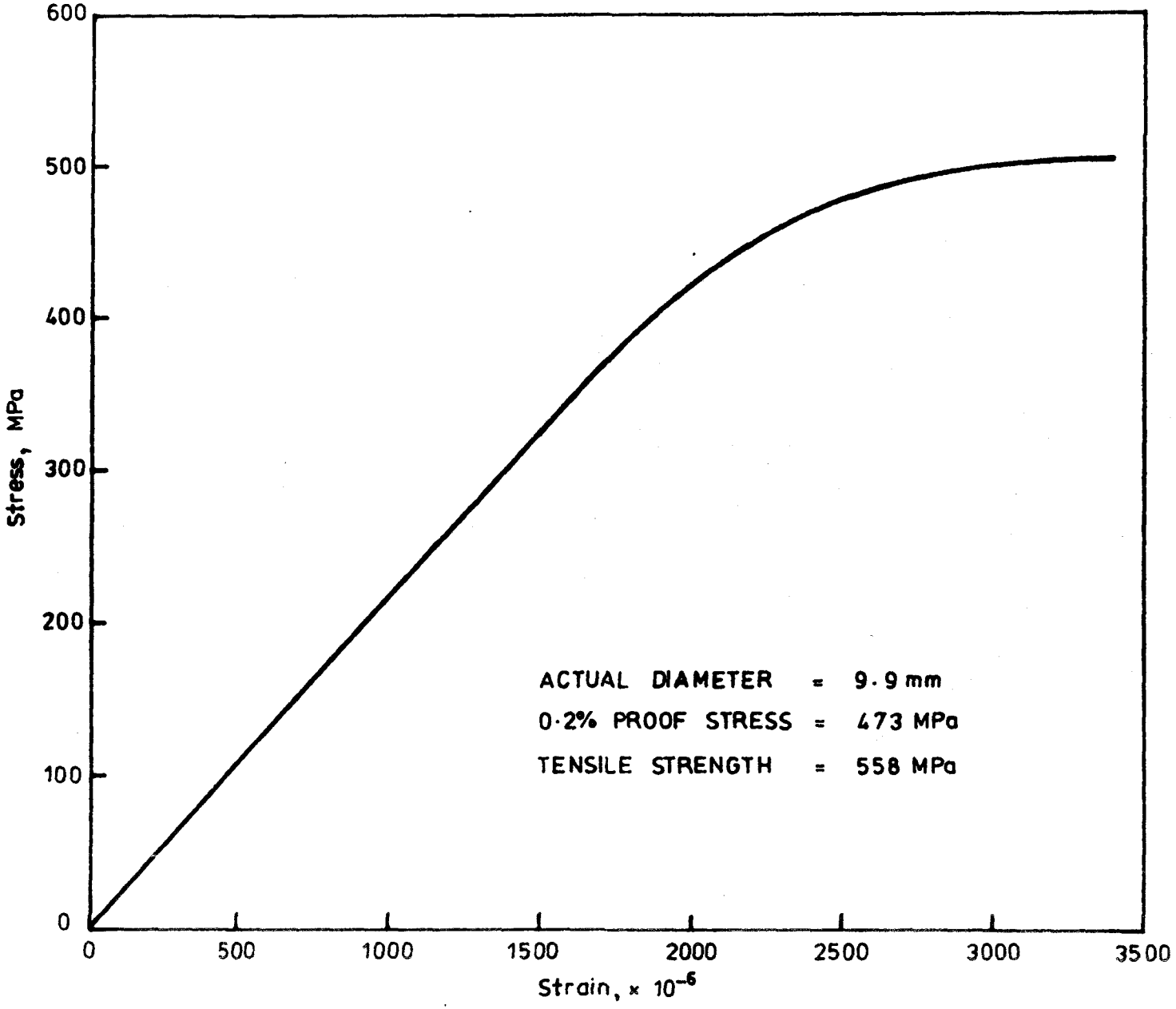

Fig. 5·9: Stress-Strain Curve for C10 Bar

5.6 STRESS-STRAIN CURVES FOR REINFORCING STEEL

Similar steel was used throughout the tests. This comprised wires or bars designated as C4, C6, C8 and C10. Of these, C4, C6 and C8 were plain hard-drawn wires and C10 was a plain round bar. One stress-strain curve was determined for each size of bar and this curve was used for every model. The four curves are given in Figs. 5.6, 5.7, 5.8 and 5.9.

5.7 RELATIONSHIP BETWEEN BENDING MOMENT AND MEASURED STEEL STRAIN

As explained in section 4.6, the purpose of the strain gauges on the reinforcement was to determine the distribution of moments at certain locations. In the early models the distribution of E-W slab moments along the face of the spandrel were sought. It was hoped that these would correlate with the total stress-resultants as measured by the load cells at the base of column A. In models 2 and 3 the distribution of mid-span moments was sought as well, and in models 4 and 5 interest extended further to the distribution along the face of the western spandrel (side B).

It was considered impossible to measure the steel strains due to dead load. In fact, the strains were taken as zero at the commencement of the vertical load test, when the dead load and the load distribution beams were already in place. In the early stages of the test the strains all varied linearly with load, so it was a fairly simple matter to estimate for each gauge, by extrapolation, the strain corresponding to the loads already existing at the start of the test. By adding this estimated strain to the measured strain, the strain corresponding to total load was obtained. It was now necessary to compute, from these strains, the slab bending moment at each load level.

Previous investigators at the University of Illinois (1961) successfully used a bi-linear moment-strain relationship to convert the steel strains to bending moments (B.M per metre width in the case of the slab). This approach was adopted here.

The moment-strain relationship is represented by two straight lines OA and AB as shown in Fig. 5.10. The co-ordinates of A are the cracking moment M_c and the steel strain ε_c at the same load

level. The co-ordinates of B are the yield moment M_y and the steel yield strain ε_y.

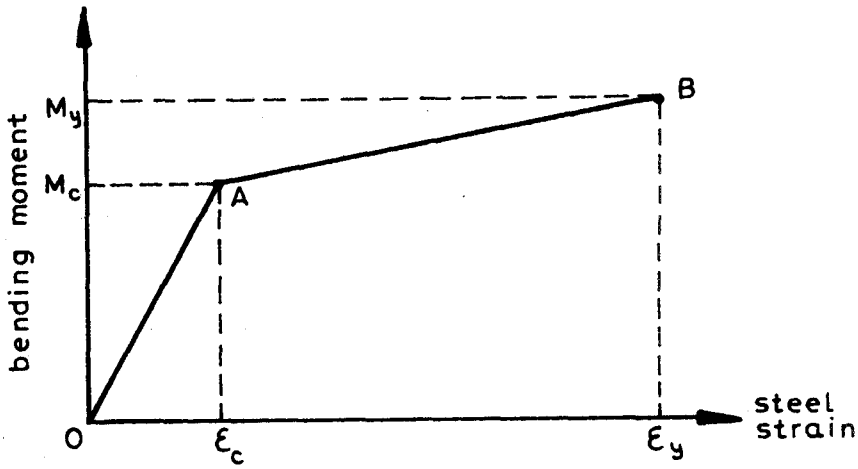

Fig. 5.10 Moment - strain relationship.

The cracking moment was calculated from the expression

$$M_c = 0.62 \sqrt{F'_c}\, I_{gt}/y_t \qquad (5.1)$$

In the case of slab moments, I_{gt} is the moment of inertia of the transformed, uncracked section of one metre width, y_t is the distance of the extreme tensile fibre from the neutral axis, F'_c is the compressive strength of the concrete at the time of the test, and M_c is the moment per metre width of slab. In the case of model 1, I_{gt} for the floor beam was calculated as for a T-beam having an outstanding flange width on each side of the stem equal to the projection of the beam below the flange.

The concrete cracking strain at the extreme fibre was assumed to be 0.00015, following the value used at the University of Illinois. The strain at the steel level, ε_c, was then obtained on the basis of a linear strain distribution across the section. Values of ε_c varied between 0.00010 and 0.00012.

In this investigation the stress-strain relations of the steel bars were non-linear. The yield strains, ε_y, were therefore taken to be the strains corresponding to the 0.2% proof stress. These were obtained from the actual stress-strain curves and the values varied from 0.0023 to 0.0027 for the different bar sizes.

The yield moment, M_y, was evaluated by means of the usual flexure theory for cracked reinforced concrete sections.

In most cases strains were measured, and hence bending moments determined, at various distances along a given E-W line. These values exhibited slight inconsistencies due to the proximity or otherwise of cracks. To compensate for this, the moments at various distances along a given line were assembled and a smooth curve of best fit was determined. The values from this curve were finally used as representing the measured bending moments. Moreover, the slopes of this curve at the ends provided a value for the slab shear adjacent to the spandrels.

5.8 TYPES OF TESTS CARRIED OUT

The main tests comprised the stiffness tests and the vertical load test.

The object of the stiffness tests was to determine the relationship between a couple, applied at the junction of column A and the slab, and the corresponding joint rotation. Such tests were carried out both before and after cracking. The difference would provide a measure of the drop in stiffness of the structure occasioned by cracking.

The application of the couple to joint A was straight-forward by virtue of the type of support at the base of column A. As described in section 4.4, this support consisted of five rocker arms (or load cells) - one vertical and four in the horizontal plane. These last will be referred to as North, East, South and West. The north and south rockers mainly supplied stability since by symmetry there was practically zero force in the north-south direction. In order to apply a couple, the west rocker was entirely loosened. A force in the east rocker would then induce a couple at the top of column A. The force in the rocker was successively increased by tightening the screw against which the outer end of the rocker was supported. Rotation of joint A was measured by means of the dial gauges described in section 4.7.

In the earlier models the stiffness tests were carried out with the five joints at the other columns only partially restrained. The values of the stiffness obtained did not therefore comply with the moment distribution concept of 'far end completely fixed', and the values could not be directly compared with any values which

might be used in an elastic stiffness analysis. They did, however, give an indication of reduction in stiffness due to cracking.

In models 4 and 5, column B was supported in the same manner as column A. In these models it was possible to obtain values which approximated closely to the 'far end fixed' condition. The method of achieving this will be described in section 6.4 which deals with the details of the tests on model 4.

The object of the vertical load test was generally to determine the distribution of moments in the slab under vertical load, and in particular to investigate bending moments, twisting moments and shears in the vicinity of edge column A. The method of applying a load which approximated to UDL was described in section 4.5. Bending moments were measured by means of the strain gauges attached to the reinforcement (section 4.6). Shears were obtained from the rate of variation of the bending moments. The twisting moments in the spandrel beam or spandrel strip were obtained from the unit bending moments and shears in the slab at the face of the spandrel. The method of calculation of these quantities will be described in Chapter 6.

In some models, tests were carried out to determine, approximately, the magnitude of the errors introduced by virtue of the fact that the model did not comprise the complete building. In effect this test would determine how realistic was the boundary condition adopted.

Steel cantilevers were bolted to a boundary remote from column A, i.e. an 'artificial' boundary. The ends of these cantilevers were then loaded by dead load, so that a moment and a shear were applied at the edge of the model. The load was calculated so that the moment and shear corresponded approximately to that which would occur due to live load on the adjacent panel which in fact was not included in the model. The assembly is shown in Fig. 5.11.

Strain gauge readings were taken before and after the application of the edge load so that the effect of the edge load on the region around column A could be estimated.

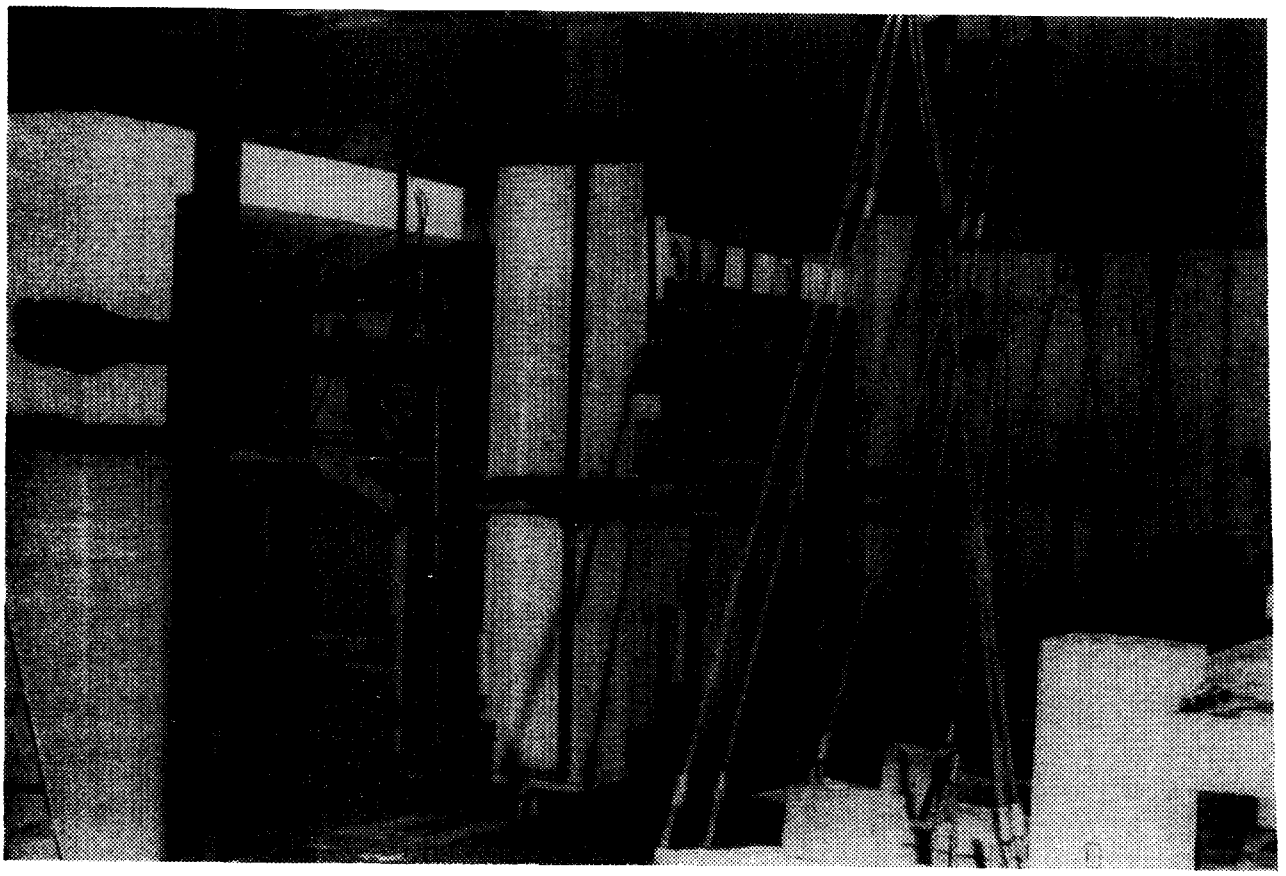

Fig. 5·11 Assembly used for Boundary Condition Tests

Chapter 6

THE TESTS - MODEL BY MODEL

6.0 GENERAL

We come now to the tests themselves. The general appearance and size of the models is shown in Fig. 6.1

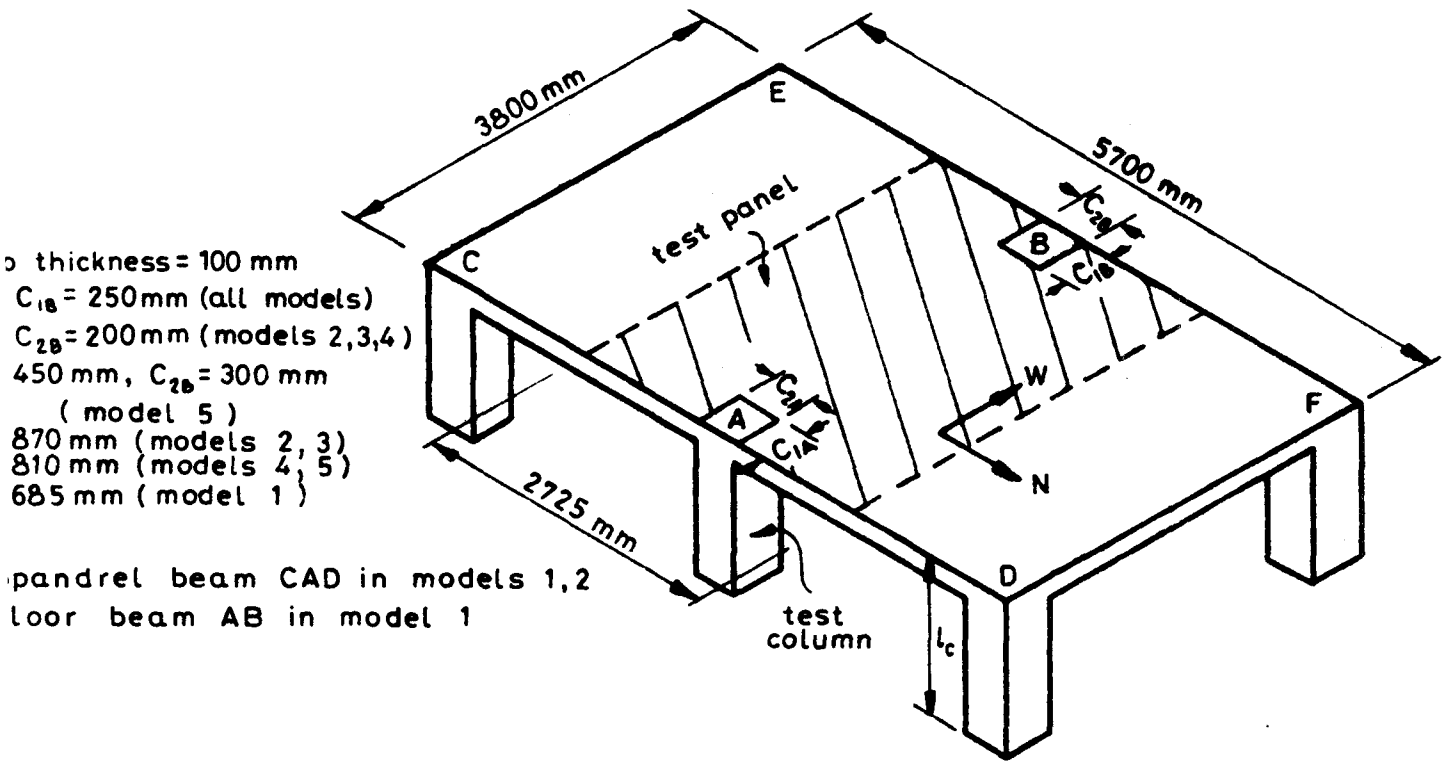

Fig. 6.1 Test Specimens.

The dimensions of beams and reinforcement details will be given for each model separately.

In some models, welded mesh reinforcement was used and this will be designated by the standard reference code in use at the time of the research. The significance of the code numbers is given in Table 6.1.

Details of design calculations for all models are given in Appendix A.

All the raw data collected in the laboratory are given in Appendix B. Test results are given in the present chapter, but these are mainly in the form of graphs obtained from the data in Appendix B.

Table 6.1 - Australian Standard Mesh Sizes

Code No.	Bar and Mesh Size (mm)		
	Dia. of Hard-Drawn Wire (mm)	Longitudinal Spacing (mm)	Transverse Spacing (mm)
F818	8	100	200
F828	8	200	250
F62	6.3	200	200

The testing of model 1 will be described in Section 6.1, that of model 2 in Section 6.2, and so on. Figures or tables which refer to model 4 (for example) will be numbered 6.4.1, 6.4.2 etc.

For ease of reference, a system of Figure numbering has been adopted so that as far as possible corresponding graphs for the various models have similar numbers. Where a Figure is not relevant in a particular model that number is omitted. For model number x, the figures 6.x.1-6.x.3 are concerned with details of the construction and testing of the model. Figures 6.x.4-6.x.9 give details of cracking during the vertical load test. Figures 6.x.10-6.x.29 give summaries of the data which are given in full in Appendix B. These figures refer to the following information:

6.x.1 Reinforcement Details and Beam Sizes
6.x.2 Picture of Laser Beam (Model 1 only)
6.x.3 Picture of Boundary Condition Test
6.x.4) Photographs of Cracks
6.x.5)
6.x.6)
6.x.7)
6.x.8 Diagram of Crack Pattern on Top of Slab
6.x.9 Diagram of Crack Pattern on Bottom of Slab
6.x.10 Vertical Reaction R_A and Shear V_A
6.x.11 Total Exterior Moment M_A
6.x.12 Unit Slab Moment at Various Values of y
6.x.13 Unit Slab Shear at Various Values of y
6.x.14 Unit Mid-span Moment at Various Values of y
6.x.15 Transverse Distribution of M_A

6.x.16 Transverse Distribution of V_A
6.x.17 Transverse Distribution of Mid-span Moment M_M
6.x.18 Variation of Torque along the Eastern Spandrel
6.x.19 Angle of Twist along Eastern Spandrel
6.x.20 Angle of Twist along Eastern Spandrel
6.x.21 Slab Deflections
6.x.22 Data Related to Stiffness Tests
6.x.23 Vertical Reaction R_B and Shear V_B
6.x.24 Total End Moment M_B
6.x.25 Unit Slab Moment along Western Spandrel
6.x.26 Unit Slab Shear along Western Spandrel
6.x.27 Transverse Distribution of M_B
6.x.28 Transverse Distribution of V_B
6.x.29 Variation of Torque along the Western Spandrel

For the purpose of defining the location of points within the models, a system of co-ordinate axes was adopted. The origin of co-ordinates was taken at the centre of the interior face of column A and at the level of the bottom of the floor slab. The x axis was taken in a westerly direction, i.e. towards column B; the y axis in a northerly direction, i.e. along the inner face of the spandrel beam or spandrel strip; the z axis vertically upward.

6.1 MODEL 1

Design

Although the investigation was concerned primarily with flat plates, it was decided to test also some models which contained beams in order to compare the behaviour of floors with and without beams. A floor with beams was tested first.

Model 1 comprised a floor slab of thickness 100 mm with a spandrel beam 250 mm wide and 300 mm overall depth. A floor beam 200 mm wide and 300 mm overall depth ran from column A to column B. These elements were intended to be half-scale representations of a real building. Column A was 200 mm x 250 mm.

In the real structure columns C and D (see Fig. 6.1) would be the same as column A and beams CE and DF would be the same as beam AB. However, in the model the whole of the perimeter except in the vicinity of column A was modified in order to provide satisfactory

boundary conditions. For example, boundary CE was made stiffer in order to simulate partially the effect of the next panel of the building. This called for a stiffening of both the columns and the edge beam. Other than these boundary modifications, the model was designed in accordance with SAA Code AS1480 (1974). Details of the design are given in Appendix A.

Columns were included in the model extending downwards to an assumed contraflexure point. According to AS1480 the design was carried out assuming that the far end of column was fixed. This would correspond to a contraflexure point 2/3 of the column height below the floor. Since the columns above were omitted it was necessary to double the stiffness of the columns which were included. This was achieved by retaining the correct I but halving the length of the columns.

Reinforcement

Details of the reinforcement which resulted from the design are shown diagrammatically in Fig. 6.1.1.

Strain Gauges

Strain gauges were attached to the top slab steel near its entry into the spandrel beam. These gauges were intended to measure the distribution of slab bending moments along the spandrel beam. Gauges were also used in the floor beam on the top steel near end A and on the bottom steel near mid-span. Further strain gauges were attached to the longitudinal steel in the spandrel beam. It was felt that the values of these strains might prove useful although their interpretation would be obscured by the fact that the spandrel beam carried bending, torsion and shear simultaneously.

The exact locations of all the strain gauges in the model are given in Section B.1.1 of Appendix B.

Laser

The idea of using a laser beam, mounted vertically, to measure angles of slope and twist was described in Section 4.7.1. The method was used in this model only. Graph paper was mounted in a

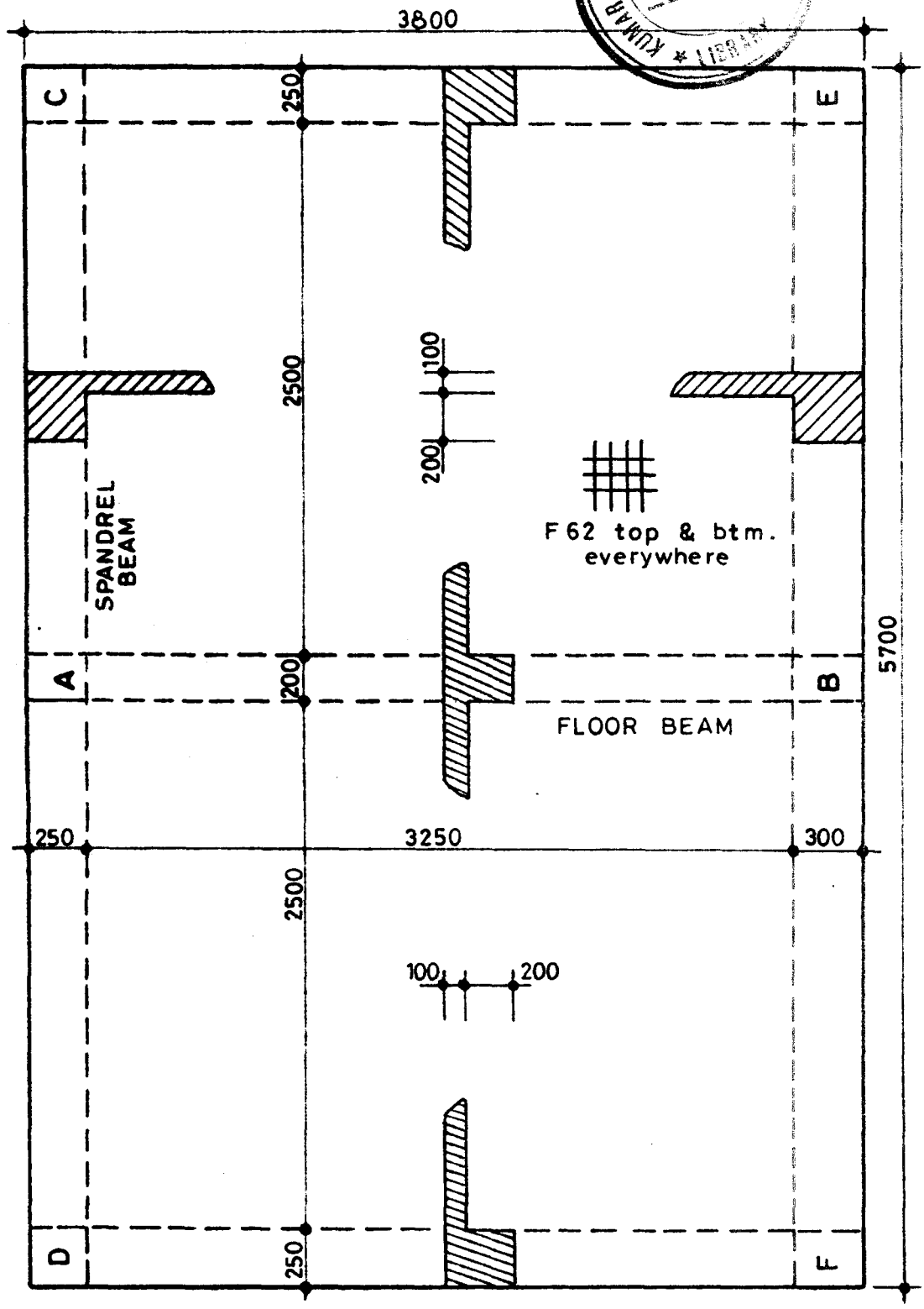

Fig. 6.1.1(a) Reinforcement Details for Model 1.

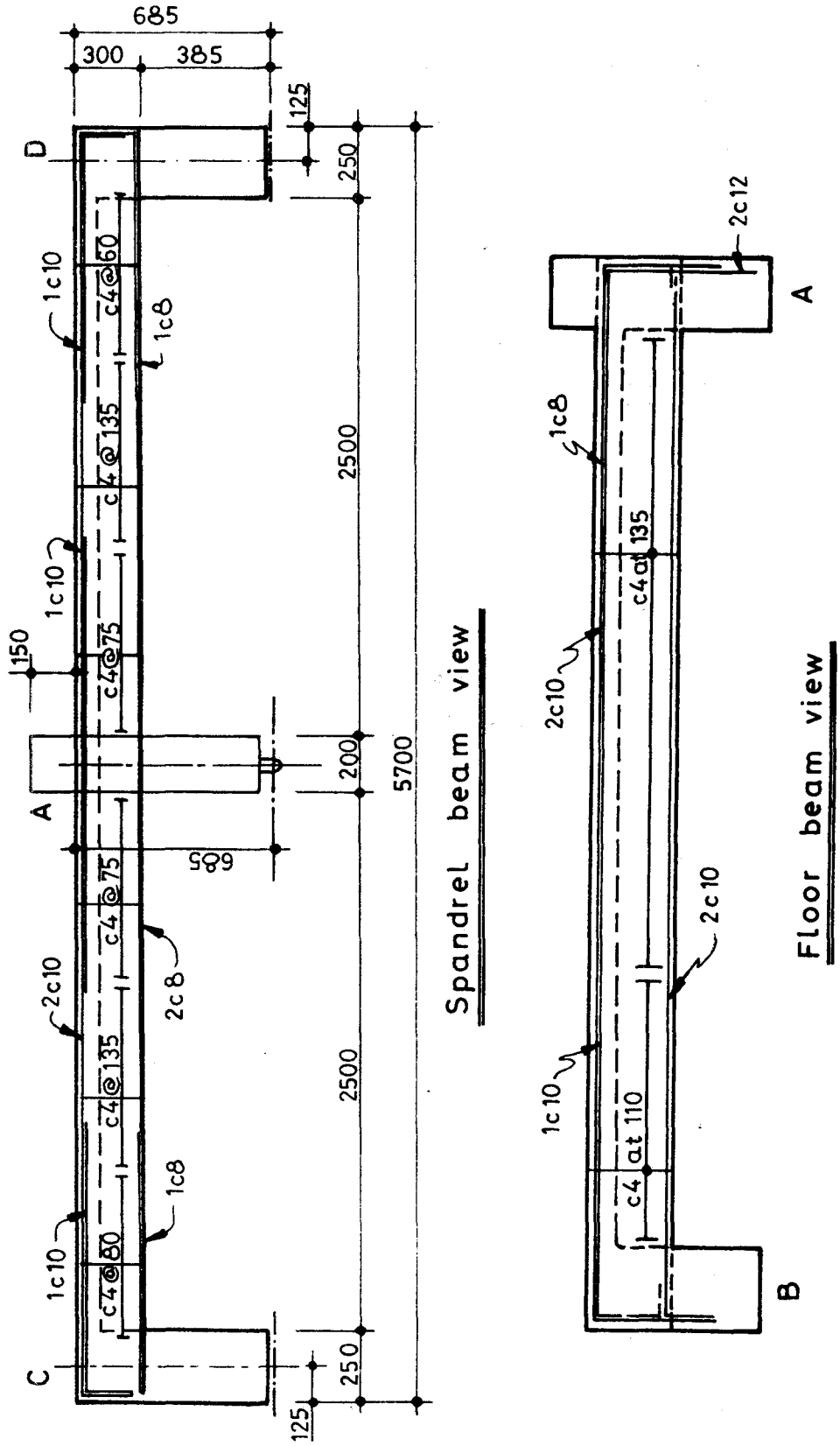

Fig 6.1.1(b) Reinforcement Details for Model 1.

horizontal plane at 2100 mm above the centreline of the beams. The paper was attached to a wooden frame which in turn was attached to the main reaction frame. The setup is shown in Fig. 6.1.2.

Dial Gauges

As described in Section 4.7.2, slopes and twists of the spandrel were also measured by dial gauges resting against angles attached vertically to the spandrel. The positions of all these spandrel gauges are given in Section B.1.2 of Appendix B.

Two dial gauges were also mounted below the model, one in the centre of each panel, in order to measure deflections (see Section B.1.3).

Concrete

At the time of the vertical load test, the concrete compressive strength was 43 MPa (cylinder strength).

Boundary Condition Test

As mentioned previously, the effectiveness of the boundary condition adopted depended on the influence which loads on other panels (not included in the model) would have on the stress conditions in the test area around column A. An attempt was made to measure this influence by applying moments and shears to the boundary of the model.

Steel cantilever beams were attached to the model boundary (see Fig. 6.1.3). By applying vertical loads to the ends of these cantilevers a moment and a shear would be applied to the model boundary. Although these forces would be concentrated instead of distributed along the boundary, as in the real structure, it was considered that the test would supply a general indication of the quantity being measured.

In the first instance, the cantilevers were attached to the northern face of the model. A dead load of 250 kg was applied to the end of each cantilever by suspending therefrom a bin containing gravel. The lever arm of the load could not be determined exactly since this depended upon the position of the resultant of the distributed reactive force near the edge of the model. Approximately

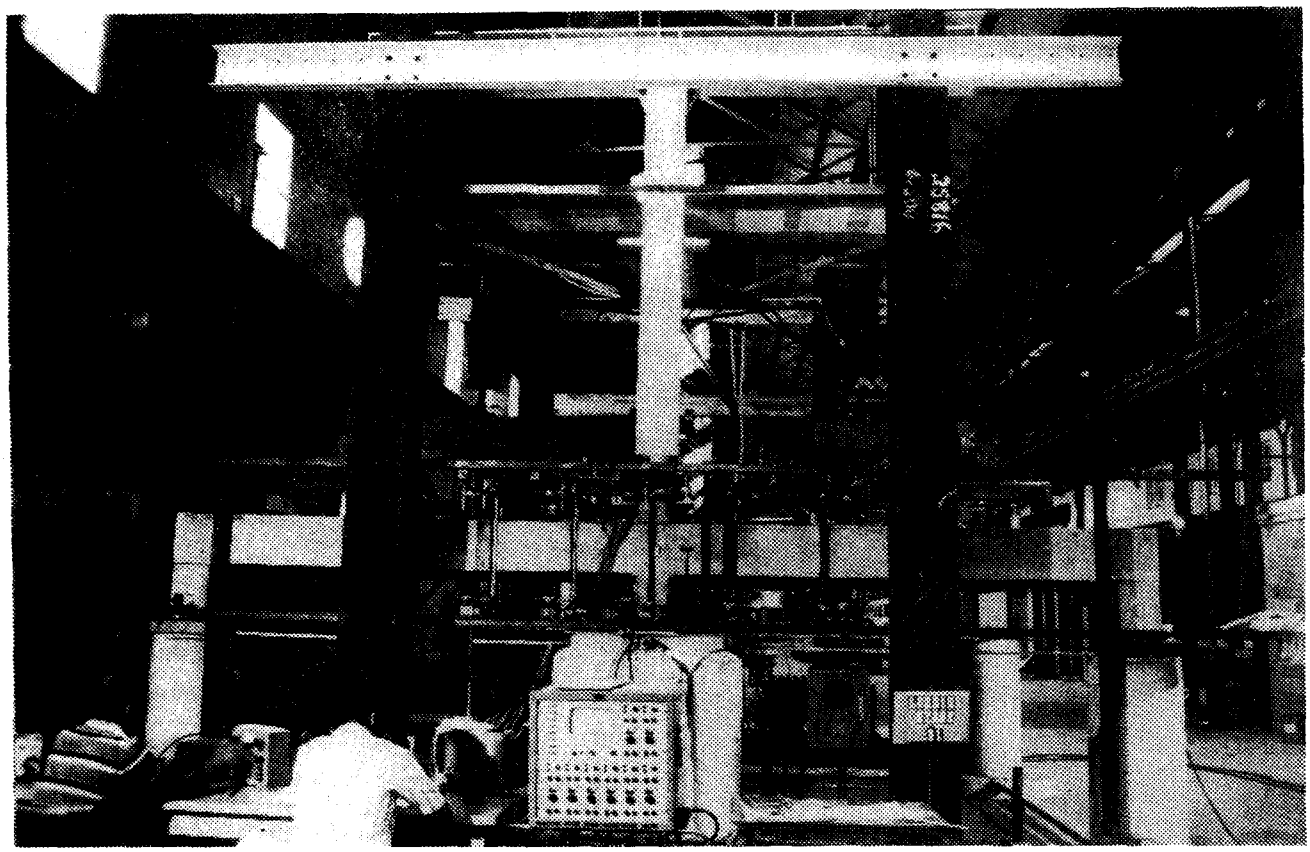

Fig. 6.1.2 Laser in Place on the Model

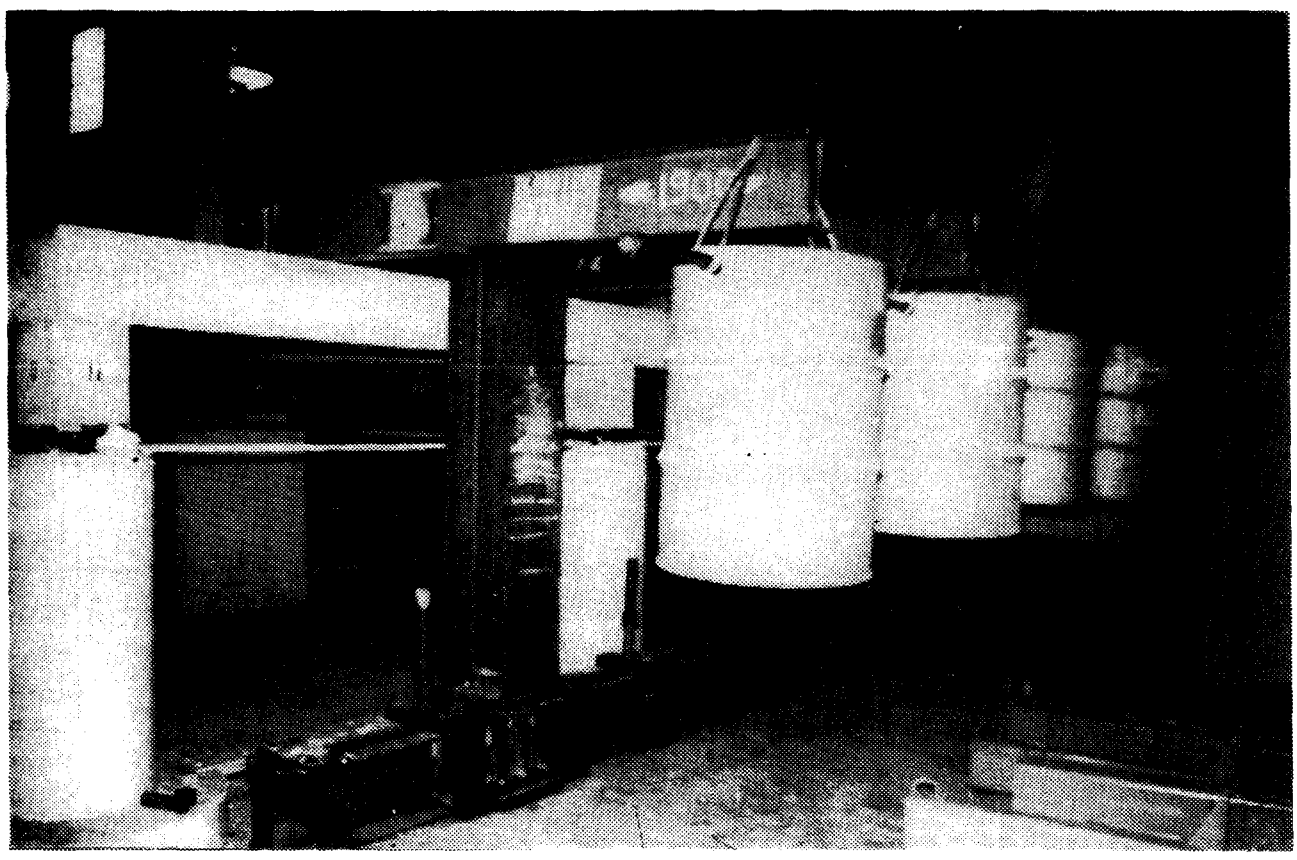

Fig. 6.1.3 Boundary Condition Test

the lever arm was 2 m, and this provided a moment of 2 x 2.5 or 5 kNm per cantilever, a total of 20 kNm for the panel. This represented approximately the edge moment which would occur if the adjacent panel in the real structure were loaded to the design ultimate load level.

Since the strain gauges registered close to zero change when this edge loading was applied, no record was made of the readings.

The cantilevers were then applied to the western edge of the model (Fig. 6.1.3) and again the influence in the test area was practically zero.

Hence for this model, the boundary conditions appeared to be satisfactory. However, the model was considerably stiffer than later models which had no beams. Hence it was decided that the test would be applied again in some of the later models.

Vertical Load Test

The presence of the beams rendered this model extremely stiff. Deformations during the test were extremely small. The slopes and twists along the spandrel beam were measured just as well by the dial gauges as by the laser. Since the dial gauges were much quicker and more convenient to reach, it was decided not to use the laser in future models.

The first cracks appeared at mid-span in the N-S direction at a load of 12.5 kN/m^2 (the service load was 7.0 kN/m^2 and the design ultimate load was 11.4 kN/m^2). At a load of 25 kN/m^2 (2.2 x the design ultimate) the capacity of the testing device was reached. It was clear that the model was still some way from failure.

At the maximum load reached, the mid-span moment in the floor beam was close to its yield value although yield had not occurred in the steel (see Fig. 6.1.14). The end moments were still well below the yield capacity.

The presence of the beams rendered the model extremely stiff as well as extremely strong.

Load cell readings taken during this test are given in Section B.1.5. The vertical load cell directly measures the vertical reaction at A, R_A. A graph of this quantity is given in Fig. 6.1.10.

The total shear along the face of the spandrel beam between the centrelines of the panels to the north and south of A is given by R_A minus the weight of the spandrel beam and column A. This total shear might be denoted by V_A. Thus

$$V_A = R_A - 5.4 \text{ kN}$$

The quantity V_A is also plotted on Fig. 6.1.10.

The total (negative) moment along the face of the spandrel beam (which is denoted by M_A) may also be obtained from the load cell readings. If E and W are the forces in east and west load cells respectively, then

$$M_A = (E-W)\ 0.635 - R_A \times 0.125 .$$

Here, 0.635 is the vertical distance from the load cells E and W to the centre of the slab, and 0.125 is half the width of the spandrel beam. Values of M_A are given in Fig. 6.1.11.

Strain gauge readings taken during the test are given in Section B.1.6. The main purpose of these readings was to permit the calculation of bending moments. The method of computing bending moments from the measured strains has been described in Section 5.7.

From the strain gauges on the top steel at the end of the floor beam AB it was possible to calculate the negative end moment in the beam adjacent to the face of column A. Actually there were strain gauges at four distances x from the column face. The moment was calculated at each of these beam sections and from these values an equation for the bending moment diagram was derived. Hence the bending moment right at the column face was calculated and these values are given in Fig. 6.1.11. From the equation, the derivative was obtained and this gave values of the shear forces at the end of the beam. These values are shown in Fig. 6.1.13.

From the strain gauges at mid-span, the positive mid-span moment in the floor beam was calculated and the values plotted in Fig. 6.1.14.

By means of the strain gauges attached to the top slab steel entering the spandrel beam it was possible to calculate the negative

slab moment at various locations along the spandrel, i.e. at various distances y from column A. Hence for any given load level the distribution of slab moments could be obtained, and these are shown in Fig. 6.1.15. Slab moments are not shown within 300 mm of the centreline of column A since this part of the slab was regarded as part of the floor beam and the total moment within this central region is accounted for as beam moment (see Fig. 6.1.11).

The values given in the graphs of Figs. 6.1.10-6.1.15 are in effect summaries of the data given in Appendix B, Section B.1. It is possible to derive further information from these graphs. Of particular interest is the variation of the twisting moment along the spandrel beam, and especially the torque which occurs at the column face.

The twisting moment in the spandrel beam is induced mainly by the negative slab moments adjacent to the beam, and to a smaller extent by the slab shears (which have a moment about the beam centreline). For any load level, the distribution of the slab moments can be obtained from Fig. 6.1.15. The slab shears can be estimated approximately since the total shear, V_A, is known (Fig. 6.1.10) and the shear in the floor beam (assumed to be concentrated in the stem) is also known (Fig. 6.1.13). The remaining shear will be assumed to be uniform along the beam. This assumption is based on the measurements in later tests.

This procedure was carried out only for one load level. In Fig. 6.1.18 the slab moments, m_s, are first plotted. These are obtained directly from Fig. 6.1.15. The slab shears, v_s, are obtained as follows:

Total Shear, V_A	=	54.0 kN (Fig. 6.1.10)
End Shear in Floor Beam	=	36.2 kN (Fig. 6.1.13)
Shear in Slab	=	17.8 kN
	=	8.9 kN each side
Length from column to panel centreline	=	1.265 metres

If v_s is assumed to be uniform

$$v_s = \frac{8.9}{1.265} = 7.0 \text{ kN/m}$$

$$0.125\ v_s = 0.88 \text{ kNm/m}$$

$$\frac{dT}{dy} = m_s + 0.125\ v_s$$

Hence by integration the curve of T may be obtained. The torque at the panel centreline (y = 1365 mm) is zero by symmetry.

As regards the angle of twist of the spandrel beam, the readings from the dial gauges were found to produce more consistent values than those from the laser. The twists calculated from the dial gauge readings are plotted in Fig. 6.1.19.

The dial gauges below the slab provided values of the vertical deflections. There was so little difference between the deflection at the beam centre (gauge 36) and the deflection at the panel centres (gauges 33 and 39) that a single curve is given in Fig. 6.1.21.

The values in the graphs are further summarized in a Summary Table, 6.1.1. This table is drawn up in such a way that it can be applied to all five models and thus simplify comparison. As explained previously several quantities were measured in later models which were not measured in the earlier models. Consequently, several items in the Summary Table for model 1 are not filled in.

Stiffness Test

The stiffness test consisted of the application of a moment to joint A (the junction of the slab and column A) and the measurement of the corresponding joint rotation. The method of applying the moment was described in Section 5.8.

The applied moment was increased up to 32 kNm and then released, readings being taken during increasing and decreasing moments. Readings of dial gauges right along the spandrel were taken so that not only could the rotation of joint A be determined but also the distribution of twist along the spandrel. These latter values proved to be of little interest, so in later models only the rotation of the joint itself was measured.

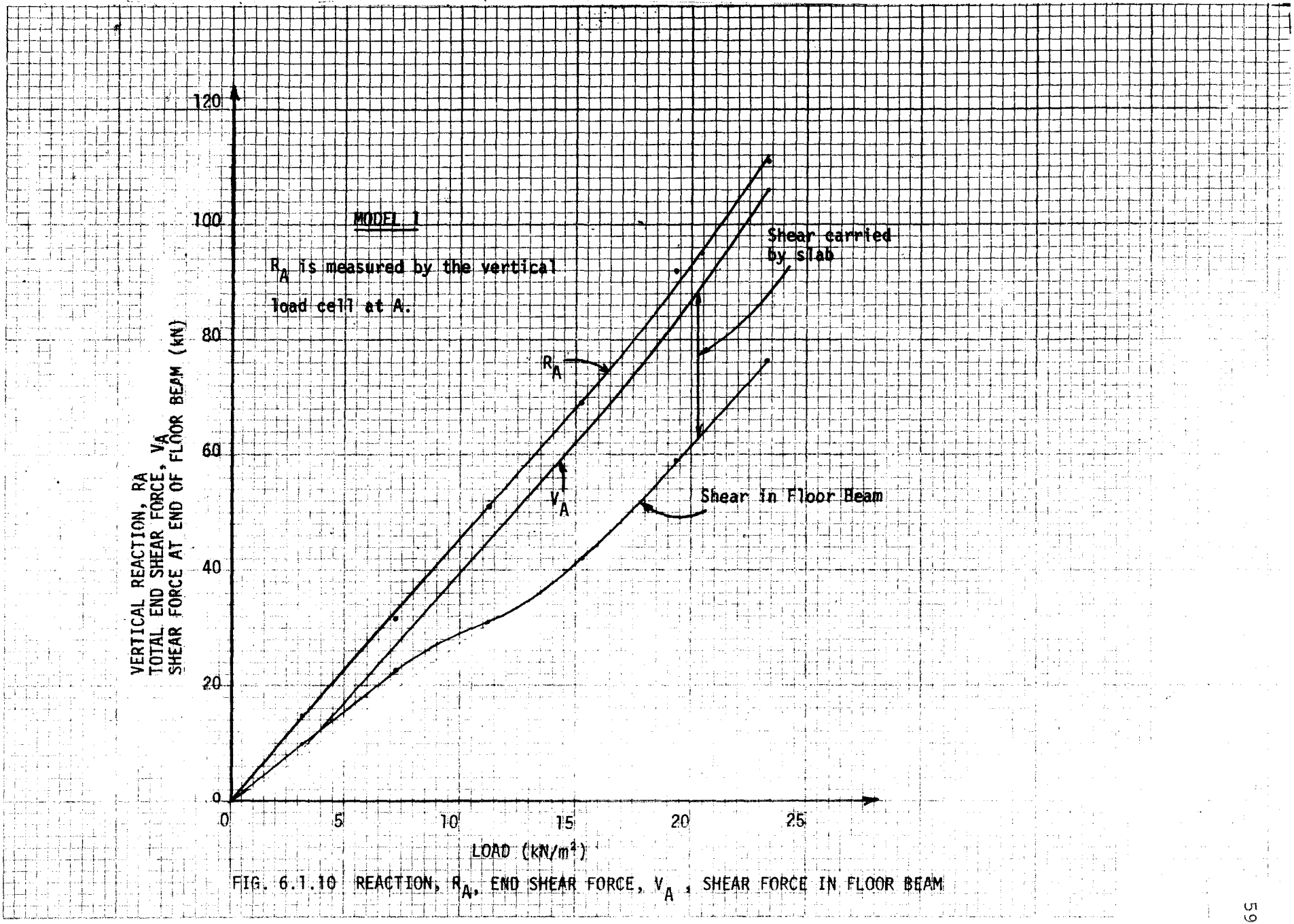

FIG. 6.1.10 REACTION, R_A, END SHEAR FORCE, V_A , SHEAR FORCE IN FLOOR BEAM

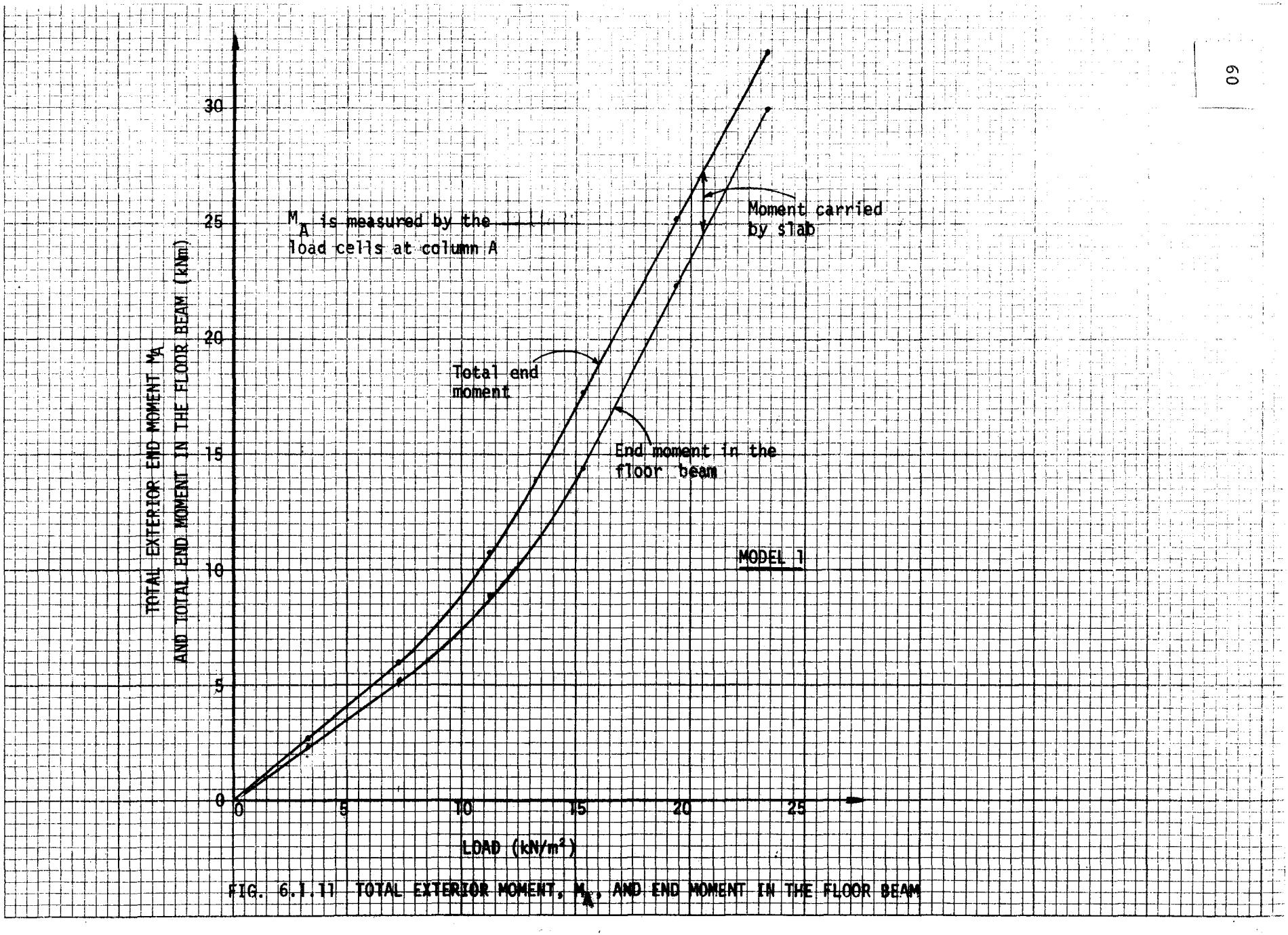

FIG. 6.1.11 TOTAL EXTERIOR MOMENT, M_A, AND END MOMENT IN THE FLOOR BEAM

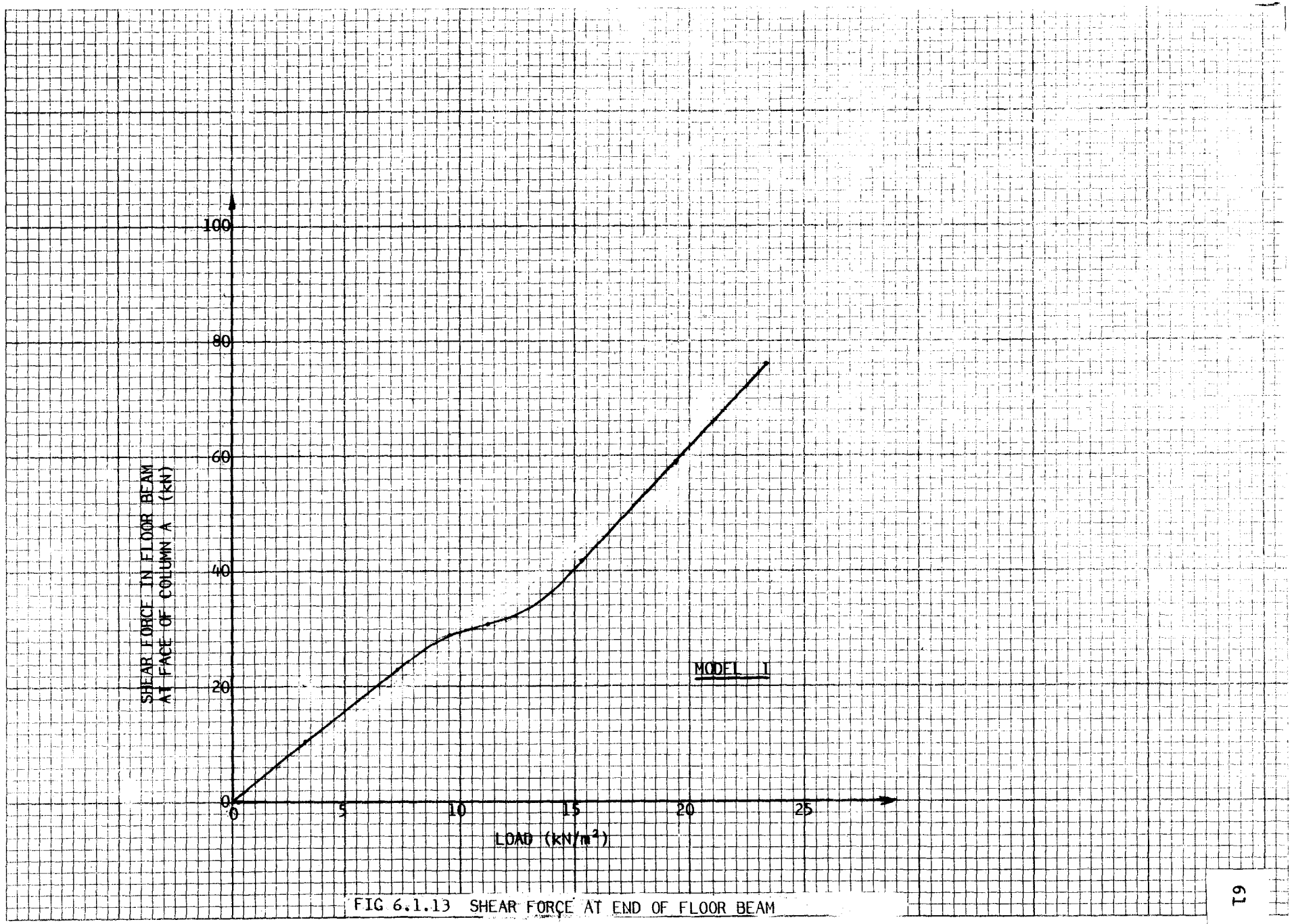

FIG 6.1.13 SHEAR FORCE AT END OF FLOOR BEAM

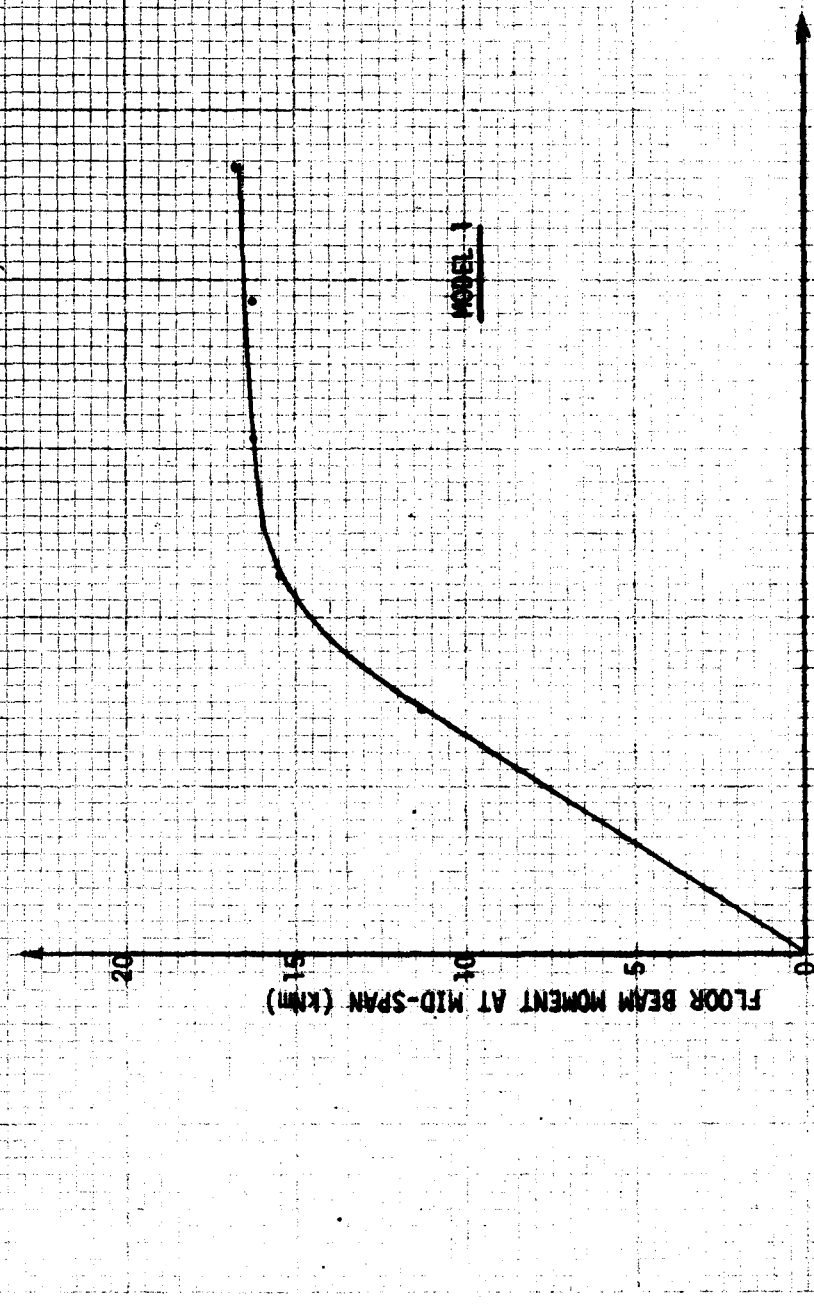

FIG. 6.1.14 MID-SPAN MOMENT IN THE FLOOR BEAM

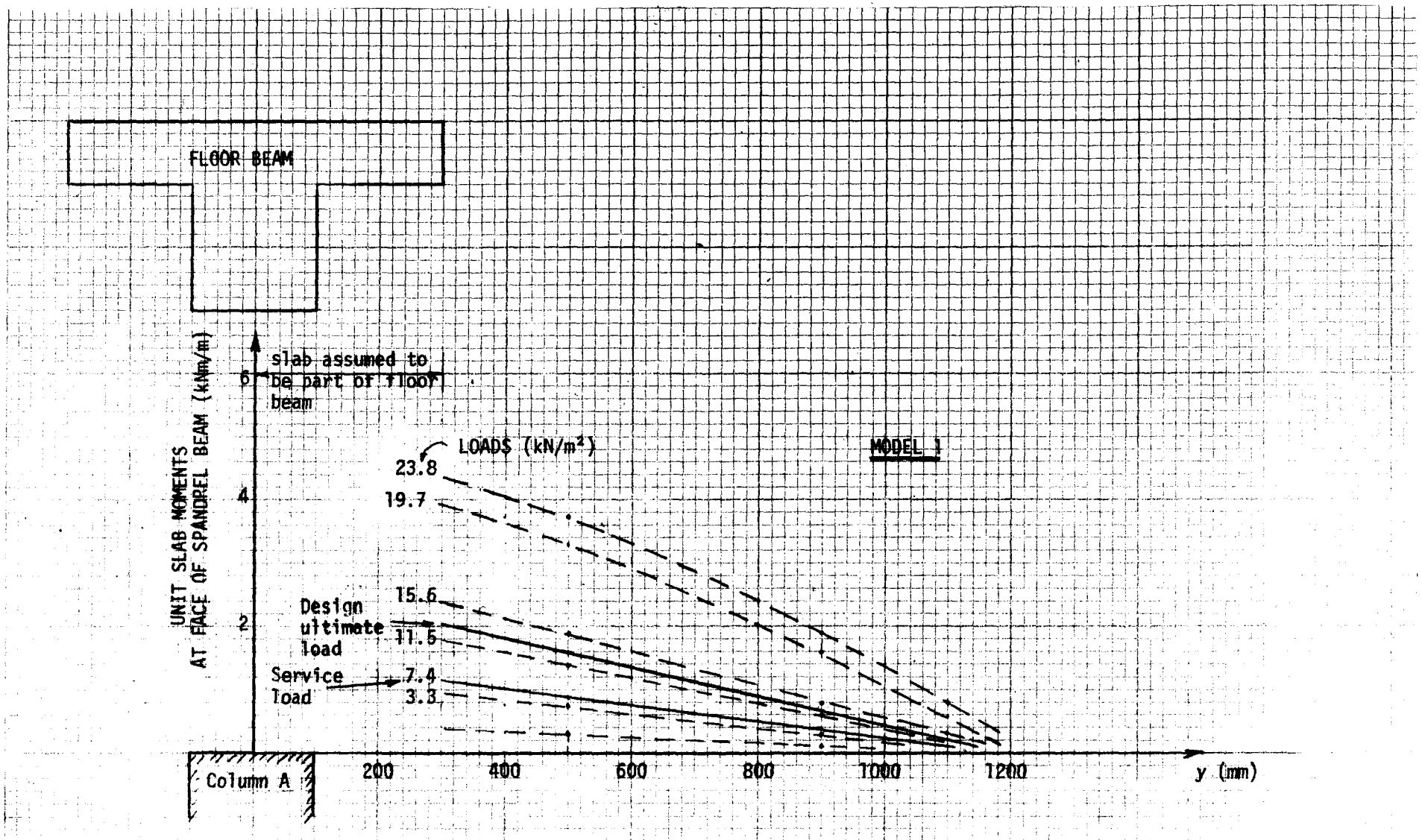

FIG. 6.1.15 TRANSVERSE DISTRIBUTION OF M_A AT VARIOUS LOADS

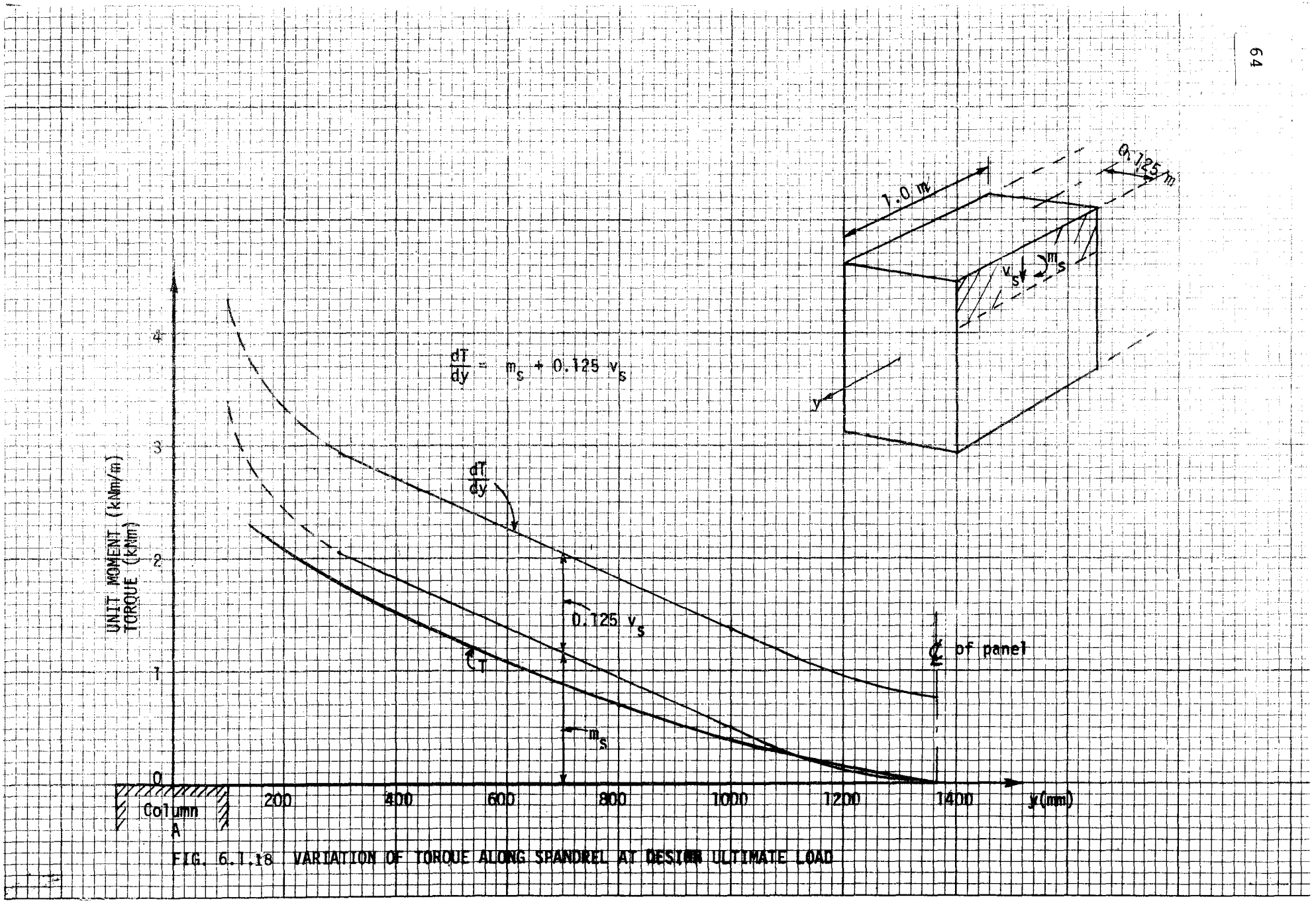

FIG. 6.1.18 VARIATION OF TORQUE ALONG SPANDREL AT DESIGN ULTIMATE LOAD

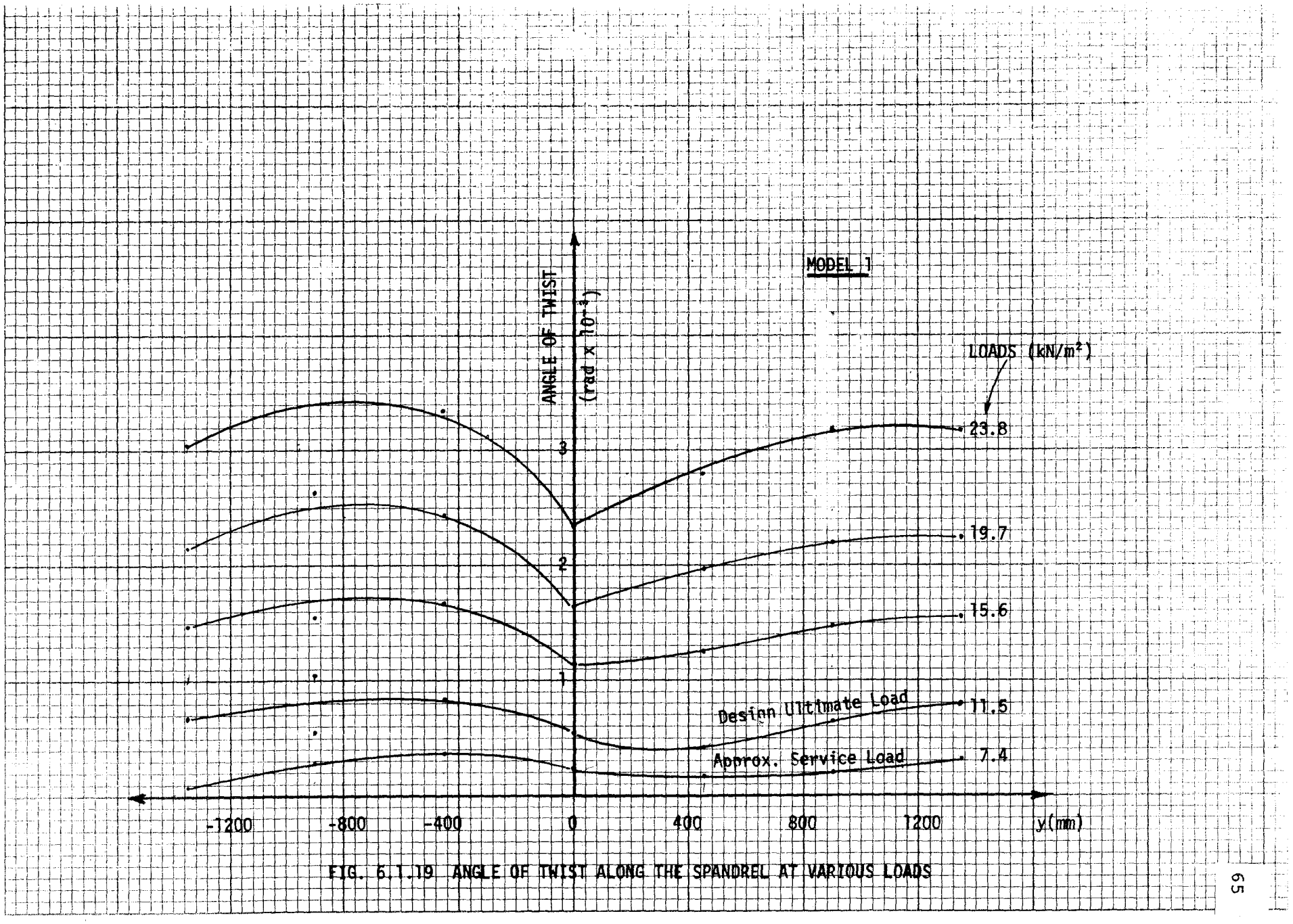

FIG. 6.1.19 ANGLE OF TWIST ALONG THE SPANDREL AT VARIOUS LOADS

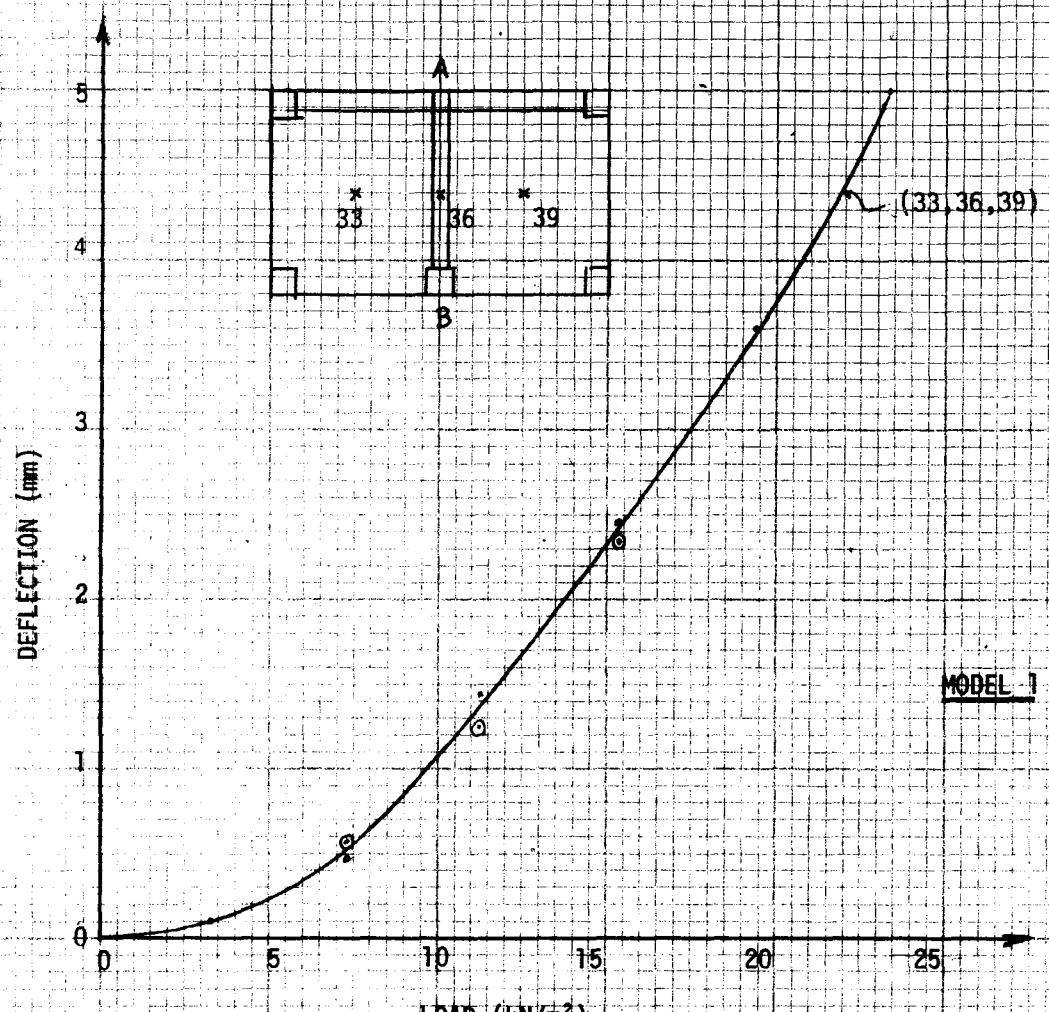

FIG. 6.1.21 SLAB DEFLECTIONS

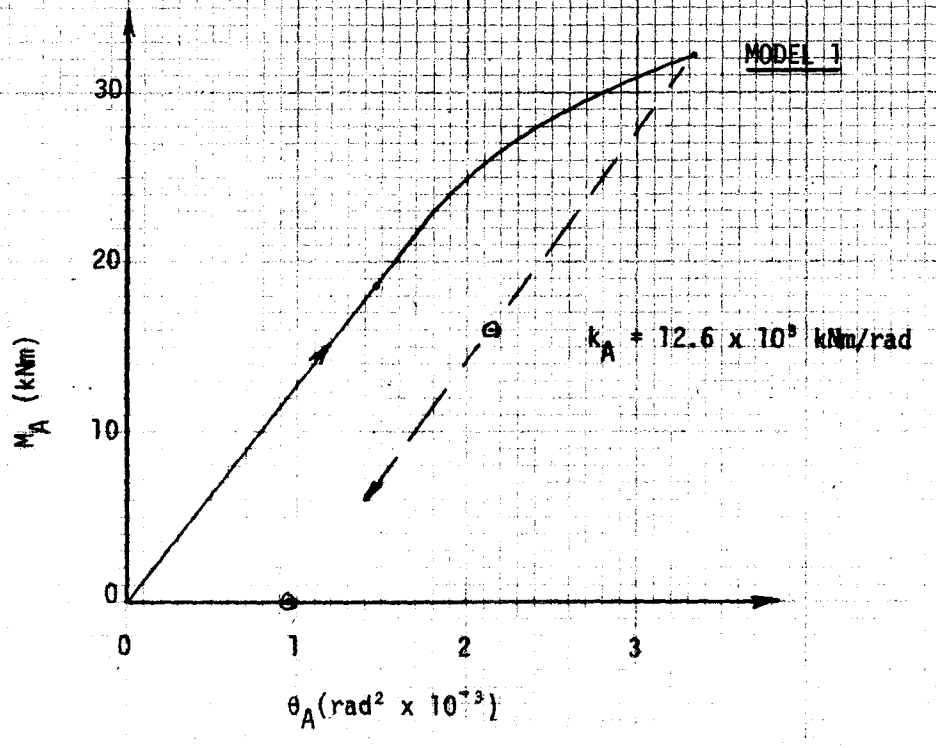

FIG. 6.1.22 ROTATIONAL STIFFNESS OF JOINT A

MODEL No. 1

TABLE 6.1.1 SUMMARY OF RESULTS OF VERTICAL LOAD TEST

Service Load = 7.0 kN/m^2
Design Ultimate Load = 11.4 kN/m^2
Failure Load = -

Item	Load Level	Test Value
1. Vertical Reaction at A = R_A (kN)	service design ult. failure	32 52 -
2. Vertical Reaction at B = R_B (kN)	service design ult. failure	
3. Total Mid-Span Moment = M_M (kNm)	service design ult. failure	
4. Total Moment at face of Spandrel A = M_A (kNm)	service design ult. failure	5.7 10.8 -
5. Total Shear Force at Face of Spandrel A = V_A (kN)	service design ult. failure	26 46 -
6. Total Moment at Face of Spandrel B = M_B (kNm)	service design ult. failure	
7. Total Shear Force at Face of Spandrel B = V_B (kN)	service design ult. failure	
8. Transverse Distribution of Mid-Span Moment M_M	service design ult. failure	
9. Transverse Distribution of M_A	service design ult. failure	See Fig.6.1.15
10. Transverse Distribution of M_B	service design ult. failure	

* Values in brackets are obtained from strain gauge readings by integration. Other values are obtained from load cells.

TABLE 6.1.1 VERTICAL LOAD TEST (cont.)

Item	Load Level	Test Value
11. Distribution of Torque along Spandrel A	design ult.	See Fig.6.1.18
12. Torque in Spandrel A at Face of Column A (kNm)	design ult.	2.3
13. End Moment in Floor Beam at Face of Column A (kNm)	service design ult. failure	5.0 8.9
14. Shear Force in Floor Beam at Face of Column A (kN)	service design ult. failure	19 31 -
15. Shear Force in Spandrel at Face of Column A (kN)	service design ult. failure	5.8 9.8 -
16. Distribution of Torque along Spandrel B	design ult.	
17. Torque in Spandrel B at Face of Column B (kNm)	design ult.	
18. End Moment in Beam Strip at Face of Column B (kNm)	service design ult. failure	
19. Shear Force in Beam Strip at Face of Column B (kN)	service design ult. failure	
20. Shear Force in Spandrel at Face of Column B (kN)	service design ult. failure	
21. Mid-span Moment in Floor Beam (kNm)	service design ult. failure	10.7 15.5

MODEL No. 1

TABLE 6.1.2 SUMMARY OF RESULTS OF STIFFNESS TESTS

	Condition of Model		
	Uncracked	Cracked	Severely Cracked
Stiffness of Joint A = k_A (kNm/radian)	12.6×10^3		
Carry-over factor from A to B = c_{BA}			
Stiffness of Joint B = k_B (kNm/radian)			
Carry-over factor from B to A = c_{AB}			

A graph of the measurements is given in Fig. 6.1.22. The stiffness value obtained from this graph is given in a summary table (Table 6.1.2). As with the summary table for the vertical load test, the stiffness table is designed to accommodate the more extensive results from later models.

During the test, column A became cracked. This revealed a weakness in the design of the model. The stiffness of column A had been doubled by keeping I constant and halving the length. While this certainly would double the stiffness, it would leave the flexural strength the same as in the real structure. However, with the upper column removed and the stiffness of the lower column doubled, the moment in the lower column would be doubled in the vertical load test. Hence, the column *strength* would be inadequate. It was realized that for future models the I should be doubled and the length retained as in the real structure.

Because of the damage to column A, the only stiffness test carried out was that with the slab in an uncracked condition, i.e. before the vertical load test.

6.2 MODEL 2

Design

Model 2 was generally similar to model 1 except that the floor beam AB was omitted. The spandrel beam remained the same as in model 1. This model thus represented a fairly common type of flat plate floor, having no internal beams but having an exterior spandrel beam.

In the real structure, there would be no beams on the three sides CE, EBF and FD. However, as before beams were provided to simulate as nearly as possible the stiffness of the removed adjacent slabs. These beams were 250 mm wide and 165 mm overall depth on the north and south sides, CE and DF. The same size beam should theoretically have been provided on the western side EBF. However, this would clearly result in the region around column B being weaker than that around column A. As it was hoped that the vertical load test of this model might be continued until failure,

the beam EBF along the western side was arbitrarily increased to the same size as CAD in order that failure would occur adjacent to column A.

The steel in the slab and in the spandrel beam CAD was retained exactly as in model 1, hence no design calculations were carried out. The only calculations required were an estimate of the size of the other perimeter beams. These calculations are given in Appendix A. The dimensions of the beams in model 2 are given in Fig. 6.2.1.

For the reasons explained at the end of section 6.1, the length of the columns was increased as compared with model 1. It was decided that it would be more representative of the conditions in an average floor of a building to assume that the contraflexure point of the columns occurs at mid storey height. The pin joints were placed at 820 mm below the centre of the floor slab. In order to double the stiffness of column A it was now necessary to double its I. The column in the real structure was 200 x 250, so the model column was made 200 x 320. However, if the model column projected 320 mm into the slab instead of 250 mm this would modify stress conditions at the floor-column junction. This problem was resolved by making the extra 70 mm of the model column project outside the slab (see Fig. 6.2.1).

Reinforcement

Details of the reinforcement in model 2 are shown in Fig. 6.2.1.

Strain Gauges

The layout of strain gauges was generally similar to that in Model 1. There was, of course, no floor beam in model 2 but a few gauges were placed on the bottom steel at mid-span close to the line AB.

The locations of all strain gauges in this model are given in Section B.2.1 of Appendix B.

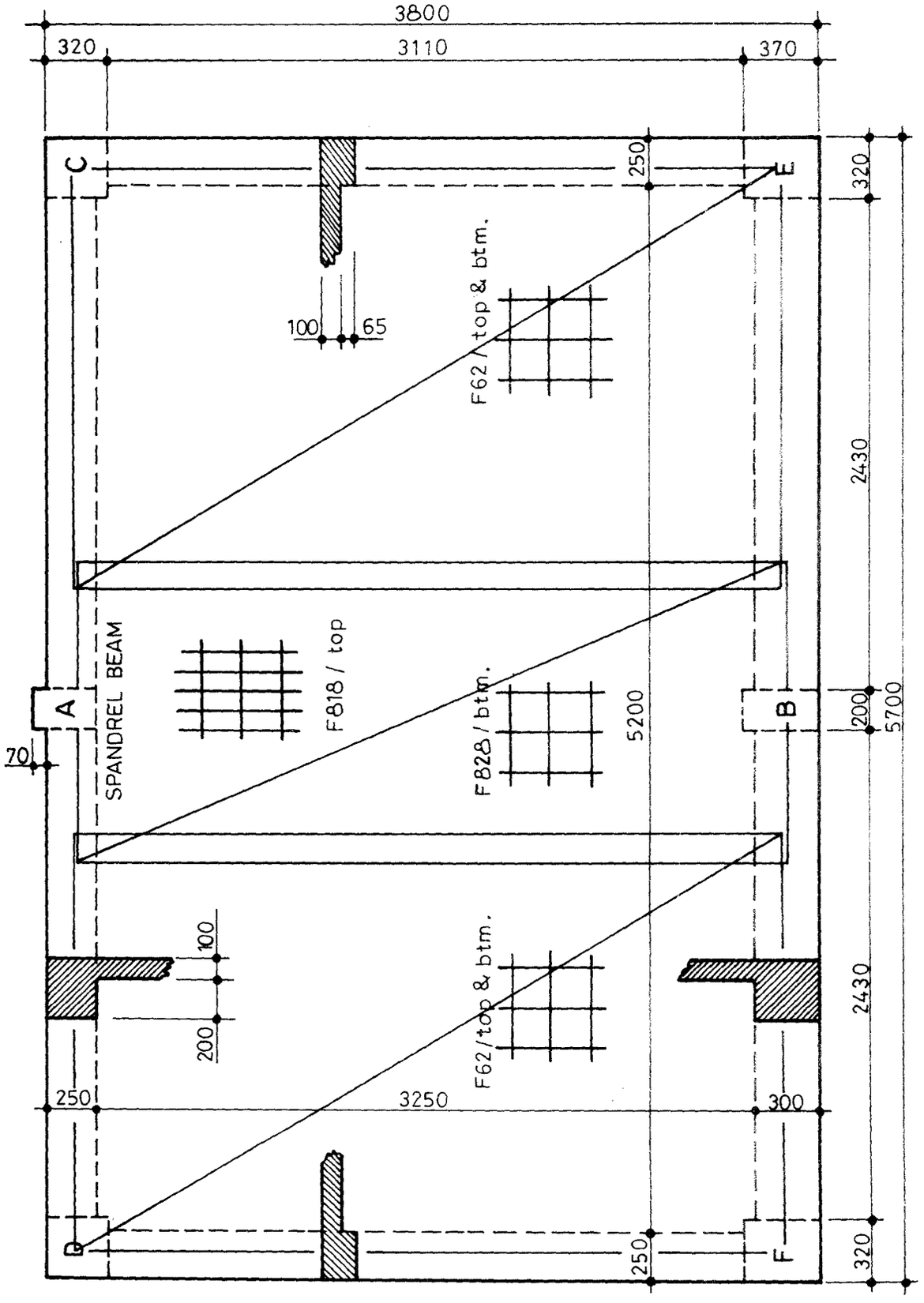

Fig.6.2.1(a) Reinforcement Details for Model 2.

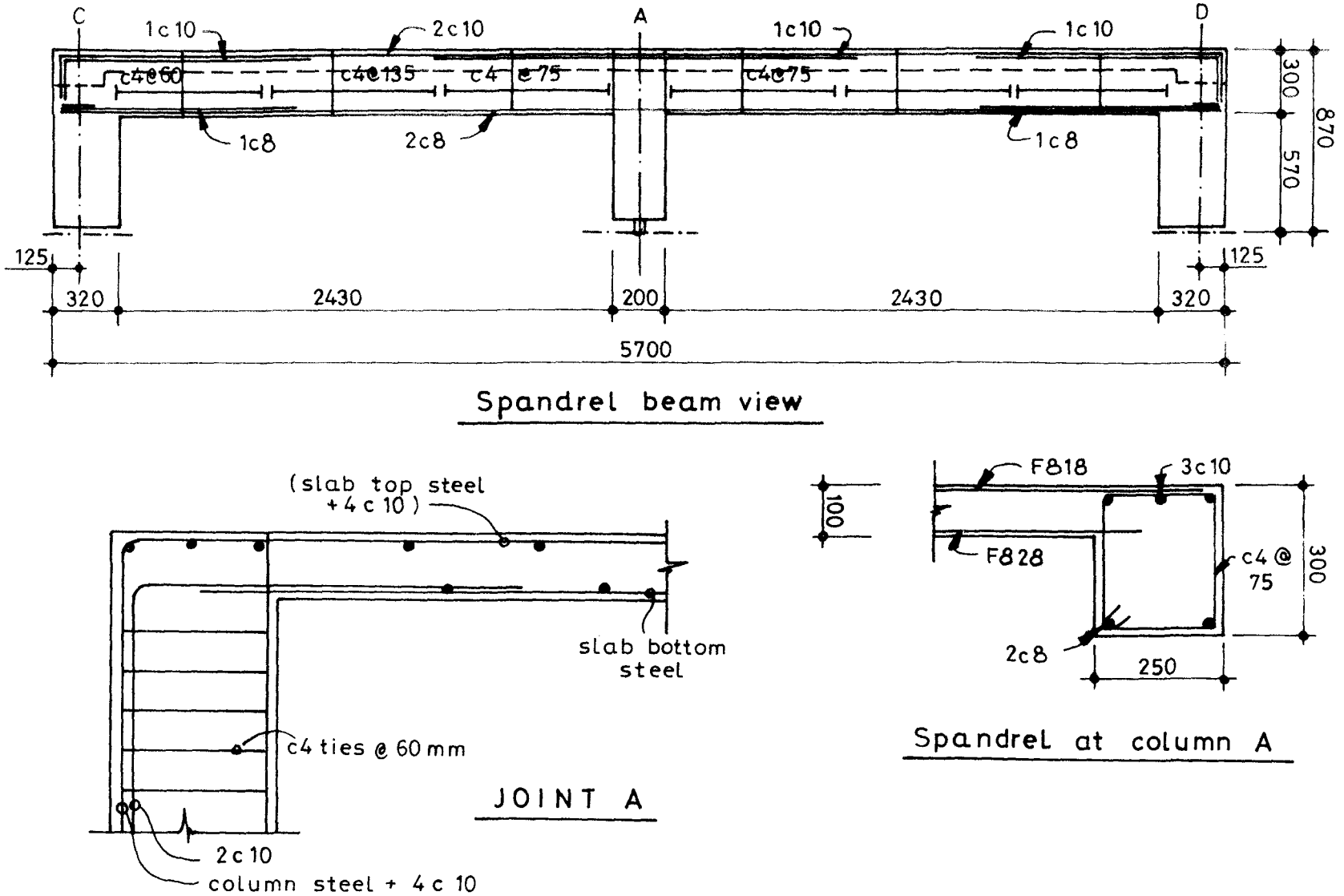

Fig. 6.2.1 (b) Reinforcement Details for Model 2.

Dial Gauges

The dial gauges for measuring angles of twist and slopes along the spandrel beam were mounted in exactly the same way as for model 1. Details of their locations are given in Section B.2.2 of Appendix B.

Three gauges were mounted below the model in this case, one at the centre of each panel and an additional one at the centre of the line AB. This layout is recorded in Section B.2.3.

Concrete

At the time of the vertical load test, the concrete compressive strength was 38 MPa.

Vertical Load Test

The absence of the floor beam in this model resulted in larger deformations, both slab deflections and angular twists in the spandrel beam.

First cracking occurred at the top of the slab at the face of columns A and B at a load of 12 kN/m^2. At 17.2 kN/m^2, cracking occurred on the bottom of the slab midway between A and B and at right-angles to the line AB. These cracks extended as the load increased.

At a load of 25 kN/m^2 the testing frame reached its capacity and the test was discontinued. The mid-span moment had reached its yield capacity but the end regions did not show signs of distress. The model appeared to be some way from collapse.

Figs. 6.2.4 and 6.2.5 are photographs of the cracks. Figs. 6.2.8 and 6.2.9 are diagrams of the cracks in the top and bottom of the slab respectively.

Load cell readings for this test are given in Section B.2.4. A graph of the vertical reaction at A (measured by the vertical load cell) is given in Fig. 6.2.10. The total shear V_A along the face of the spandrel beam is derived as before by subtracting from R_A the weight of the column A and the spandrel beam.

$$V_A = R_A - 5.4 \text{ kN}$$

This quantity is also shown in Fig. 6.2.10.

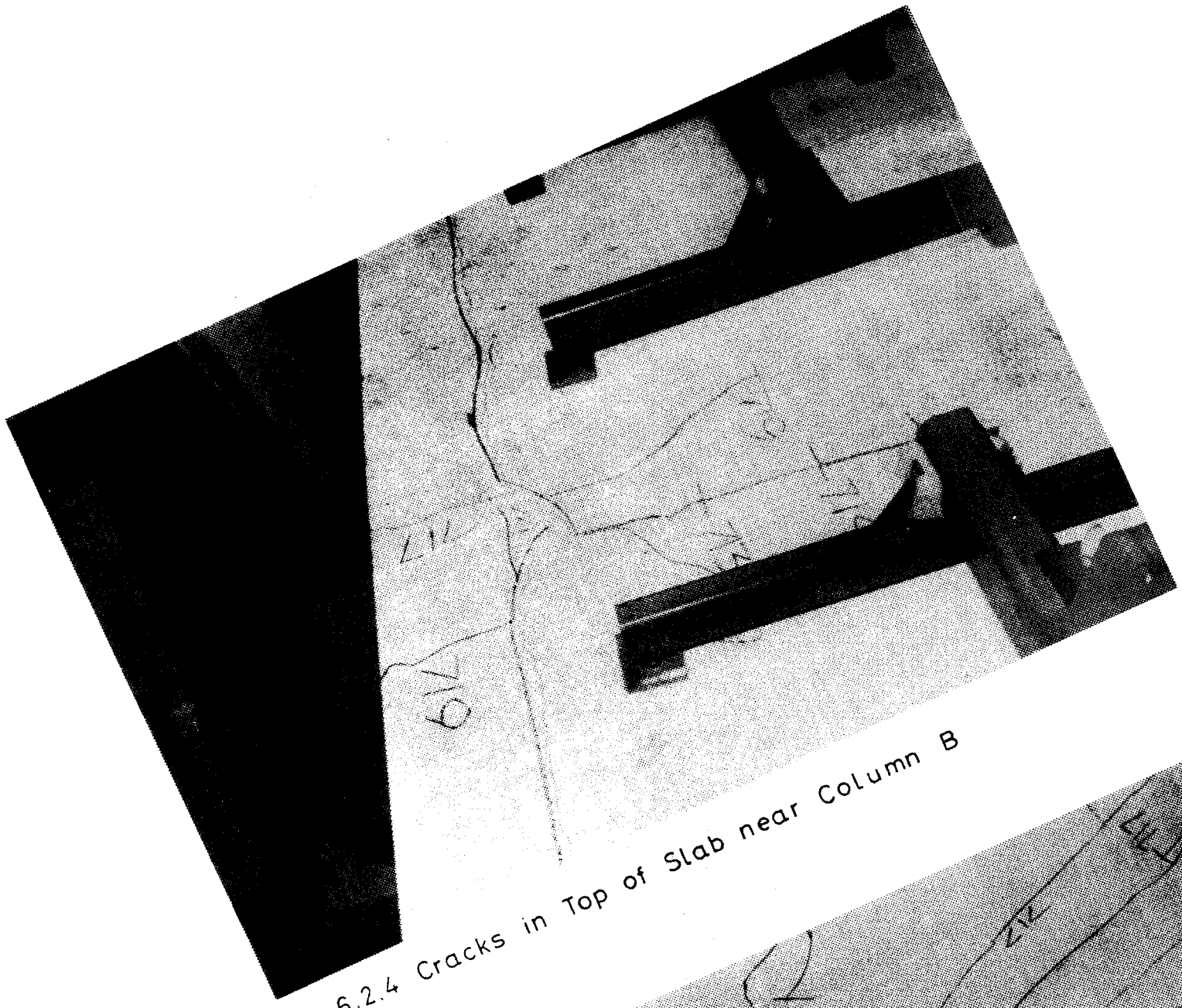

Fig. 6.2.4 Cracks in Top of Slab near Column B

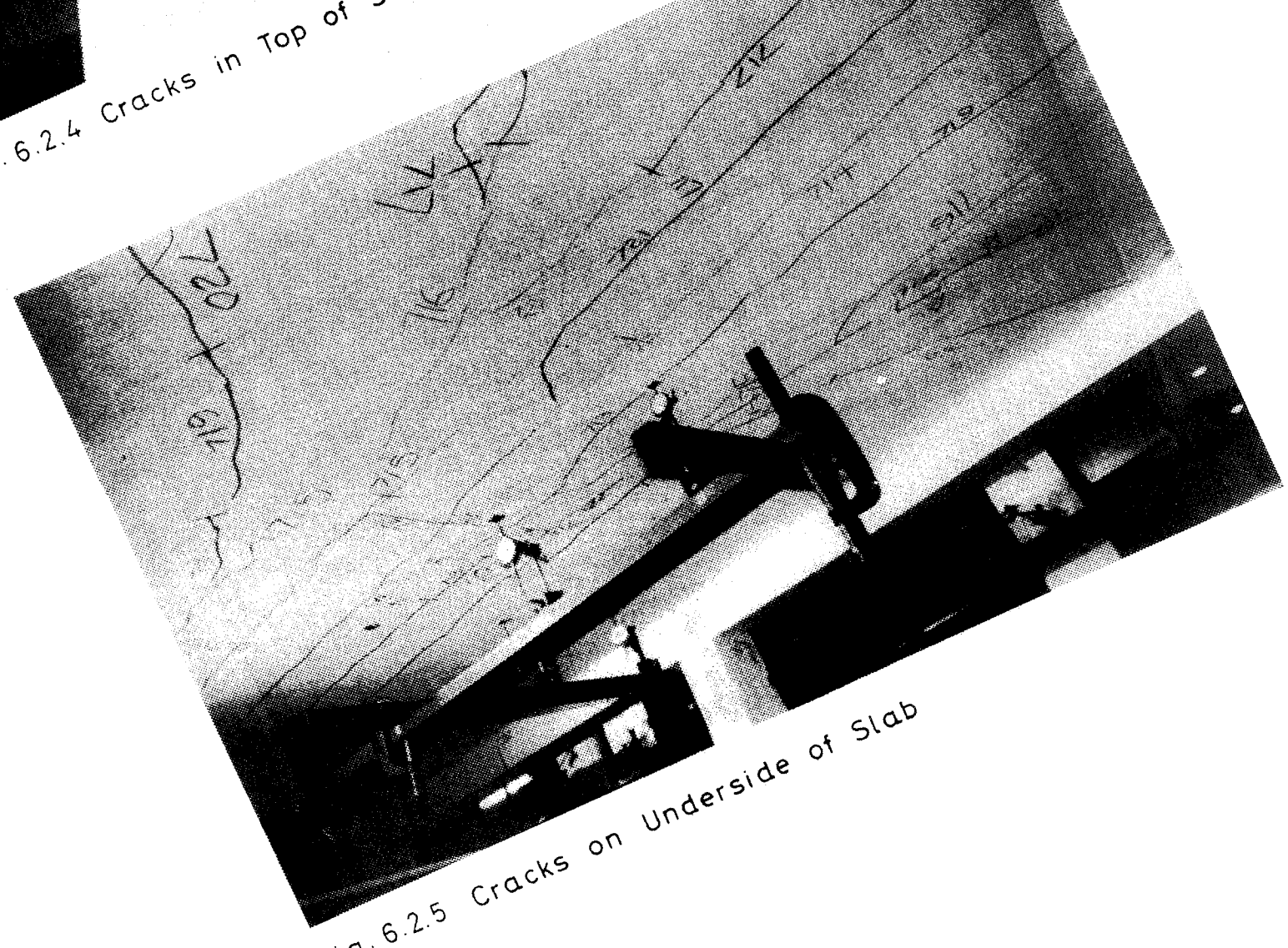

Fig. 6.2.5 Cracks on Underside of Slab

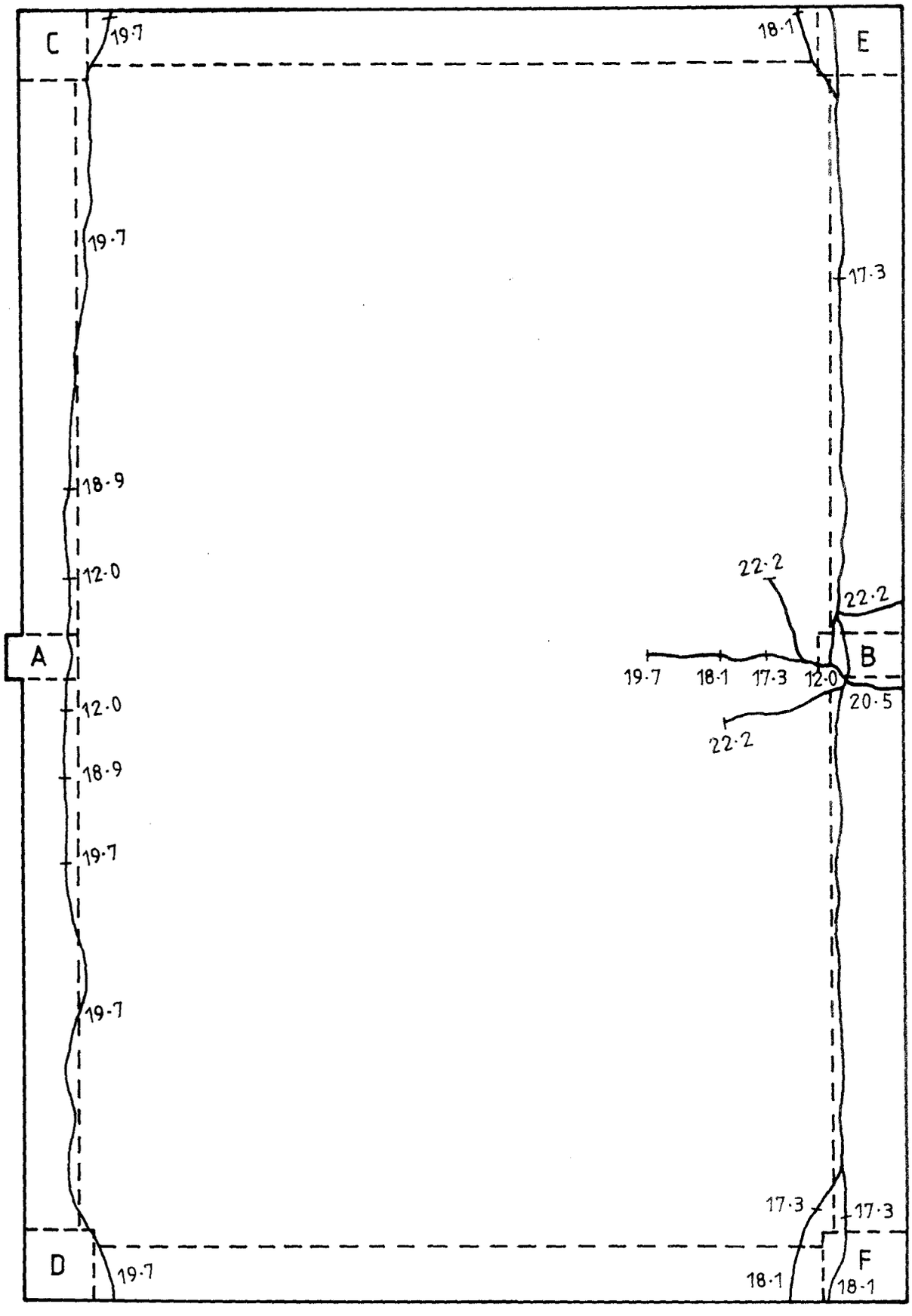

(NUMBERS ON THE CRACKS ARE LOAD IN kN/m^2)

Fig. 6.2.8 : Crack Pattern on the Top of Model 2

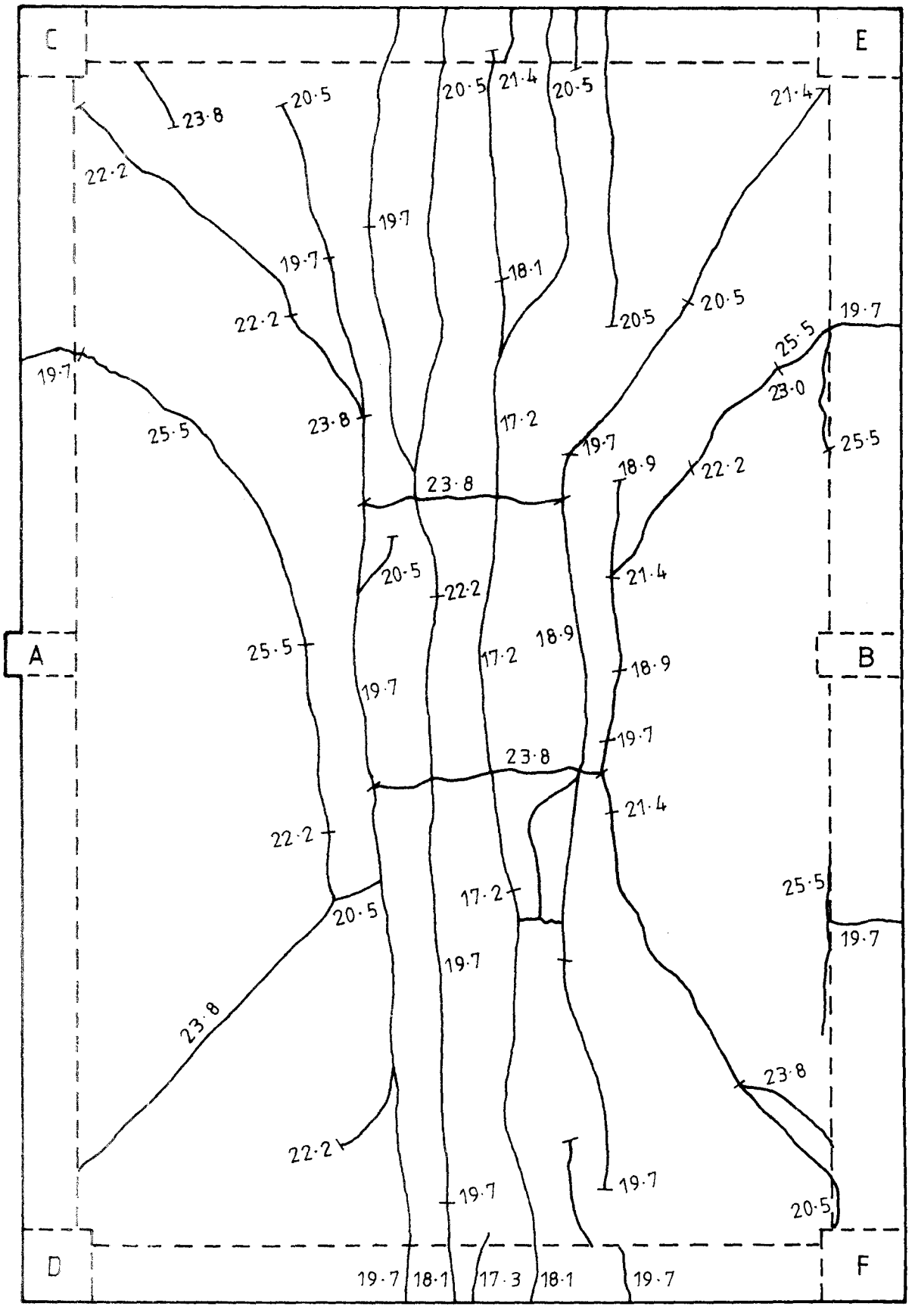

(NUMBERS ON THE CRACKS ARE LOAD IN kN/m^2)

Fig. 6.2.9: Crack Pattern on the Bottom of Model 2

From the load cell readings, the total moment M_A is also derived. In this model the height of column A was different from that in model 1 and M_A is now given by

$$M_A = (E-W)0.820 - R_A\ 0.125$$

Values of M_A are plotted in Fig. 6.2.11.

Strain gauge readings taken during the vertical load test are recorded in Section B.2.5.

From the strain gauges on the top steel in the slab adjacent to the spandrel beam it was possible to calculate the unit negative moment (moment per unit width of slab) at various distances from column A. Graphs of these quantities as the load was increased are given in Fig. 6.2.12.

Opposite the centre of column A (actually at y = 25 mm) the slab moment was calculated at various distances x from the face of the spandrel beam. The derivative of m could then be estimated and this gave the unit shear force (shear per unit width of slab) at the column face. This value is shown in Fig. 6.2.13.

The unit mid-span moments could be similarly calculated at those locations where the bars were strain gauged. Unfortunately at this stage of the project interest was focused on the region around column A and only the three central bars (y = -220, y = -22 and y = 178 mm) were gauged. The moment did not vary very much across this rather narrow central band and hence the average value is given in Fig. 6.2.14. This may be regarded as the moment per unit width in the "beam strip", i.e. the strip of slab more or less opposite the columns.

The graphs 6.2.10 - 6.2.14 are derived directly from the raw data given in Appendix B.2. They may be regarded as the summarized form of these data. From these graphs it is possible to derive further graphs which refer more nearly to quantities which are of direct interest in the research.

From the graphs of unit moment at various y positions (Fig. 6.2.12) it is possible to construct a graph which shows the transverse distribution of the end moment M_A (i.e. the variation of slab moment along the face of the spandrel beam) at any load level.

In Fig. 6.2.15 this distribution is shown at various load levels.

Owing to lack of data, it was not possible to construct similar graphs showing the distribution of slab shear force along the face of the spandrel beam. For the purpose of calculating spandrel torsion, an estimate of shears is made in Fig. 6.2.16. The slab shear at the column centreline was measured (see Fig. 6.2.13). The total shear was measured by the load cells (Fig. 6.2.10). A linear variation of shear was assumed and from the two measured quantities this permitted the graph shown in Fig. 6.2.16 to be drawn. The shape of these graphs should not be interpreted as experimentally derived.

The lateral distribution of mid-span moment was not measured. To preserve a similarity of figure numbering with other models, the number 6.2.17 is omitted for model 2.

The variation of twisting moment, T, along the spandrel beam was calculated from the unit slab moments (Fig. 6.2.15) and the estimated values of unit slab shears (Fig. 6.2.16). Although the assumption of shear distribution must have involved some error, it should be borne in mind that the contribution of slab shear to the spandrel torque is much less than the contribution of slab moment.

The calculation of T was made only for design ultimate load. In Fig. 6.2.18 is shown the variation of slab moment m_s. This is taken directly from Fig. 6.2.15. Also shown added to this is the variation of slab shear v_s (derived as described) multiplied by 0.125 m (half the width of the spandrel beam). The sum of these two quantities gives dT/dy. The integral of this summation graph provides the value of T. By symmetry T must be zero at mid-panel (y = 1362).

Dial gauge readings taken during the vertical load test are recorded in Appendix B, Section B.2.6. For those gauges situated along the spandrel beam (gauges 1-28), the readings may be translated into angles of twist and slope along the spandrel. The values of these angular deformations are given in Section B.2.7. Fig. 6.2.19 shows graphs of the twist values for the different load levels. Fig. 6.2.20 is similar but gives values only for

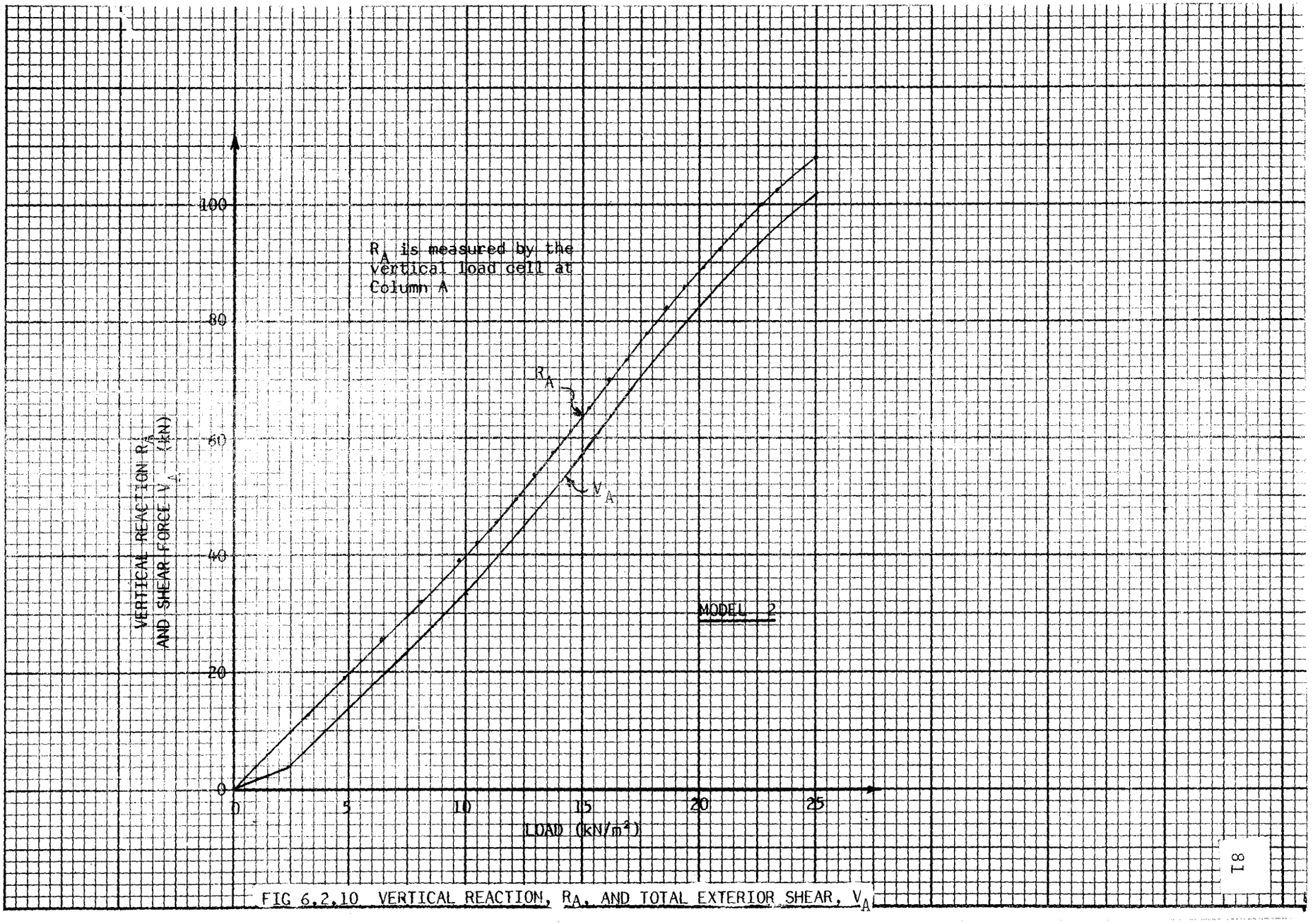

FIG 6.2.10 VERTICAL REACTION, R_A, AND TOTAL EXTERIOR SHEAR, V_A

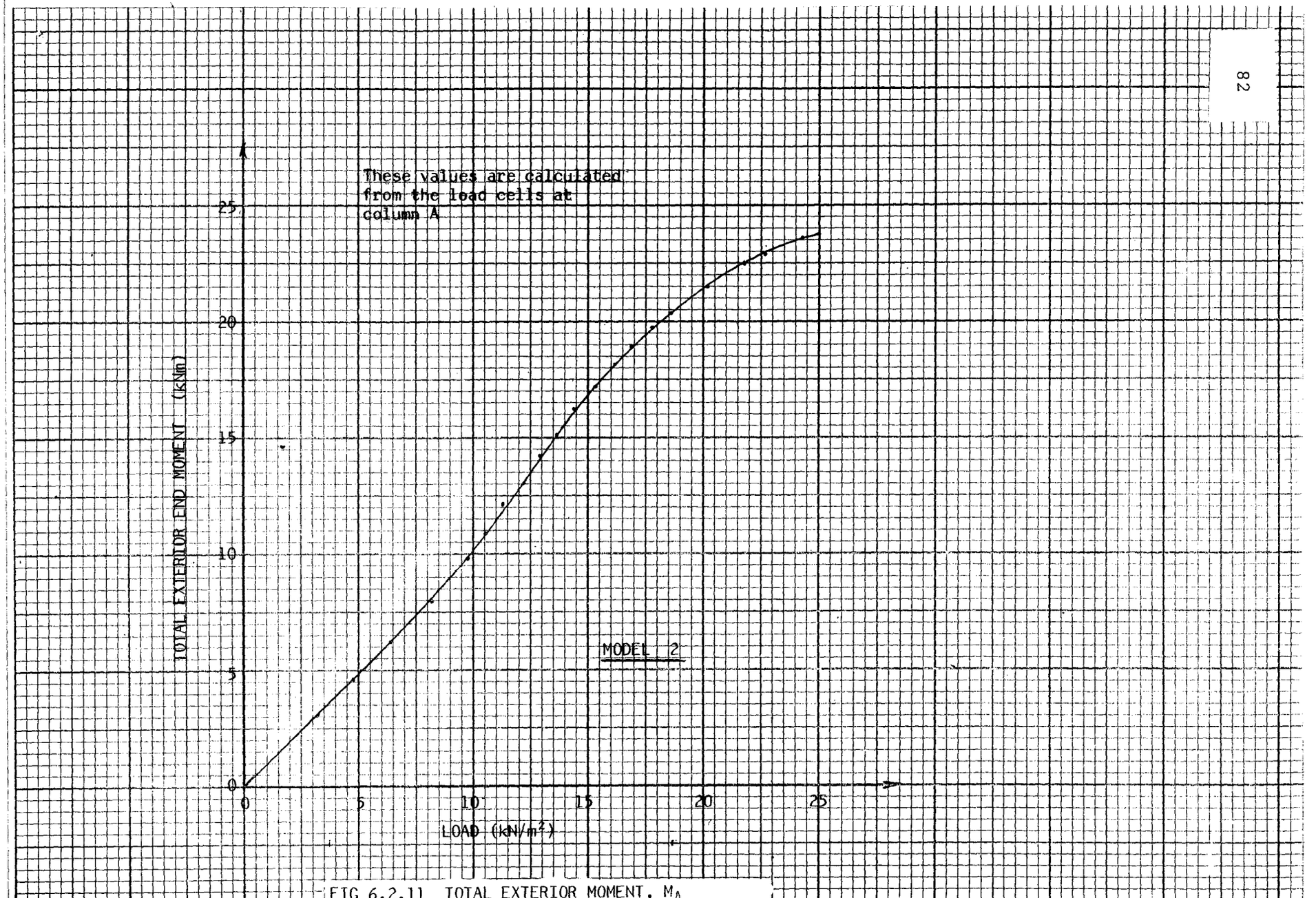

FIG 6.2.11 TOTAL EXTERIOR MOMENT, M_A

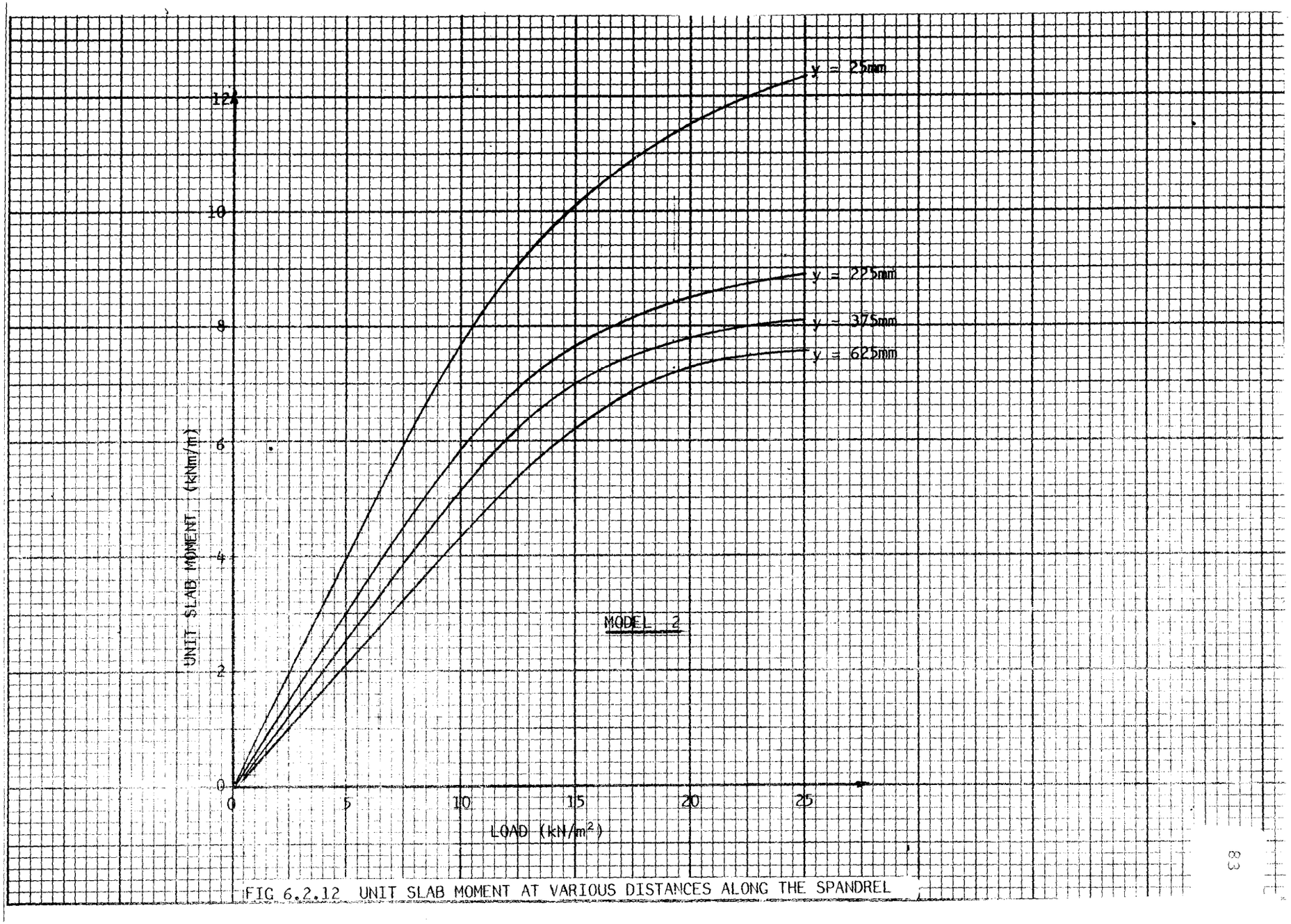

FIG 6.2.12 UNIT SLAB MOMENT AT VARIOUS DISTANCES ALONG THE SPANDREL

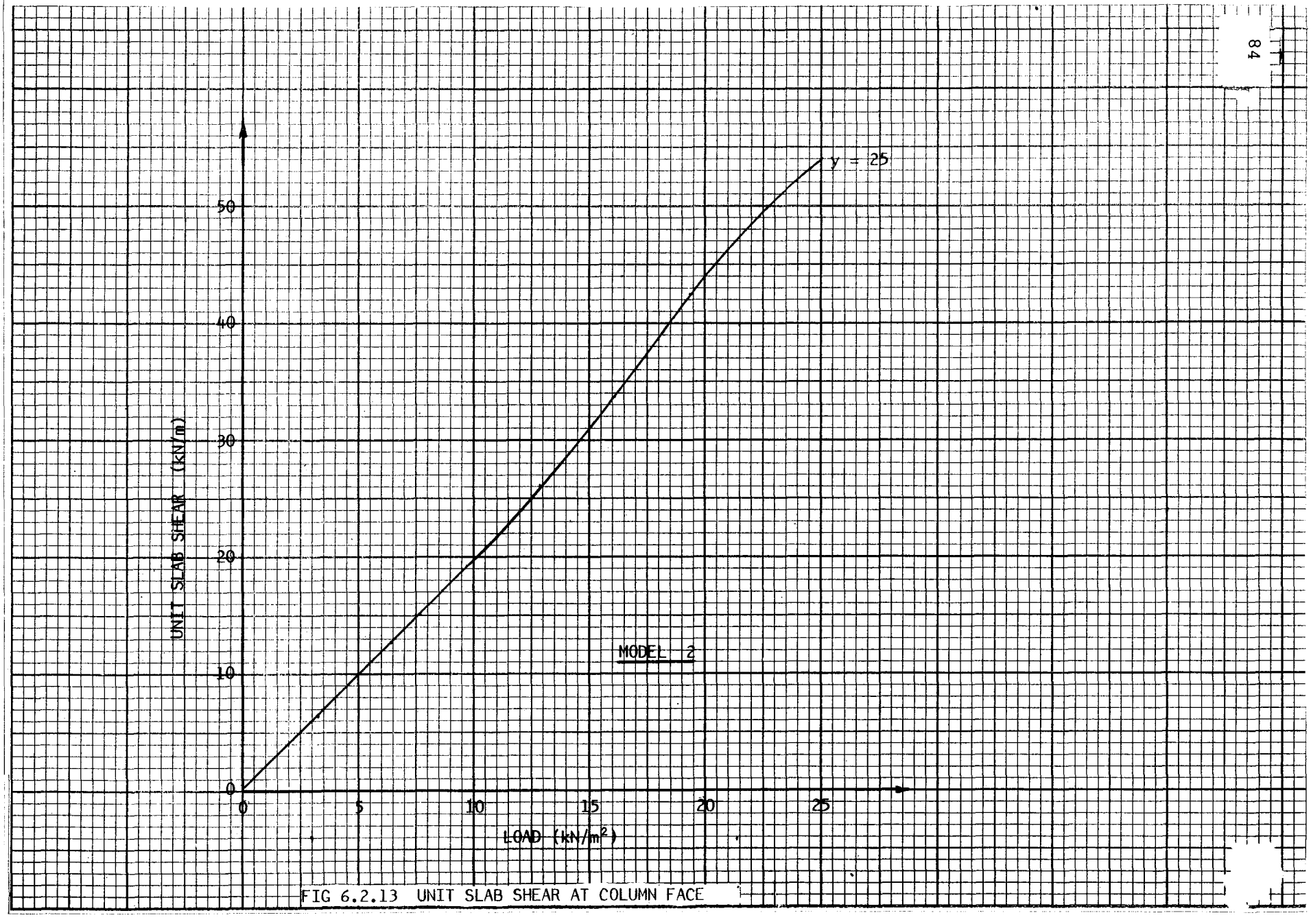

FIG 6.2.13 UNIT SLAB SHEAR AT COLUMN FACE

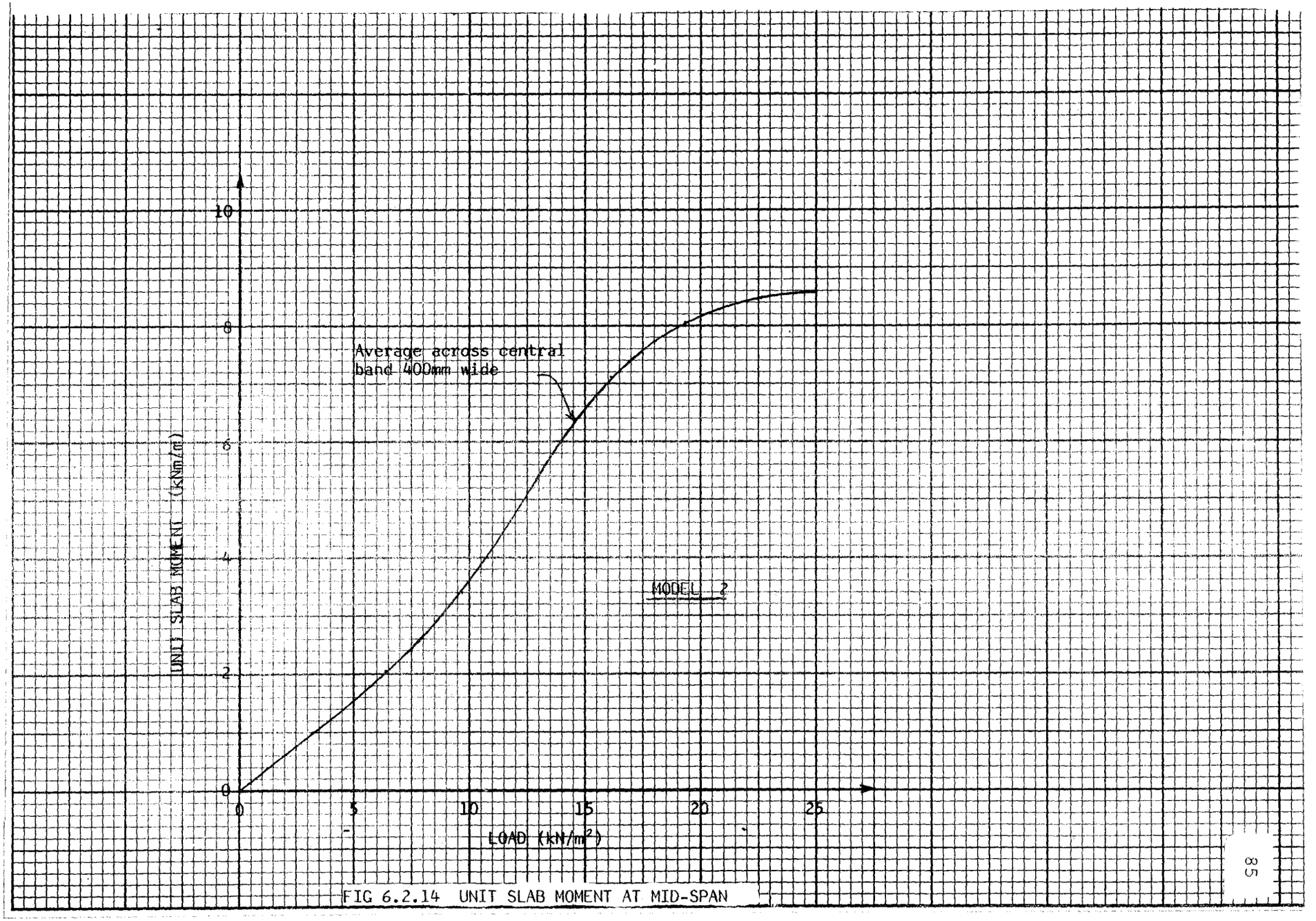

FIG 6.2.14 UNIT SLAB MOMENT AT MID-SPAN

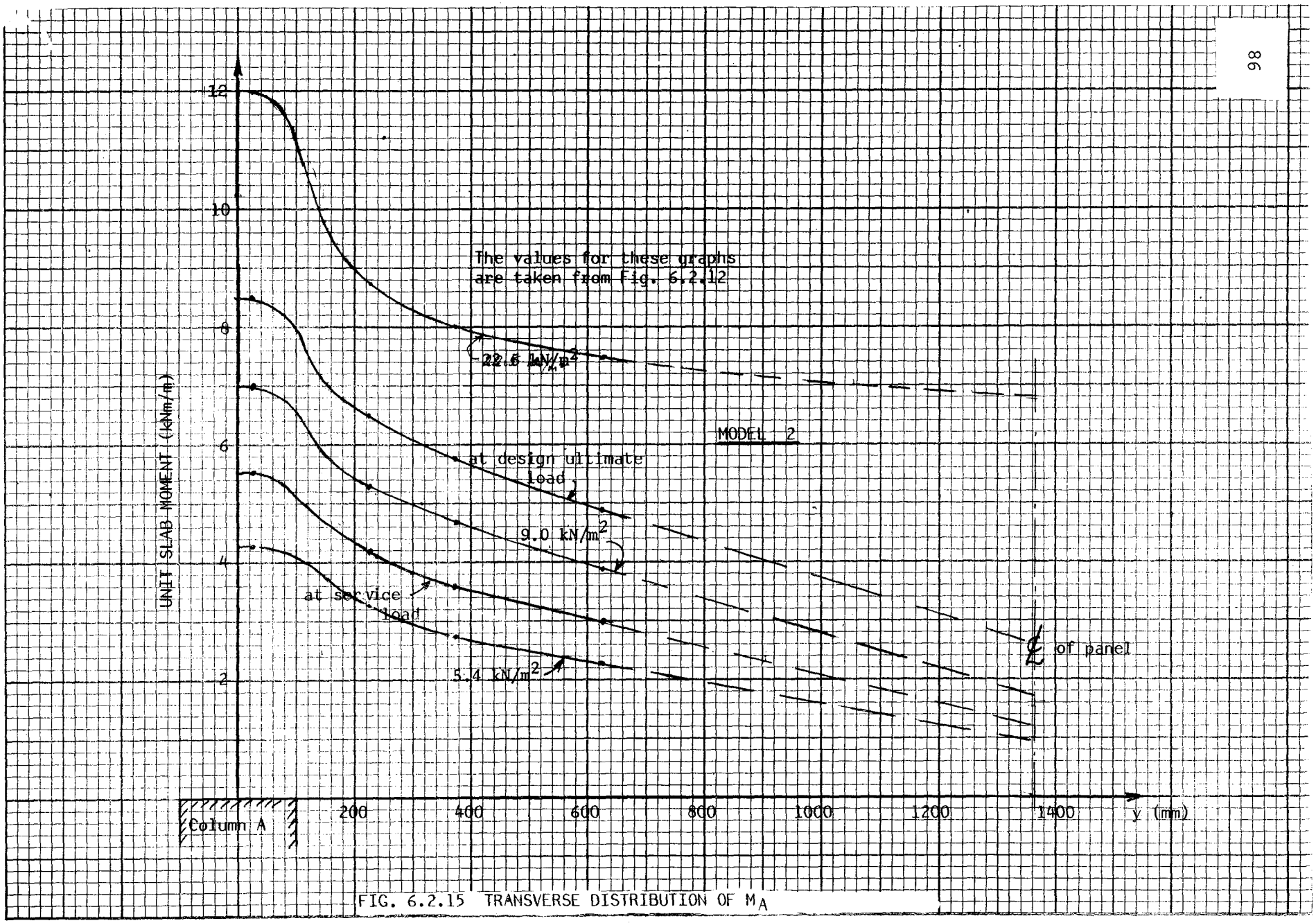

FIG. 6.2.15 TRANSVERSE DISTRIBUTION OF M_A

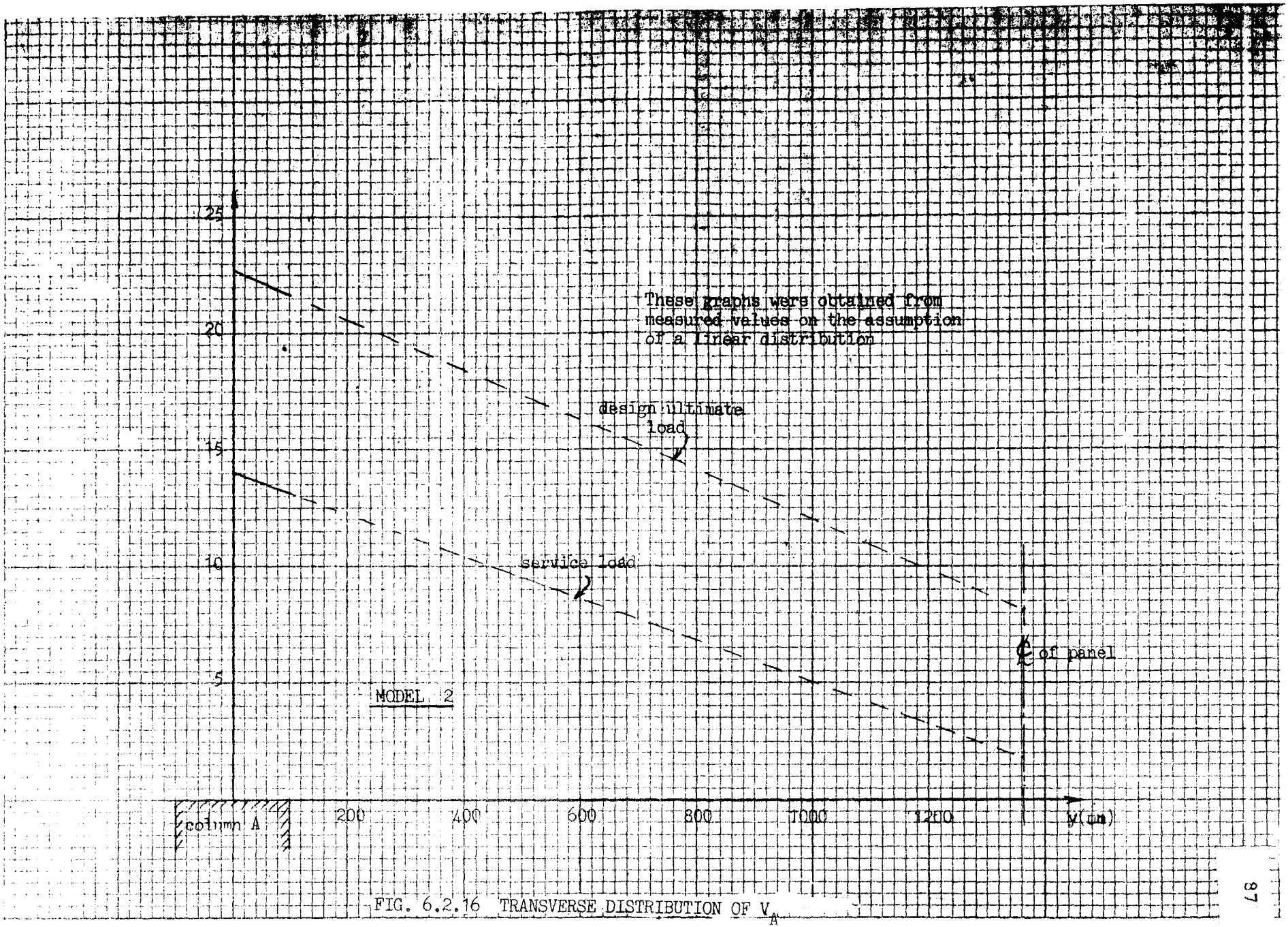

FIG. 6.2.16 TRANSVERSE DISTRIBUTION OF V_A

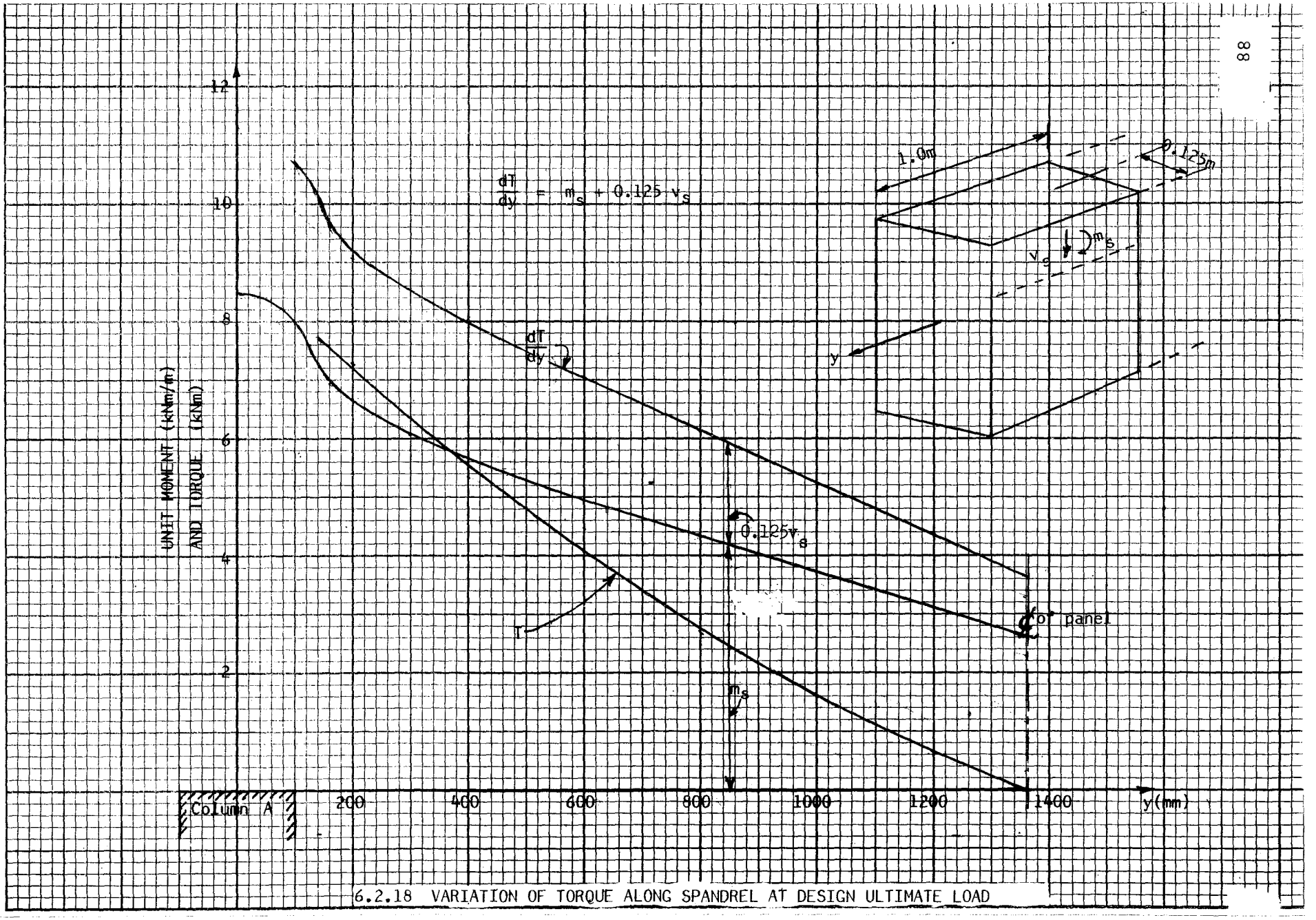

6.2.18 VARIATION OF TORQUE ALONG SPANDREL AT DESIGN ULTIMATE LOAD

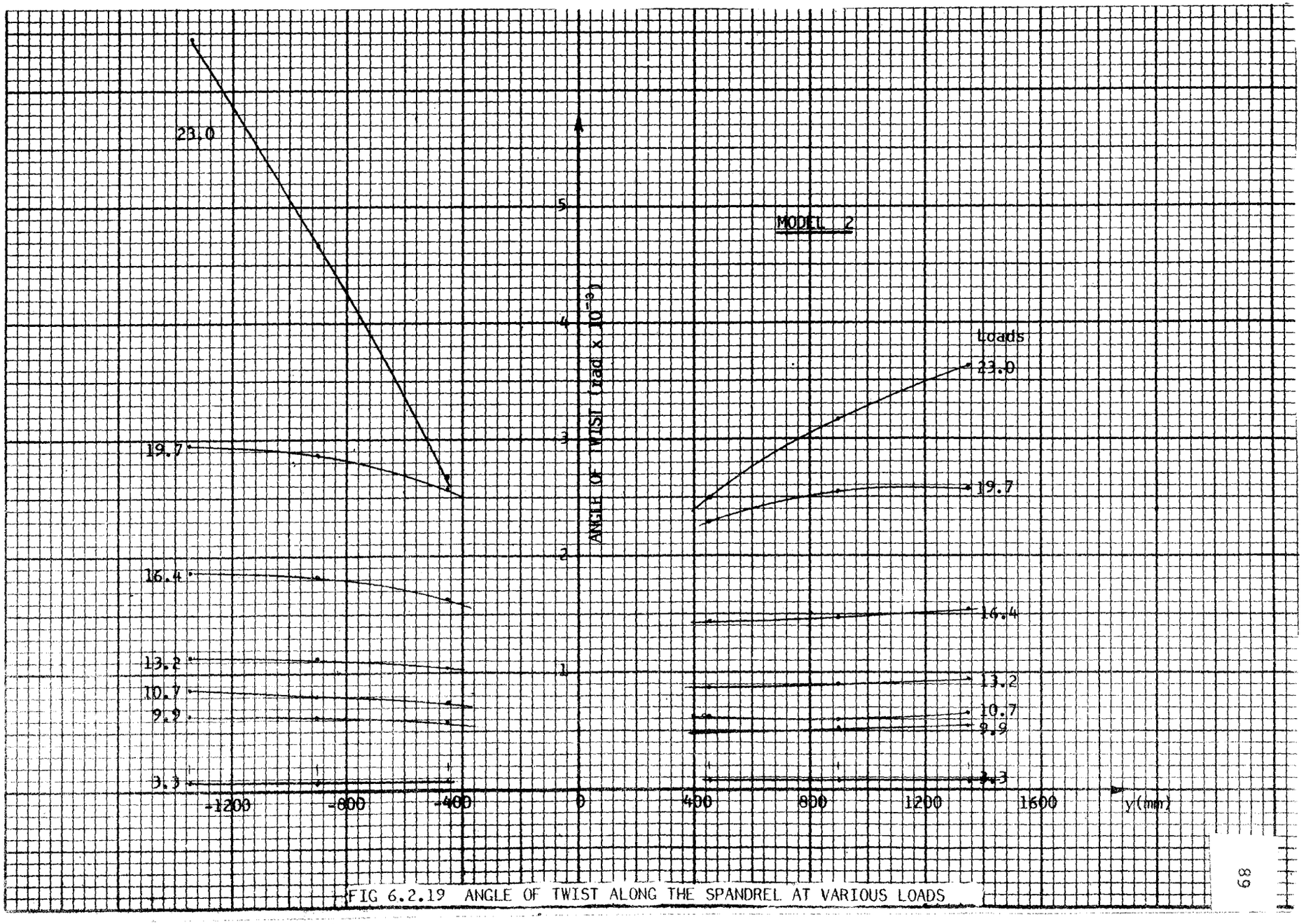

FIG 6.2.19 ANGLE OF TWIST ALONG THE SPANDREL AT VARIOUS LOADS

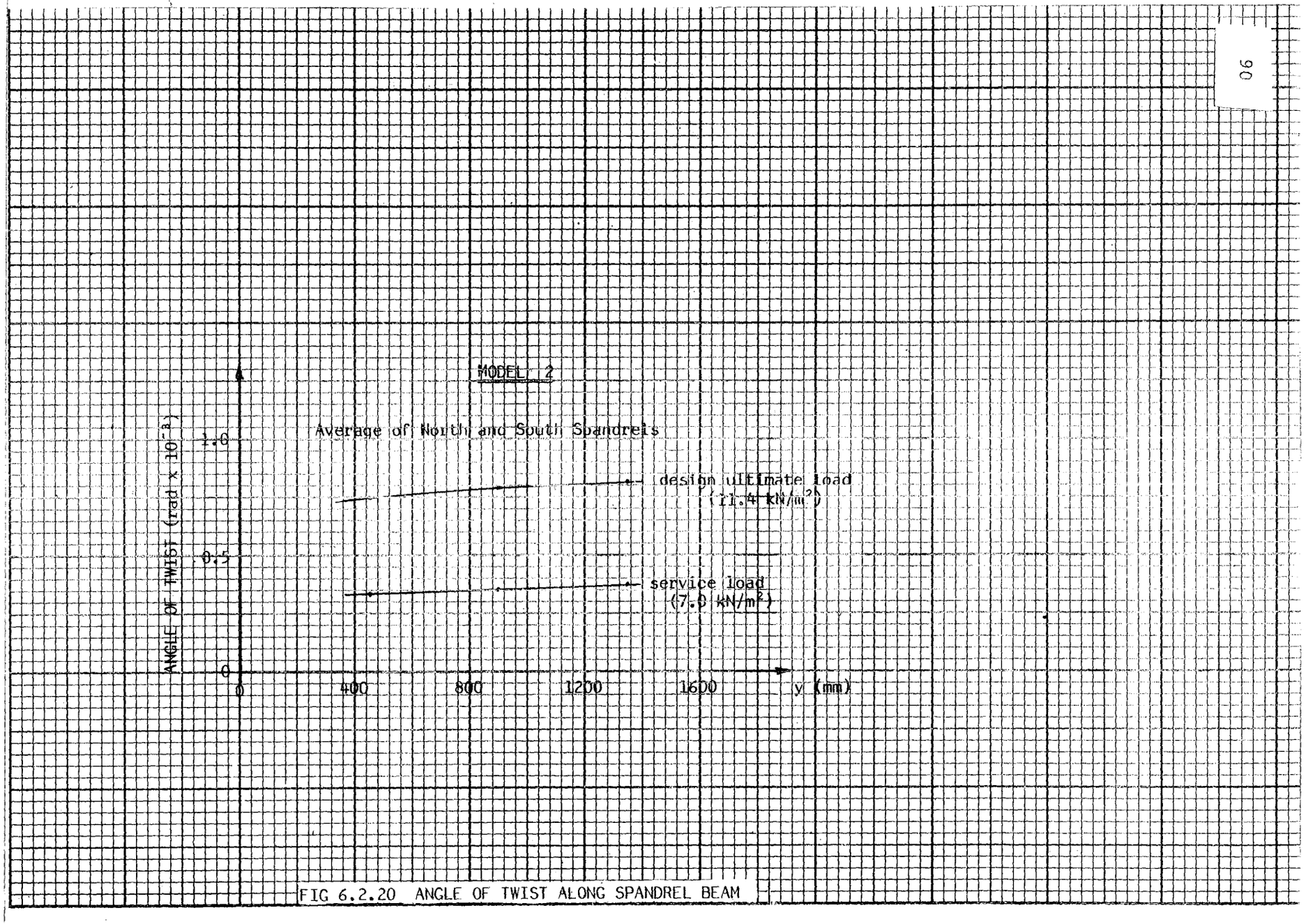

FIG 6.2.20 ANGLE OF TWIST ALONG SPANDREL BEAM

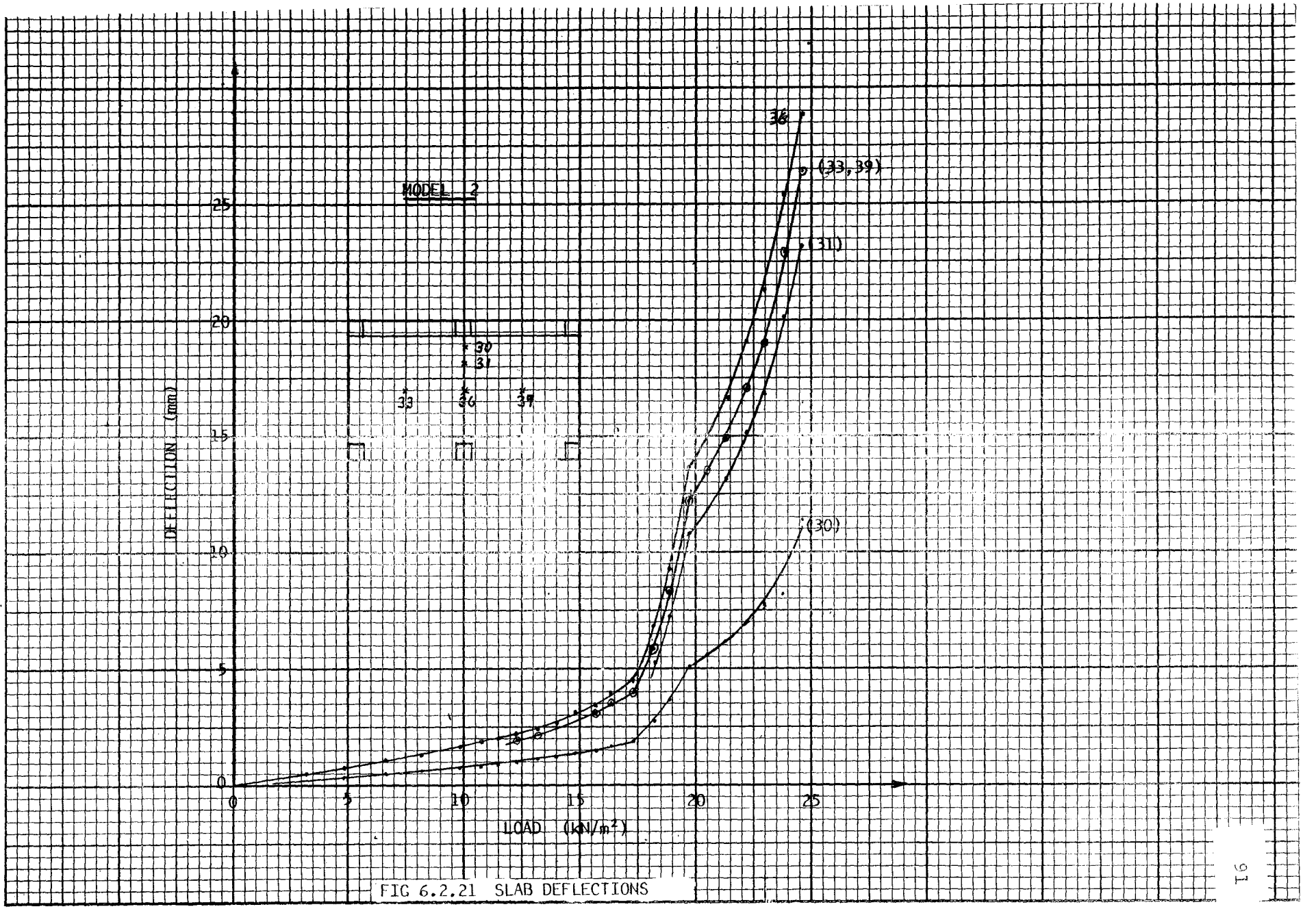

FIG 6.2.21 SLAB DEFLECTIONS

MODEL No. 2
SUMMARY OF RESULTS OF VERTICAL LOAD TEST

TABLE 6.2.1

Service Load = 7.0 kN/m^2
Design Ultimate Load = 11.4 kN/m^2
Failure Load =

Item	Load Level (kN/m^2)	Test Value
1. Vertical Reaction at A = R_A (kN)	5.4 9.0 22.5	21.5 35.5 99.5
2. Vertical Reaction at B = R_B (kN)	5.4 9.0 22.5	
3. Total Mid-Span Moment = M_M (kNm)	5.4 9.0 22.5	
4. Total Moment at face of Spandrel A = M_A (kNm)	5.4 9.0 22.5	5.3 (6.2) 9.0(10.6) 22.9 (21.7)
5. Total Shear Force at Face of Spandrel A = V_A (kN)	5.4 9.0 22.5	15.5 29.5 93
6. Total Moment at Face of Spandrel B = M_B (kNm)	5.4 9.0 22.5	
7. Total Shear Force at Face of Spandrel B = V_B (kN)	5.4 9.0 22.5	
8. Transverse Distribution of Mid-Span Moment M_M		
9. Transverse Distribution of M_A		See Fig. 6.2.15
10. Transverse Distribution of M_B		

* Values in brackets are obtained from strain gauge readings by integration. Other values are obtained from load cells.

MODEL No. 2.

VERTICAL LOAD TEST (cont.)

Item	Load Level (kN/m^2)	Test Value
11. Distribution of Torque along Spandrel A	design ultimate load	See Fig. 6.2.18
12. Torque in Spandrel A at Face of Column A (kNm)	design ultimate load	(7.7)
13. End Moment in Beam Strip at Face of Column A (kNm)	5.4	(1.2)
	9.0	(1.9)
	22.5	(3.3)
14. Shear Force in Beam Strip at Face of Column A (kN)	5.4	(2.9)
	9.0	(4.9)
	22.5	(13.7)
15. Shear Force in Spandrel at Face of Column A (kN)	5.4	
	9.0	
	22.5	
16. Distribution of Torque along Spandrel B	design ultimate load	
17. Torque in Spandrel B at Face of Column B (kNm)	design ultimate load	
18. End Moment in Beam Strip at Face of Column B (kNm)	5.4	
	9.0	
	22.5	
19. Shear Force in Beam Strip at Face of Column B (kN)	5.4	
	9.0	
	22.5	
20. Shear Force in Spandrel at Face of Column B (kN)	5.4	
	9.0	
	22.5	
21. Mid-span Moment in Beam Strip (kNm)	5.4	(0.5)
	9.0	(0.9)
	22.5	(2.4)

design ultimate load and service load. Also the values for the north and south spandrels are here averaged.

The dial gauges below the slab measured deflections. Gauges 33 and 39 measured mid-panel deflections and the mean of these (they differed very little) is graphed in Fig. 6.2.21. Gauge 36 measured the deflection at the mid-span of the beam strip (i.e. midway between columns A and B). This deflection is also graphed in Fig. 6.2.21.

A summary of the results in the graphs is given in the Summary Table 6.2.1.

It was realized at the conclusion of the vertical load test on model 2 that further useful information could have been obtained if more strain gauges had been used in the regions outside the immediate vicinity of column A. In particular a more complete group of gauges at mid-span would provide the value of the total mid-span moment M_m and its transverse distribution. These modifications were put into effect in model 3.

6.3 MODEL 3

Design

In model 3 the spandrel beam was omitted as well as the floor beam. The real building, of which this model represented a portion, was therefore entirely a flat plate. In the model, beams 250 mm wide and 165 mm deep were included on the southern, western and northern boundaries to simulate approximately the stiffness of adjacent panels. The slab steel was retained the same as for model 2, and therefore no design calculations were carried out.

Since there was no actual spandrel beam in this model, the strip of slab 250 mm wide along the spandrel (i.e. where the beam was in previous models) will be referred to as the "spandrel strip" in this model.

The dimensions of model 3 are given in Fig. 6.3.1.

Reinforcement

Details of the reinforcement in model 3 are given in Fig. 6.3.1.

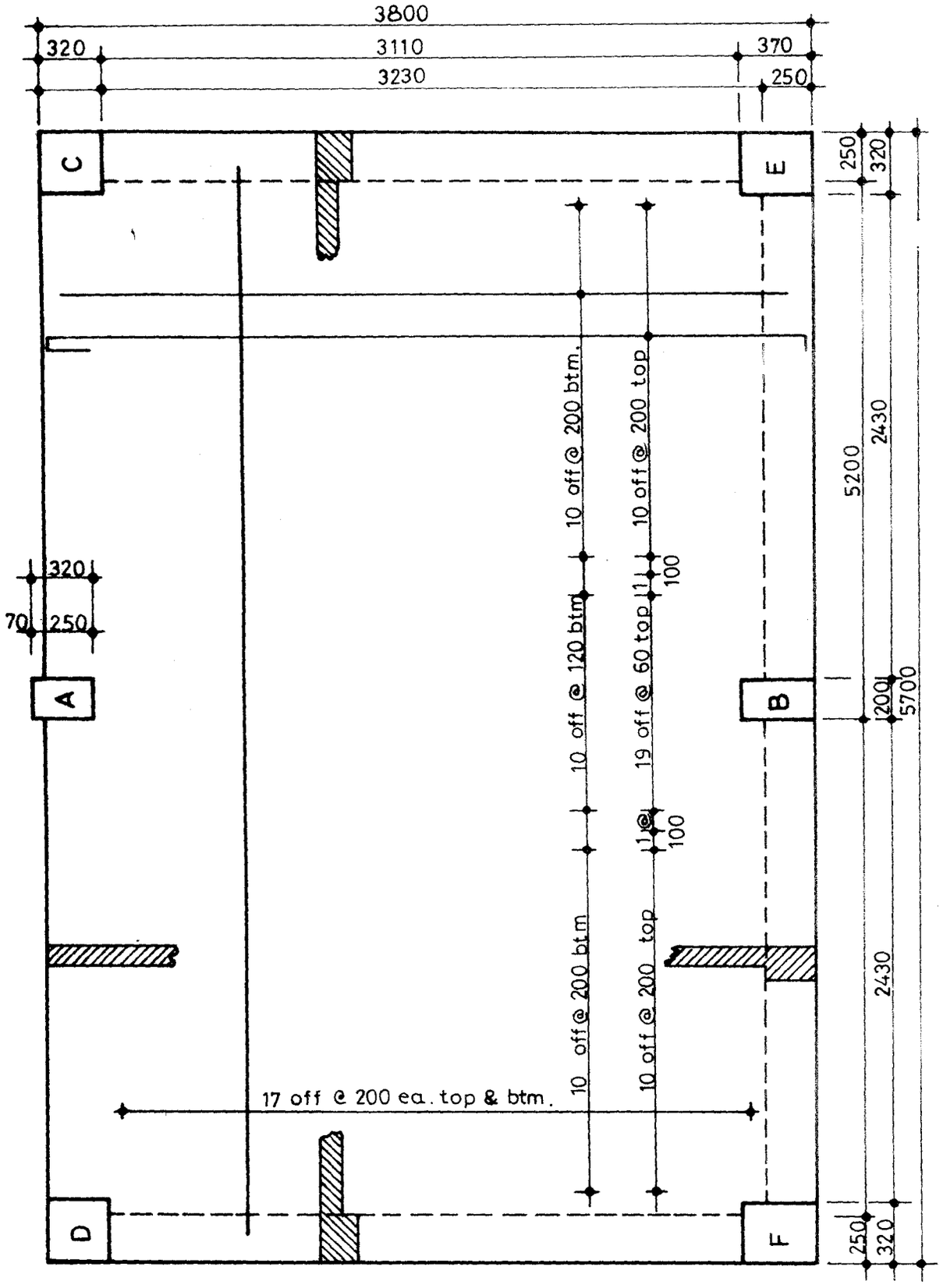

Note : all reinforcement shown is 6.3 mm dia. hard drawn wire.

Fig. 6.3.1(a) Reinforcement Details for Model 3.

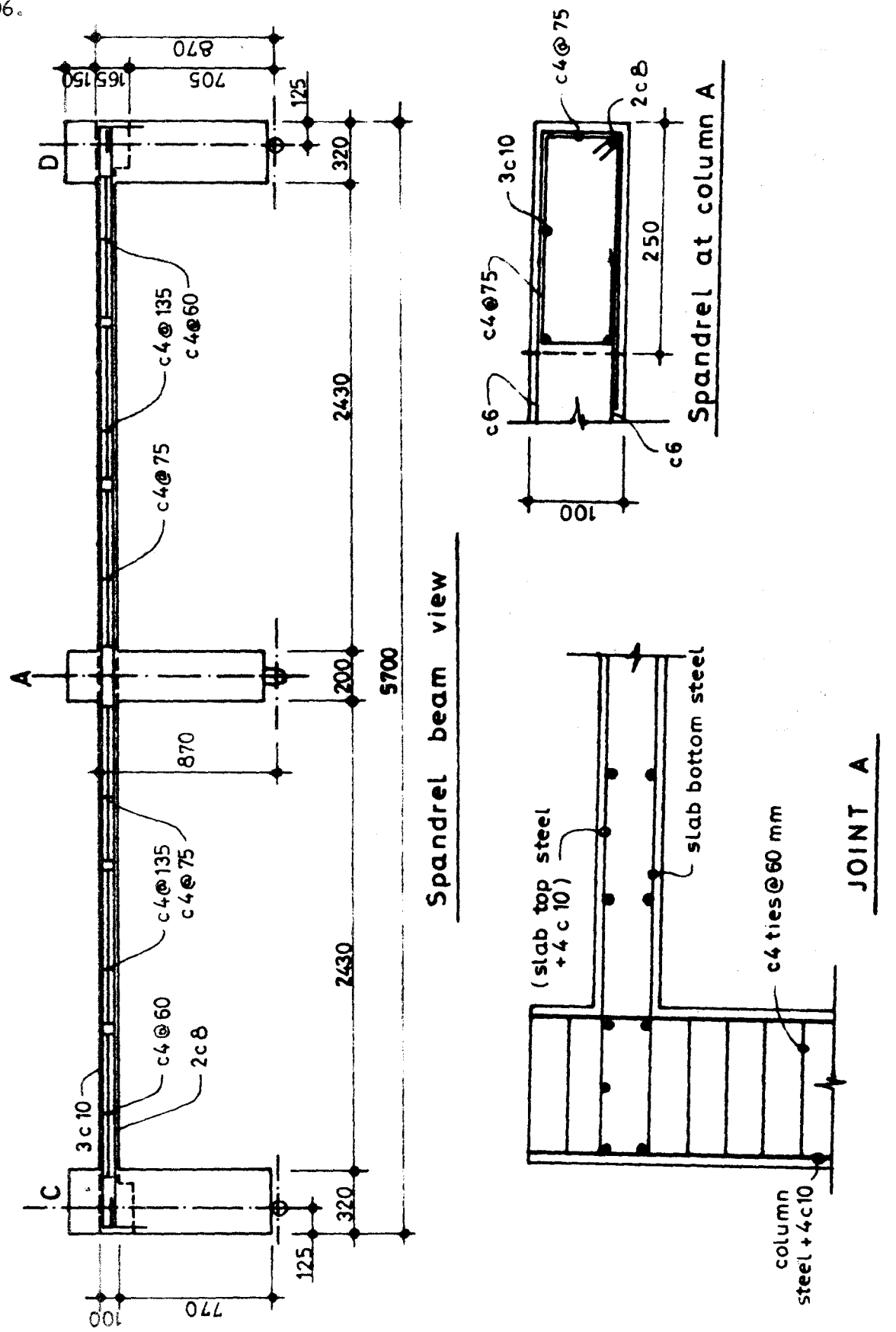

Fig 6.3.1(b) Reinforcement Details for Model 3.

Strain Gauges

It was decided that in this model it would be desirable to obtain fuller information about the distribution of mid-span moments. Consequently all the bottom bars between the panel centrelines north and south of line AB were gauged at mid-span. Three gauges were attached to each bar in case some gauges failed to operate correctly. To compensate partly for the increased number of gauges at mid-span, fewer gauges were used on the top steel at the end of the span. In model 2, six gauges were used on each top bar, but results showed that this was excessive and only four gauges per bar were used in model 3. This was sufficient to give not only the end moment but the local rate of change of moment (end shear).

Details of the location of all gauges are given in Section B.3.1 of Appendix B.

Dial Gauges

The dial gauges along the spandrel strip were generally the same as before. The locations at which twists and slopes were measured were 500 mm apart in this model instead of 450 mm as in previous models. Exact locations of the gauges are given in Section B.3.2.

Eleven gauges were mounted below the model this time so that a more extensive picture could be obtained of the variation of deflection along the line AB and along the centreline at right angles to AB. The locations of these gauges are given in Section B.3.3.

Concrete

At the time of the vertical load test the concrete compressive strength was 44 MPa.

Vertical Load Test

The vertical load test was generally carried out in a manner similar to that of the previous models.

First cracking occurred at the top of the slab near the faces of columns A and B at a load of 7 kN/m^2. This was followed, at a load of 11 kN/m^2 by bottom cracking at midspan. At 14 kN/m^2 a crack occurred in the top of the slab starting at column A and running towards column B (Fig. 6.3.4). This crack extended as the load increased. The top crack across the face of column A extended across the top of the spandrel strip at approximately 45^o, reaching the edge of the model. This crack was indicative of torsion in the spandrel. Parallel cracks occurred at higher loads. Similar cracks occurred adjacent to column B. Radial cracks also appeared radiating from column A.

The mid-span moment reached yield first. At 23.8 kN/m^2 the end regions showed signs of distress and the model refused to accept further load, although deformation was increasing. The longitudinal steel in the spandrels at A reached yield. Figs. 6.3.4 and 6.3.5 show the cracking on the top and bottom of the slab respectively at this advanced load. At this stage the model was unloaded and a stiffness test was carried out as reported below.

After the stiffness test the vertical loading was then resumed with increase in deformation. The torsion cracks in the spandrel strips widened considerably (photograph in Fig. 6.3.6). A punching shear occurred suddenly at column A. Fig. 6.3.6 shows the appearance of this punching failure in the top of the slab. Fig. 6.3.7 shows the appearance of the underside at column A, where the failure crack is at the junction of the slab and the column.

Figs. 6.3.8 and 6.3.9 are diagrams of top and bottom cracking respectively.

Load cell readings for this test are given in Section B.3.4. A graph of the vertical reaction at A is given in Fig. 6.3.10. Also shown in this graph is the total shear, V_A, along the face of the spandrel strip. For this model

$$V_A = R_A - 3.1 \text{ kN}$$

From the load cell readings, the total moment M_A is derived. The vertical distance from the pin support to the centre of the slab was 0.820 m in model 3. Hence M_A is given by

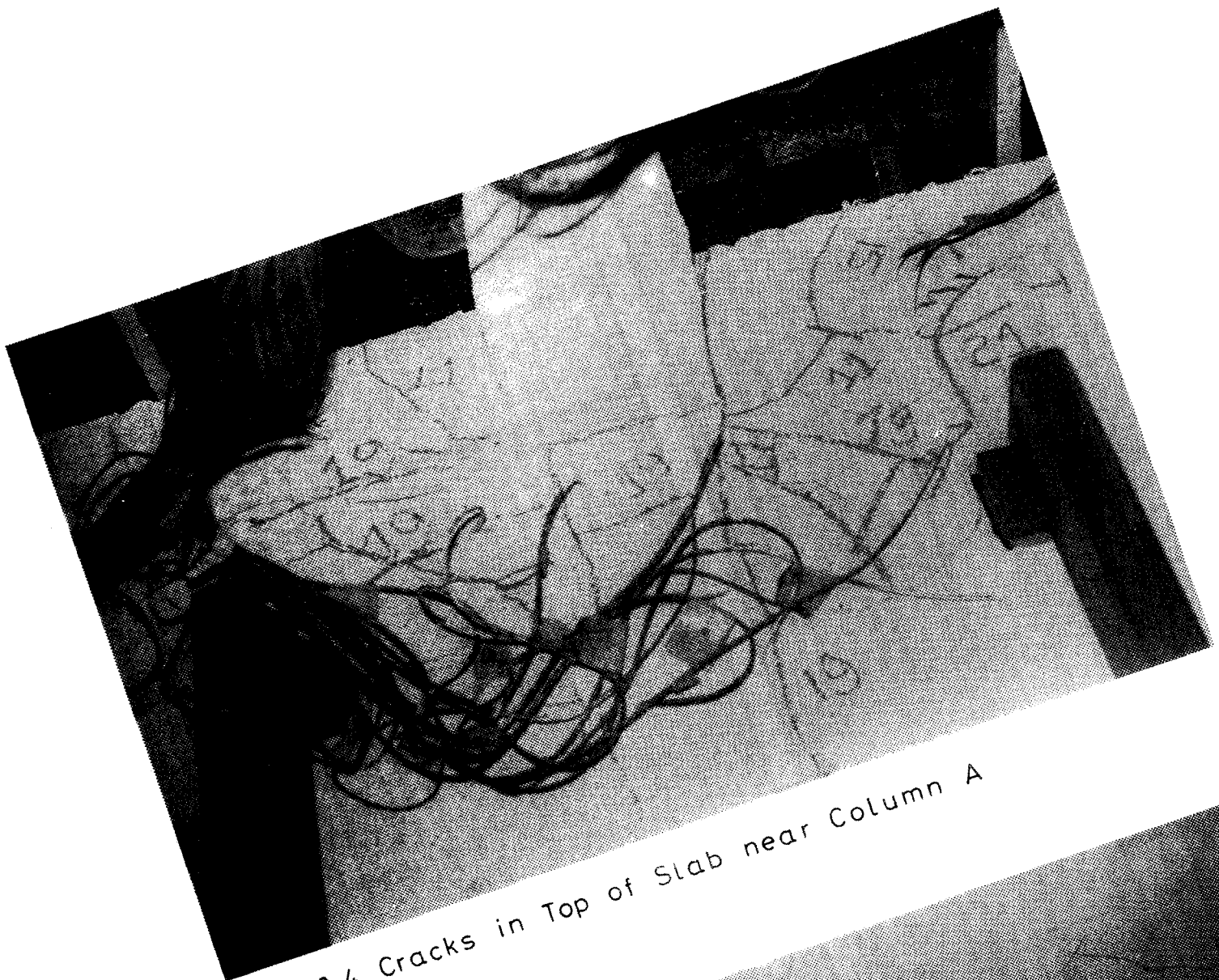

Fig.6.3.4 Cracks in Top of Slab near Column A

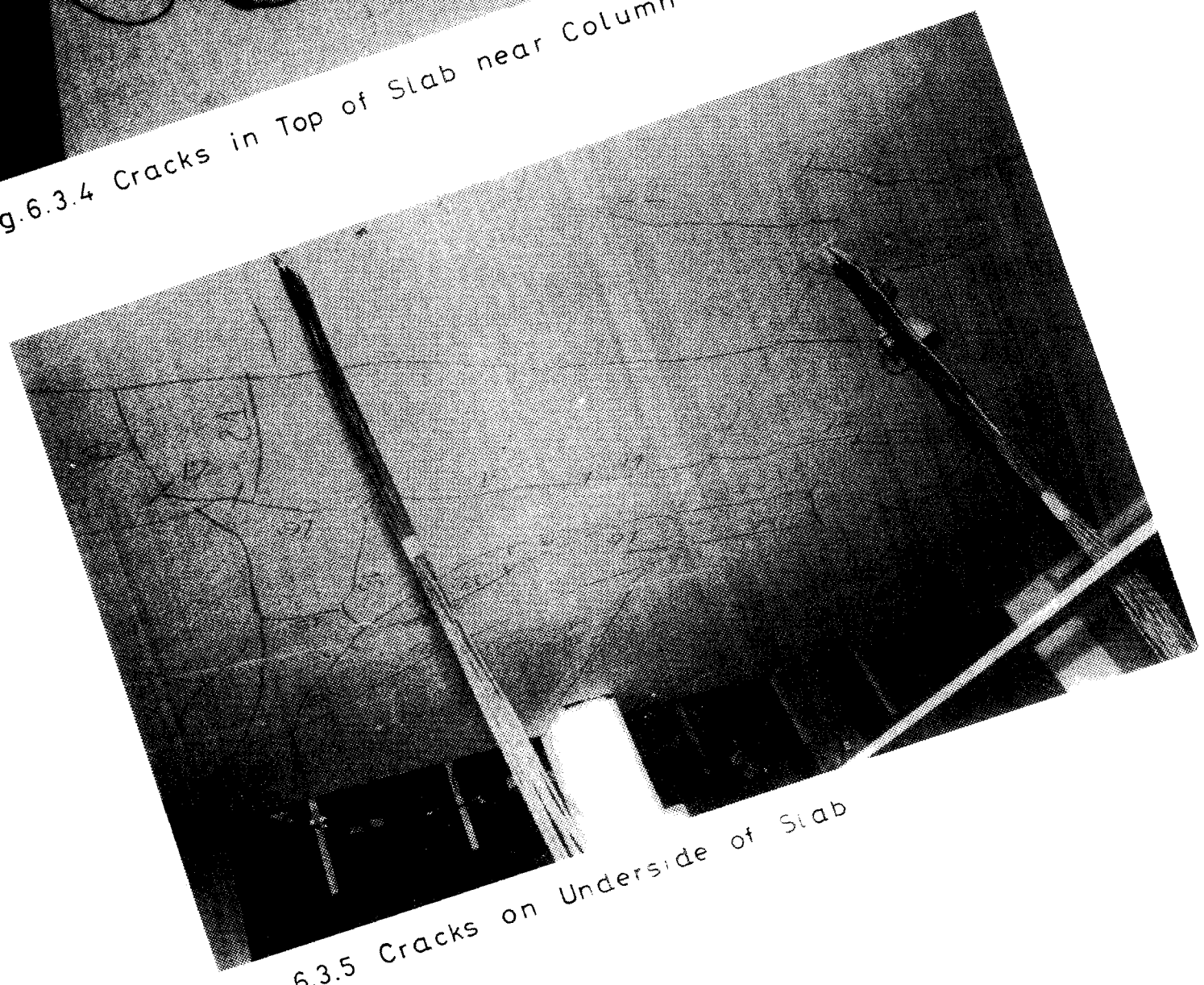

Fig. 6.3.5 Cracks on Underside of Slab

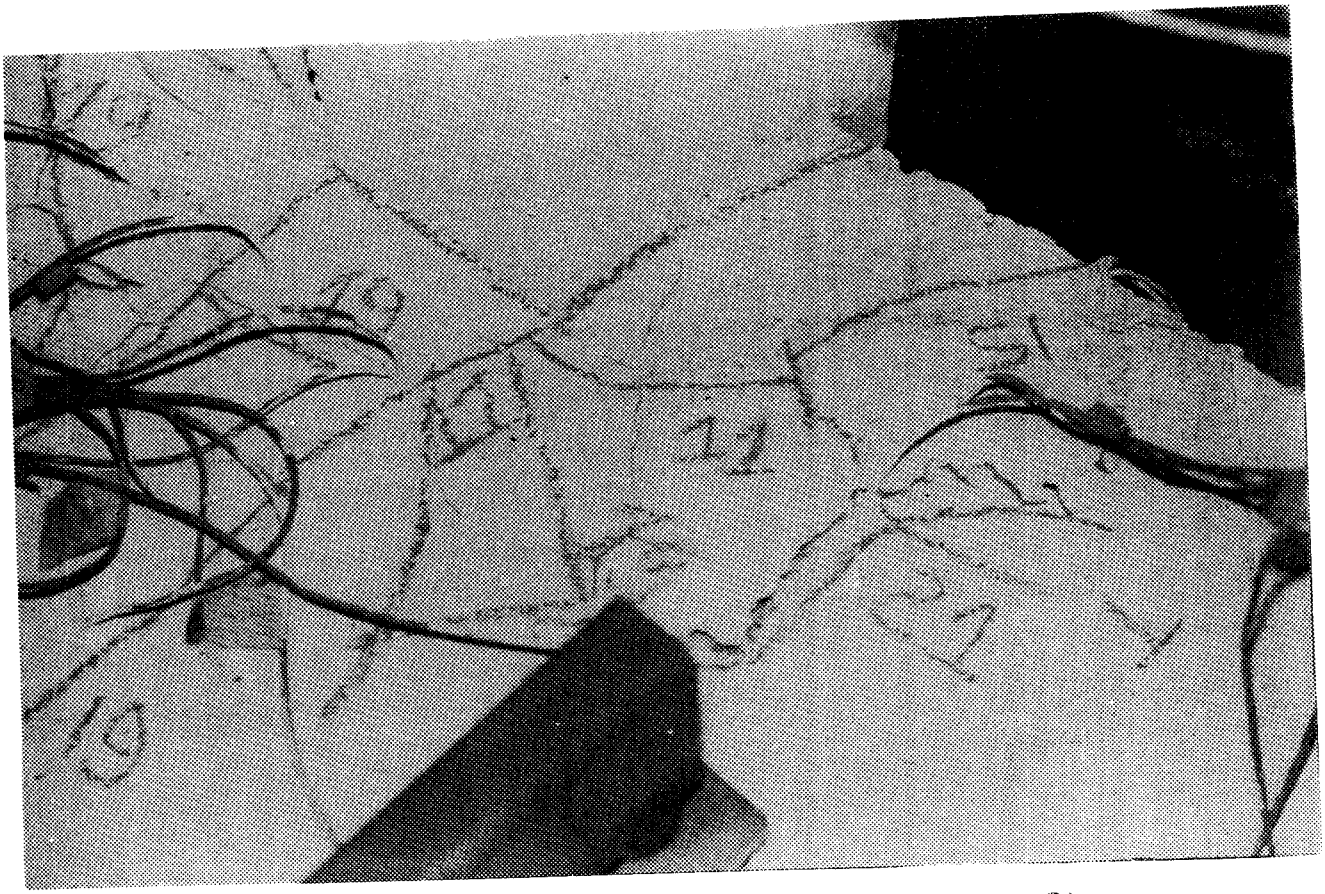

Fig. 6.3.6 Top of Slab at Column A after Punching Shear

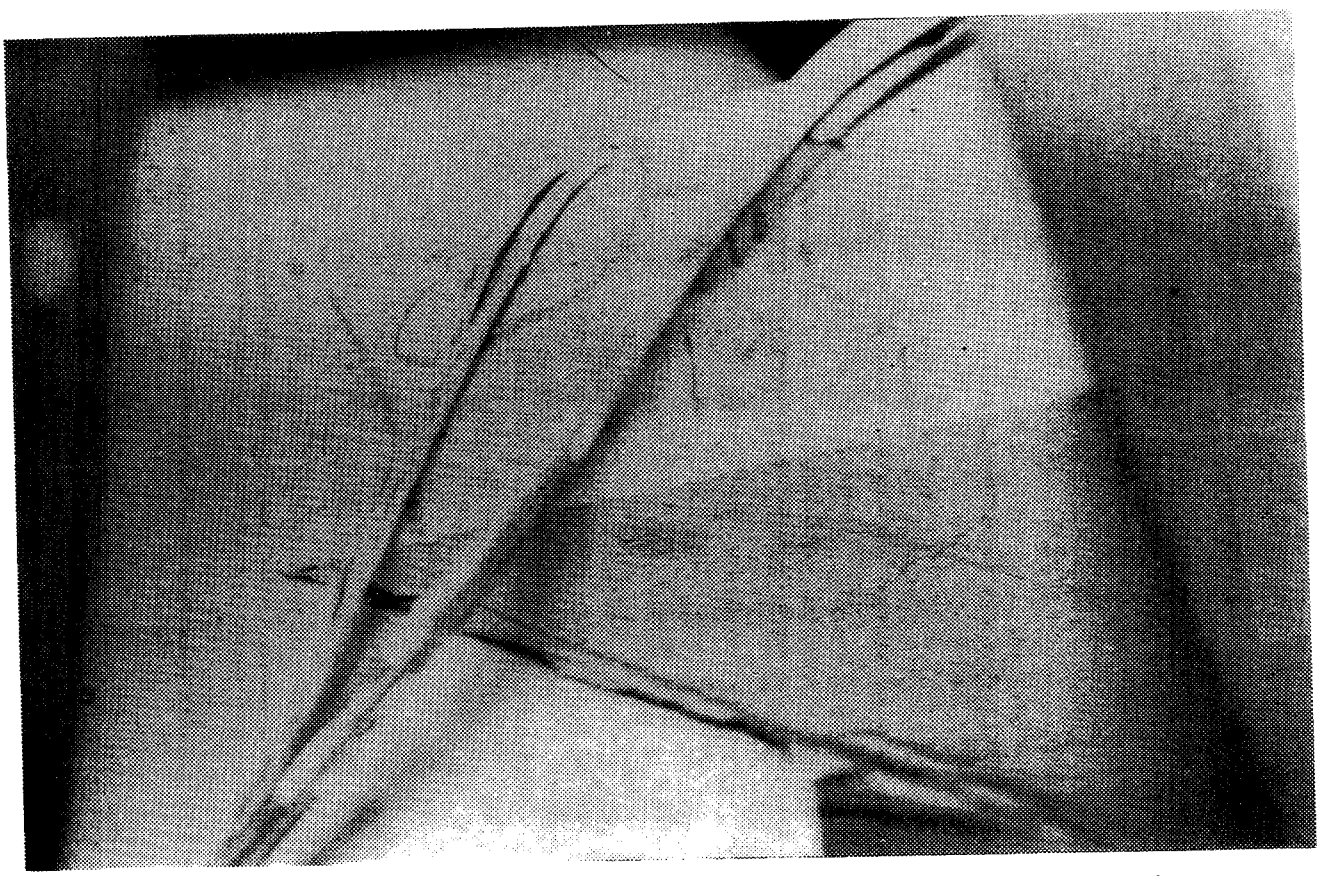

Fig 6.3 7 Bottom of Slab at Column A after Punching Shear

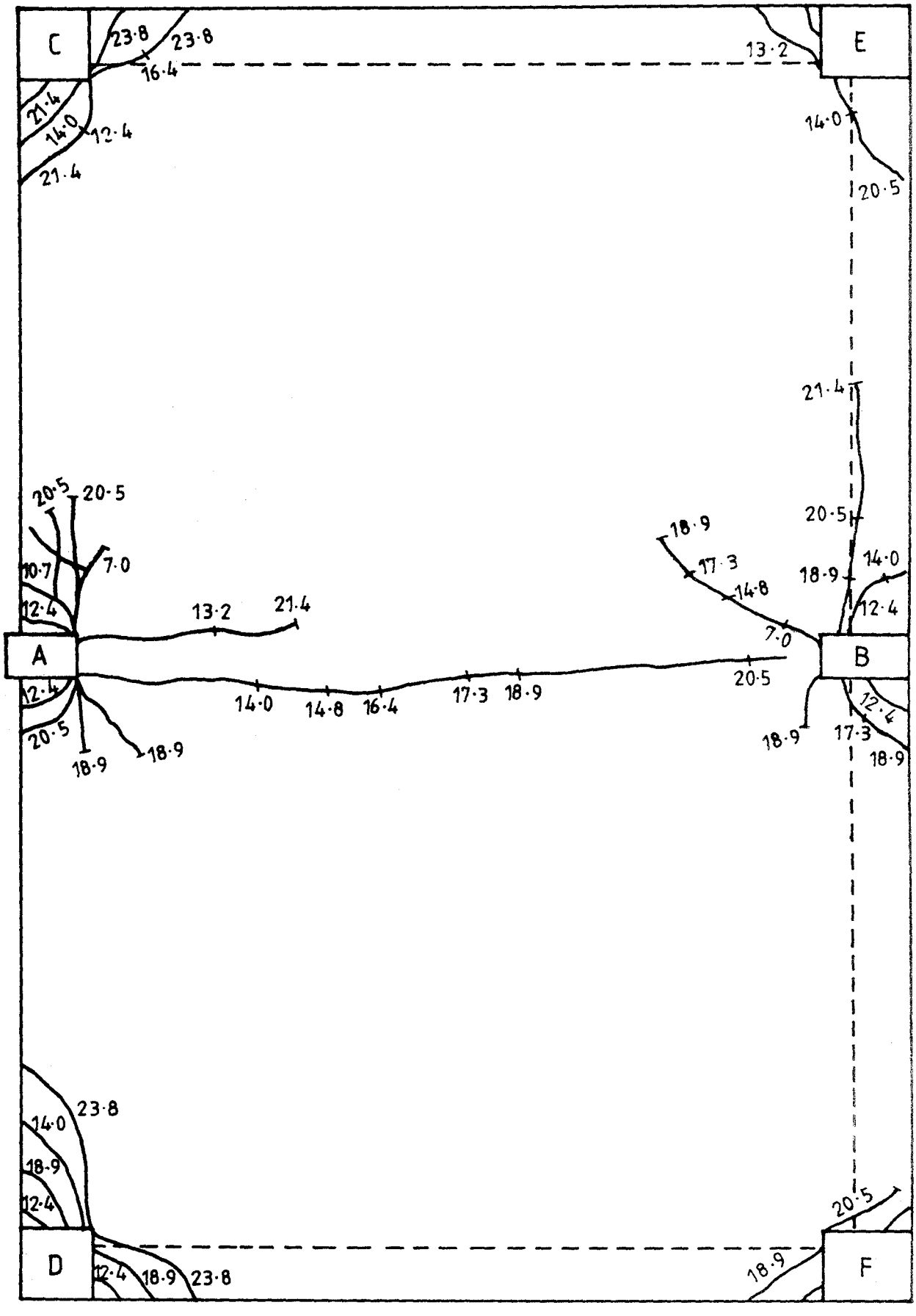

(NUMBERS ON THE CRACKS ARE LOAD IN kN/m^2)

Fig. 6.3.8 : Crack Pattern on the Top of Model 3

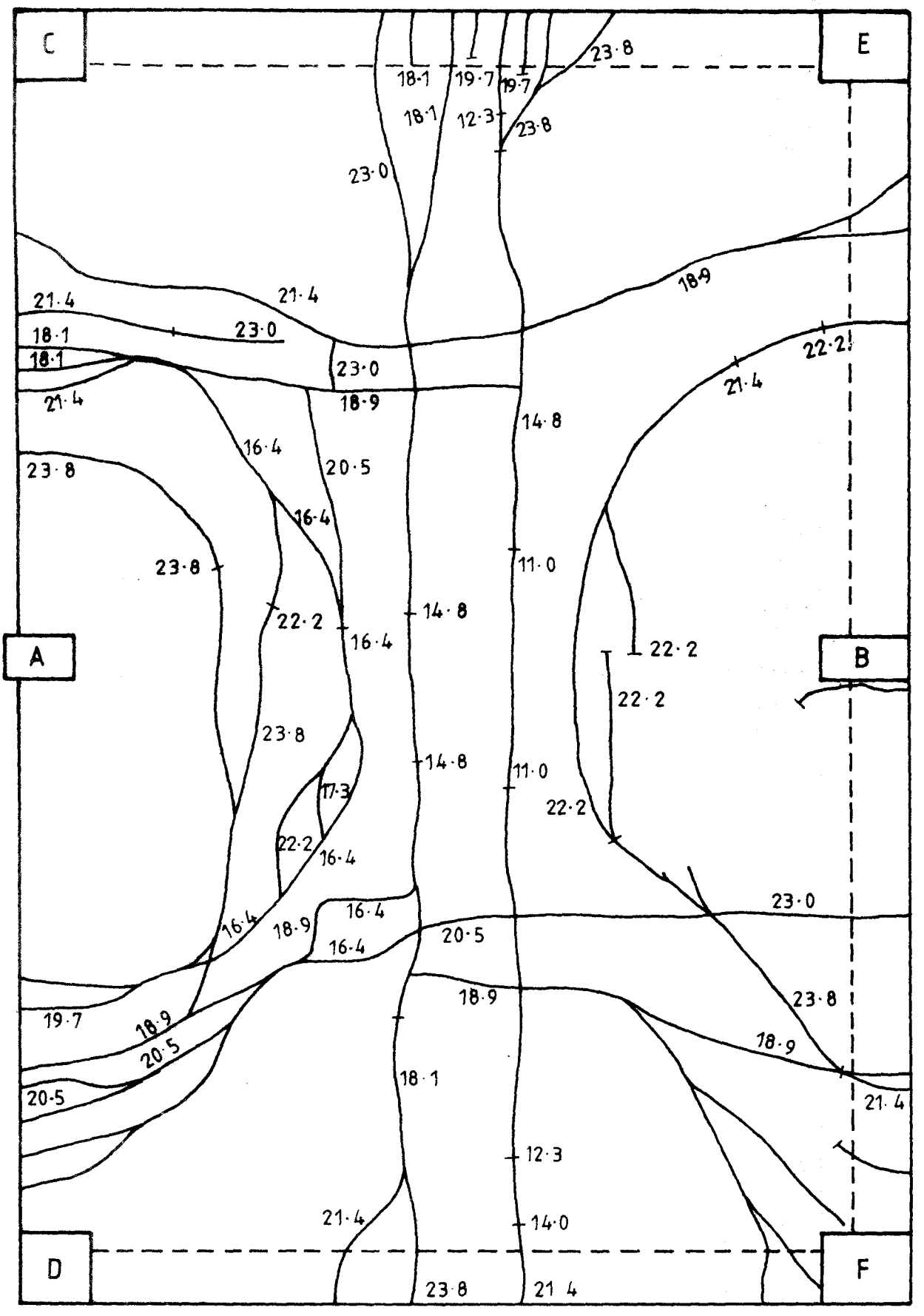

(NUMBERS ON THE CRACKS ARE LOAD IN kN/m^2)

Fig. 6.3.9: Crack Pattern on the Bottom of Model 3

$$M_A = (E-W)0.820 - R_A\ 0.125$$

Values of M_A are plotted in Fig. 6.3.11.

Strain gauge readings taken during the vertical load test are recorded in Section B.3.5.

Fig. 6.3.12 shows values of the unit negative moment at various distances from A. These values were obtained from the strain gauges on the top steel adjacent to the spandrel strip.

As before, the unit shear force at various distances from A was calculated from the derivative of m at these locations. These unit shears are plotted in Fig. 6.3.13.

In model 3 it was possible for the first time to make similar calculations at mid-span. Fig. 6.3.14 shows the unit moment at various values of y. The mid-span moment was much more uniformly distributed across the panel width than was the end moment. Consequently it was not considered worthwhile to plot a large number of graphs.

At mid-span the shear force is, of course, close to zero so that the calculation of derivatives of m was not necessary.

Graphs 6.3.10 - 6.3.14 provide summaries of the data in Appendix B.3. From these graphs further quantities are now obtained as described for model 2.

From the graph of unit moment along the face of the spandrel (Fig. 6.3.12) graphs are constructed showing the transverse distribution of M_A. Such graphs are given in Fig. 6.3.15 for various load levels.

In a similar way graphs of the transverse distribution of the shear force, V_A, are constructed from the unit shear graphs of Fig. 6.3.13. The shear distributions are shown in Fig. 6.3.16.

From the graphs of unit moment at mid-span (Fig. 6.3.14) graphs can be constructed in a similar manner to show the transverse distribution of the total mid-span moment M_m. These graphs are given in Fig. 6.3.17.

Now that the distribution of M_A and of V_A along the face of the spandrel strip are known, these may be used to derive the variation of torque, T, along the spandrel strip. This calculation

was carried out only for design ultimate load. In Fig. 6.3.18, values of the unit moment, m_s, are taken directly from Fig. 6.3.12. Values of the unit shear, v_s, are taken from Fig. 6.3.13 but multiplied by 0.125 (half the width of the spandrel strip). Summation of these quantities gives dT/dy. Then T is obtained by integration together with the condition that T = 0 at mid panel.

Dial gauge readings taken during the vertical load test are recorded in Section B.3.6. Values of angles of twist and slope along the spandrel strip are derived from these readings and are recorded in Section B.3.7. Graphs of the angles of twist are plotted in Fig. 6.3.19 for various load levels. In Fig. 6.3.20, the twist along the spandrel is given for service load and design ultimate load. Since the dial gauges were removed before final failure graphs at this load level were not available.

Readings from the dial gauges below the slab (gauges 29-39) give the slab deflections at several points. It will be seen from Fig. 6.3.21 that the deflections at mid-panel were only very slightly different from the deflections midway between A and B.

A summary of the results in the graphs is given in Summary Table 6.3.1.

Stiffness Tests

For model 3, a more complete series of stiffness tests was carried out than for previous models. Tests were carried out (a) before cracking (i.e. before the commencement of the vertical load test), (b) after extensive cracking (i.e. when the model refused to accept any more load but before final failure), and (c) after a punching shear failure had occurred around column A.

The results for these tests are recorded in Section B.3.8 and graphs of these results are given in Fig. 6.3.22.

Before cracking, only one stiffness test was carried out, namely the application of negative moment to joint A. This is referred to in the graphs as test 1.

After cracking, a negative moment test (test 2) was first carried out. It was then decided to investigate whether there was any marked difference between the stiffnesses as determined

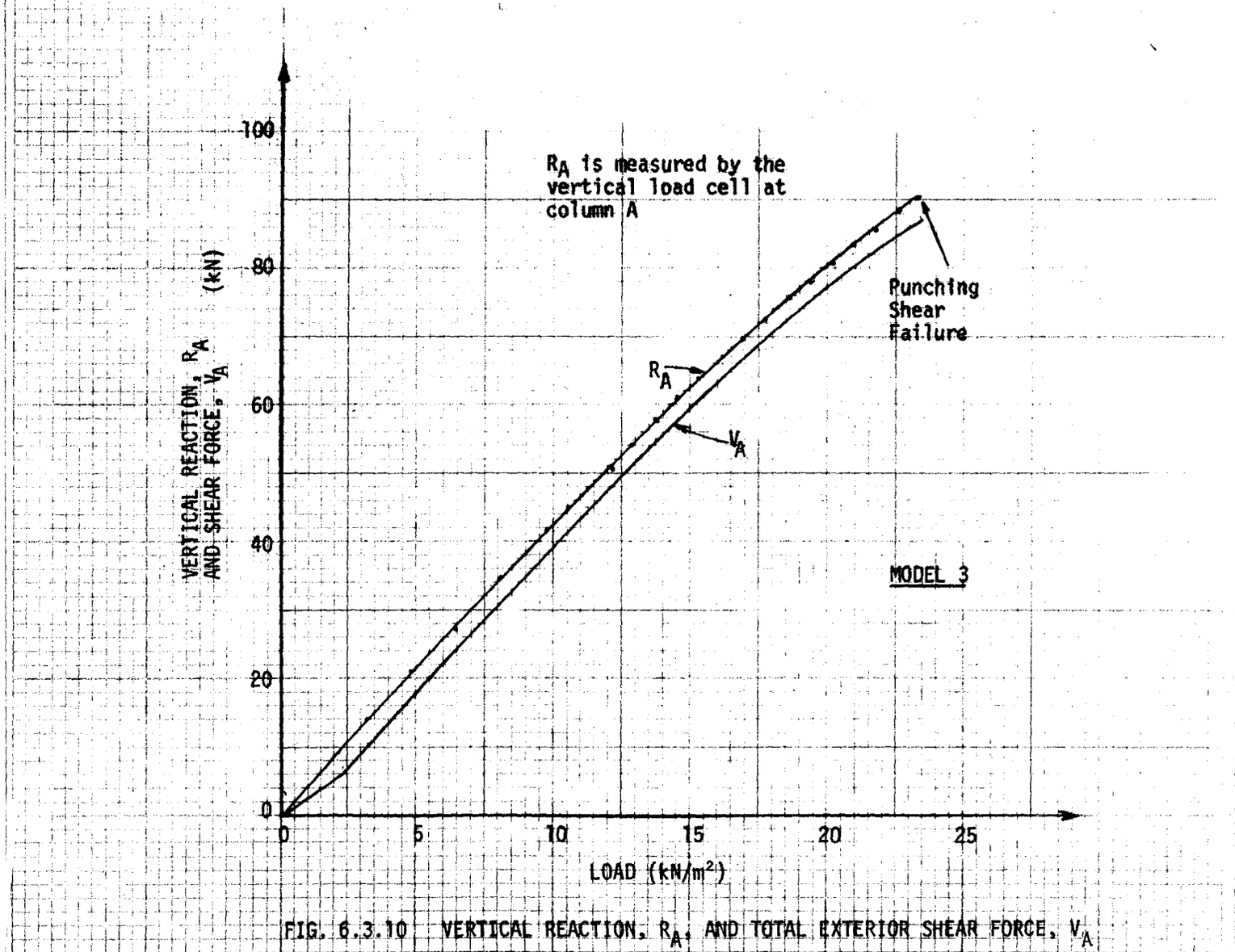

FIG. 6.3.10 VERTICAL REACTION, R_A, AND TOTAL EXTERIOR SHEAR FORCE, V_A

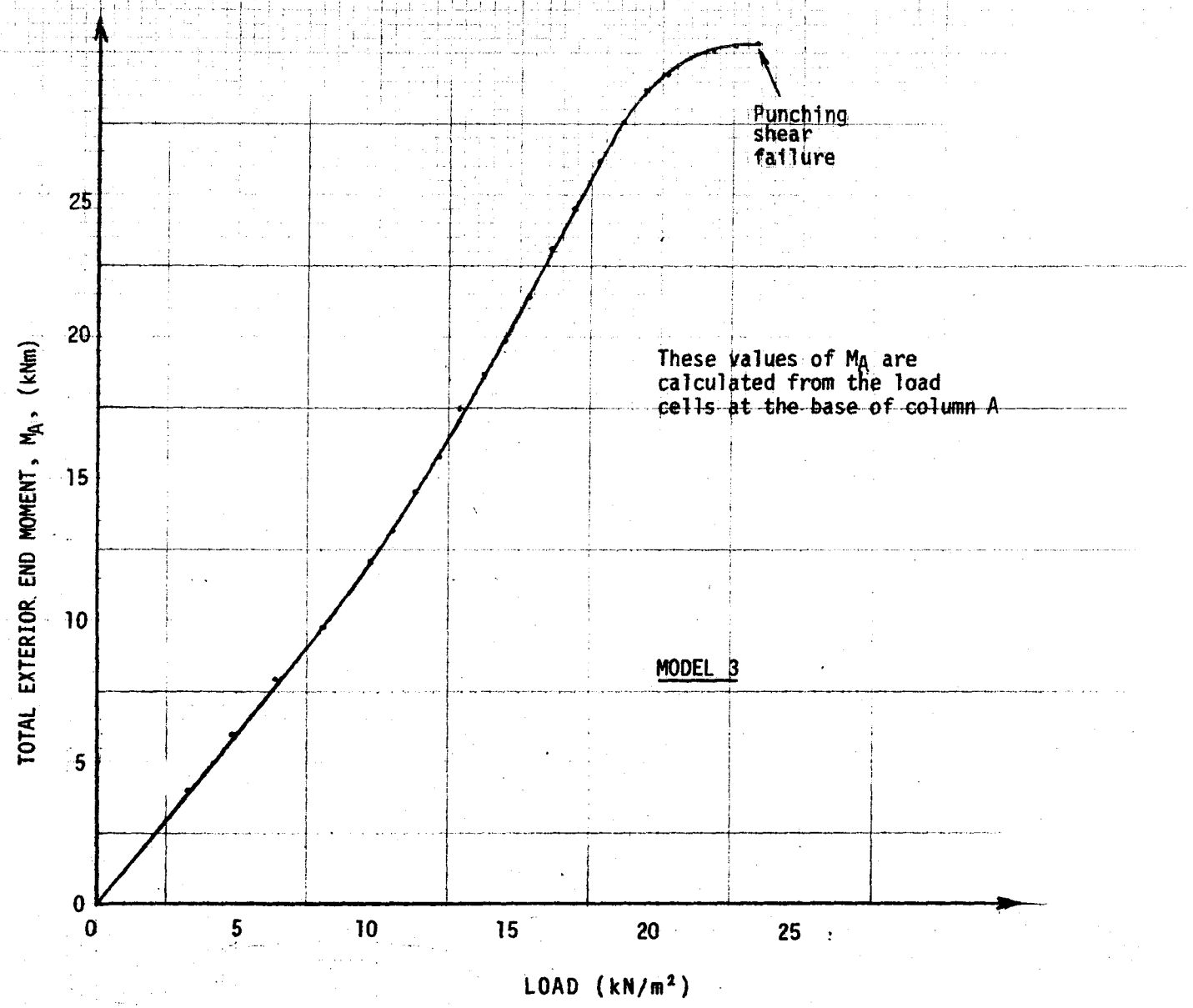

FIG. 6.3.11 TOTAL EXTERIOR END MOMENT M_A

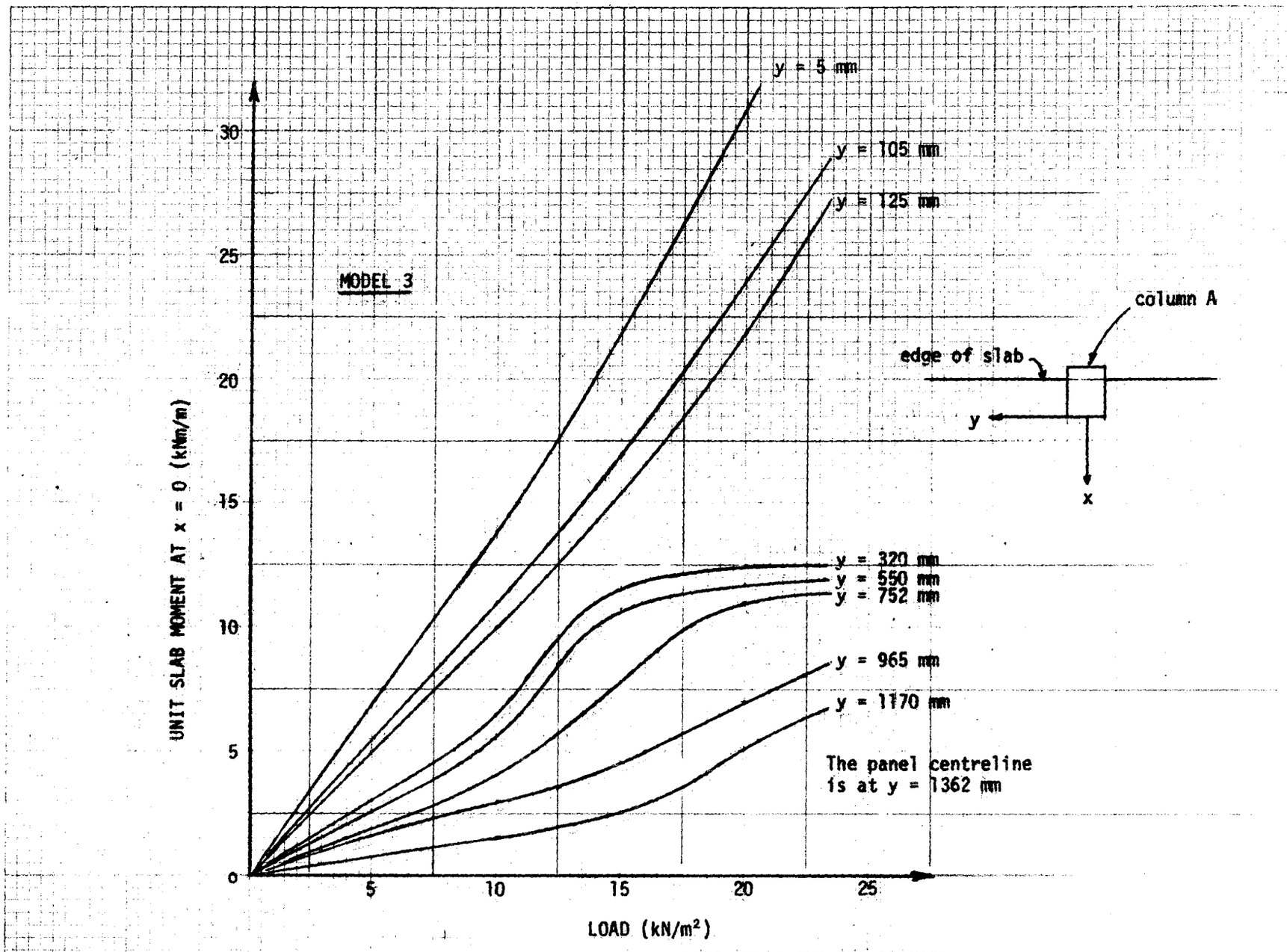

FIG. 6.3.12 UNIT SLAB MOMENT AT VARIOUS DISTANCES ALONG THE SPANDREL

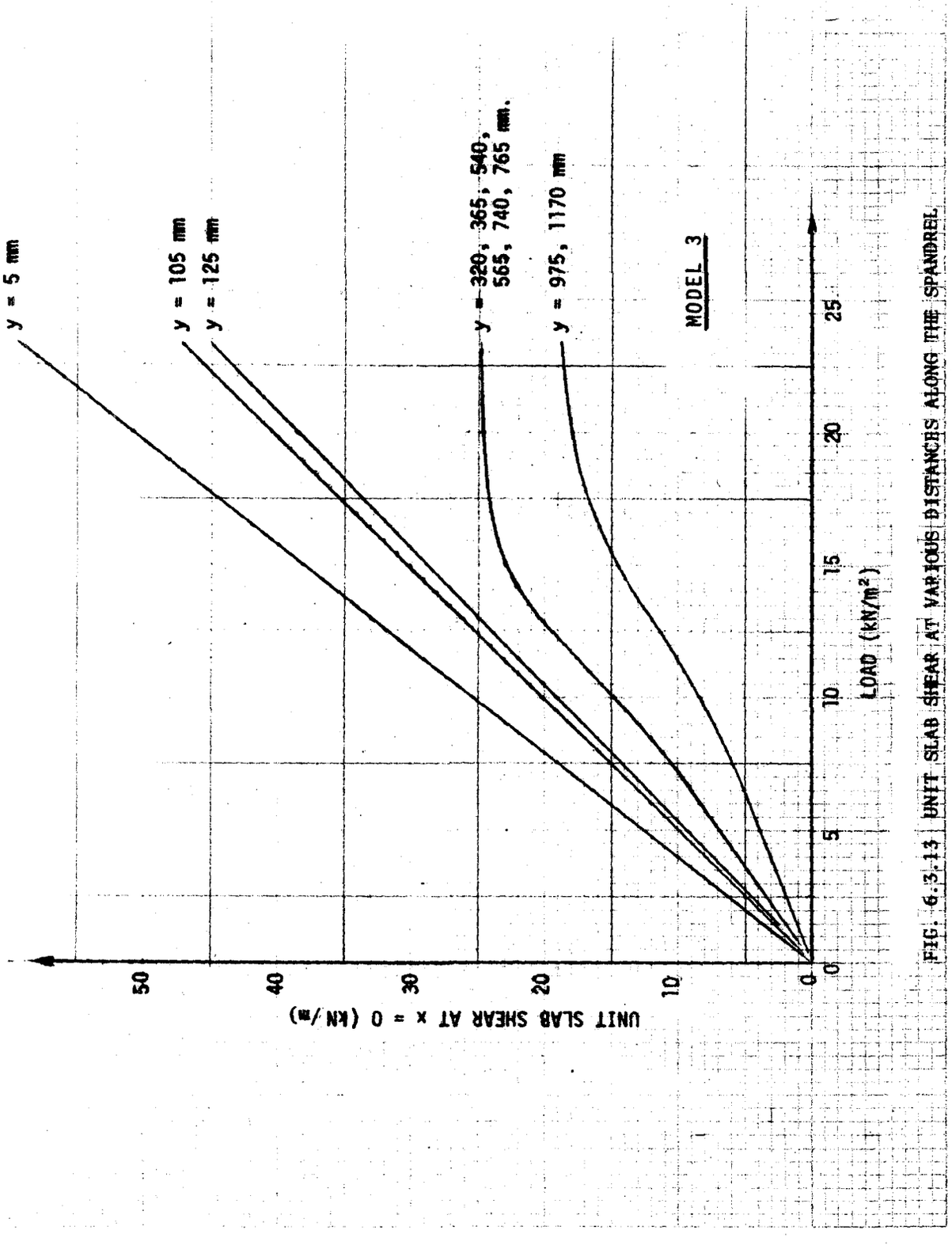

FIG. 6.3.13 UNIT SLAB SHEAR AT VARIOUS DISTANCES ALONG THE SPANDREL

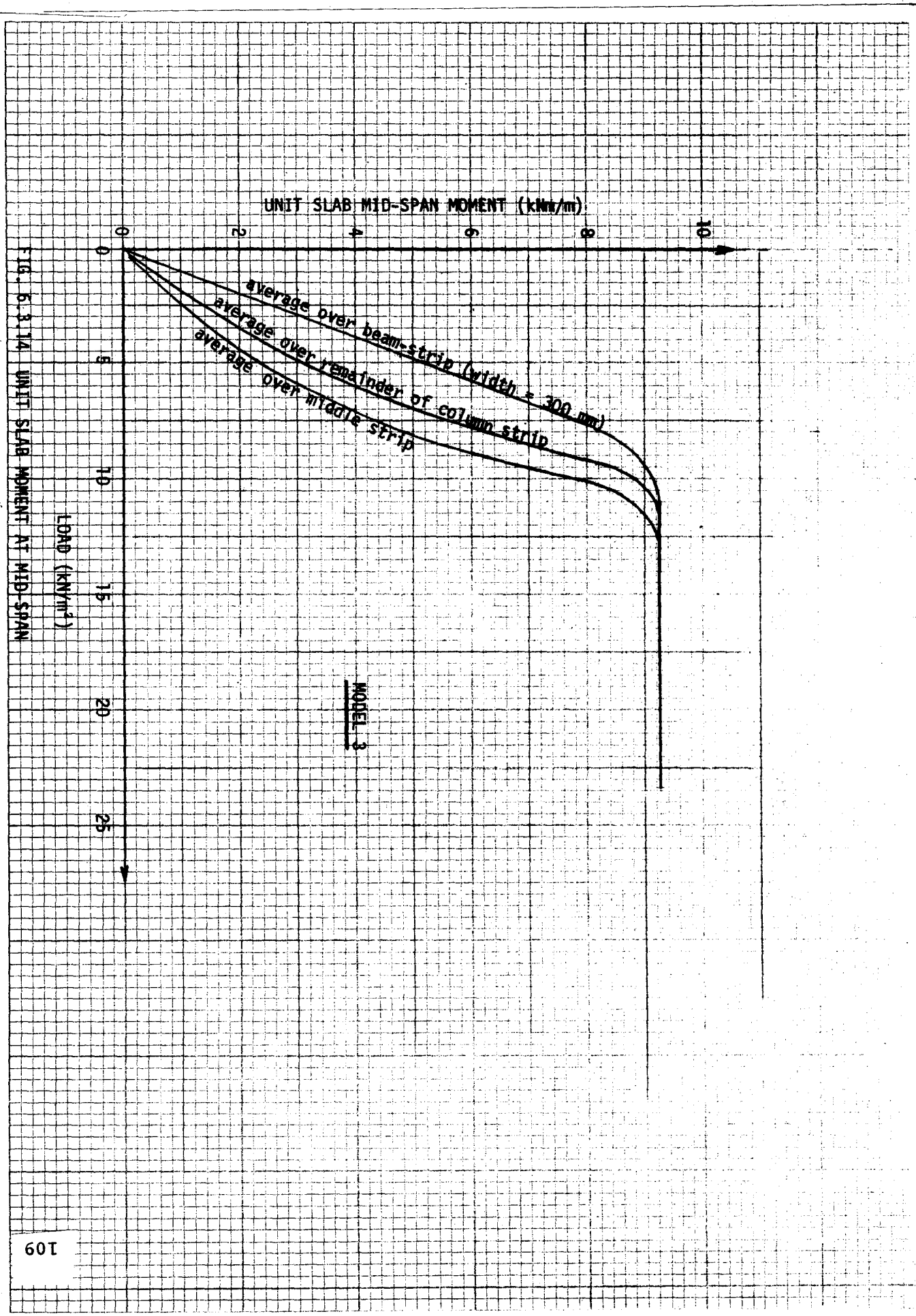

FIG. 6.3.14 UNIT SLAB MOMENT AT MID-SPAN

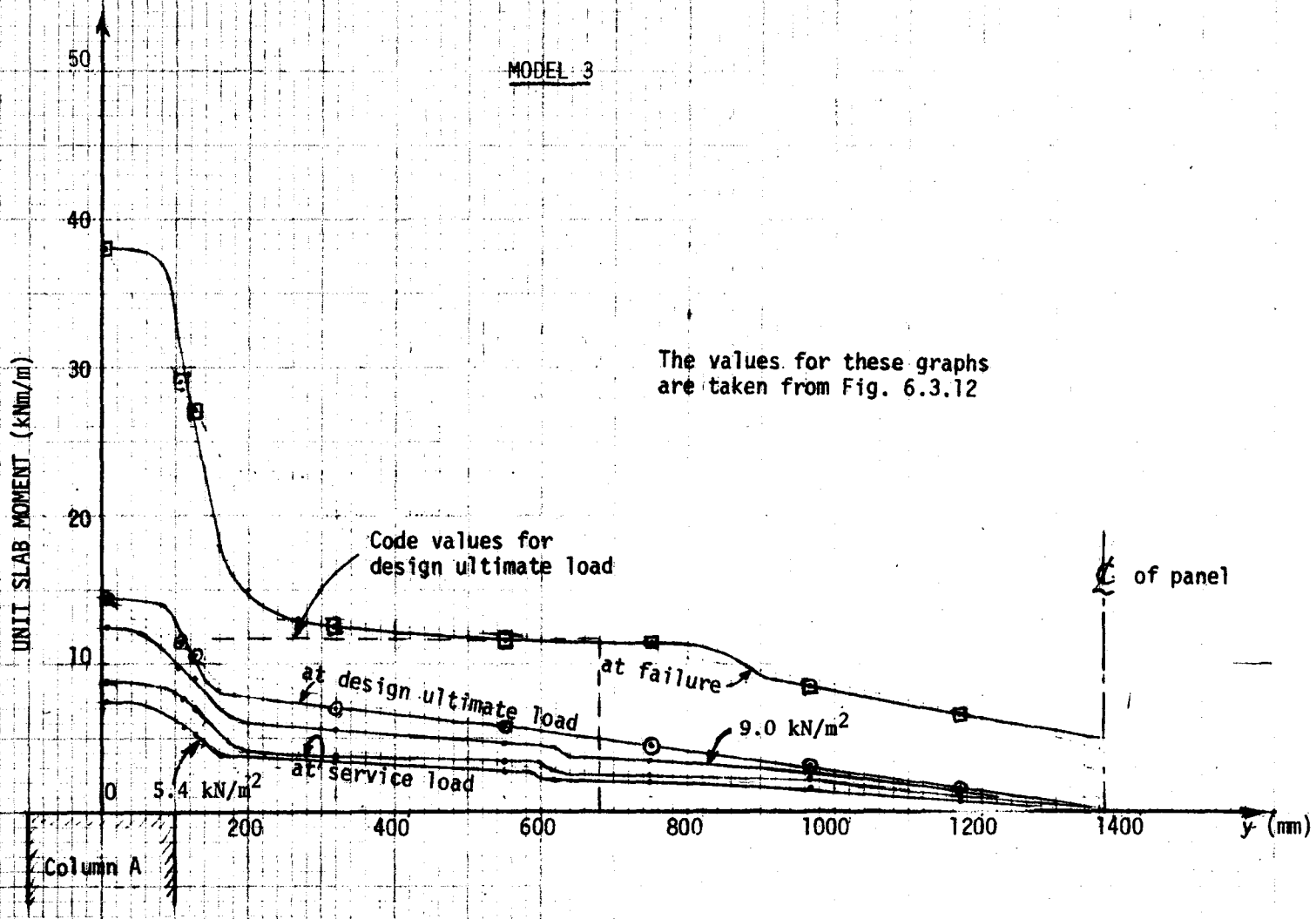

FIG. 6.3.15 TRANSVERSE DISTRIBUTION OF M_A

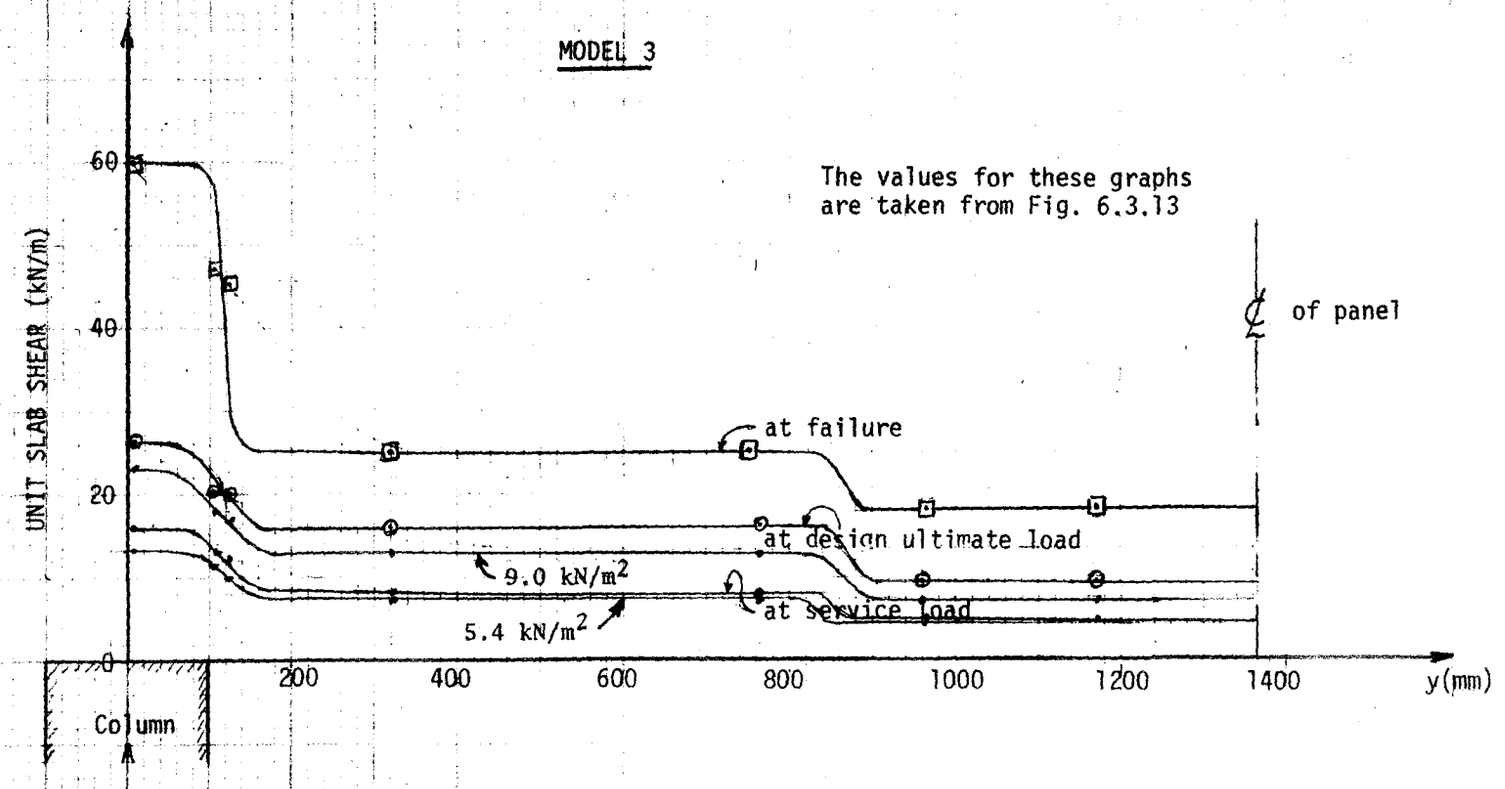

FIG. 6.3.16 TRANSVERSE DISTRIBUTION OF SLAB SHEAR ALONG SPANDREL

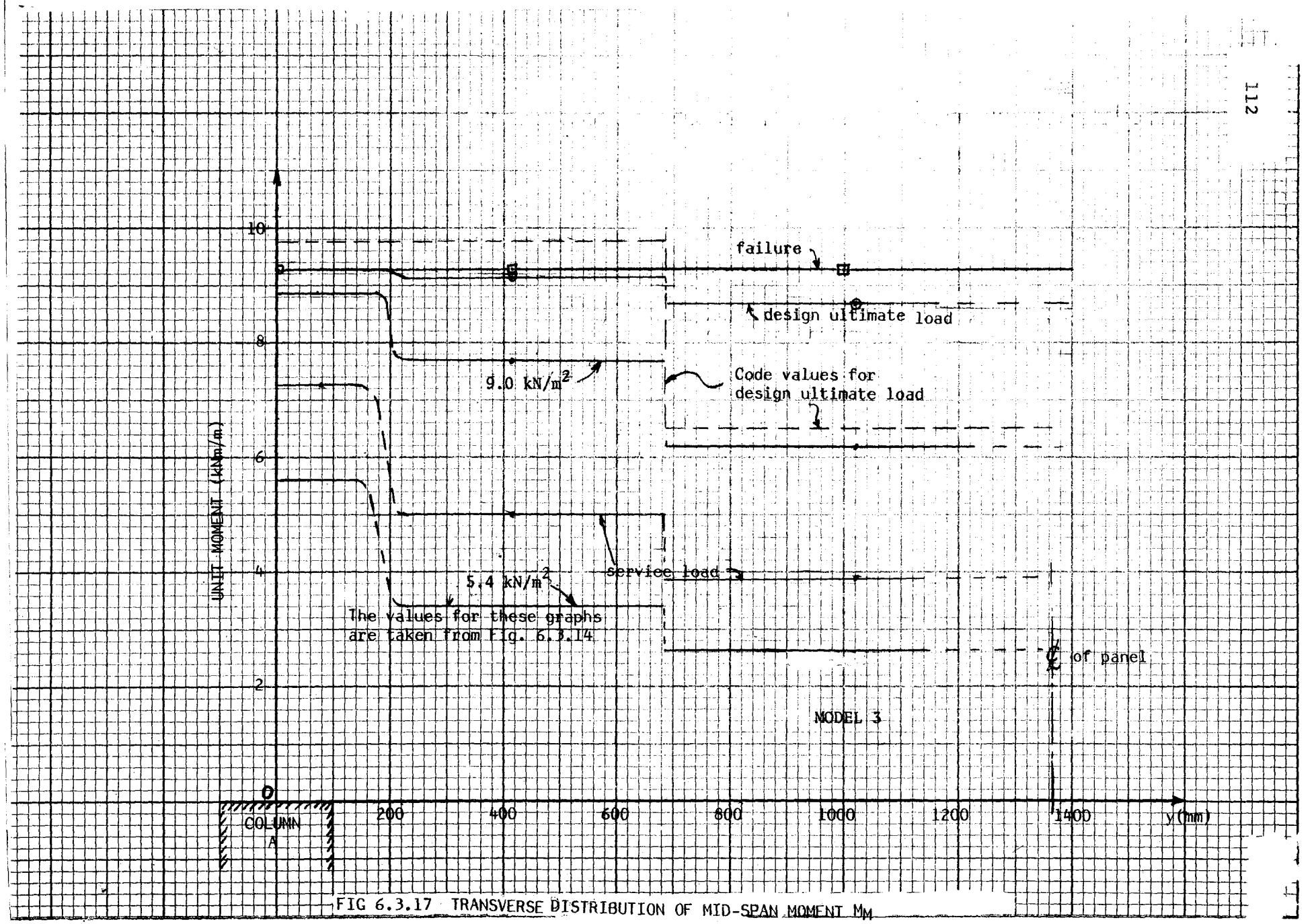

FIG 6.3.17 TRANSVERSE DISTRIBUTION OF MID-SPAN MOMENT M_M

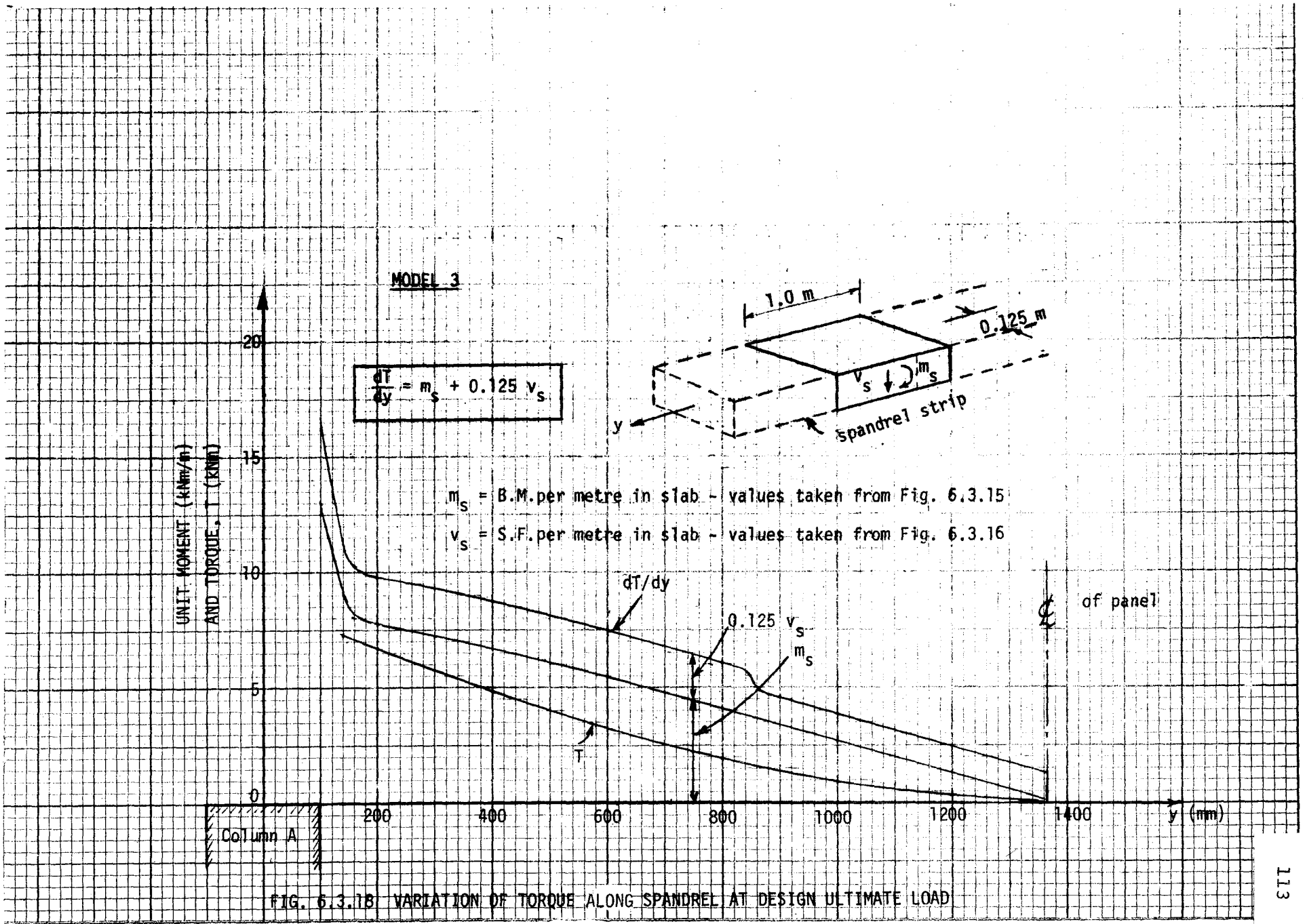

FIG. 6.3.18 VARIATION OF TORQUE ALONG SPANDREL AT DESIGN ULTIMATE LOAD

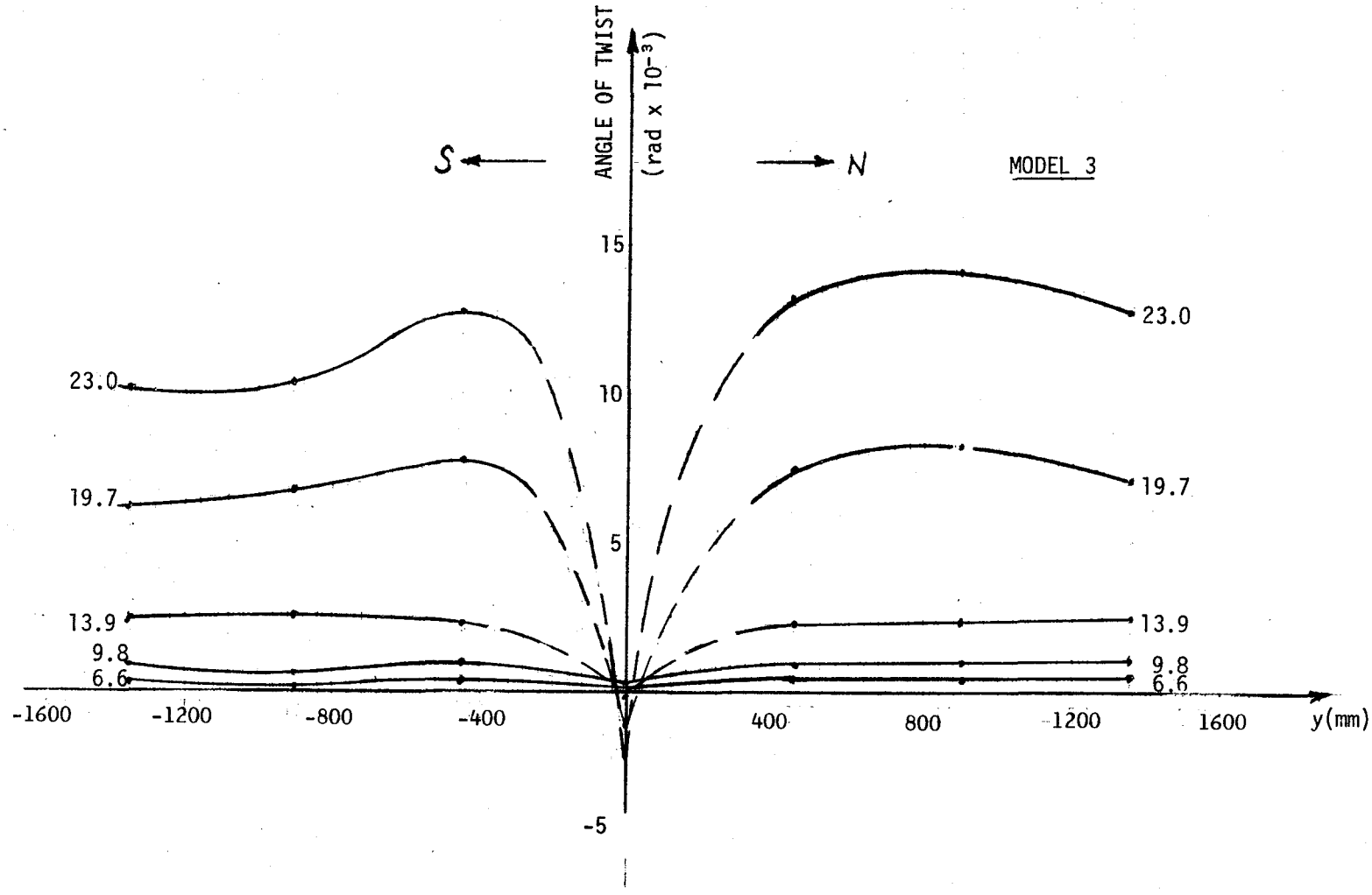

FIG 6.3.19 ANGLE OF TWIST ALONG THE SPANDREL AT VARIOUS LOADS

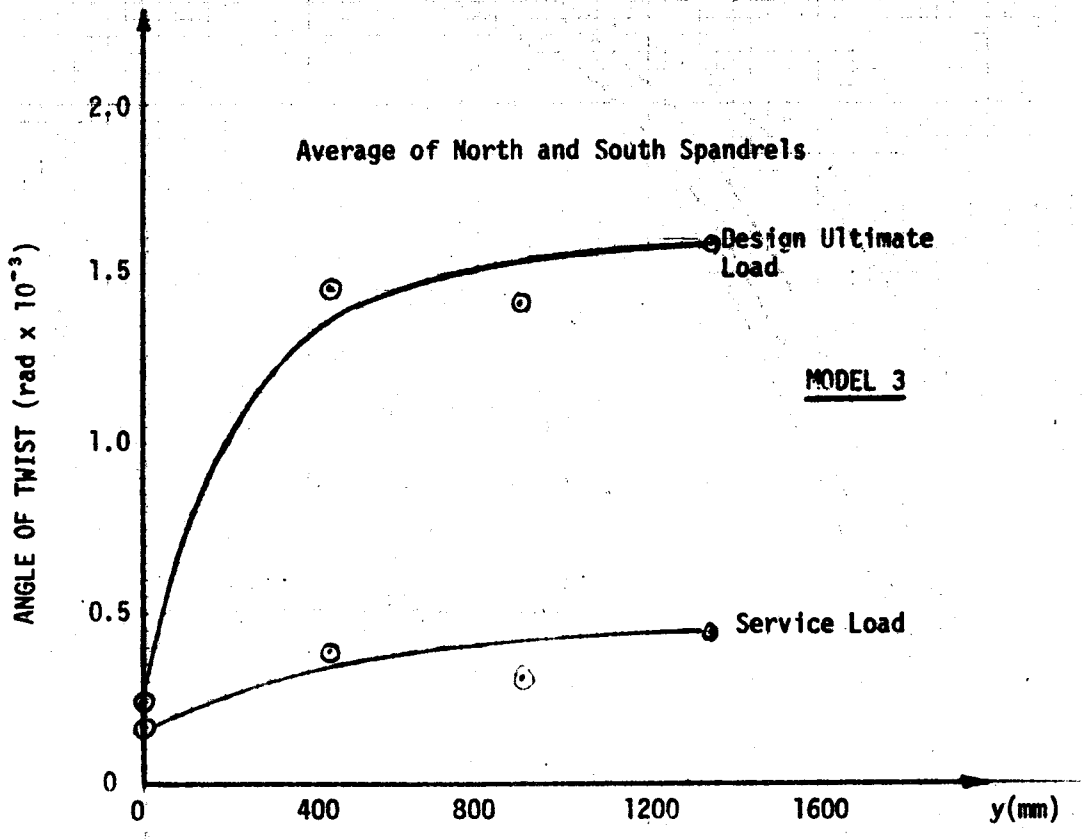

FIG. 6.3.20 ANGLE OF TWIST ALONG SPANDREL

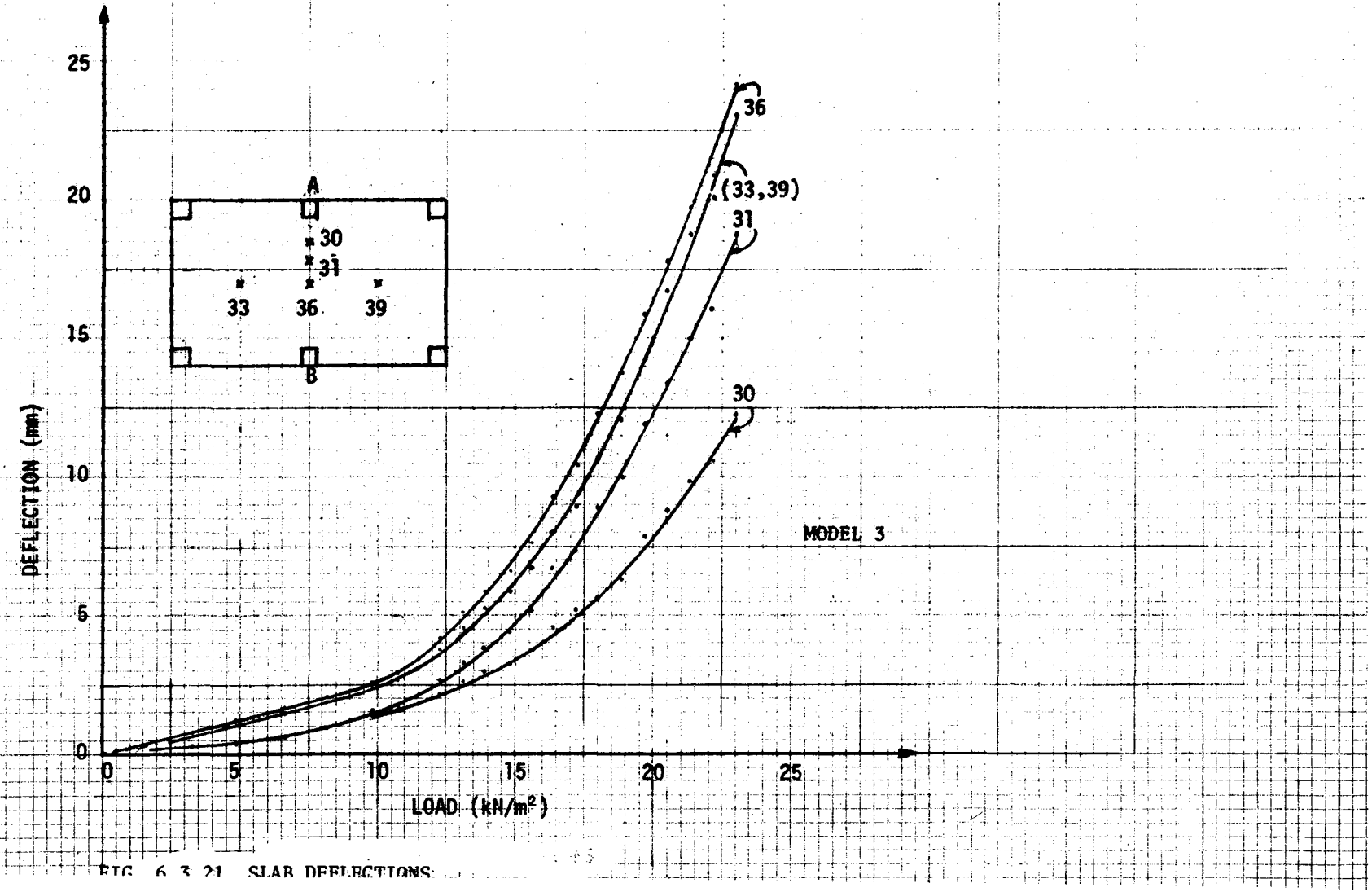

FIG. 6.3.21 SLAB DEFLECTIONS

		k (=M/θ) kNm/rad
1. Uncracked	(-M)	7.5×10^3
2. Cracked	(-M)	1.3
3. Cracked	(+M)	1.5
4. Cracked	(-M after 3)	1.0
5. Failed	(-M)	0.55
6. Failed	(+M)	0.57

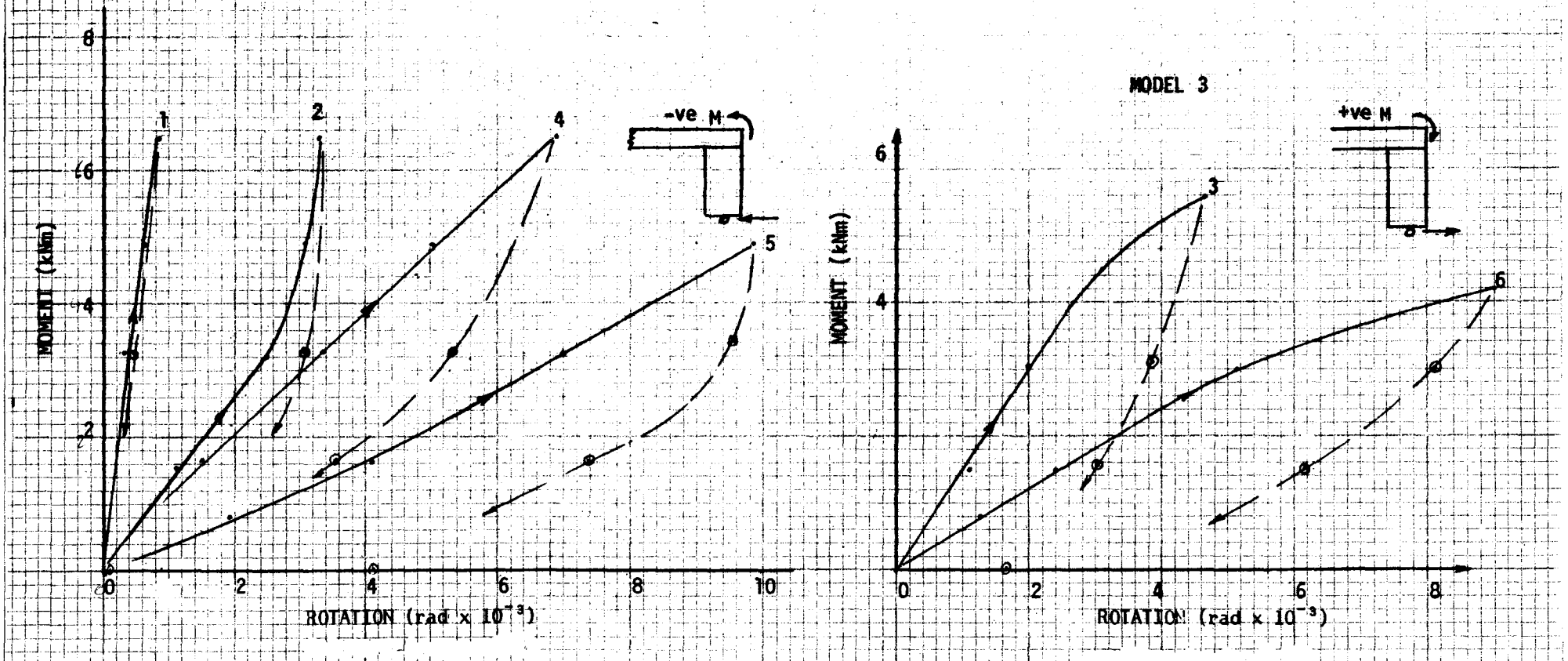

(a) NEGATIVE MOMENT

(b) POSITIVE MOMENT

FIG. 6.3.22 ROTATION STIFFNESS OF JOINT A

MODEL No. 3

TABLE 6.3.1 SUMMARY OF RESULTS OF VERTICAL LOAD TEST

Service Load = 7.0 kN/m²
Design Ultimate Load = 11.4 kN/m²
Failure Load = 23.8 kN/m²

Item	Load Level (kN/m^2)	Test Value
1. Vertical Reaction at A = R_A (kN)	5.4 9.0 22.5	23.5 38.2 88.2
2. Vertical Reaction at B = R_B (kN)	5.4 9.0 22.5	
3. Total Mid-Span Moment = M_M (kNm)	5.4 9.0 22.5	(8.8) (19.3) (25.2)
4. Total Moment at face of Spandrel A = M_A (kNm)	5.4 9.0 22.5	6.4 (7.2) 11.0 (12.5) 30.3 (33.3)
5. Total Shear Force at Face of Spandrel A = V_A (kN)	5.4 9.0 22.5	19.6 (18.0) 35.0 (31.0) 84.5 (69.1)
6. Total Moment at Face of Spandrel B = M_B (kNm)	5.4 9.0 22.5	
7. Total Shear Force at Face of Spandrel B = V_B (kN)	5.4 9.0 22.5	
8. Transverse Distribution of Mid-Span Moment M_M		See Fig. 6. 3.17
9. Transverse Distribution of M_A		See Fig. 6. 3.15
10. Transverse Distribution of M_B		

* Values in brackets are obtained from strain gauge readings by integration. Other values are obtained from load cells.

Item	Load Level (kN/m^2)	Test Value
11. Distribution of Torque along Spandrel A	design ultimate load	See Fig. 6.3.18
12. Torque in Spandrel A at Face of Column A (kNm)	design ultimate load	7
13. End Moment in Beam Strip at Face of Column A (kNm)	5.4 9.0 22.5	(1.9) (3.7) (8.9)
14. Shear Force in Beam Strip at Face of Column A (kN)	5.4 9.0 22.5	(3.4) (5.8) (14.7)
15. Shear Force in Spandrel at Face of Column A (kN)	5.4 9.0 22.5	
16. Distribution of Torque along Spandrel B	design ultimate load	
17. Torque in Spandrel B at Face of Column B (kNm)	design ultimate load	
18. End Moment in Beam Strip at Face of Column B (kNm)	5.4 9.0 22.5	
19. Shear Force in Beam Strip at Face of Column B (kN)	5.4 9.0 22.5	
20. Shear Force in Spandrel at Face of Column B (kN)	5.4 9.0 22.5	
21. Mid-span Moment in Beam Strip (kNm)	5.4 9.0 22.5	(1.6) (2.5) (2.6)

MODEL No. 3

TABLE 6.3.2 - SUMMARY OF RESULTS OF STIFFNESS TESTS

	Condition of Model		
	Uncracked	Cracked	Severely Cracked
Stiffness of Joint A = k_A (kNm/radian)	7.5×10^3	1.3×10^3	0.55×10^3
Carry-over factor from A to B = c_{BA}			
Stiffness of Joint B = k_B (kNm/radian)			
Carry-over factor from B to A = c_{AB}			

for negative and for positive moment. Hence test 3 was carried out with a positive moment applied. Test 4 was carried out with a negative moment again to see if the application of the positive moment had changed the slab characteristics.

After failure two tests were carried out - test 5 with negative moment and test 6 with positive moment.

The stiffness values, k, determined from these graphs are also indicated in Fig. 6.3.22. Compared with the difference in k caused by cracking or by slab failure, the difference as determined by positive or negative moment is relatively insignificant. It was therefore decided that in future models only tests with negative moment would be carried out. The stiffness values are summarized in Table 6.3.2.

As mentioned earlier, the stiffness values determined from this test are not directly applicable to analysis since it was not possible in the test to simulate the condition of full fixity at joint B. The test values are indicative, however, of the percentage reduction which might be expected as a result of extensive cracking in the slab.

It was decided that in the next model an attempt would be made to measure true stiffness and carry-over factors as used in analysis.

6.4 MODEL 4

Design

The overall dimensions of model 4 were generally the same as those of model 3. There were, however, several differences between the models.

In the first place, the reinforcement of slab 3 was the same as that in slabs 1 and 2, since the objective in these models was to determine the effect of removing the floor beam and the spandrel beam respectively. As a consequence of this procedure, the slab of model 3 was not reinforced in accordance with AS 1480. It was felt that a slab designed strictly according to AS 1480 should be tested. This would also indicate whether the behaviour of the slab is influenced in any way by minor variations in the reinforcement.

In model 4 it was decided to measure the reactions at column B as well as those at column A. This involved building, at column B, a large hollow concrete pedestal similar to the one at A (see Section 4.6) and providing a set of five rocker arms, one vertical and four in the horizontal plane.

It was also decided that to some extent the model might be used as a 'double-sided' model. Hitherto, the eastern side had been regarded as the edge of the building, with column A as an 'exterior' column. Column B was an 'interior' column and an attempt had been made to make some allowance for those floor panels which were not included in the model. However it seemed likely that the edge conditions at B had only a very minor effect on the moments around column A. To the extent that this effect could be ignored it would then be possible to regard the western side as the edge of the building, with column B as the 'exterior' column and column A as the 'interior' column.

Side A would represent the case of no spandrel beam, while side B would represent the case of a building with a fairly shallow spandrel beam.

Details of the design of model 4 are given in Appendix A, Section A.4. The dimensions of model 4 are given in Fig. 6.4.1.

Peinforcement

Details of the reinforcement in model 4 are given in Fig. 6.4.1.

Strain Gauges

More strain gauges were used in this model than in previous models. For each top slab bar (in the EW direction) three strain gauges were attached at end A and three at end B. These gauges provided a moment profile for the slab strip adjacent to its junction with the spandrel strip at end A (the eastern side of the model) and also adjacent to its junction with the beam at end B (the western side of the model).

For each bottom bar in the EW direction, two gauges were attached at mid-span. It was not necessary to measure the variation

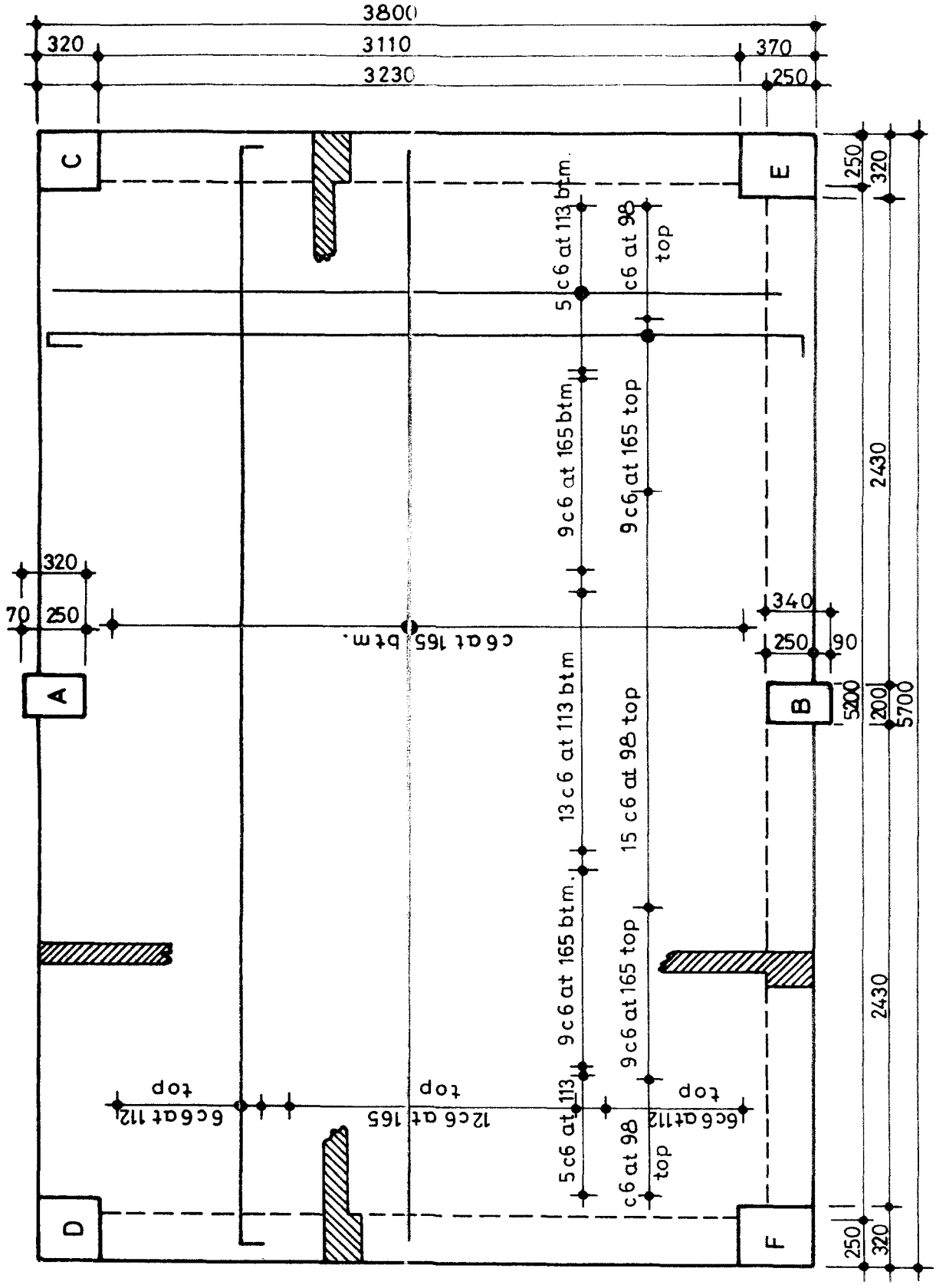

Fig. 6.4.1 (a) Reinforcement Details for Model 4.

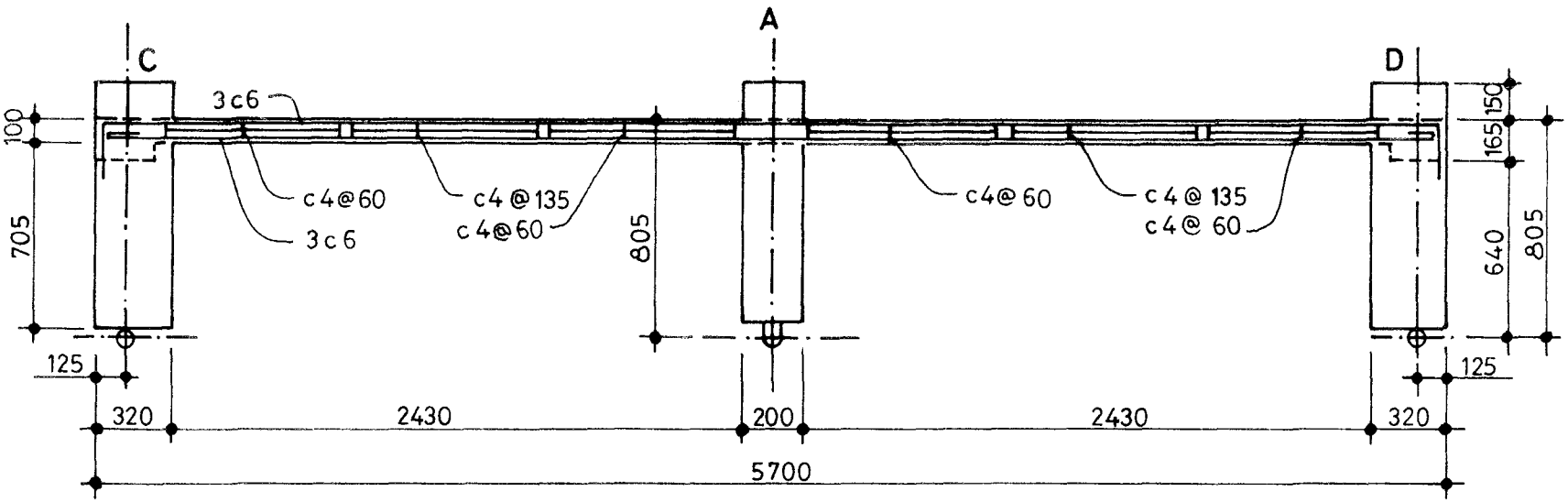

Spandrel beam view

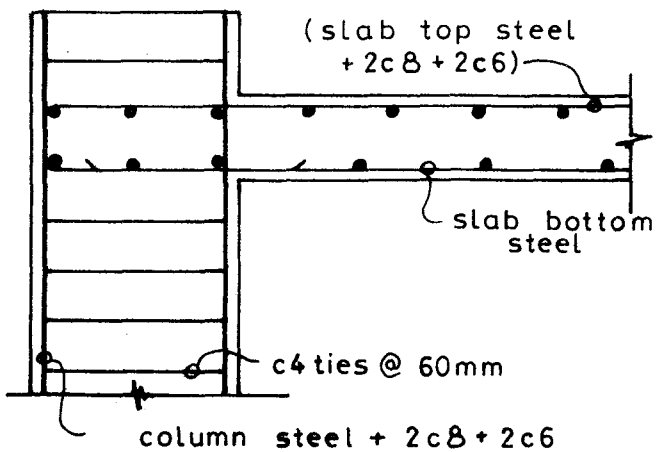

JOINTS A & B

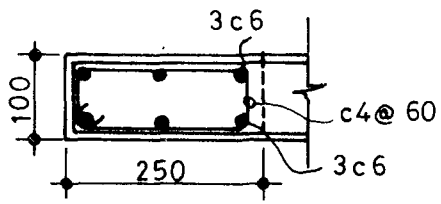

Spandrel at column A

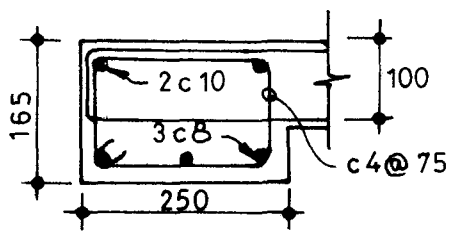

Spandrel at column B

Fig. 6.4.1 (b) Reinforcement Details for Model 4.

of moment at this location, so theoretically one gauge per bar would have been sufficient. Two were used in case of malfunction of one gauge.

As before, gauges were provided on the longitudinal (NS) bars in the spandrel strip at the eastern side. But in this model, similar gauges were also provided to the longitudinal bars in the beam along the western edge.

Details of the location of all gauges are given in Section B.4.1 of Appendix B.

Dial Gauges

The dial gauge layout for this model was generally the same as for model 3. Two extra dial gauges, 41 and 42, were provided at joint B in order that the rotation of this joint could be measured during stiffness tests.

The location of the dial gauges is given in Sections B.4.2 and B.4.3 of Appendix B.

Concrete

At the time of the vertical load test, the concrete compressive strength was 28 MPa.

Vertical Load Test

Cracks appeared in the top of the slab at the faces of columns A and B at a load of 5 kN/m^2. Bottom cracks appeared at midspan at 8 kN/m^2. The yield moment at midspan was only slightly greater than the cracking moment because of the light reinforcement at midspan. For this reason, the midspan moment reached its yield value shortly afterwards.

At 11.5 kN/m^2 radial top cracks occurred around column A. At 13.2 kN/m^2 a top crack along the line AB started from the ends. As in model 3, torsion cracks appeared in the top of the spandrel strips close to the column faces.

At 22.5 kN/m^2 the model refused further load, and the vertical load test was interrupted in order to carry out a stiffness test (see below). Vertical loading was then resumed with increase in

deformation. The torsion cracks in the spandrel strips near column A widened and eventually a punching shear took place.

The longitudinal steel in the spandrels at A reached yield whereas the steel in spandrels B did not. The longitudinal spandrel steel at B reached a stress of approximately 220 MPa.

Figs. 6.4.4 and 6.4.5 are photographs of top and bottom cracks respectively. Torsion cracking in the spandrel is shown clearly in Fig. 6.4.4. Fig. 6.4.6 shows cracking in the top near corner column D. Clearly torsion is present in this region. Figs. 6.4.8 and 6.4.9 are diagrams of the top and bottom cracking respectively.

Load cell readings for this test are given in Section B.4.4. A graph of the reaction at A is given in Fig. 6.4.10. Also shown in this graph is the shear V_A at the face of the spandrel strip. For this model

$$V_A = R_A - 2.7 \text{ kN}$$

From the load cell readings, the value of M_A is derived.

$$M_A = (E-W)0.760 - R_A\ 0.125$$

Values of M_A are plotted in Fig. 6.4.11.

Strain gauge readings for this model are recorded in Section B.4.5.

Unit negative moments and unit shears along the face of the spandrel were obtained as in previous models and are plotted in Figs. 6.4.12 and 6.4.13 respectively. Fig. 6.4.14 shows unit midspan moments at various distances y from the line AB.

From the foregoing graphs, the lateral distribution of M_A, V_A and M_m are obtained and are plotted in Figs. 6.4.15, 6.4.16 and 6.4.17. The distribution of torque T along the spandrel is obtained from Figs. 6.4.12 and 6.4.13 and plotted in Fig. 6.4.18.

In this model, for the first time, data regarding the moments and shears at end B were also obtained. These data, and information derived therefrom, are summarized in Figs. 6.4.23 - 6.4.29 in a manner similar to that used for the end A.

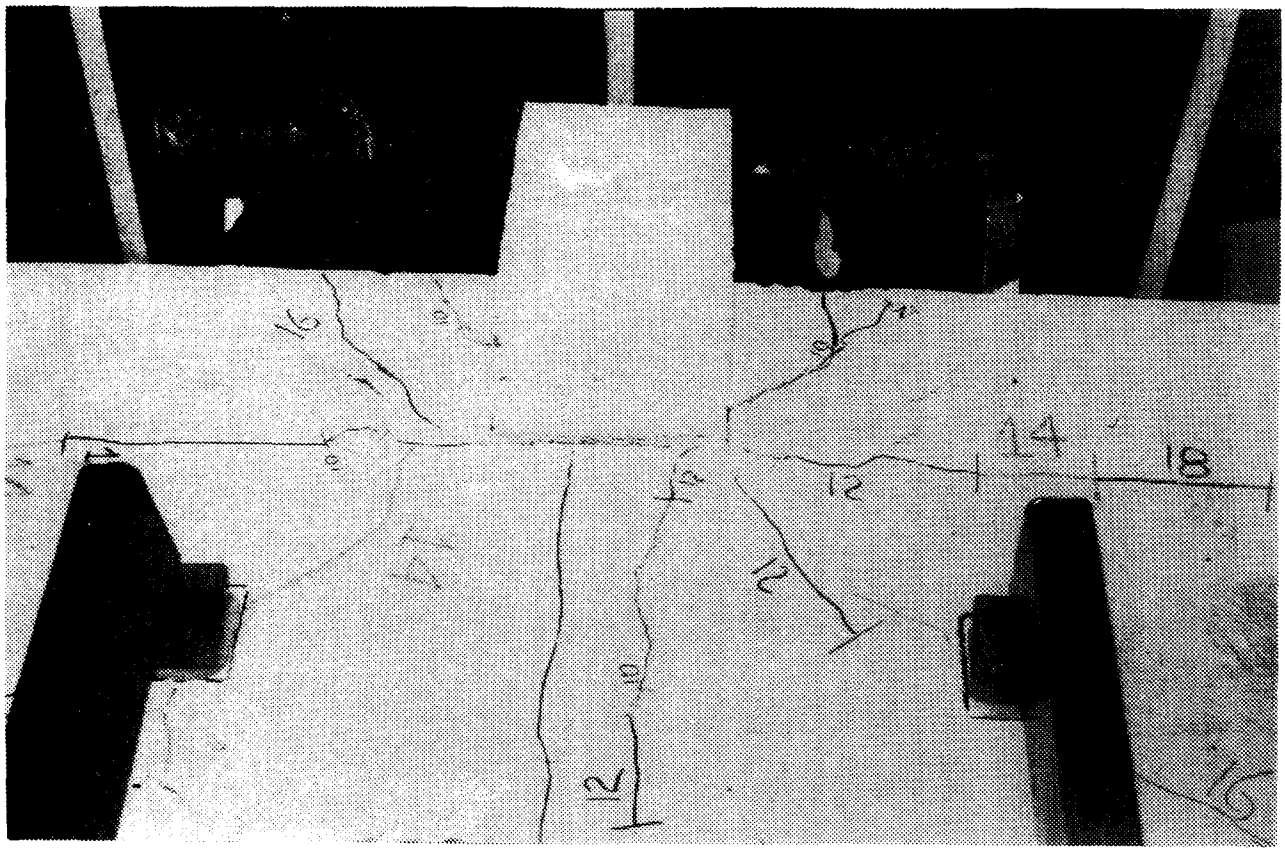

Fig. 6.4.4 Cracks in Top of Slab

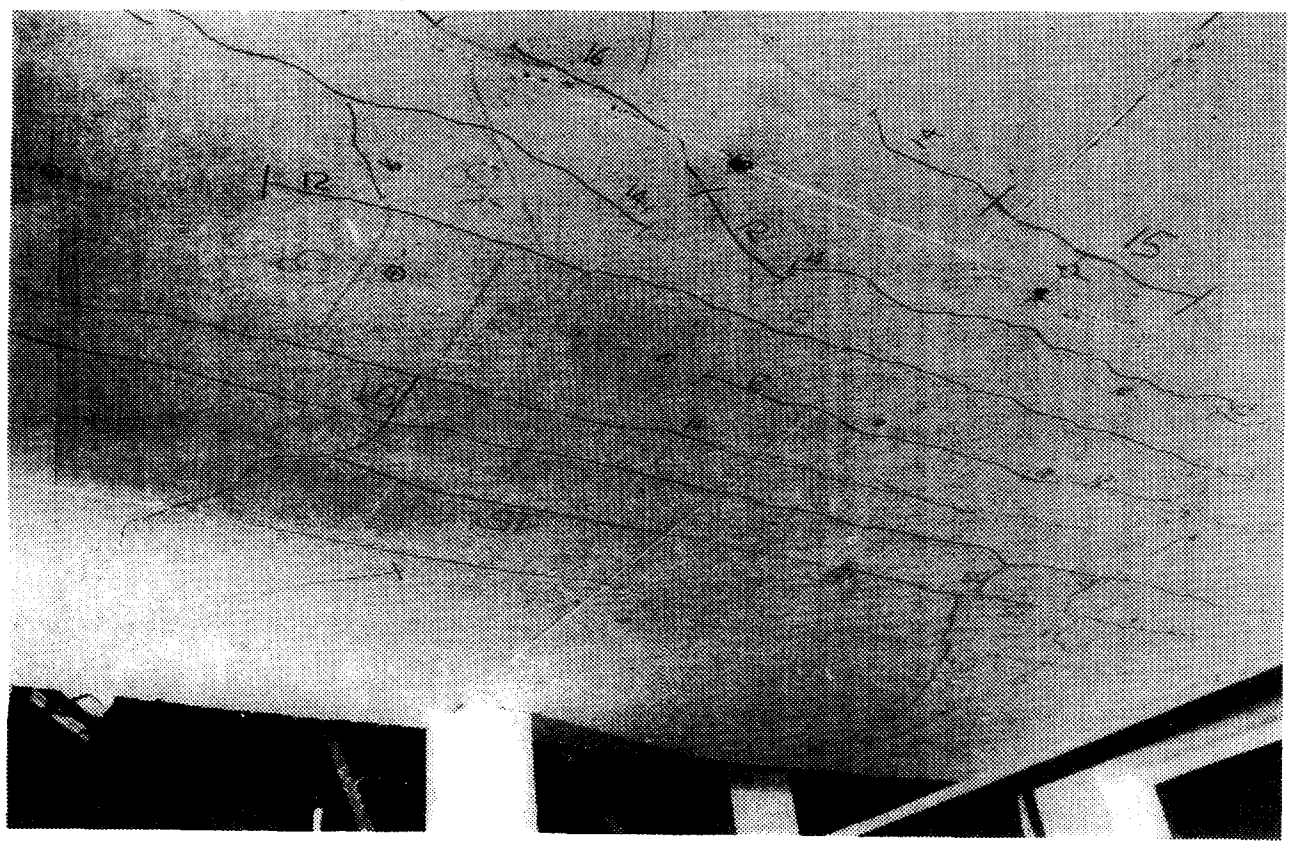

Fig. 6.4.5 Cracks on Underside of Slab

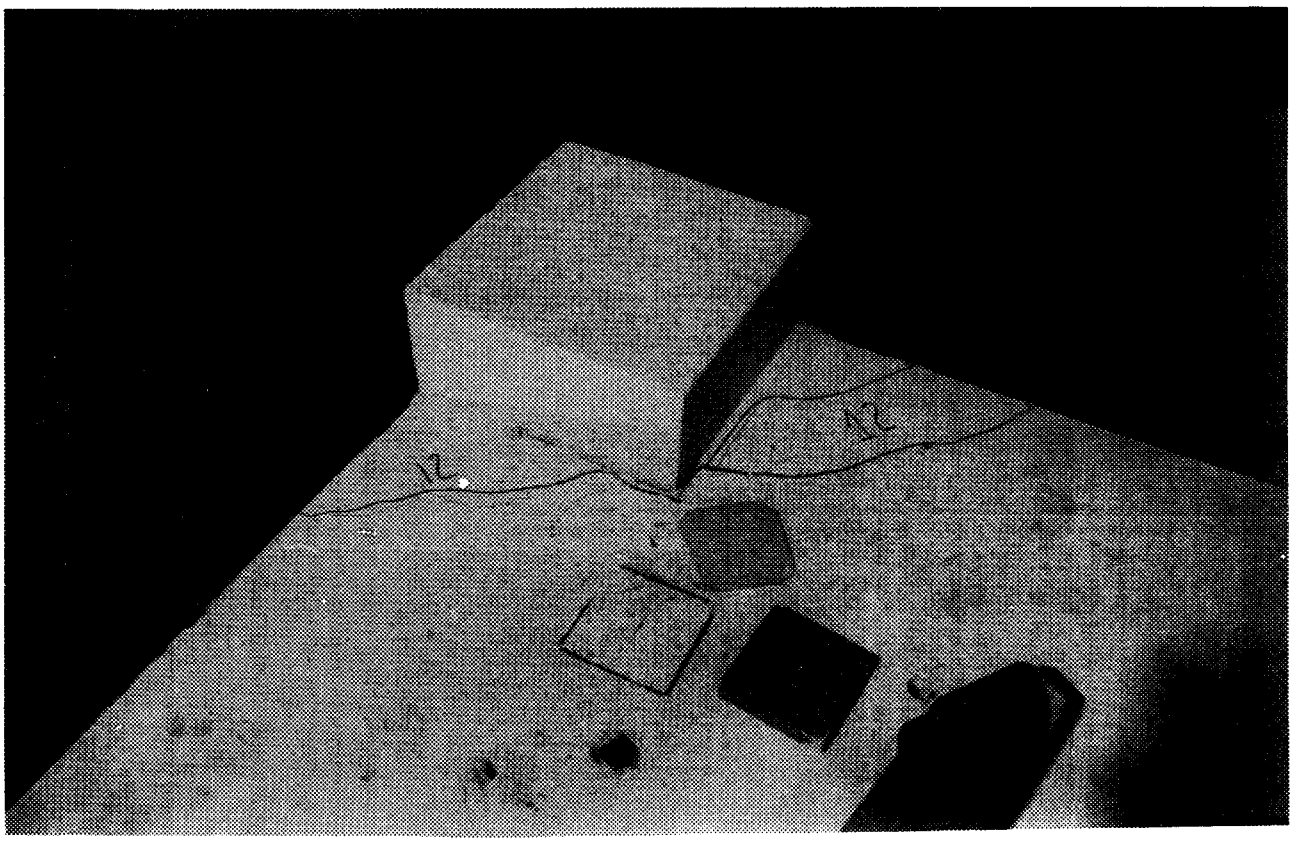

Fig. 6.4.6 Torsion Cracks near Corner Column

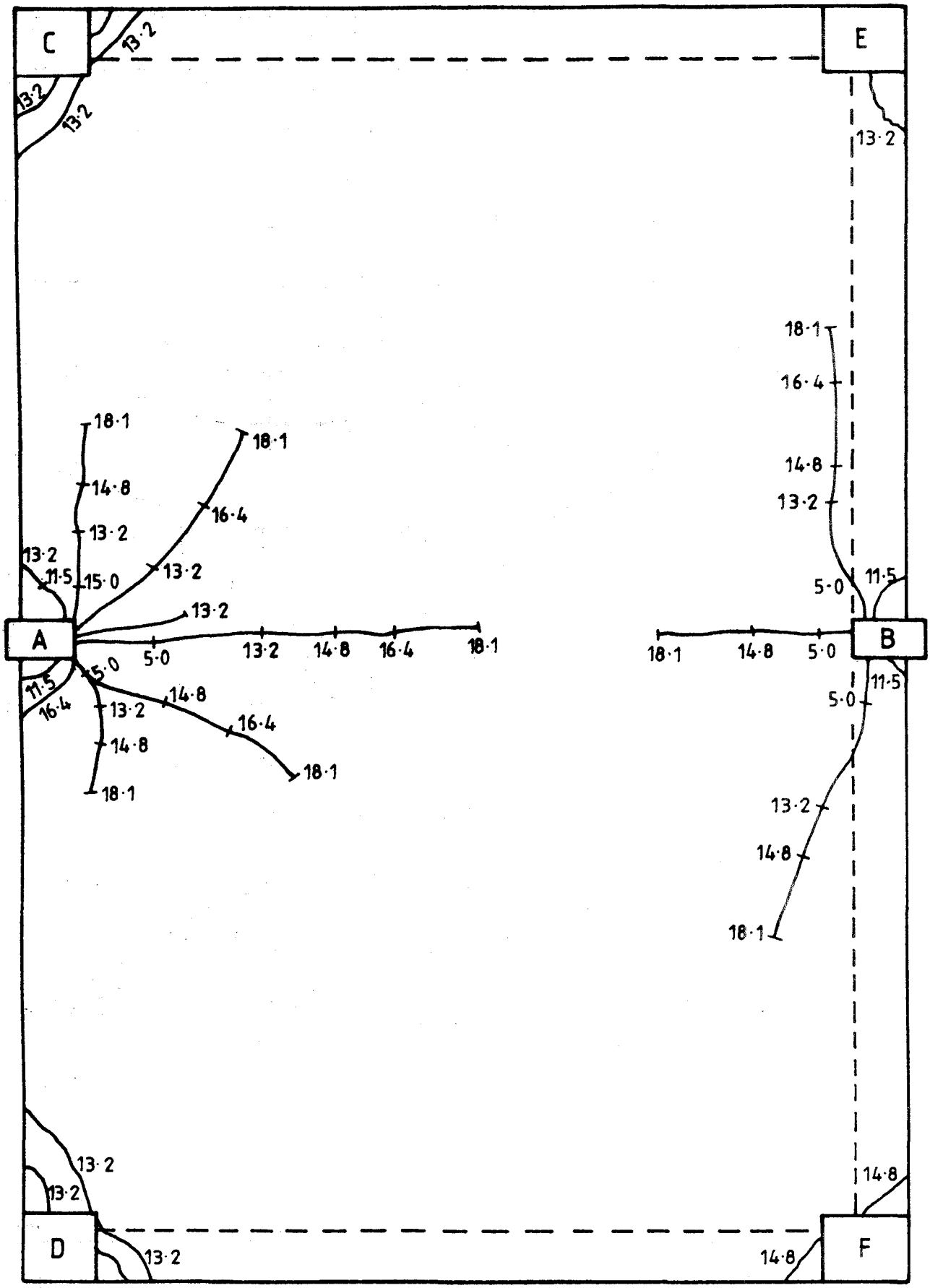

(NUMBERS ON THE CRACKS ARE LOAD IN kN/m²)

Fig. 6.4.8: Crack Pattern on the Top of Model 4

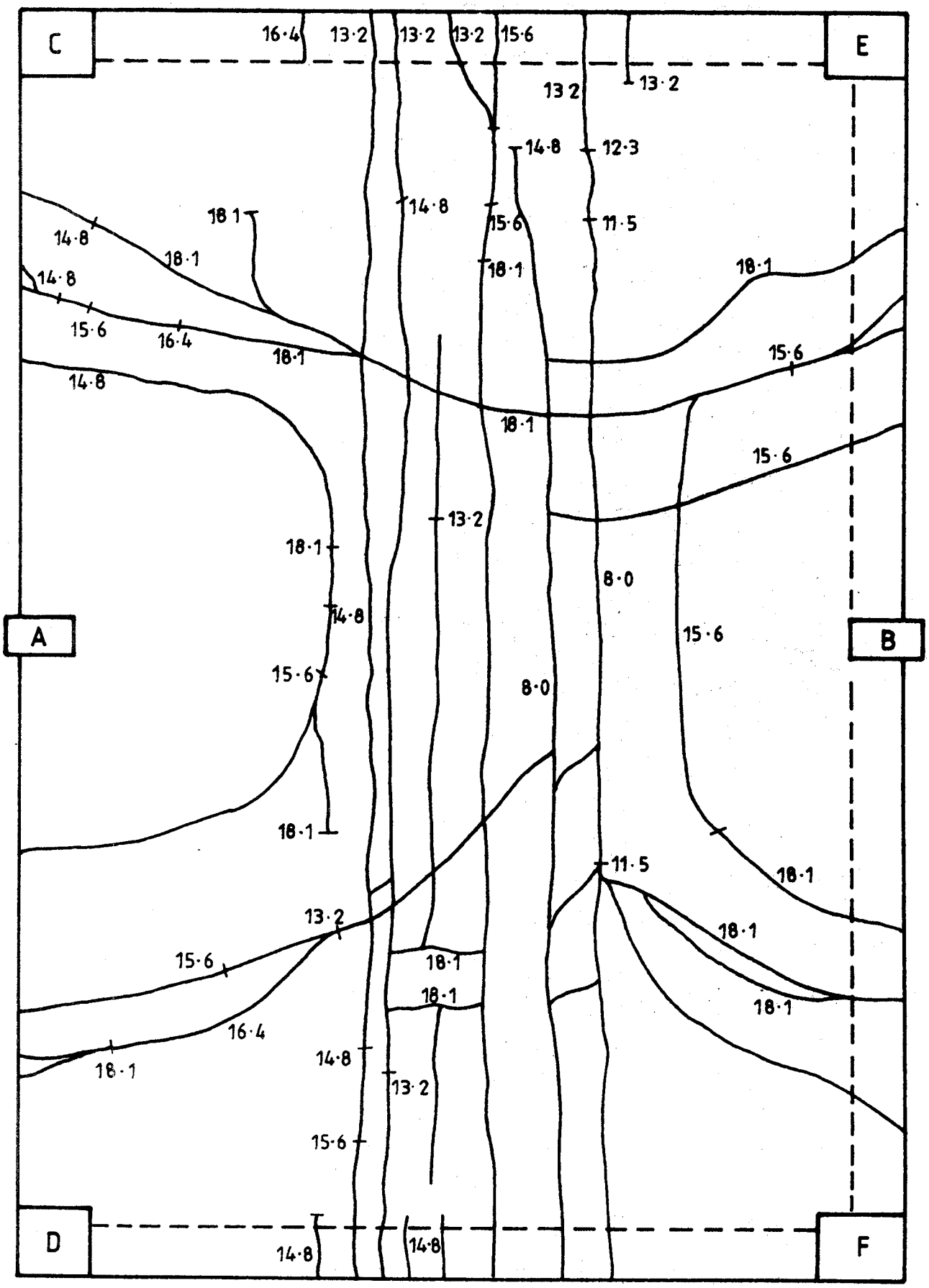

(NUMBERS ON THE CRACKS ARE LOAD IN kN/m^2)

Fig. 6.4.9: Crack Pattern on the Bottom of Model 4

Dial gauge readings are recorded in Section B.4.6. Figs. 6.4.19 and 6.4.20 show the variation of the angle of twist along the spandrel. Fig. 6.4.21 shows slab deflections at the various locations.

The results depicted in these various graphs are summarized in Table 6.4.1.

Boundary Condition Test

It was intended in this model to carry out a boundary condition test as described in Section 5.8. A test of this sort was carried out for model 1, and showed that moments applied at the artificial boundary (the western, southern and northern edges) had a negligible effect around column A. However model 1, which contained beams, was extremely stiff. It was considered desirable to repeat the tests on a flat plate model.

Unfortunately, experimental problems prevented the carrying out of these tests as planned. Instead of the applied edge moment being distributed along the edges, it was only possible to apply concentrated moments at the corners. A moment was applied at corner D in a N-S direction and at corner F in both the N-S and the E-W directions. Strain readings in the region around A were extremely small, which suggested that the adopted boundaries were satisfactory.

It was decided to make provision for the distributed edge moment in the next model.

Stiffness Tests

As in the case of model 3, stiffness tests were carried out (a) before cracking, (b) after extensive cracking, and (c) after the final punching shear failure at joint A.

In previous models the stiffness (M/θ) measured for joint A was only approximately the quantity used in analysis. The value required for analysis is the stiffness of joint A when joint B is fully restrained against rotation. In models 1-3, however, there was no method of holding joint B against rotation. In model 4 it was possible to lock joint B. One method of achieving this would

have been to apply the moment to joint A and then to adjust the load cells at B until the rotation of joint B is restored to its original value.

It was decided that instead of adopting this procedure, which might prove tedious in practice, it would be quicker to measure moments and rotations at both A and B and then derive the desired information analytically.

In the test, all horizontal load cells were released except the East cell at A and the West cell at B. A moment was applied at A by screwing in A-East to a pre-determined value. The 'carry-over' moment at B could then be read by means of load cell B-West. The rotations of joints A and B were both measured by means of the dial gauges at these joints. The four quantities measured in this operation, which can be called test 1, will be denoted by M_{A_1} M_{B_1} θ_{A_1} and θ_{B_1}. Several graphs could then be drawn relating these quantities. It was decided to plot graphs of θ_{A_1}, θ_{B_1} and M_{B_1} successively, as functions of M_{A_1} regarded as the independent variable. These three graphs are shown in Fig. 6.4.22a(i). The slopes of these graphs provide values of M_{A_1}/θ_{A_1}, M_{A_1}/θ_{B_1}, and M_{A_1}/M_{B_1}. Any other ratios could then be obtained from these.

A second test was then carried out in which a negative moment was applied at B, the moment at A being regarded as the carry-over effect. As before, rotations at A and B were measured. The values obtained in this test will be called M_{A_2} M_{B_2} θ_{A_2} and θ_{B_2}. Graphs, in which M_B is now regarded as the independent variable, are shown in Fig. 6.4.22a(ii). From these graphs the ratios M_{B_2}/θ_{A_2}, M_{B_2}/θ_{B_2} and M_{B_2}/M_{A_2} were obtained.

The quantities required in analysis may be defined as follows:

when joint B is locked against rotation,

k_A = stiffness at A

c_{BA} = carry-over *factor* from A to B

when joint A is locked against rotation,

k_B = stiffness at B

c_{AB} = carry-over *factor* from B to A

We may also define

$$k_{AB} = c_{AB}\, k_B \tag{6.1}$$

$$k_{BA} = c_{BA}\, k_A \tag{6.2}$$

There are, of course, carry-over effects from A to joints other than B but it is known that these effects are small and they will be ignored. Then A and B can be regarded as adjacent joints in a two-dimensional frame.

A couple applied at A or at B will be regarded as positive if it causes negative bending moment in the slab, at that point. The same sign conventions will be used for the rotations θ_A and θ_B.

If now, both A and B are allowed to rotate, then in terms of the basic quantities, the total couples at A and B will be

$$M_A = k_A\, \theta_A - k_{AB}\, \theta_B \tag{6.3}$$

and

$$M_B = k_B\, \theta_B - k_{BA}\, \theta_A \tag{6.4}$$

The relationships between the quantities measured in the first test are, therefore,

$$M_{A1} = k_A\, \theta_{A1} - k_{AB}\, \theta_{B1} \tag{6.5}$$

and

$$M_{B1} = k_B\, \theta_{B1} - k_{BA}\, \theta_{A1} \tag{6.6}$$

These equations may be re-arranged in the form

$$k_A - k_{AB}\left(\frac{\theta_{B1}}{\theta_{A1}}\right) = \left(\frac{M_{A1}}{\theta_{A1}}\right) \tag{6.7}$$

$$k_B - k_{BA}\left(\frac{\theta_{A1}}{\theta_{B1}}\right) = \left(\frac{M_{B1}}{\theta_{B1}}\right) \tag{6.8}$$

In a similar manner, the quantities measured in the second test are related by

$$k_A - k_{AB}\left(\frac{\theta_{B2}}{\theta_{A2}}\right) = \left(\frac{M_{A2}}{\theta_{A2}}\right) \tag{6.9}$$

$$k_B - k_{BA}\left(\frac{\theta_{A2}}{\theta_{B2}}\right) = \left(\frac{M_{B2}}{\theta_{B2}}\right) \tag{6.10}$$

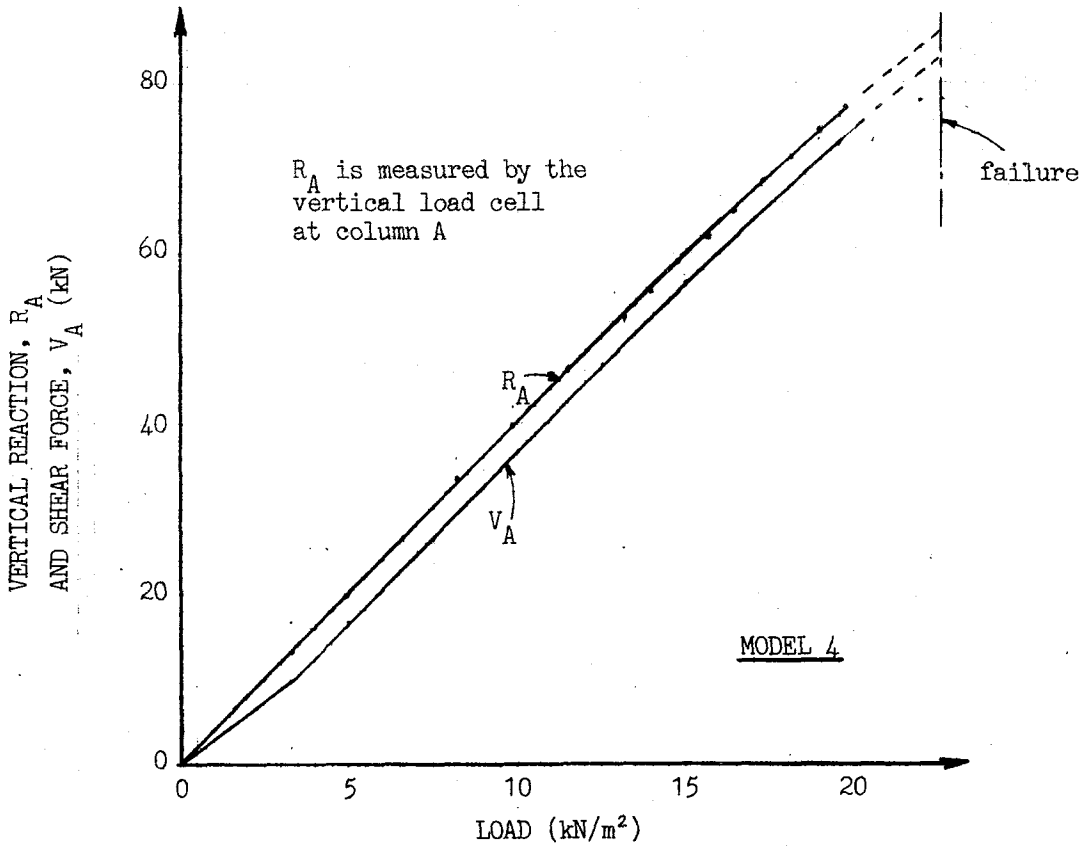

FIG. 6.4.10 VERTICAL REACTION R_A, AND TOTAL SHEAR FORCE, V_A

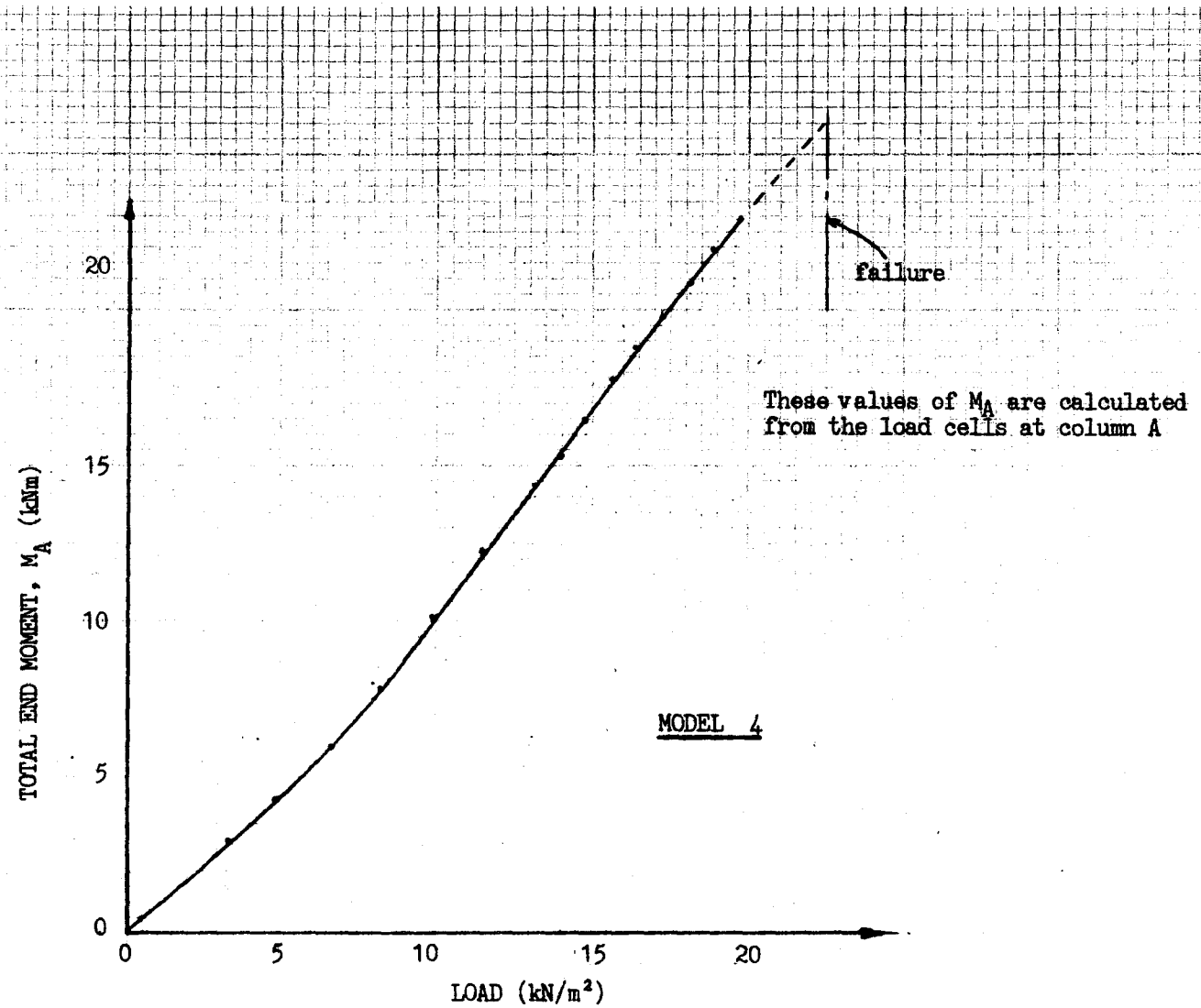

FIG. 6.4.11 TOTAL END MOMENT, M_A

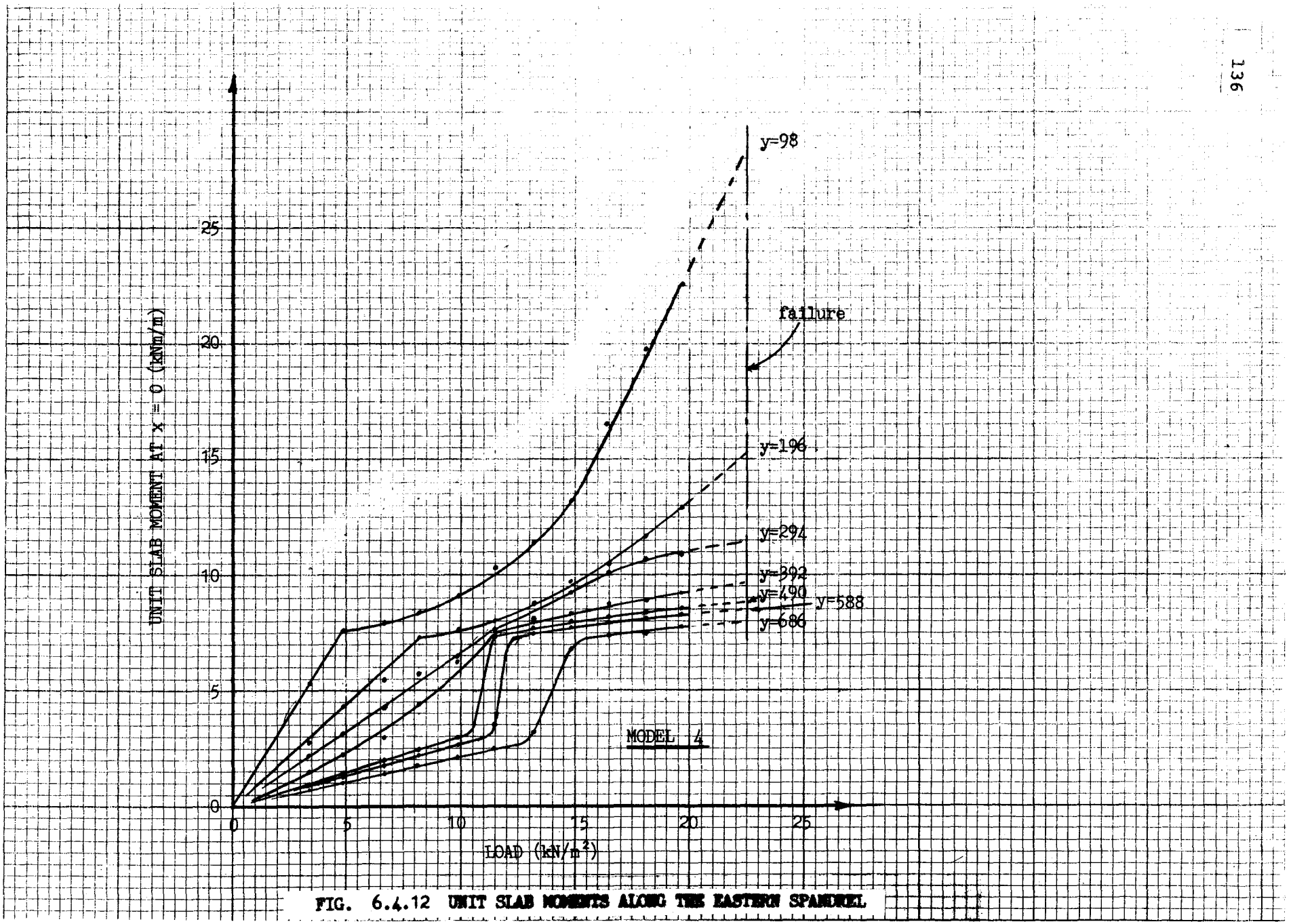

FIG. 6.4.12 UNIT SLAB MOMENTS ALONG THE EASTERN SPANDREL

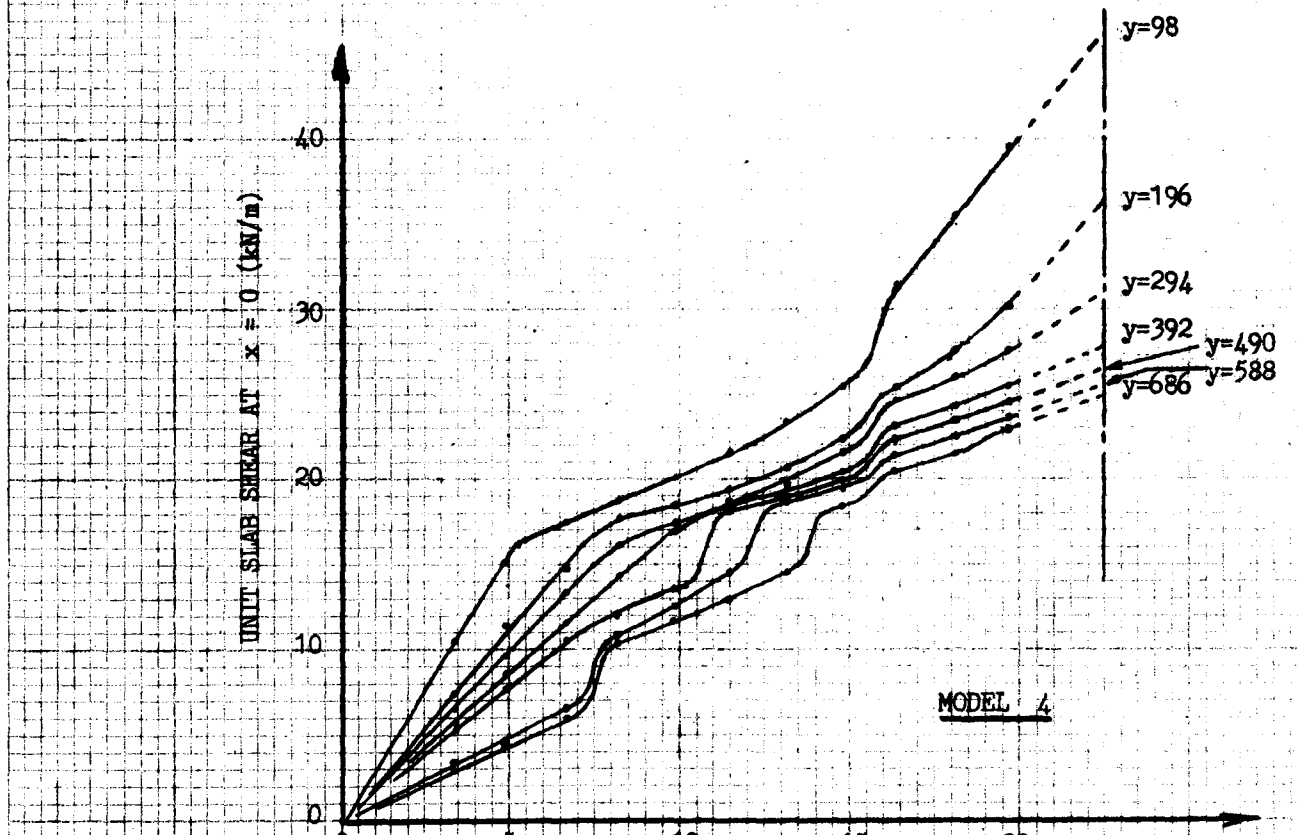

FIG. 6.4.13 UNIT SLAB SHEAR ALONG THE EASTERN SPANDREL

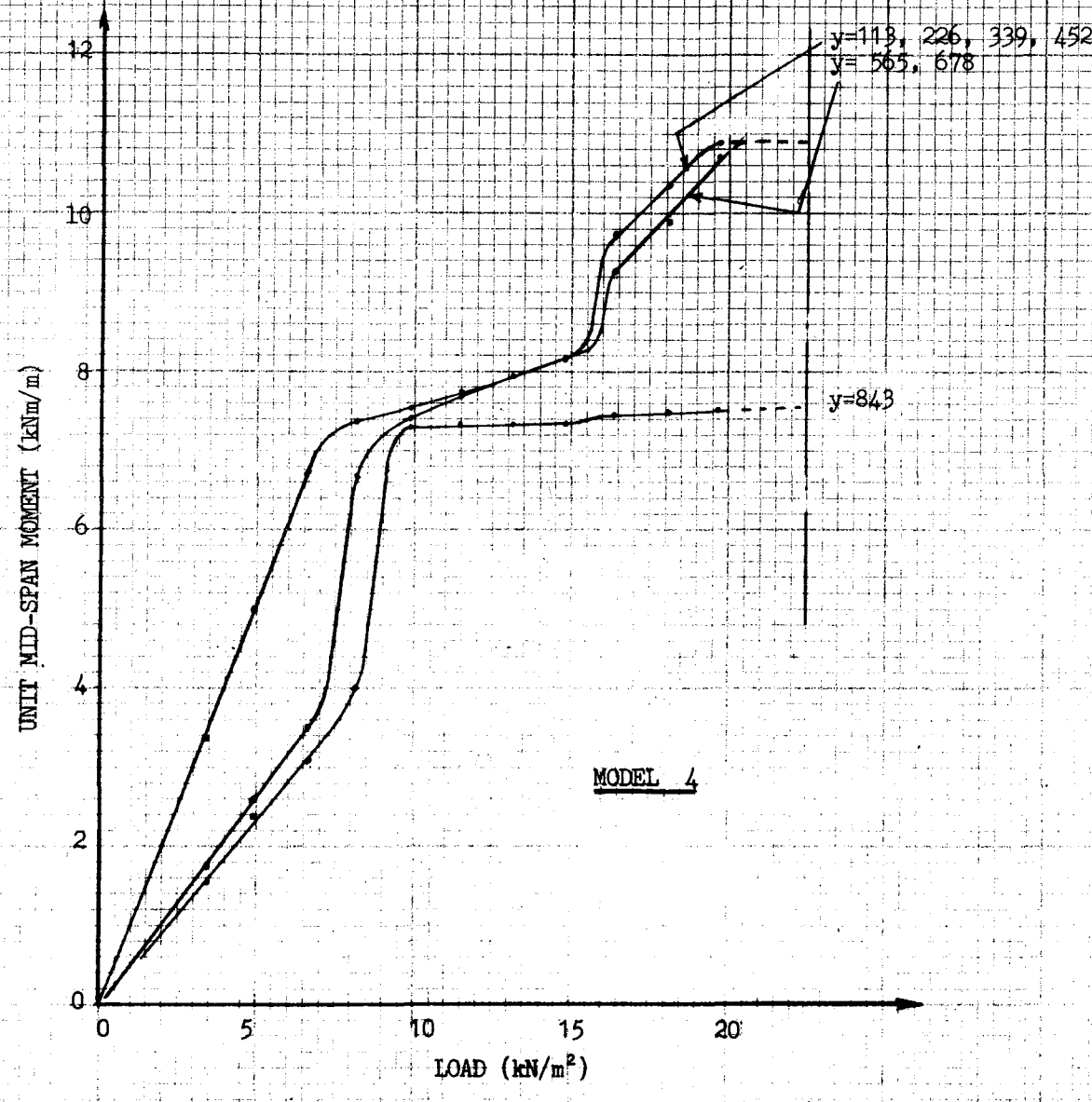

FIG. 6.4.14 UNIT SLAB MOMENT AT MID-SPAN

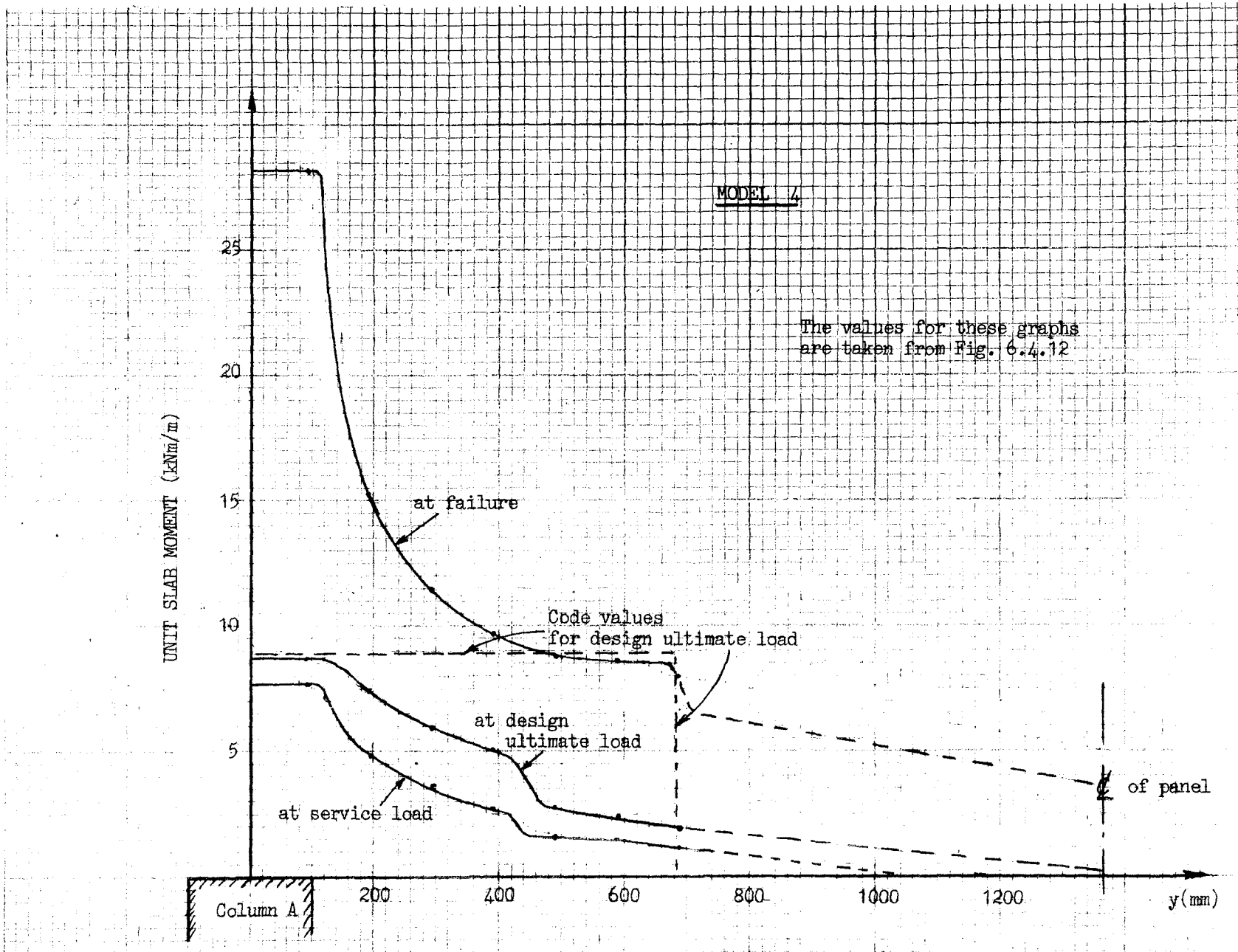

FIG. 6.4.15 TRANSVERSE DISTRIBUTION OF M_A

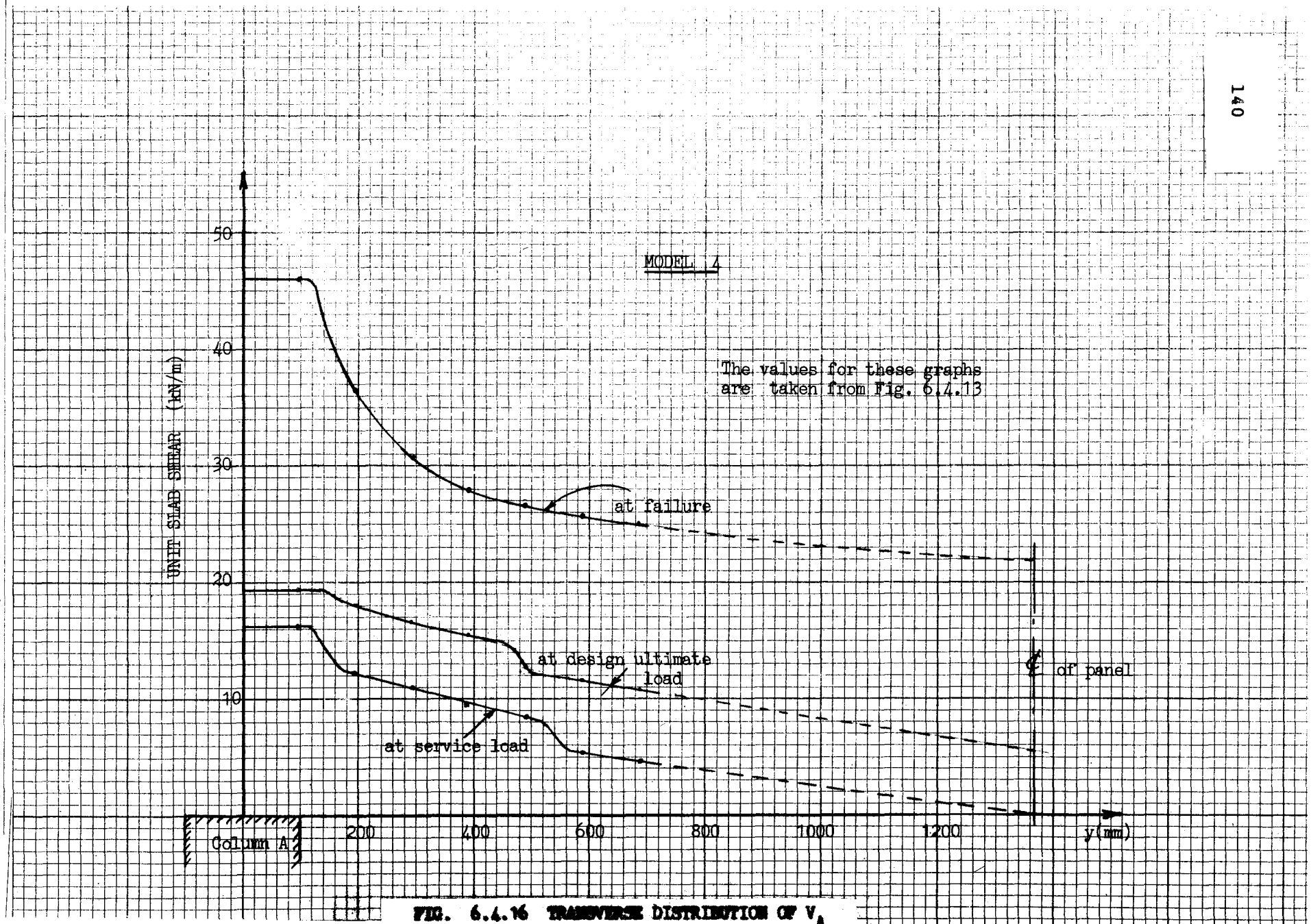

FIG. 6.4.16 TRANSVERSE DISTRIBUTION OF V_s

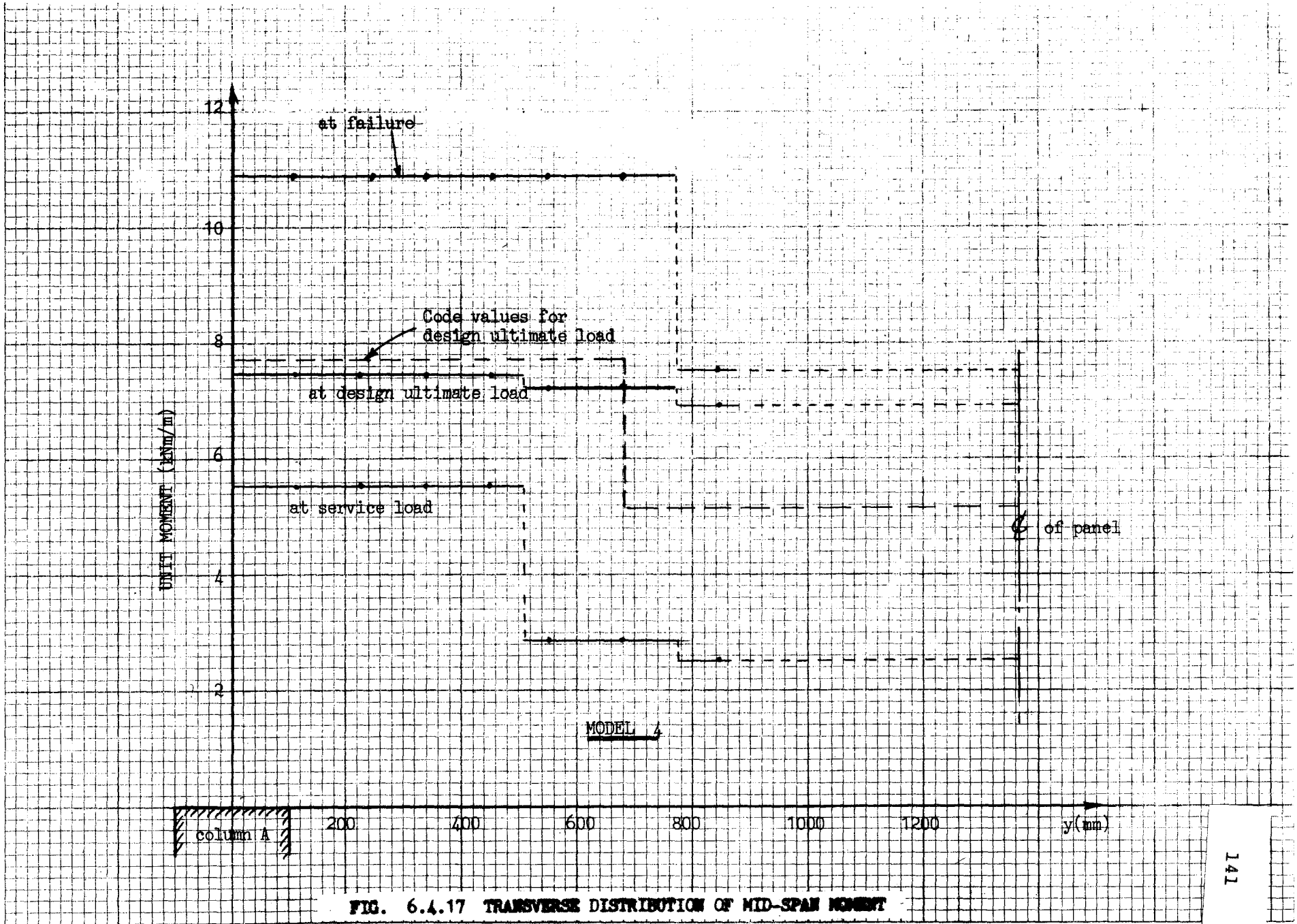

FIG. 6.4.17 TRANSVERSE DISTRIBUTION OF MID-SPAN MOMENT

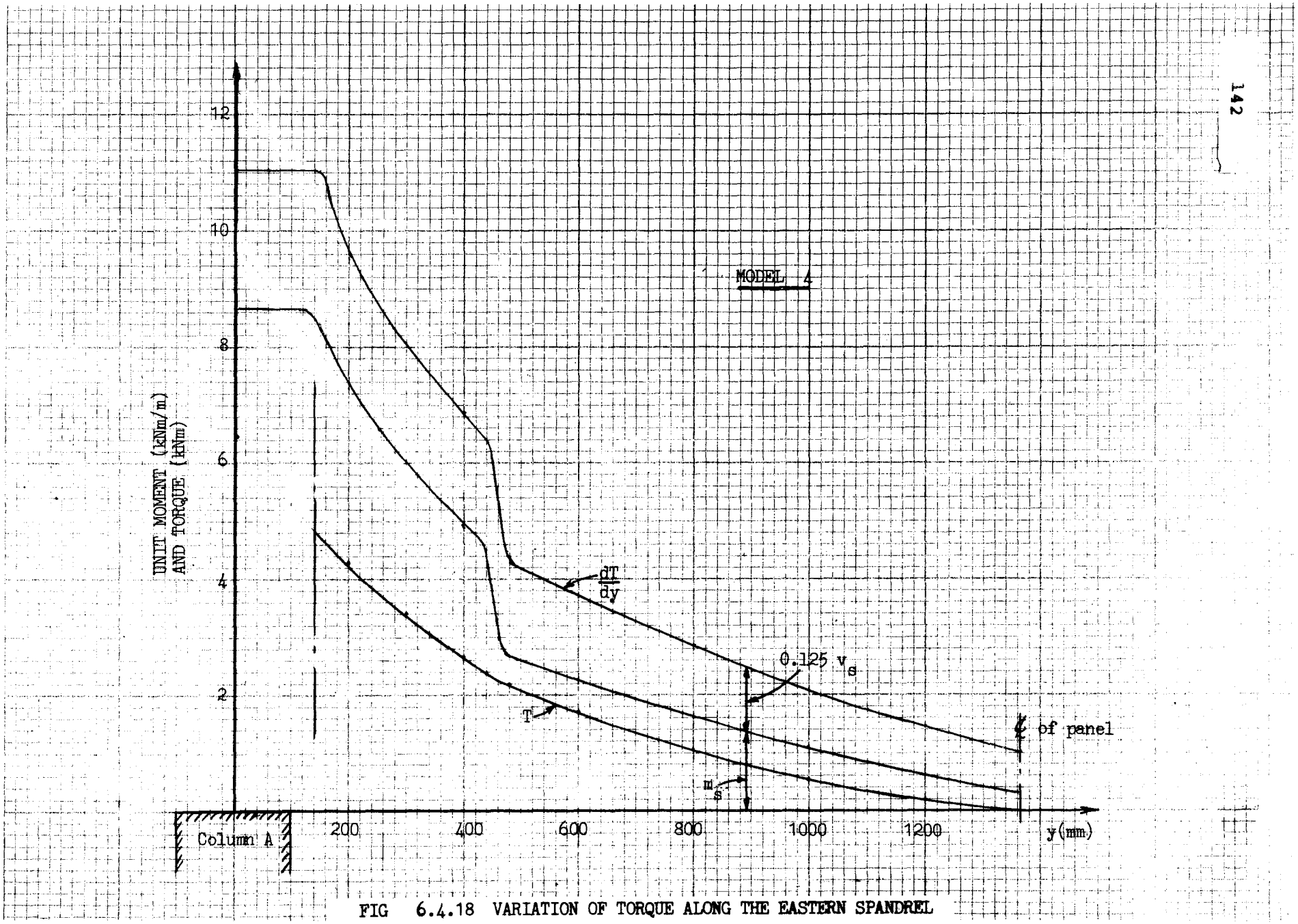

FIG 6.4.18 VARIATION OF TORQUE ALONG THE EASTERN SPANDREL

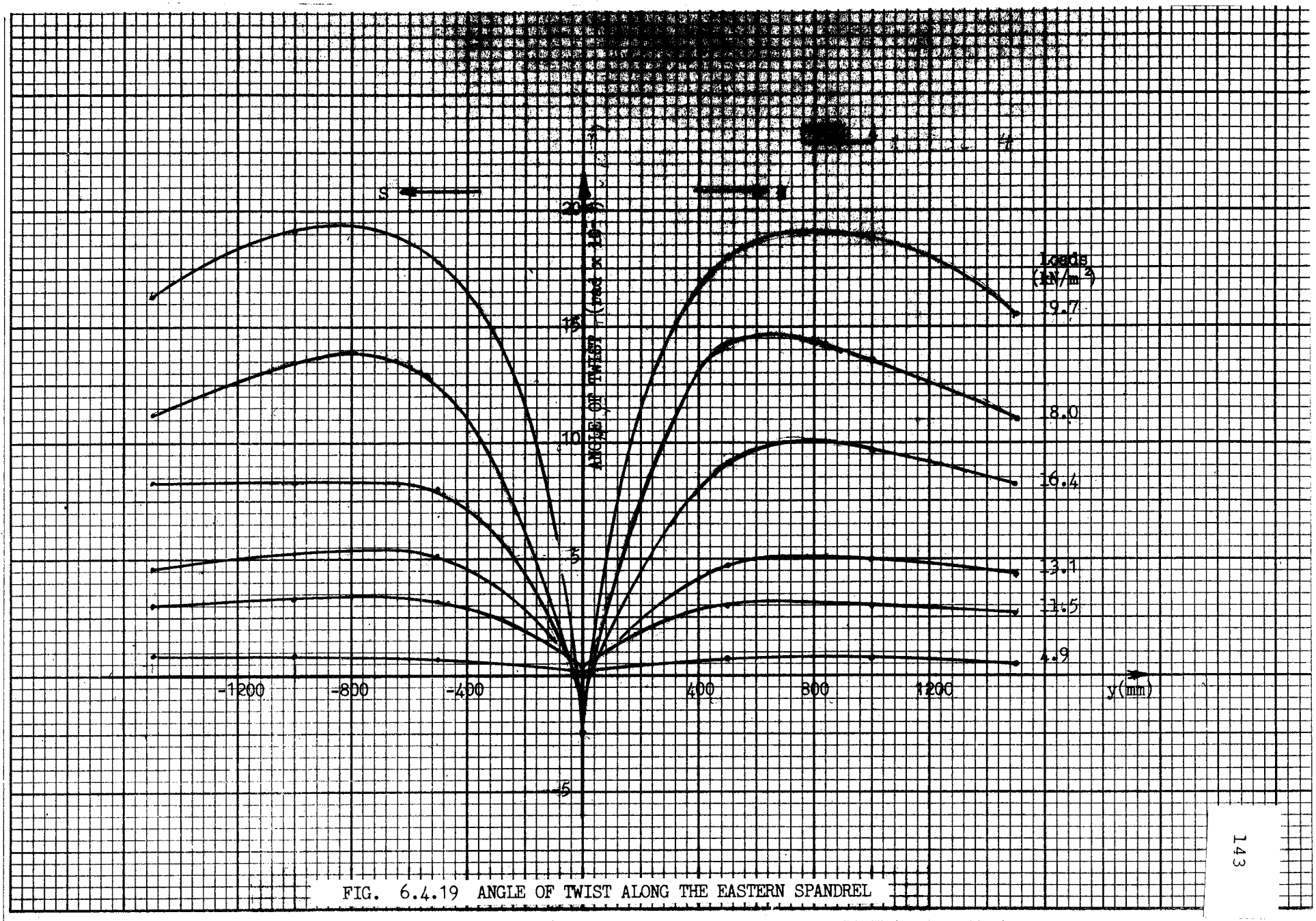

FIG. 6.4.19 ANGLE OF TWIST ALONG THE EASTERN SPANDREL

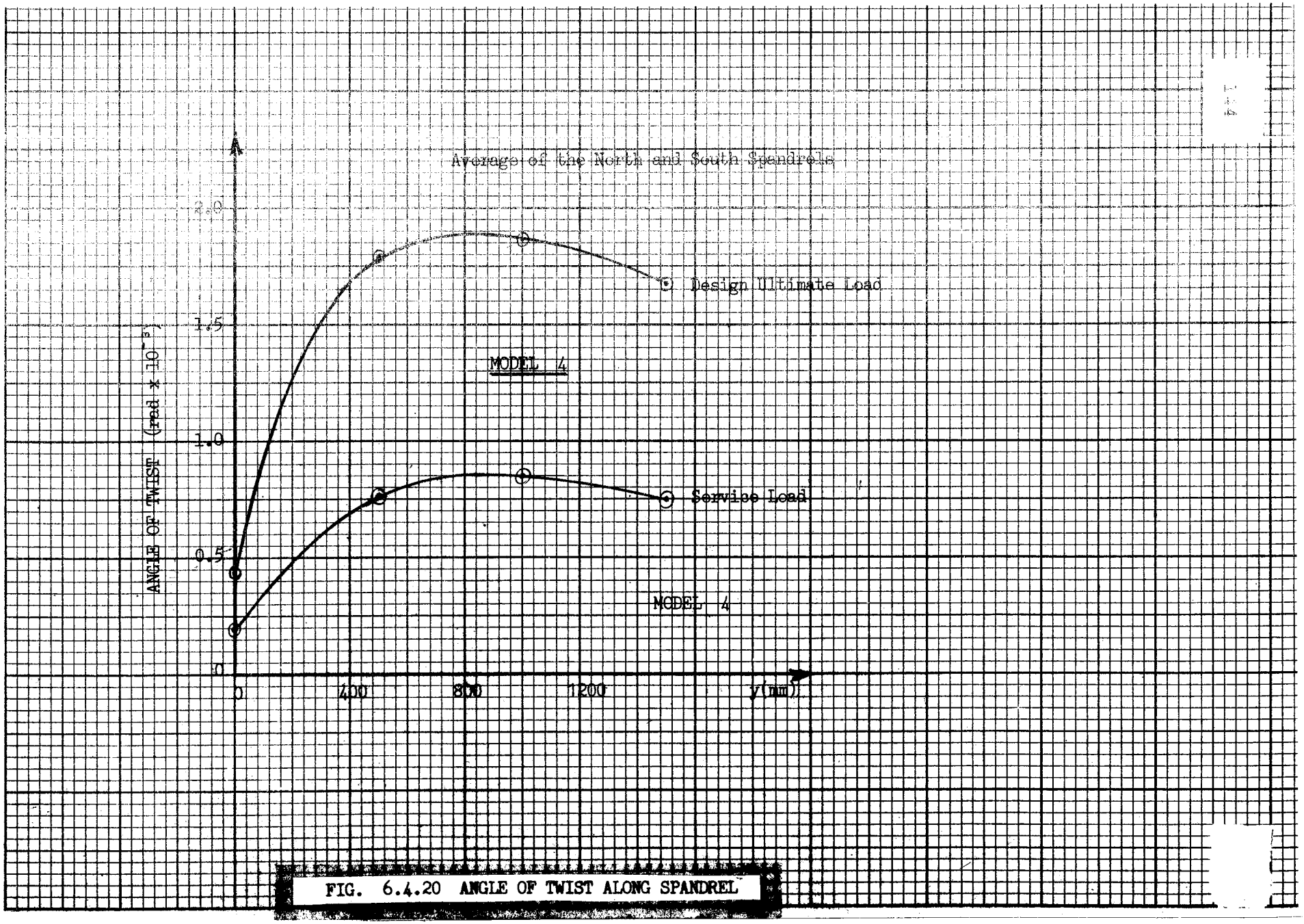

FIG. 6.4.20 ANGLE OF TWIST ALONG SPANDREL

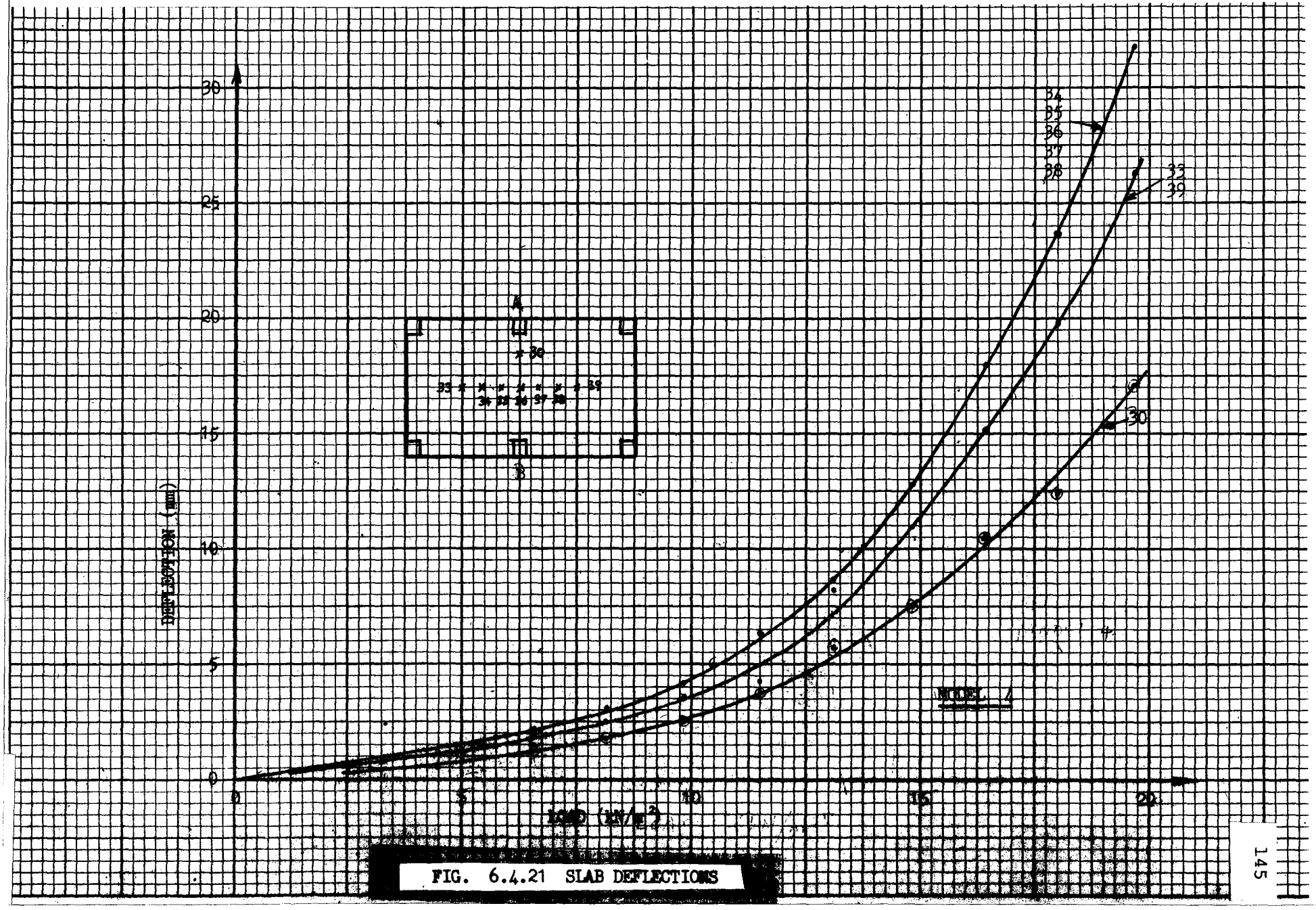

FIG. 6.4.21 SLAB DEFLECTIONS

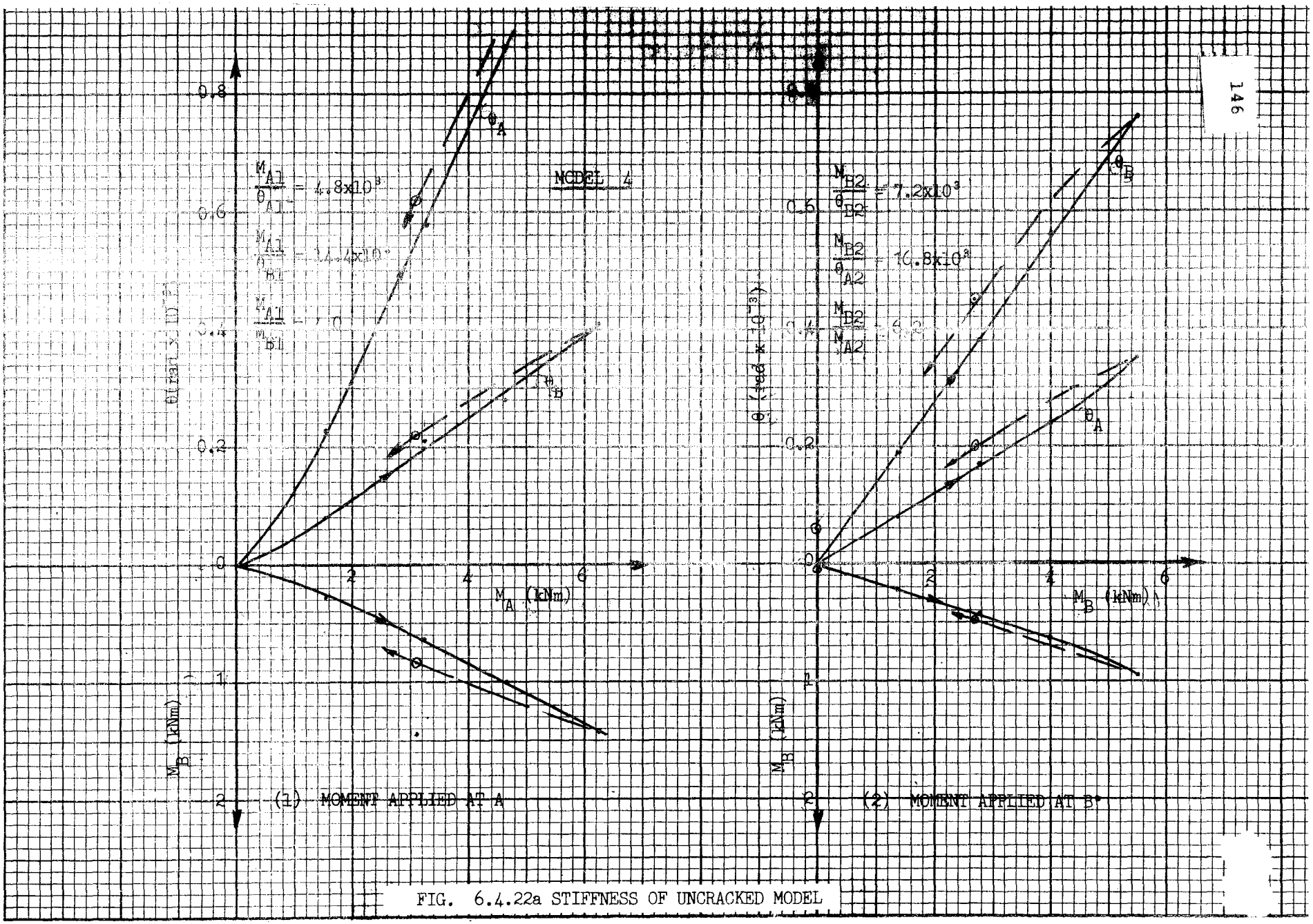

FIG. 6.4.22a STIFFNESS OF UNCRACKED MODEL

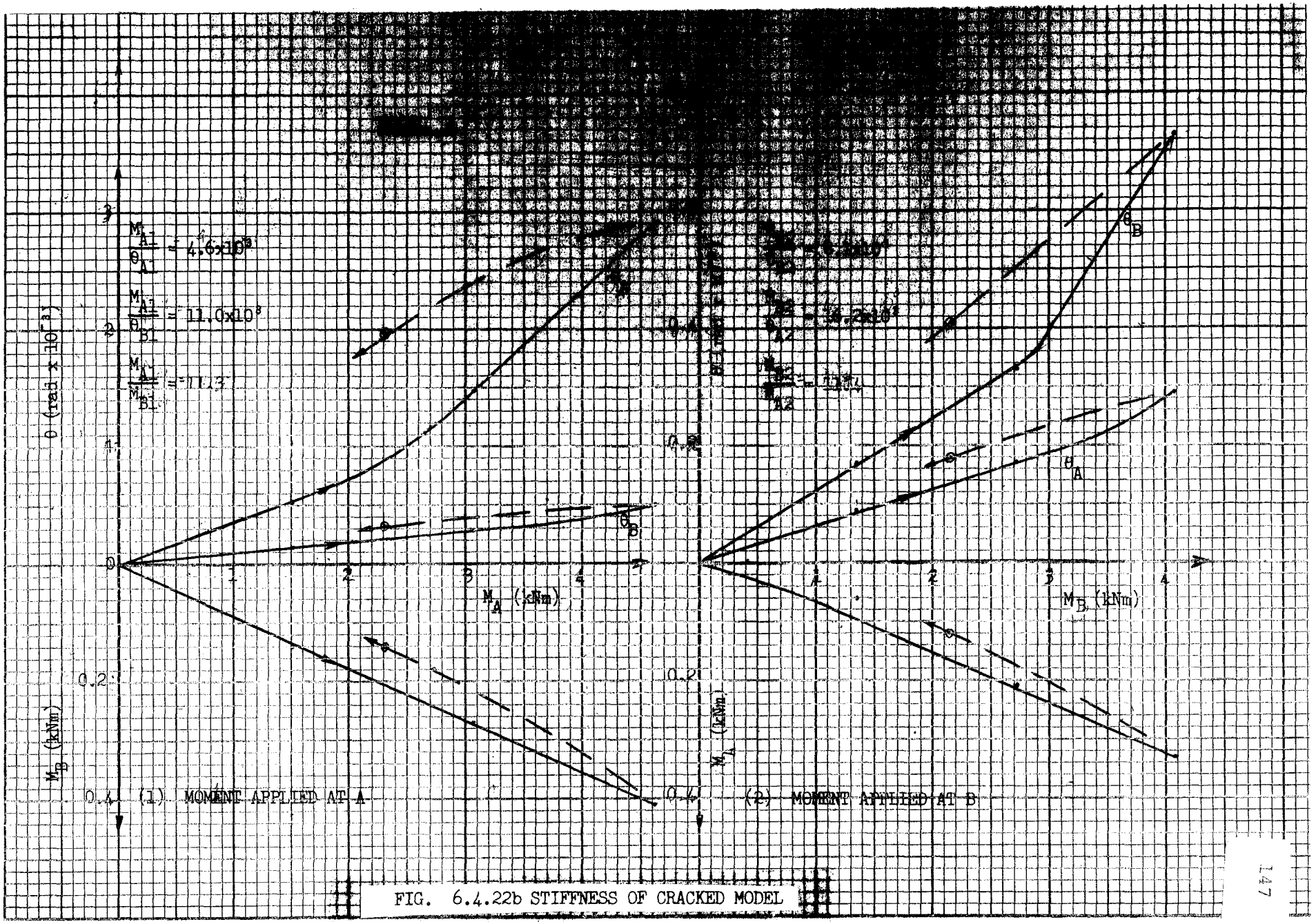

FIG. 6.4.22b STIFFNESS OF CRACKED MODEL

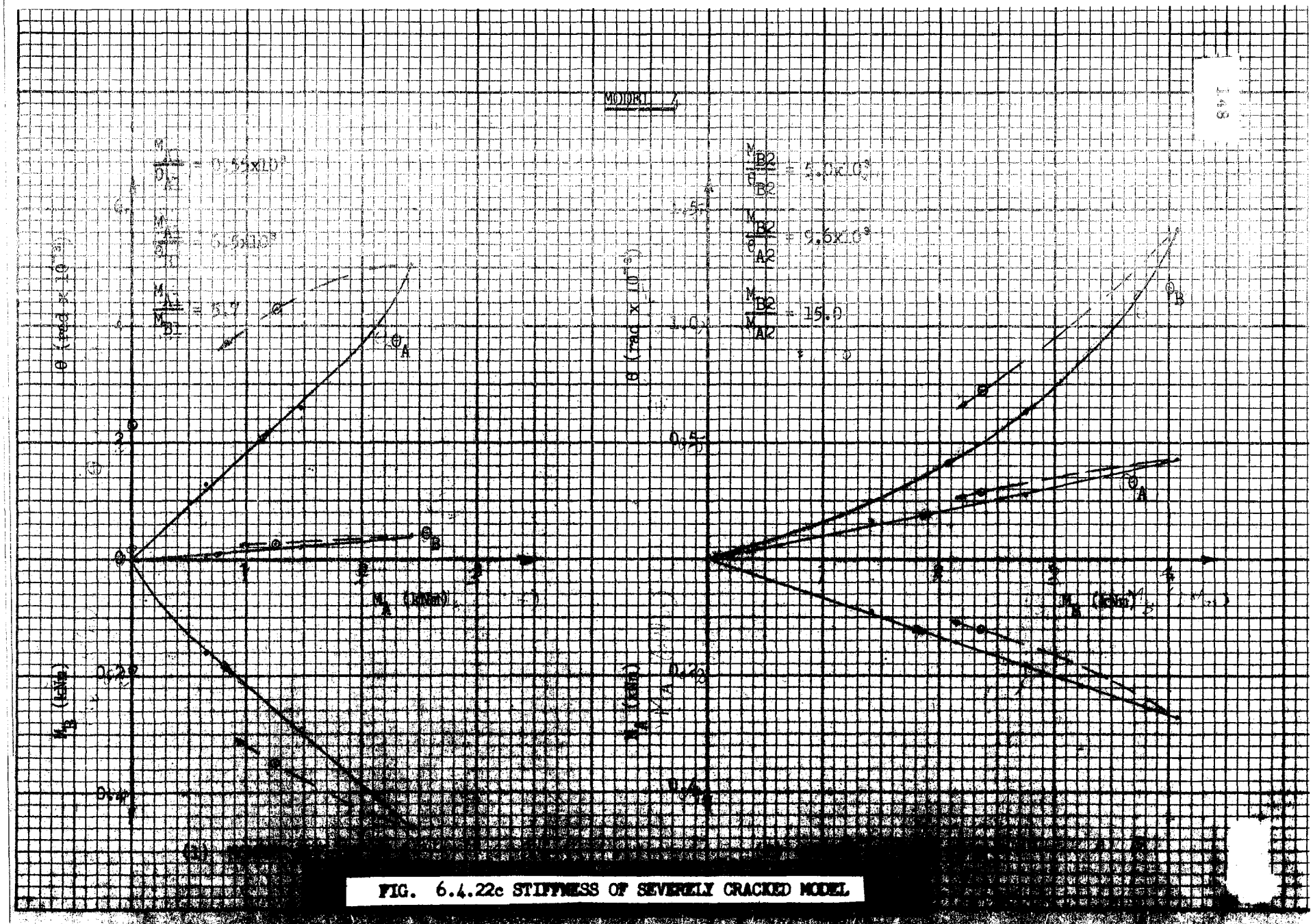

FIG. 6.4.22c STIFFNESS OF SEVERELY CRACKED MODEL

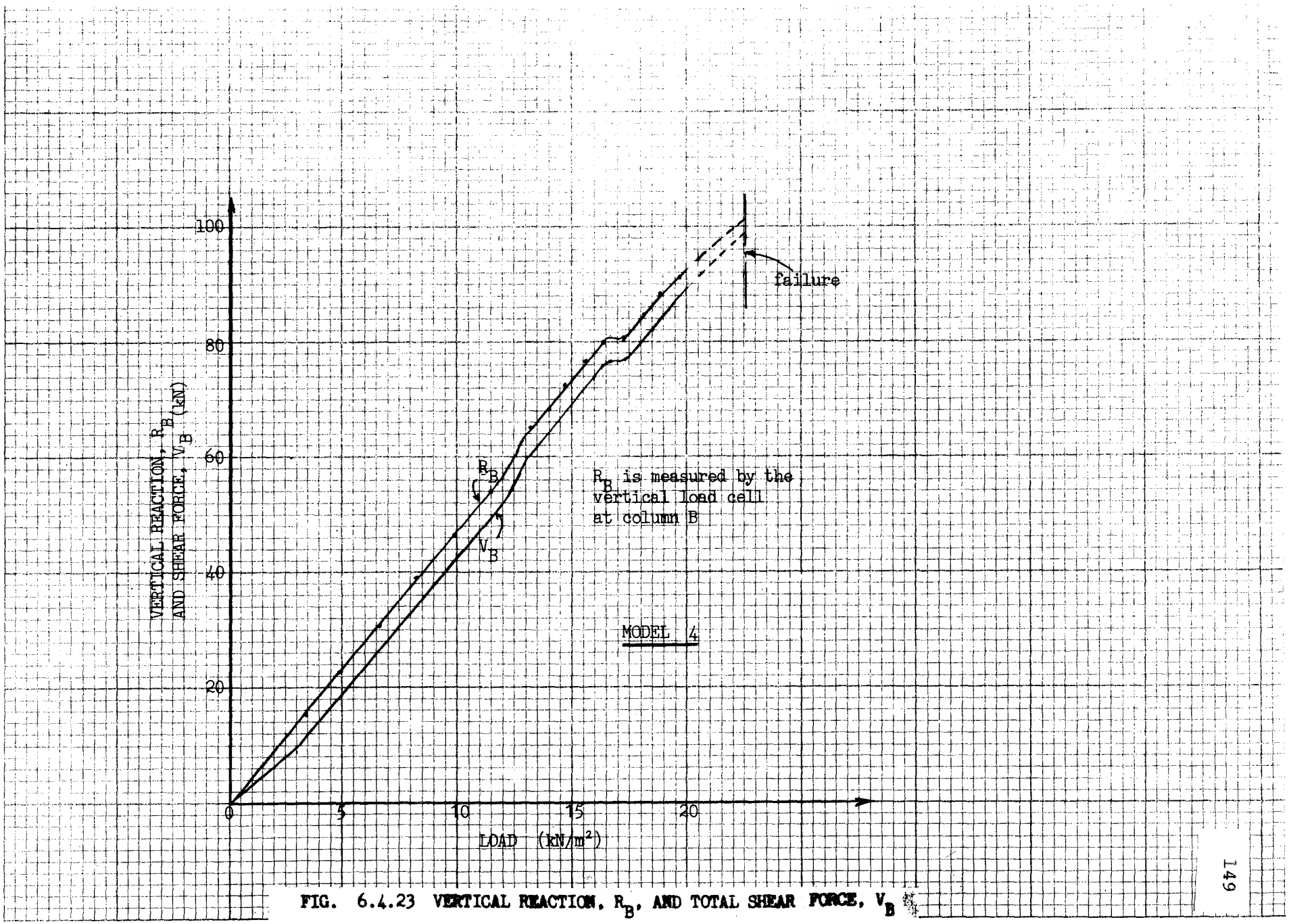

FIG. 6.4.23 VERTICAL REACTION, R_B, AND TOTAL SHEAR FORCE, V_B

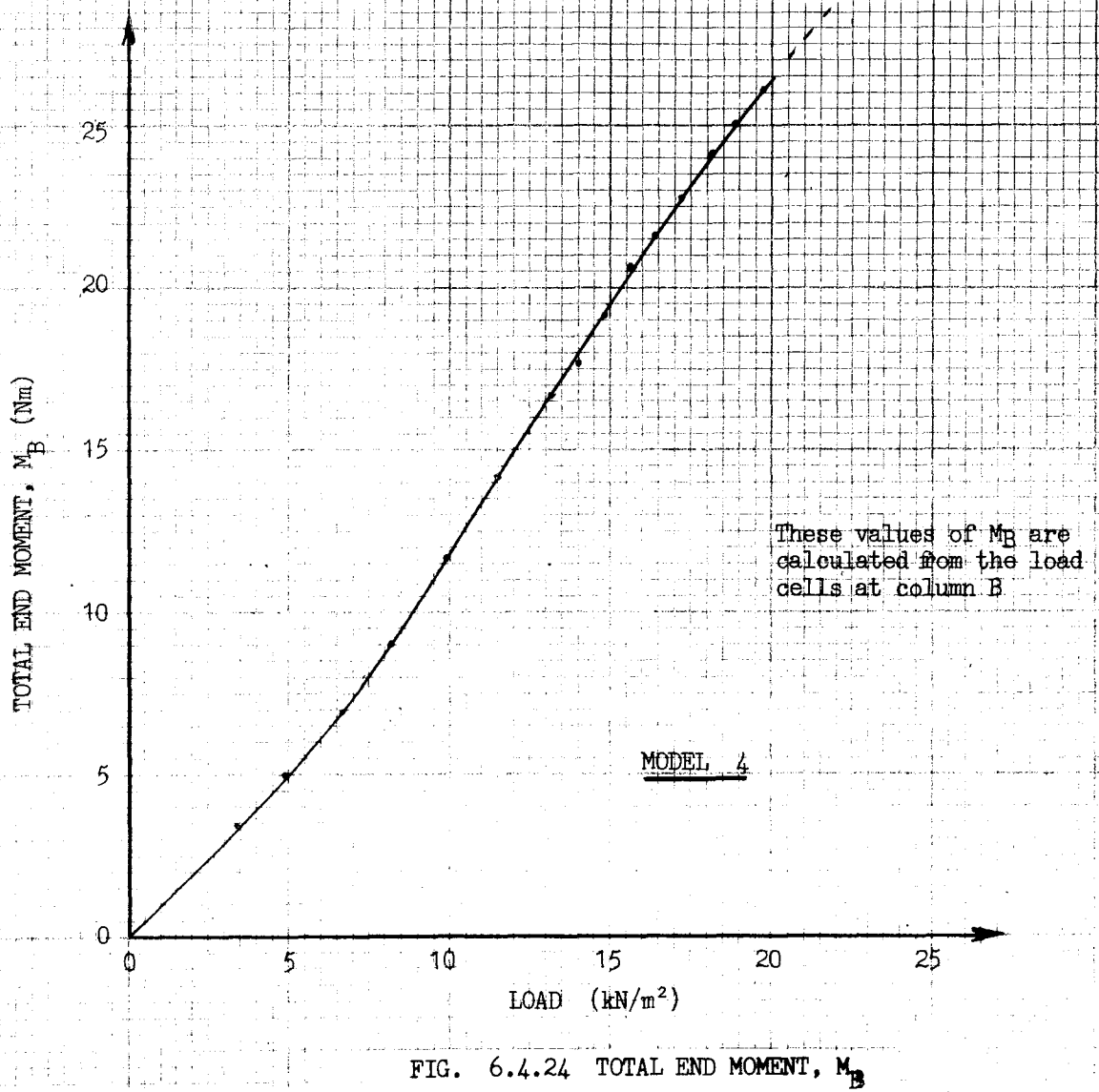

FIG. 6.4.24 TOTAL END MOMENT, M_B

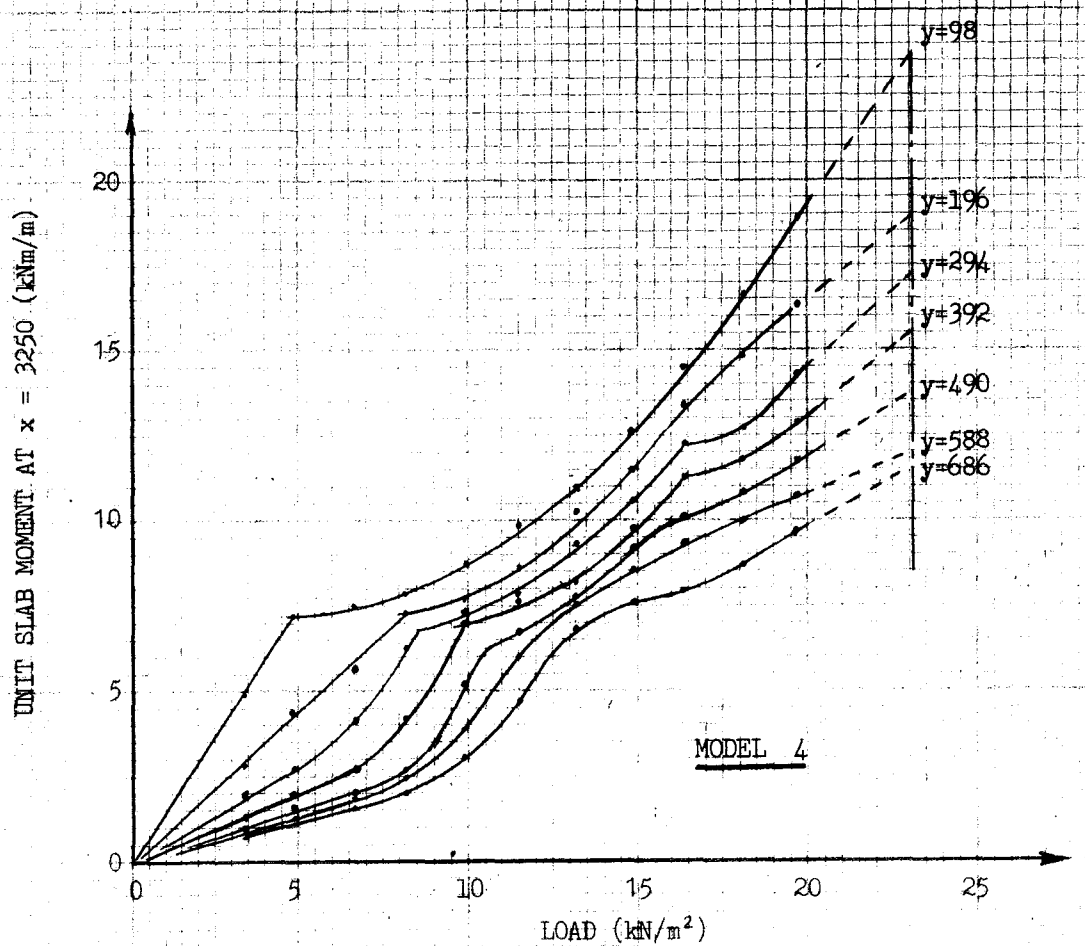

FIG. 6.4.25 UNIT SLAB MOMENTS ALONG THE WESTERN SPANDREL

FIG. 6.1.26 UNIT SLAB SHEAR ALONG THE WESTERN SPANDREL

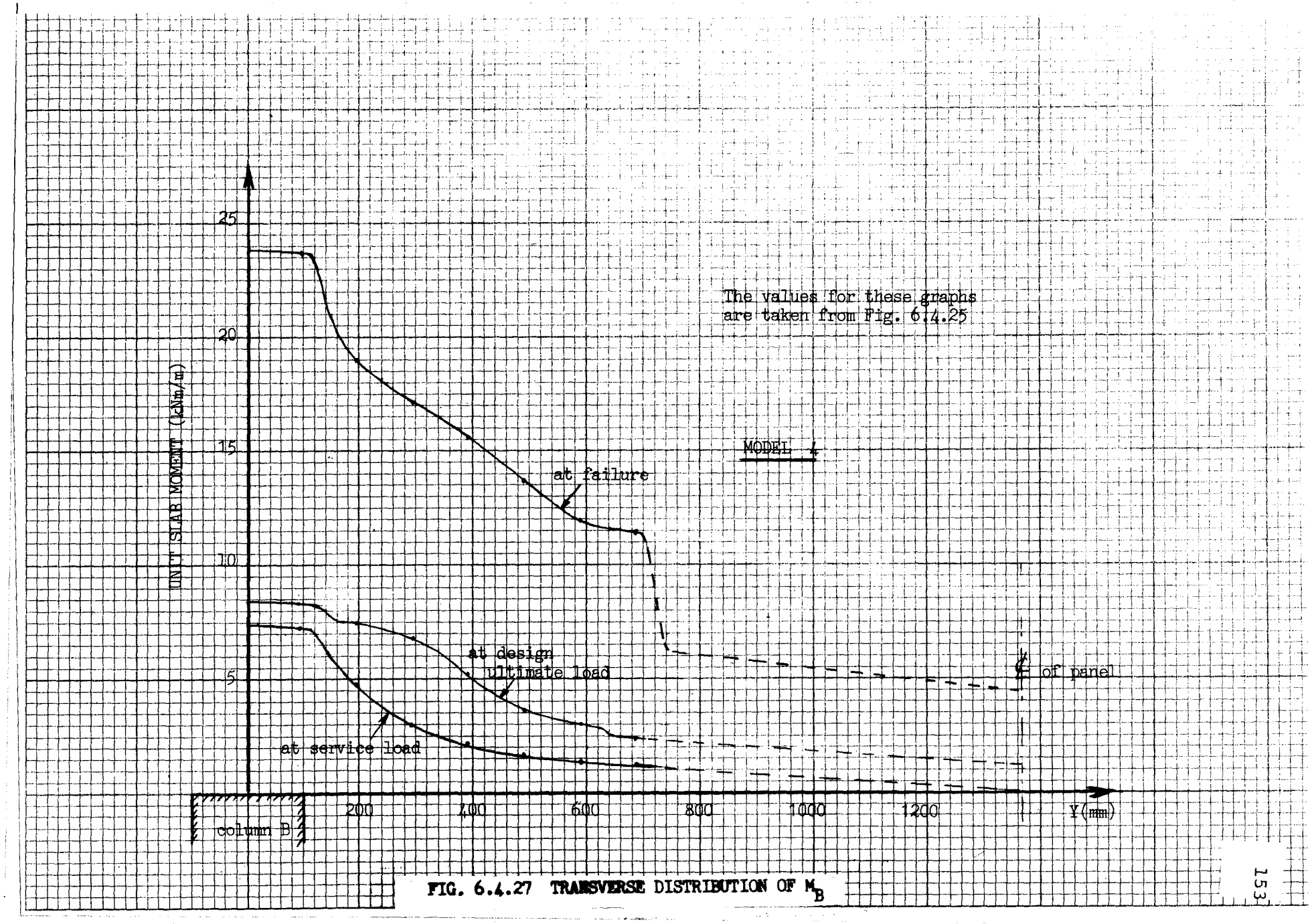

FIG. 6.4.27 TRANSVERSE DISTRIBUTION OF M_B

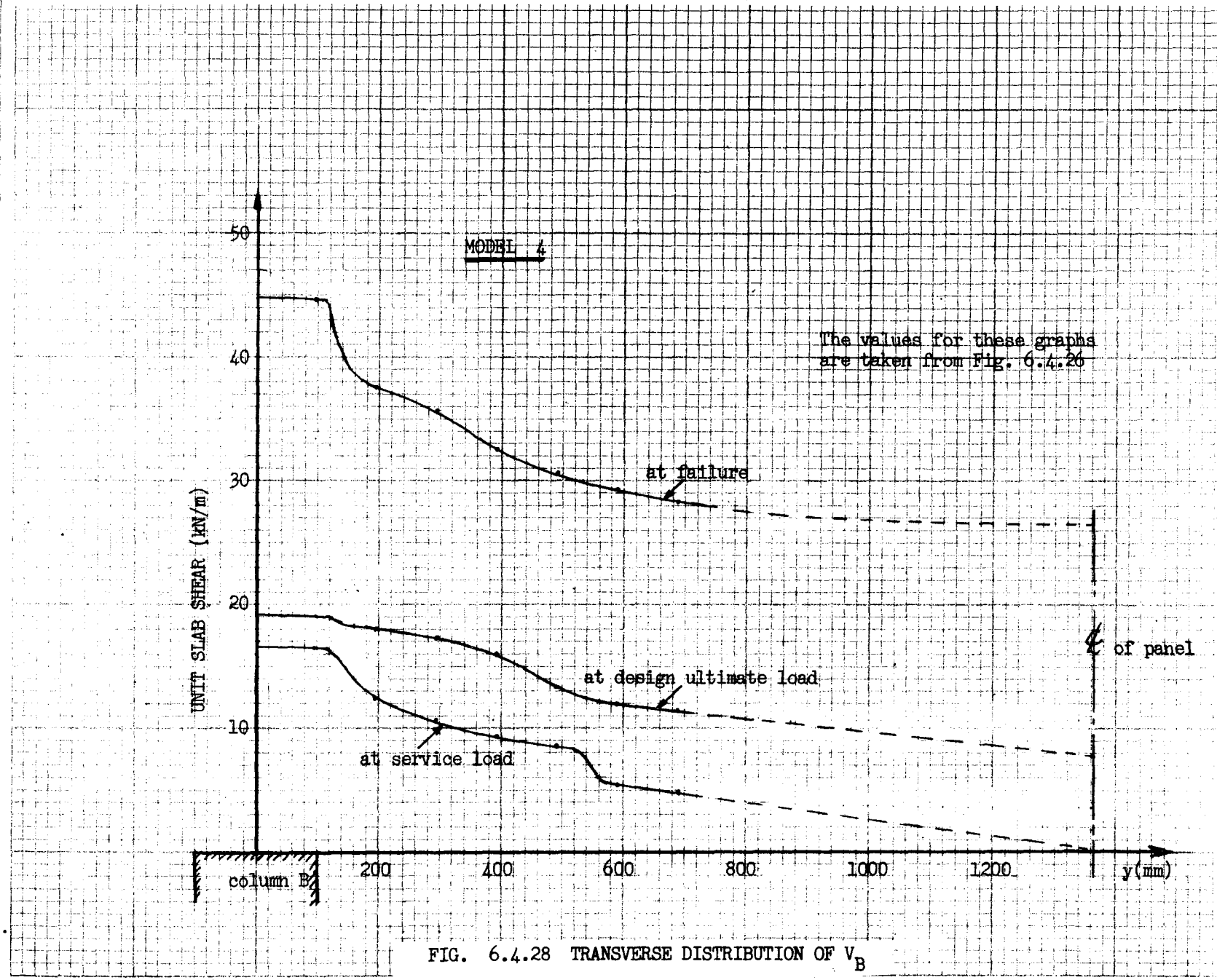

FIG. 6.4.28 TRANSVERSE DISTRIBUTION OF V_B

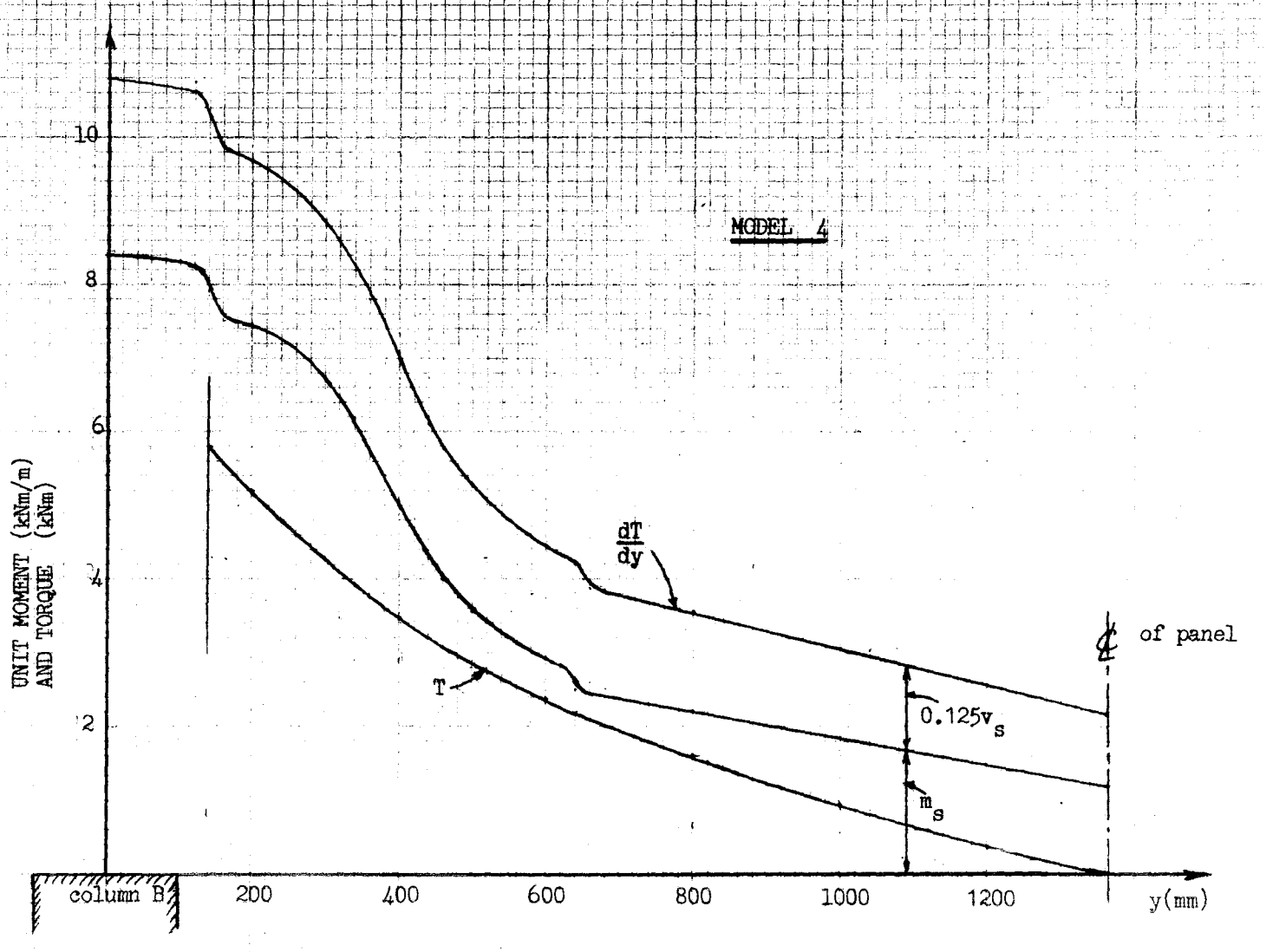

FIG. 6.4.29 VARIATION OF TORQUE ALONG THE WESTERN SPANDREL

MODEL No. 4.

SUMMARY OF RESULTS OF VERTICAL LOAD TEST

TABLE 6.4.1

Service Load = 5.4 kN/m^2
Design Ultimate Load = 9.0 kN/m^2
Failure Load = 22.5 kN/m^2

Item	Load Level (kN/m^2)	Test Value
1. Vertical Reaction at A = R_A (kN)	5.4	21.8
	9.0	36.2
	22.5	86
2. Vertical Reaction at B = R_B (kN)	5.4	25.5
	9.0	42
	22.5	102
3. Total Mid-Span Moment = M_M (kNm)	5.4	(10.0)
	9.0	(19.5)
	22.5	(25.2)
4. Total Moment at face of Spandrel A = M_A (kNm)	5.4	4.7 (5.4)
	9.0	8.7 (8.7)
	22.5	26.0 (26.2)
5. Total Shear Force at Face of Spandrel A = V_A (kN)	5.4	18.0 (17.5)
	9.0	32.5 (32.3)
	22.5	83 (76.2)
6. Total Moment at Face of Spandrel B = M_B (kNm)	5.4	5.4 (5.4)
	9.0	10.2 (10.2)
	22.5	29.4 (30.6)
7. Total Shear Force at Face of Spandrel B = V_B (kN)	5.4	21.0 (17.6)
	9.0	37.5 (34.8)
	22.5	98 (85)
8. Transverse Distribution of Mid-Span Moment M_M		See Fig. 6.4.17
9. Transverse Distribution of M_A		See Fig. 6.4.15
10. Transverse Distribution of M_B		See Fig. 6.4.27

* Values in brackets are obtained from strain gauge readings by integration. Other values are obtained from load cells.

Table 6.4.1 MODEL No.4.

VERTICAL LOAD TEST (cont.)

Item	Load Level (kN/m^2)	Test Value
11. Distribution of Torque along Spandrel A	design ultimate load	See Fig. 6.4.18
12. Torque in Spandrel A at Face of Column A (kNm)	design ultimate load	(4.8)
13. End Moment in Beam Strip at Face of Column A (kNm)	5.4	(2.1)
	9.0	(2.4)
	22.5	(7.8)
14. Shear Force in Beam Strip at Face of Column A (kN)	5.4	(4.5)
	9.0	(5.4)
	22.5	(12.8)
15. Shear Force in Spandrel at Face of Column A (kN)	5.4	7.5 (7.2)
	9.0	14.3 (14.2)
	22.5	35.8 (32.4)
16. Distribution of Torque along Spandrel B	design ultimate load	See Fig. 6.4.29
17. Torque in Spandrel B at Face of Column B (kNm)	design ultimate load	(5.8)
18. End Moment in Beam Strip at Face of Column B (kNm)	5.4	(2.0)
	9.0	(2.3)
	22.5	(6.7)
19. Shear Force in Beam Strip at Face of Column B (kN)	5.4	(4.5)
	9.0	(5.3)
	22.5	(12.7)
20. Shear Force in Spandrel at Face of Column B (kN)	5.4	9.5 (7.8)
	9.0	17.3 (16.0)
	22.5	47 (40)
21. Mid-span Moment in Beam Strip (kNm)	5.4	(0.8)
	9.0	(1.0)
	22.5	(1.7)

MODEL No. 4

TABLE 6.4.2 SUMMARY OF RESULTS OF STIFFNESS TESTS

	Condition of Model		
	Uncracked	Cracked	Severely Cracked
Stiffness of Joint A = k_A (kNm/radian)	5.2×10^3	1.6×10^3	0.55×10^3
Carry-over factor from A to B = c_{BA}	0.28	0.4	0.6
Stiffness of Joint B = k_B (kNm/radian)	7.9×10^3	5.8×10^3	5.2×10^3
Carry-over factor from B to A = c_{AB}	0.16	0	0

These four equations - (6.7), (6.8), (6.9) and (6.10) - provide values of the quantities k_A k_B k_{BA} k_{AB}. From (6.7) and (6.9) we have

$$k_{AB}\left[\frac{\theta_{B2}}{\theta_{A2}} - \frac{\theta_{B1}}{\theta_{A1}}\right] = \left[\frac{M_{A1}}{\theta_{A1}} - \frac{M_{A2}}{\theta_{A2}}\right] \qquad (6.11)$$

and with k_{AB} known, k_A may be evaluated from (6.7). From (6.8) and (6.10) we have

$$k_{BA}\left[\frac{\theta_{A2}}{\theta_{B2}} - \frac{\theta_{A1}}{\theta_{B1}}\right] = \left[\frac{M_{B1}}{\theta_{B1}} - \frac{M_{B2}}{\theta_{B2}}\right] \qquad (6.12)$$

and with k_{BA} known, k_B may be evaluated from (6.10).

Finally, the carry-over factors c_{AB} and c_{BA} can be evaluated from (6.1) and (6.2). The values of the measured ratios are shown in Fig. 6.4.22a. Then from the above equations we find that

$$k_A = 5.2 \times 10^3 \text{ kNm/rad}$$
$$k_B = 7.9 \times 10^3 \text{ kNm/rad}$$
$$c_{AB} = 0.16$$
$$c_{BA} = 0.28$$

Similar tests were carried out after severe cracking had occurred, and again after a punching shear failure around column A. The results of these tests are plotted in Figs. 6.4.22b and 6.4.22c respectively. The values obtained from all three tests are summarized in Table 6.4.2.

6.5 MODEL 5

Design

Earlier research (ACI-ASCE Committee 426 (1974), Faulkes et al (1973)) had indicated that the width of a column, c_2, in a direction at right-angles to the equivalent frame being designed, has a major influence on the slab behaviour. That is to say, in this model the width of column A in the N-S direction might be expected to have a major effect on the various quantities being investigated.

So far, this dimension had remained constant at 200 mm. For model 5 it was decided to increase this to 450 mm. This would

simulate a fairly common type of blade column with its large dimension along the exterior wall of the building. It would not be practical to assume that interior columns would be identical to this. Instead, the 'interior' column at B was taken as having approximately the same area as column A.

Design details are given in Section A.5 of Appendix A. The dimensions of the model are shown in Fig. 6.5.1.

It was hoped that a certain amount of information might be obtained by regarding edge B as an exterior edge. To this extent the width of column B would provide an additional value of c_2.

Reinforcement

Details of the reinforcement in model 5 are shown in Fig. 6.5.1.

Strain Gauges

The arrangement of strain gauges for this model was similar to that for model 4. The exact location of every gauge is given in Section B.5.1 of Appendix B.

Dial Gauges

In previous models, 28 dial gauges were provided along the spandrel beam at side A. Of these, 14 were used to measure angles of twist at 7 locations along the edge, and 14 were used to measure the slope of the spandrel in the N-S direction.

It had been found that the slopes were much smaller than the angles of twist. With the order of accuracy provided by the instrumentation the measured slopes were unreliable. In any case, it is doubtful whether the values of the slopes could have been related to the quantities under investigation.

It was decided not to measure slopes along the spandrel CAD. Instead, angles of twist along the side EBF were measured. Thus 14 dial gauges were used each side. For consistency with previous models the gauges along the eastern side were numbered with the odd numbers from 1 - 27. Those along the western boundary were numbered with even numbers from 2 - 28.

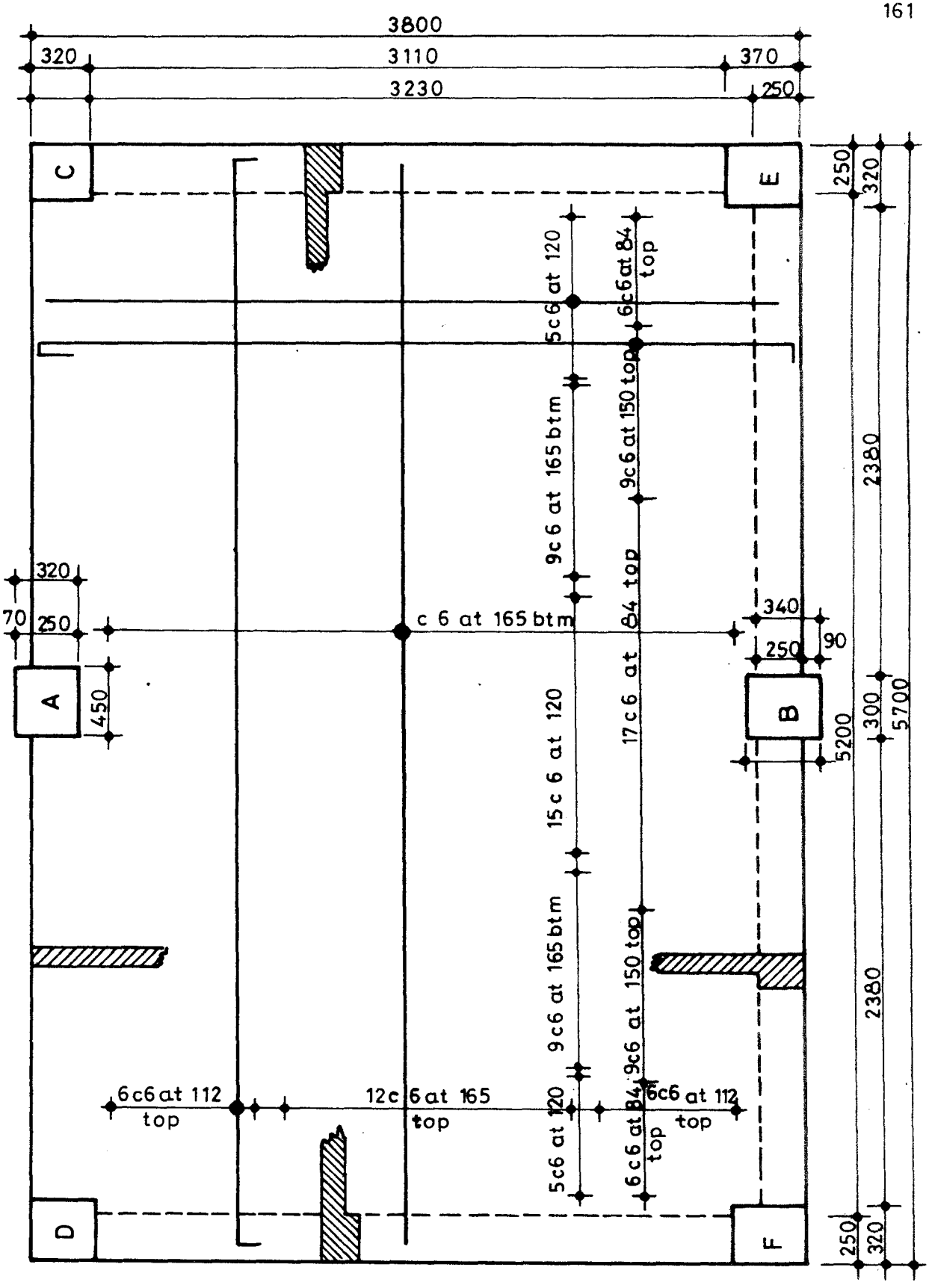

Fig. 6.5.1 (a) Reinforcement Details for Model 5 .

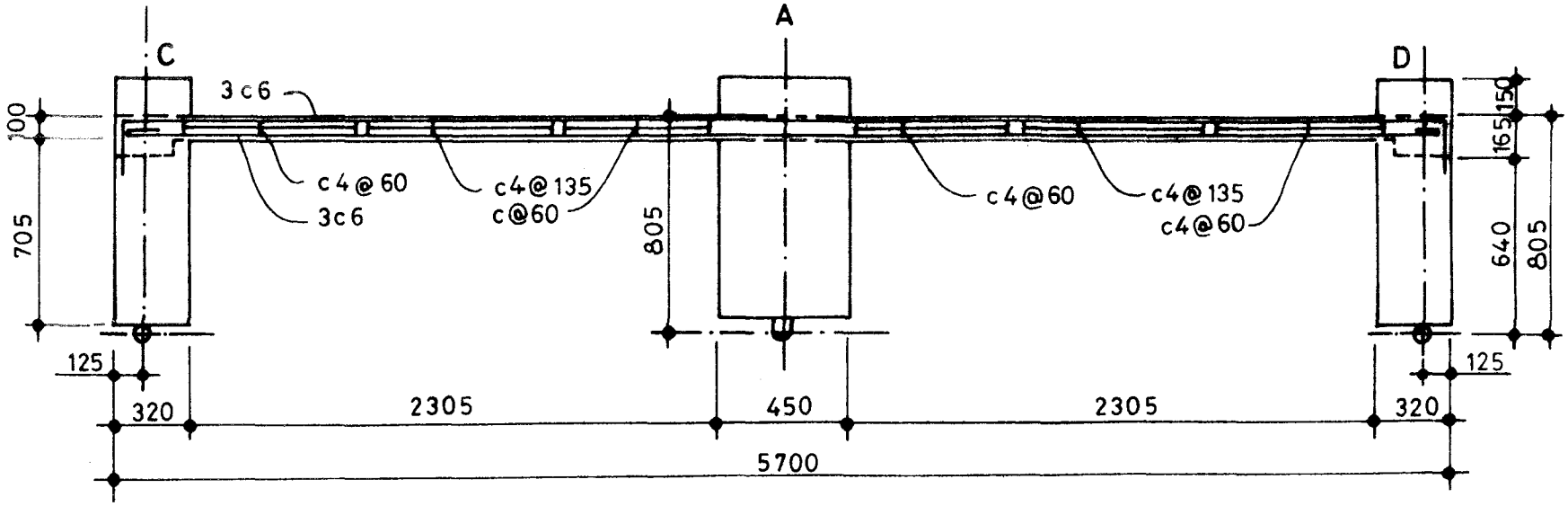

Spandrel beam view

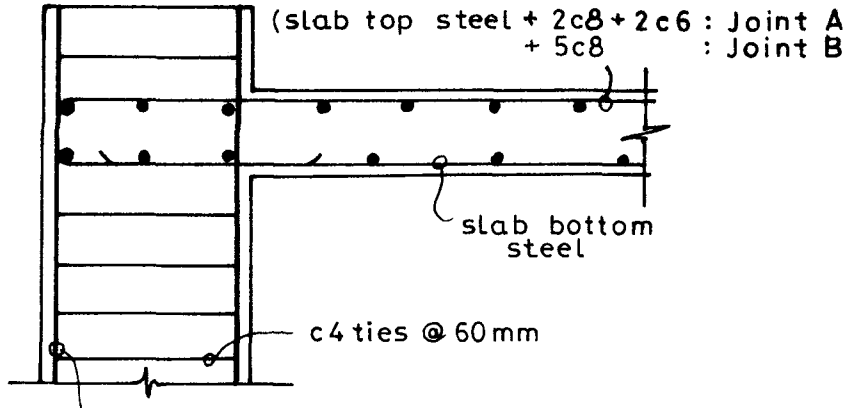

JOINTS A & B

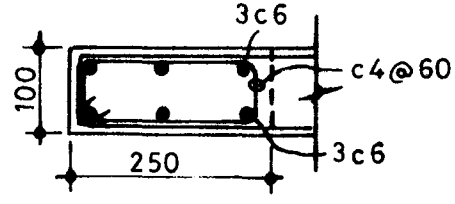

Spandrel at column A

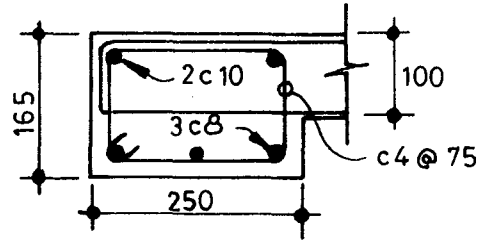

Spandrel at column B

Fig. 6.5.1(b) Reinforcement Details for Model 5.

The positions of these gauges is shown in Section B.5.2.

Dial gauges below the slab were positioned as before. The location of those gauges is shown in Section B.5.3.

Concrete

The compressive strength of the concrete was 31 MPa at the time of the vertical load test.

Boundary Condition Test

In this model a boundary test was made by applying a distributed moment along the edges. As described in Section 5.8 four cantilever beams were bolted on to the northern edge of the model. Each of these were then loaded at the end with 250 kg. The moment thus applied was equivalent to approximately 20 kNm. This approximates the bending moments which would be present due to design ultimate load on the adjacent panel to the north of the model.

The strains due to this applied moment were measured. Since they were very small they were not recorded.

The cantilever beams were removed from the northern edge and attached to the western edge between F and B (see Fig. 5.11). Again the strains measured were very small.

Vertical Load Test

Qualitatively, the behaviour of model 5 was quite similar to that of models 3 and 4.

First cracking occurred at the column faces (5 kN/m^2) followed by midspan cracking (9 kN/m^2). Midspan yield occurred shortly afterwards. Radial top cracking at columns A and B took place at 13.2 kN/m^2. Cracking along the line AB commenced at 14.2 kN/m^2, and at 15.6 kN/m^2 torsion cracking was visible in the spandrels close to the columns.

At a load of 19.7 kN/m^2 the load distribution system became unstable and collapsed. All load was removed and the spreader beam system was re-assembled. The loading was resumed and continued up to 22.8 kN/m^2, the maximum which the model would accept.

Although strain gauge and load cell readings were taken after this re-assembly, it seemed possible that these might be unreliable. It was found later that the two sets of readings did not display the close agreement which had been noticeable hitherto. It can be seen from the results that an error had probably been introduced into the load cells.

A stiffness test was performed at this stage, after which the loading system again collapsed. The only matter still to be investigated was the possibility of punching shear at column A. It was considered not feasible to continue in view of the state of the equipment.

At the maximum load, the longitudinal steel in the spandrel strip on side A had yielded while that in the beam on side B reached a stress of 305 MPa.

Figs. 6.5.4 and 6.5.5 are photographs of the top and bottom cracks respectively, while Figs. 6.5.8 and 6.5.9 give the same information in diagrammatic form.

For this test, load cell readings are given in Section B.5.4, strain gauge readings in Section B.5.5 and dial gauge readings in Section B.5.6, all in Appendix B.

Information about measured and derived quantities is given in graphical form at the end of this section and the nature and numbering of the graphs follows the same sequence as for model 4. Results are summarized in Table 6.5.1.

Stiffness Tests

Stiffness tests were carried out on model 5 in exactly the same way as for model 4. Graphs of the readings are shown in Fig. 6.5.22. The stiffness values obtained from these graphs are summarized in Table 6.5.2.

It should be noted that a shear failure did not occur around column A in this model. The final stiffness values in Table 6.5.1 refer to the condition of the model well after it had refused to accept more load. At this stage the region around column A was very extensively cracked.

Fig. 6.5.4 Cracks on Top of Slab near Column A

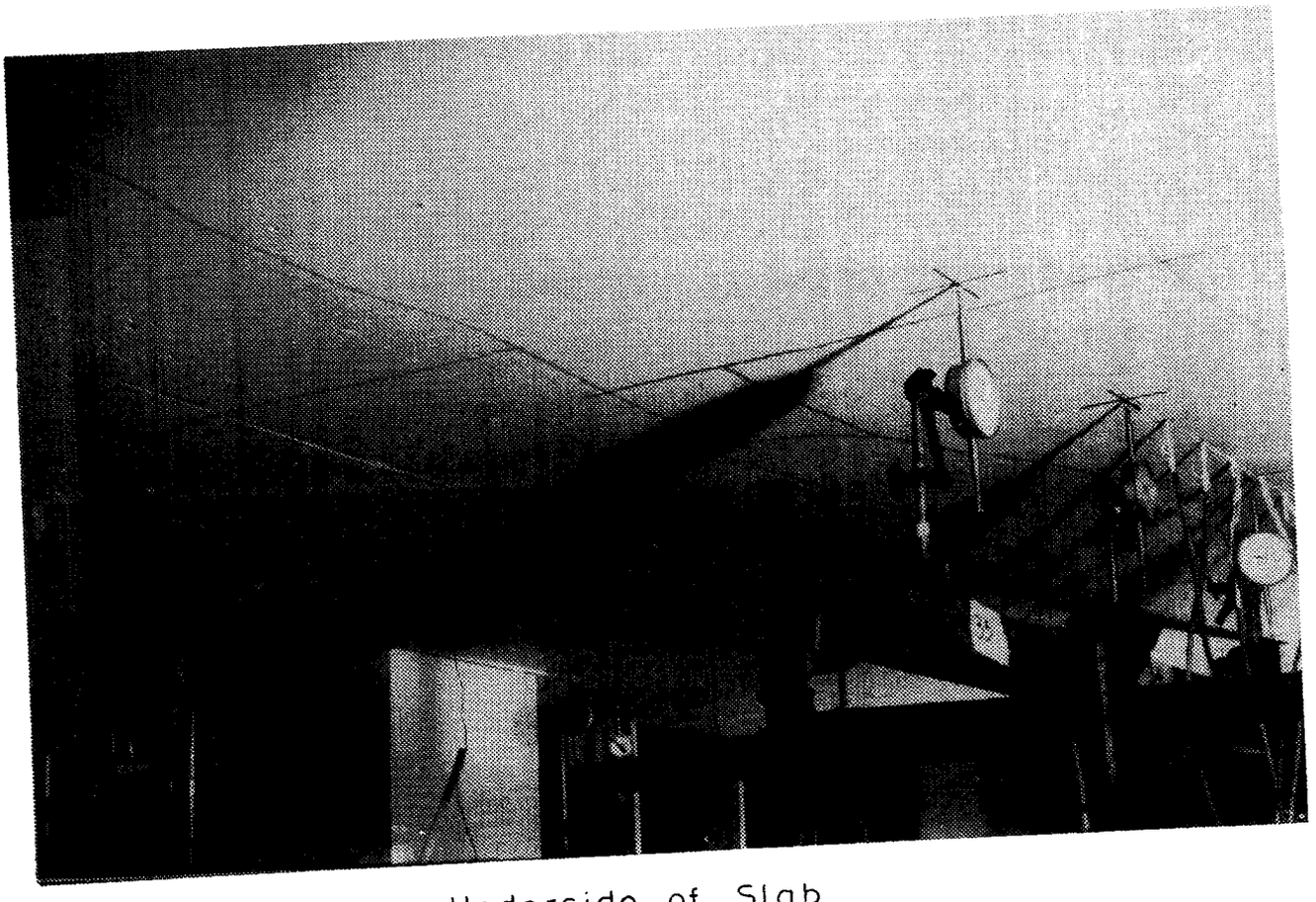

Fig. 6.5.5 Cracks on Underside of Slab

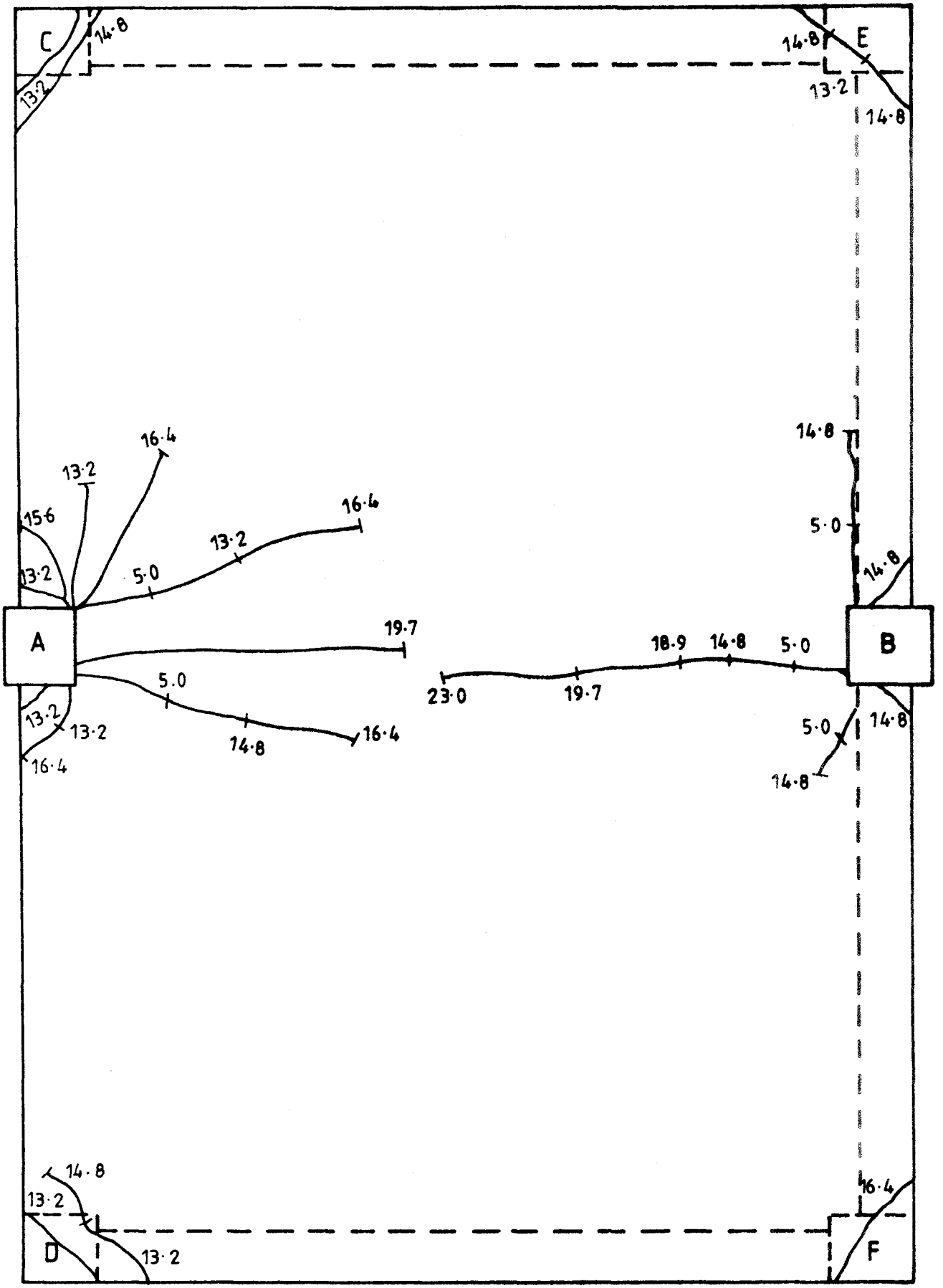

(NUMBERS ON THE CRACKS ARE LOAD IN kN/m^2)

Fig. 6.5.8: Crack Pattern on the Top of Model 5

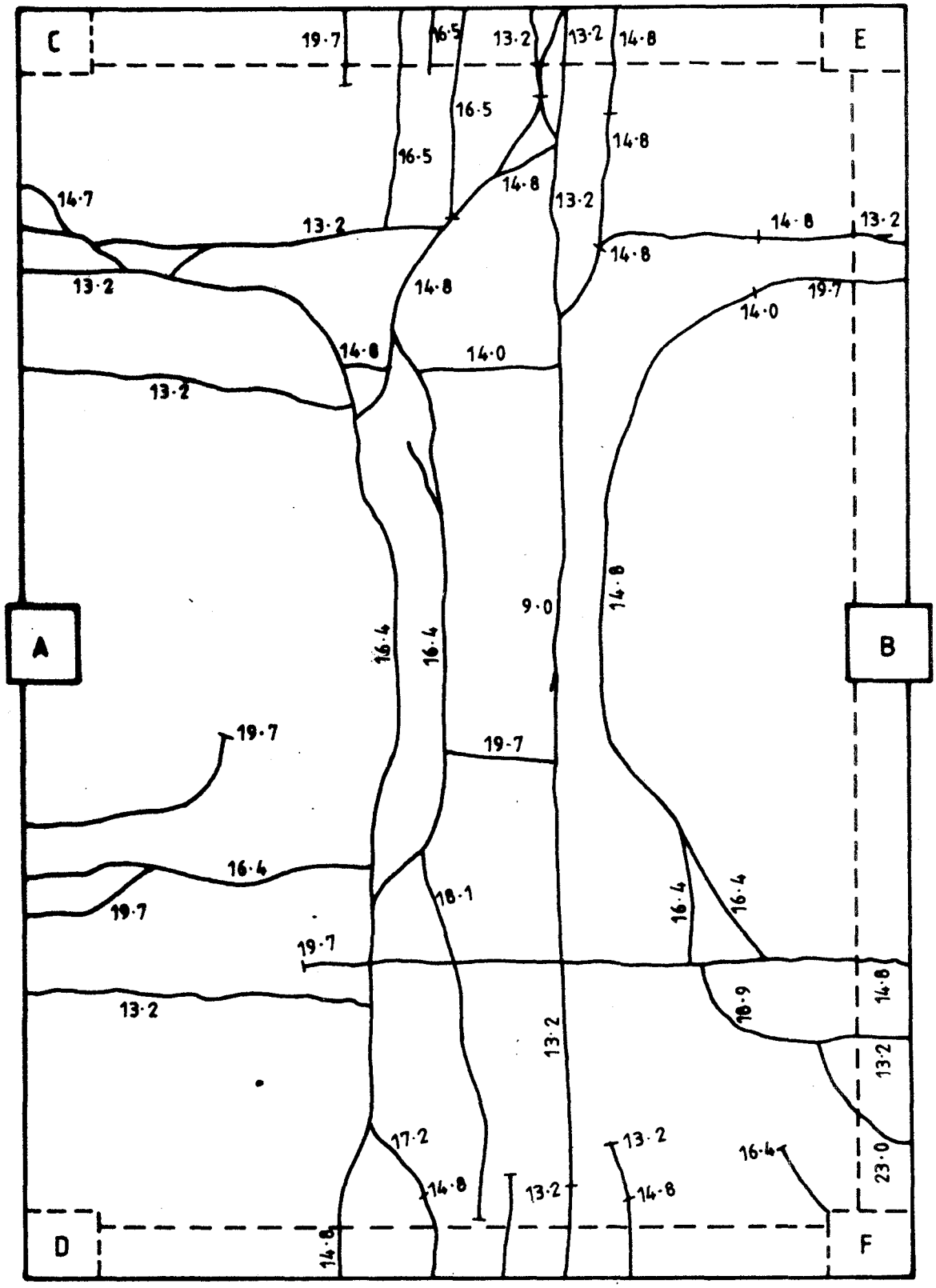

(NUMBERS ON THE CRACKS ARE LOAD IN kN/m²)

Fig. 6.5.9: Crack Pattern on the Bottom of Model 5

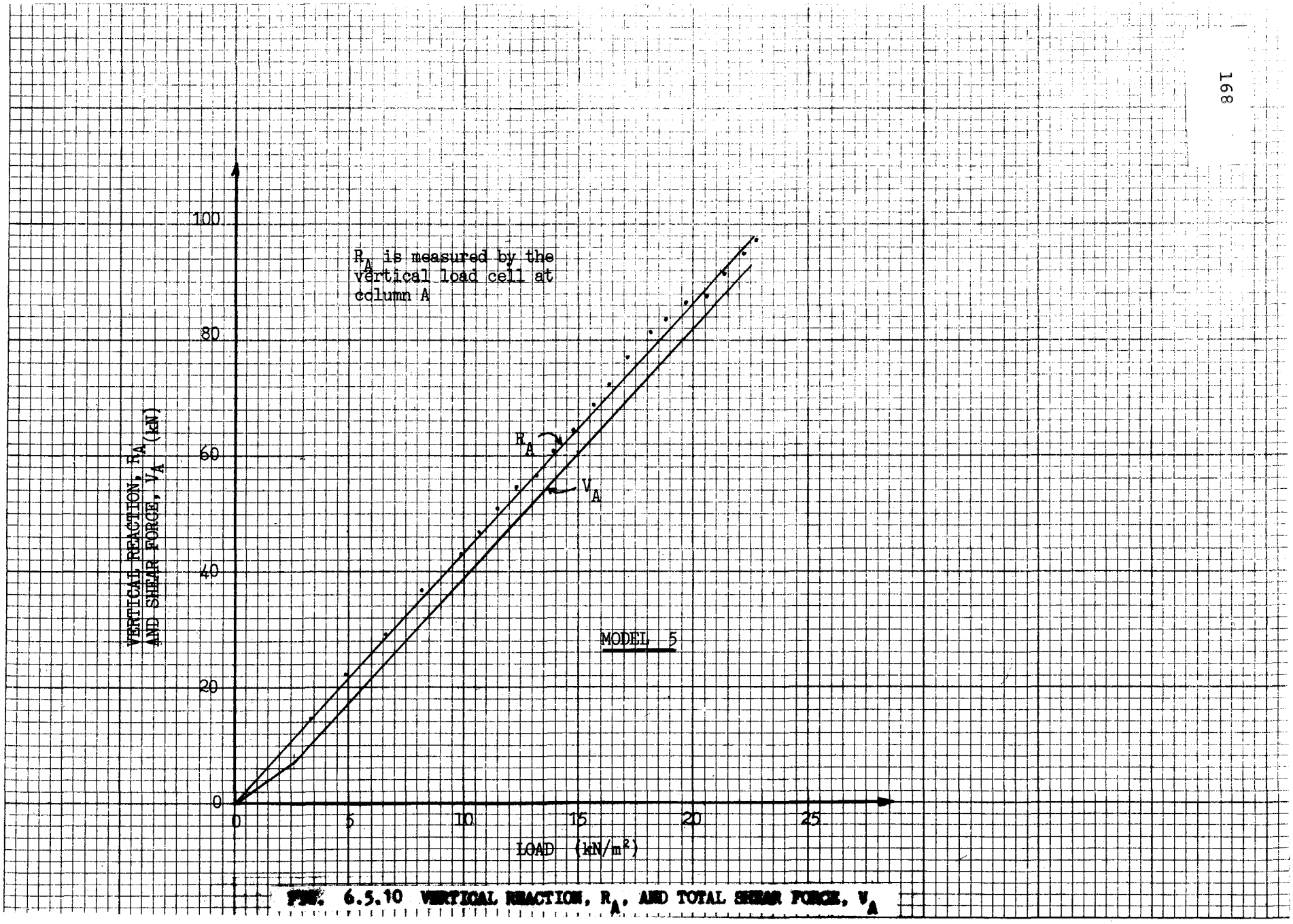

FIG. 6.5.10 VERTICAL REACTION, R_A, AND TOTAL SHEAR FORCE, V_A

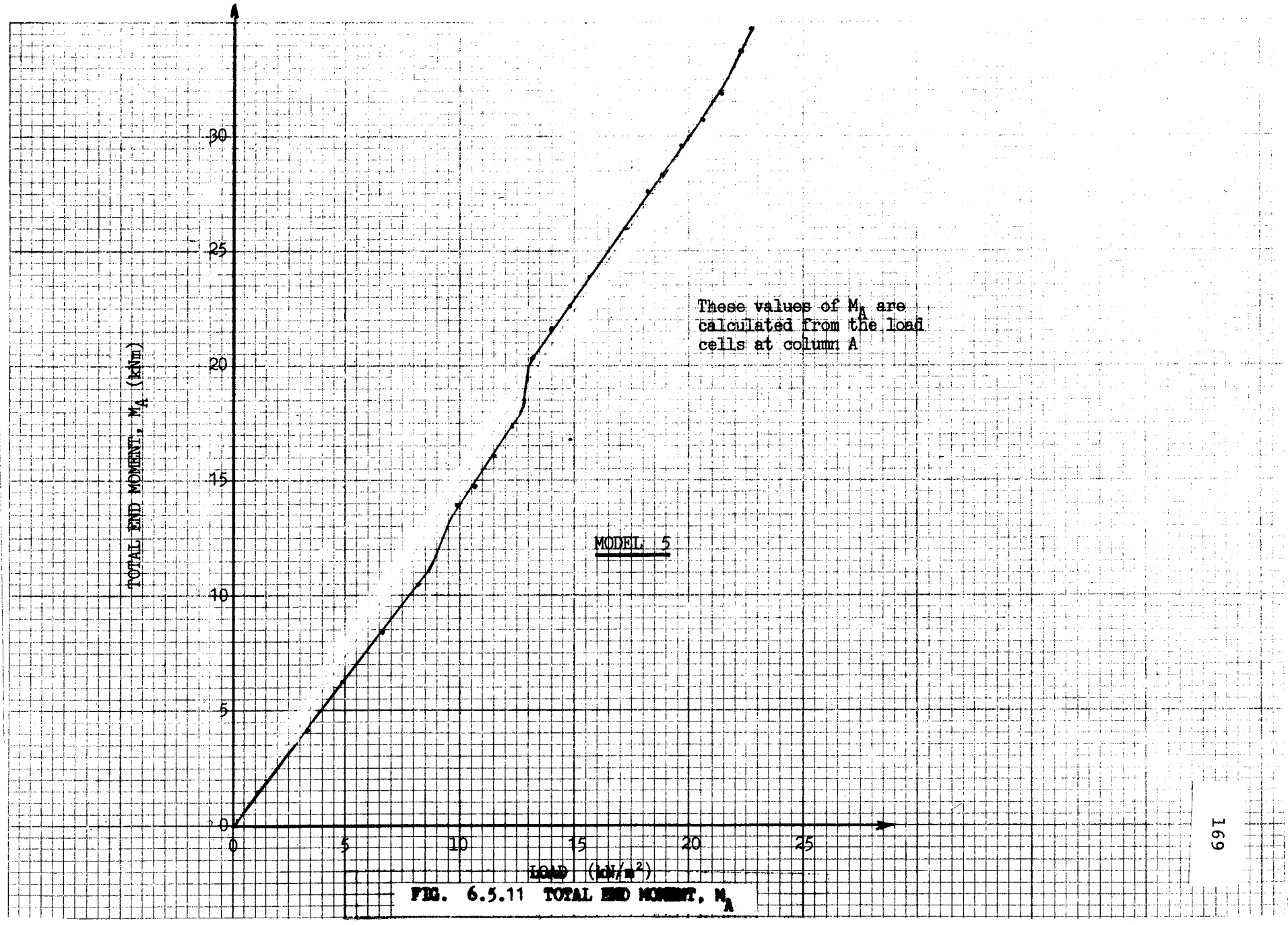

FIG. 6.5.11 TOTAL END MOMENT, M_A

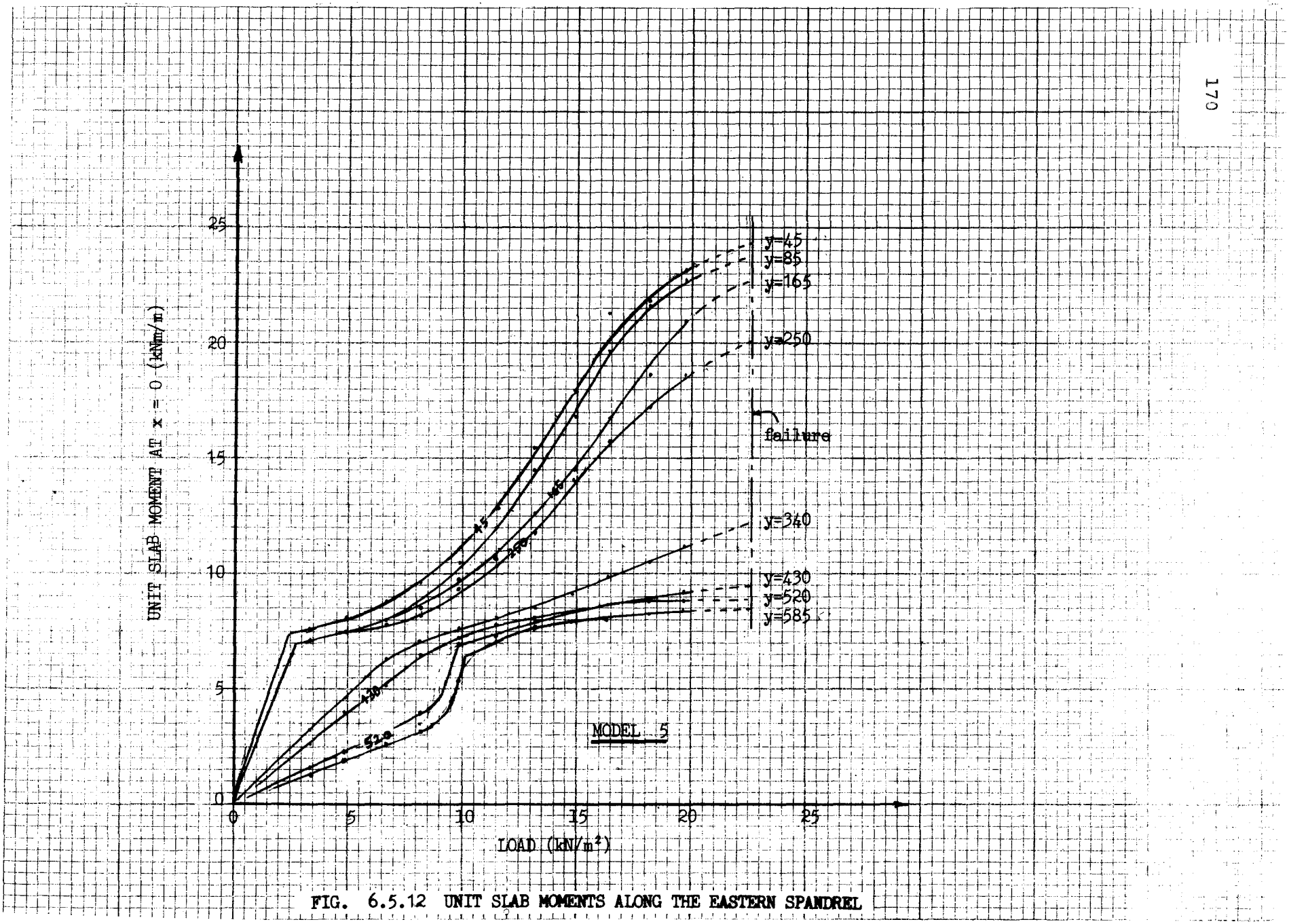

FIG. 6.5.12 UNIT SLAB MOMENTS ALONG THE EASTERN SPANDREL

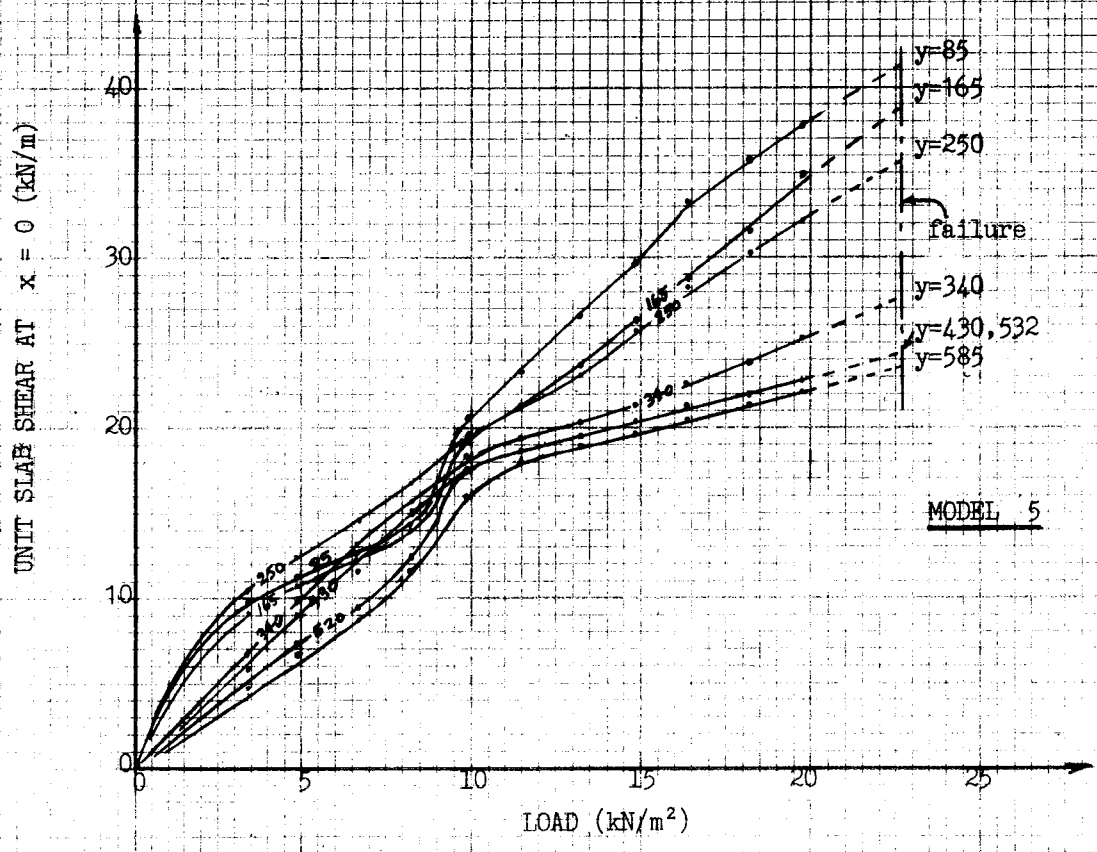

FIG. 6.5.13 UNIT SLAB SHEAR ALONG THE EASTERN SPANDREL

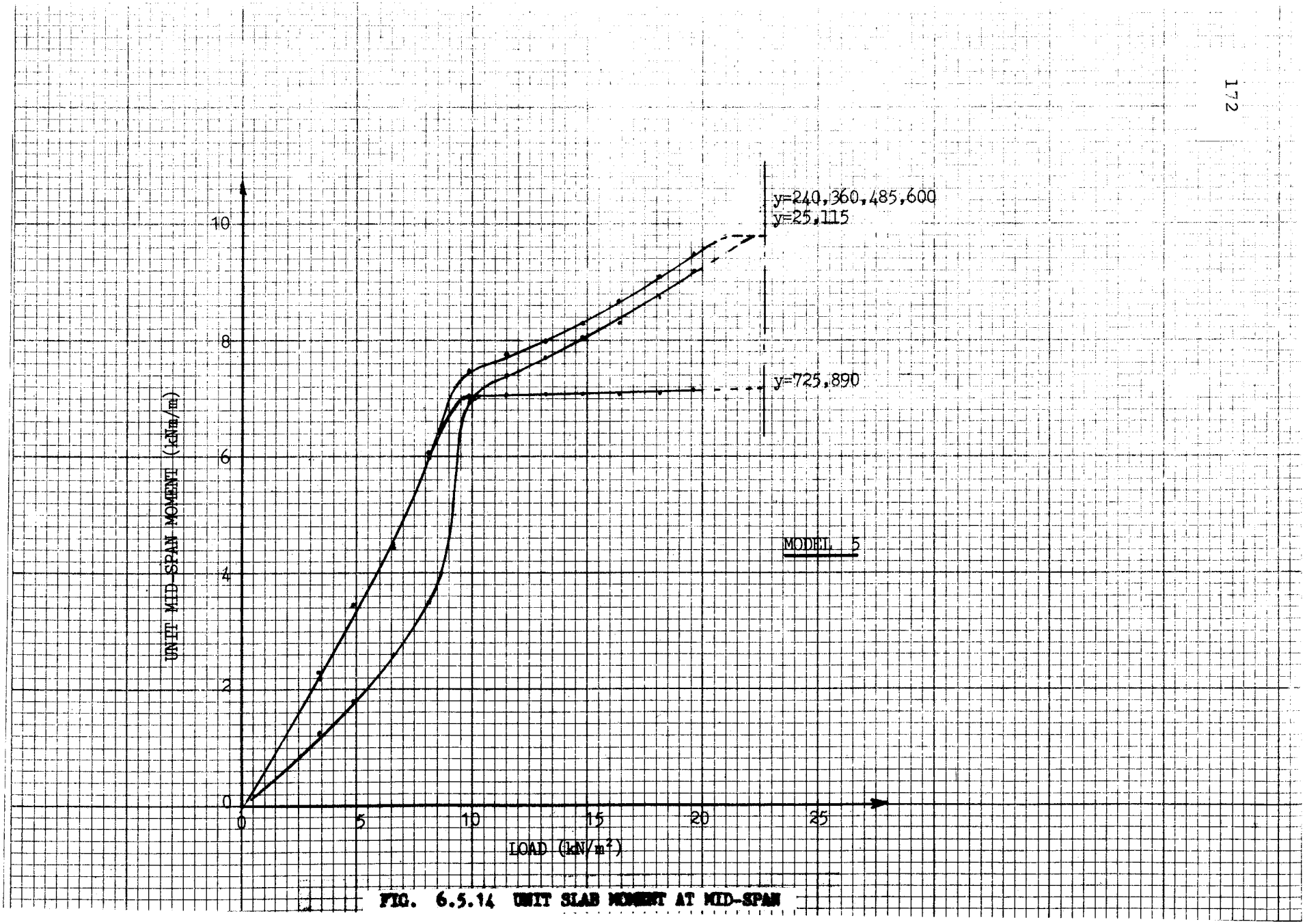

FIG. 6.5.14 UNIT SLAB MOMENT AT MID-SPAN

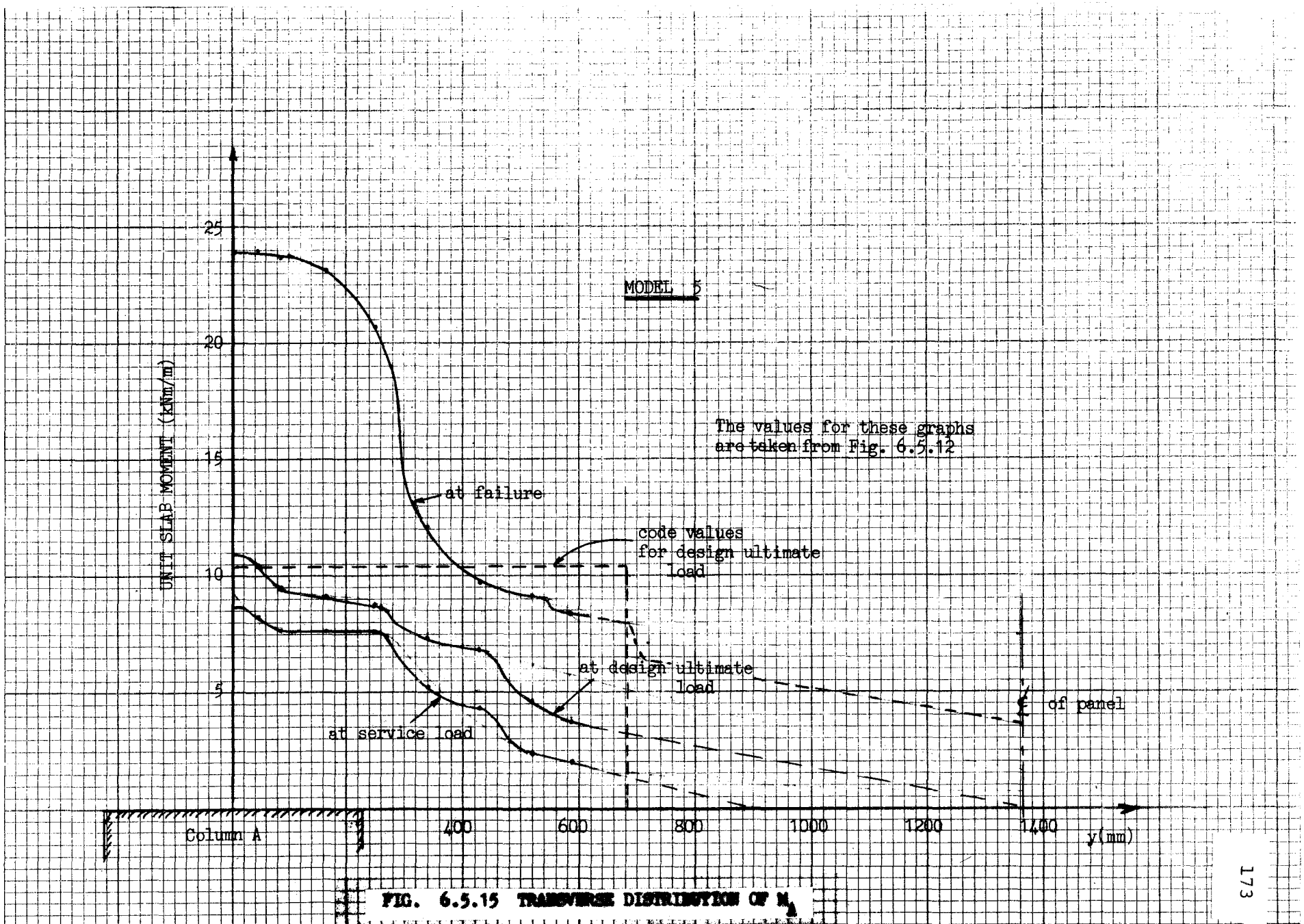

FIG. 6.5.15 TRANSVERSE DISTRIBUTION OF M_A

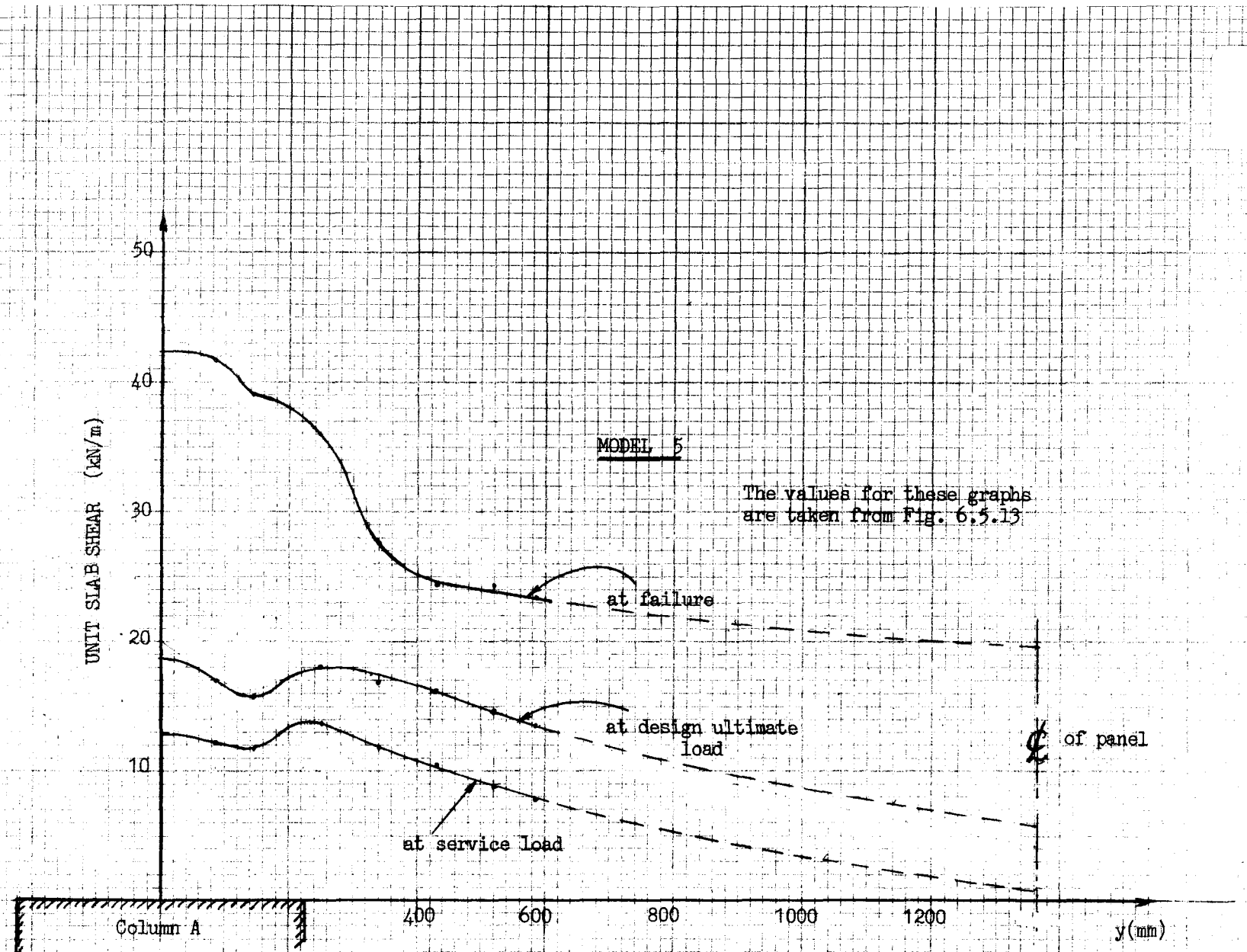

FIG. 6.5.16 TRANSVERSE DISTRIBUTION OF V_A

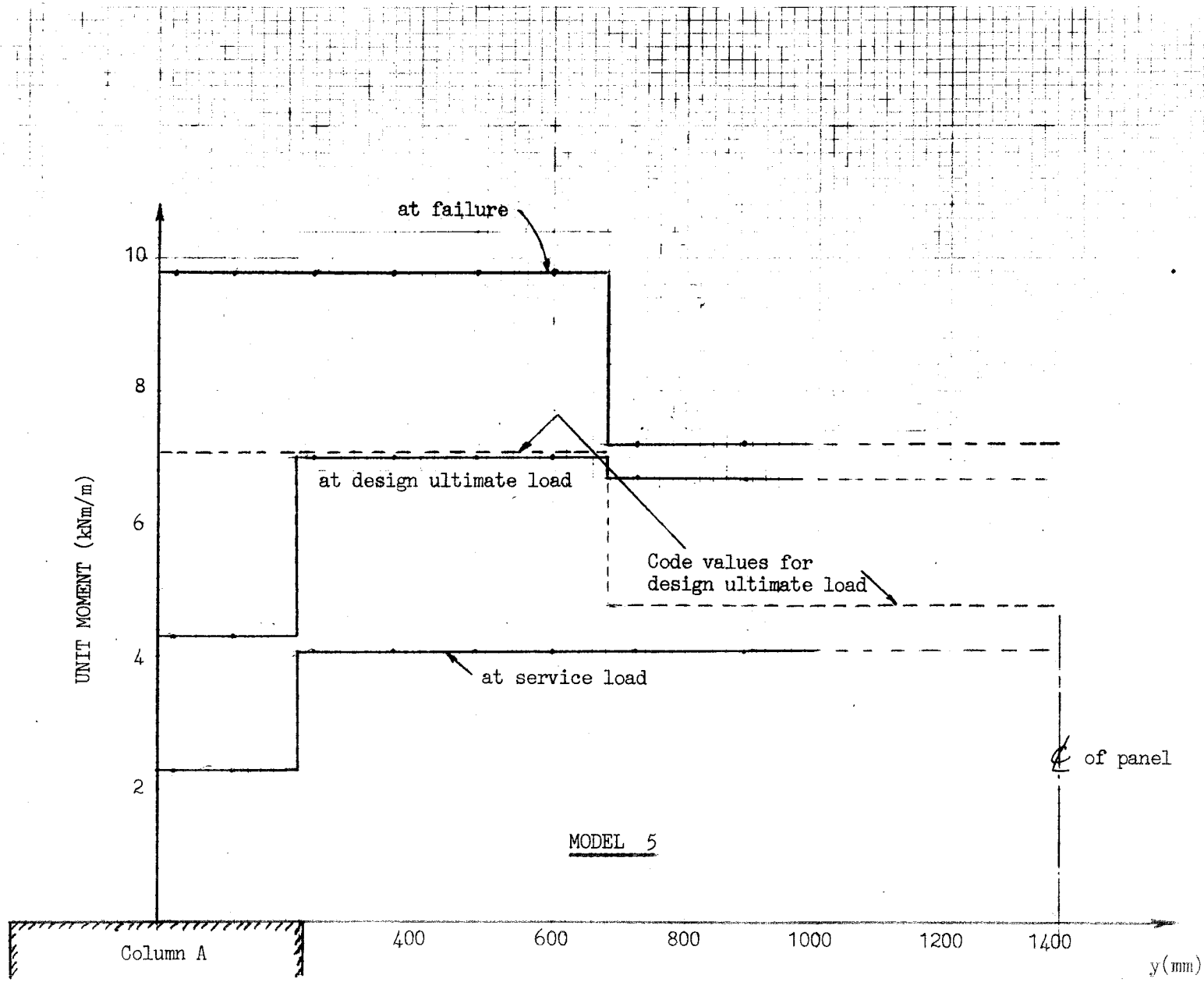

FIG. 6.5.17 TRANSVERSE DISTRIBUTION OF MID-SPAN MOMENT

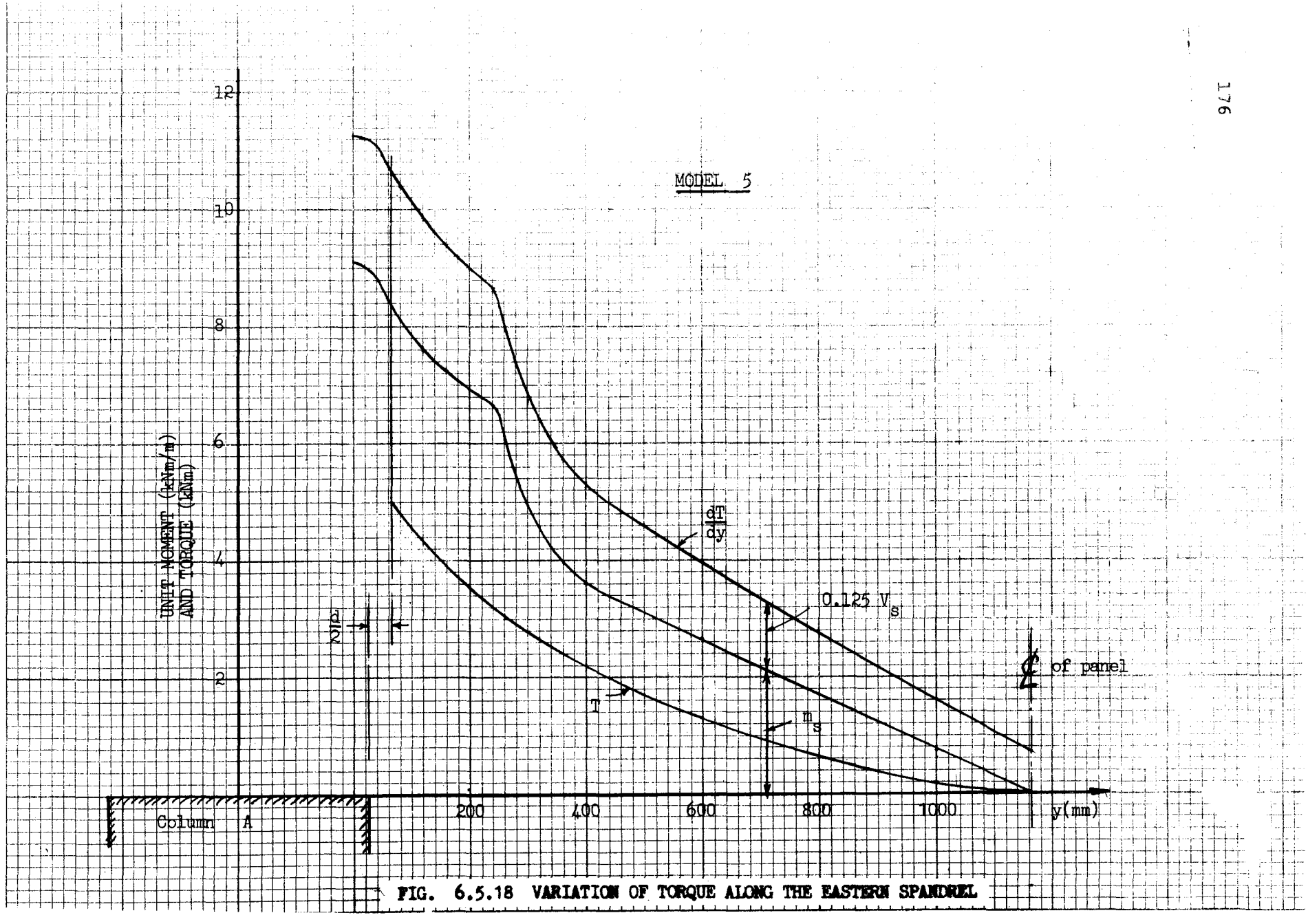

FIG. 6.5.18 VARIATION OF TORQUE ALONG THE EASTERN SPANDREL

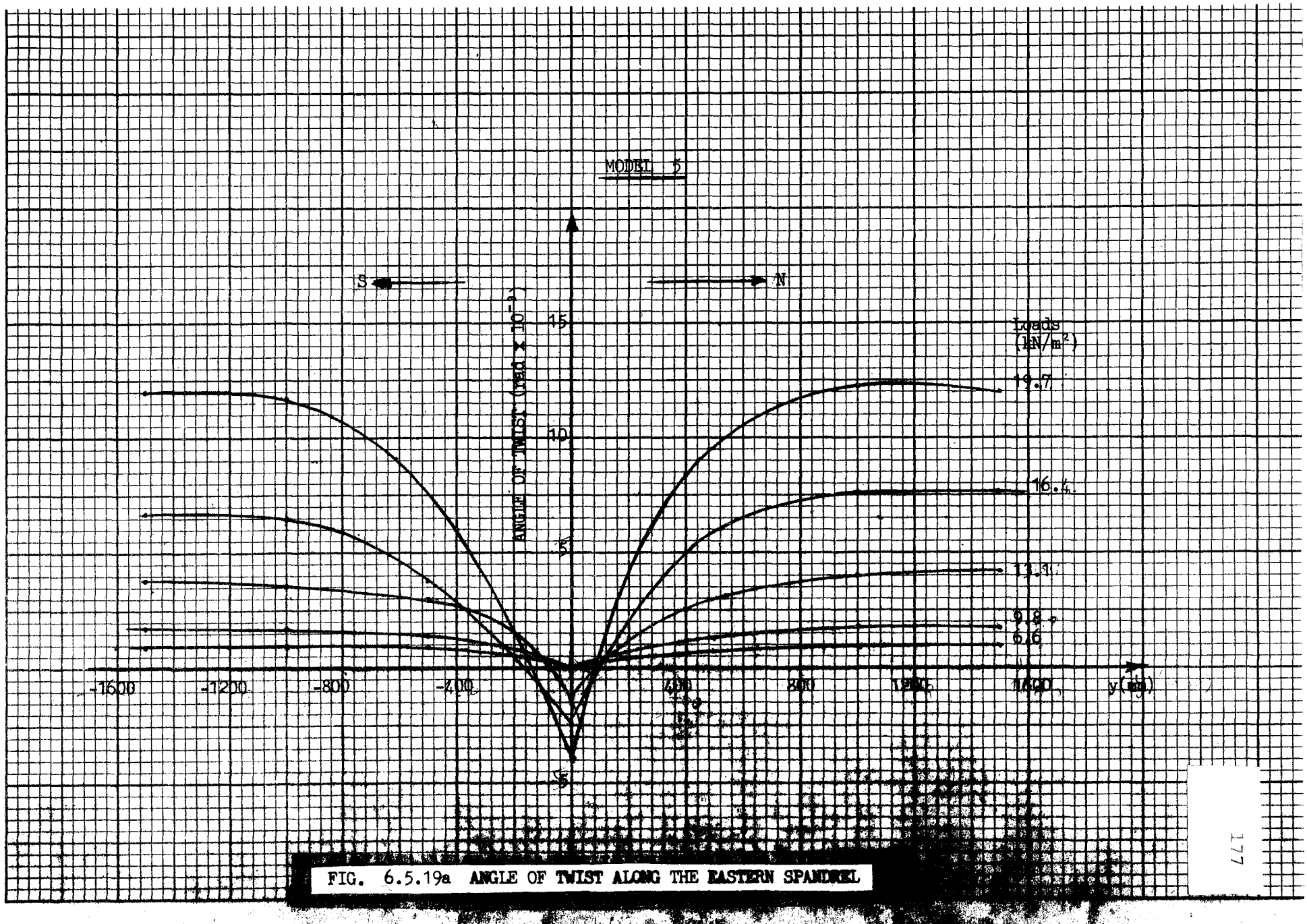

FIG. 6.5.19a ANGLE OF TWIST ALONG THE EASTERN SPANDREL

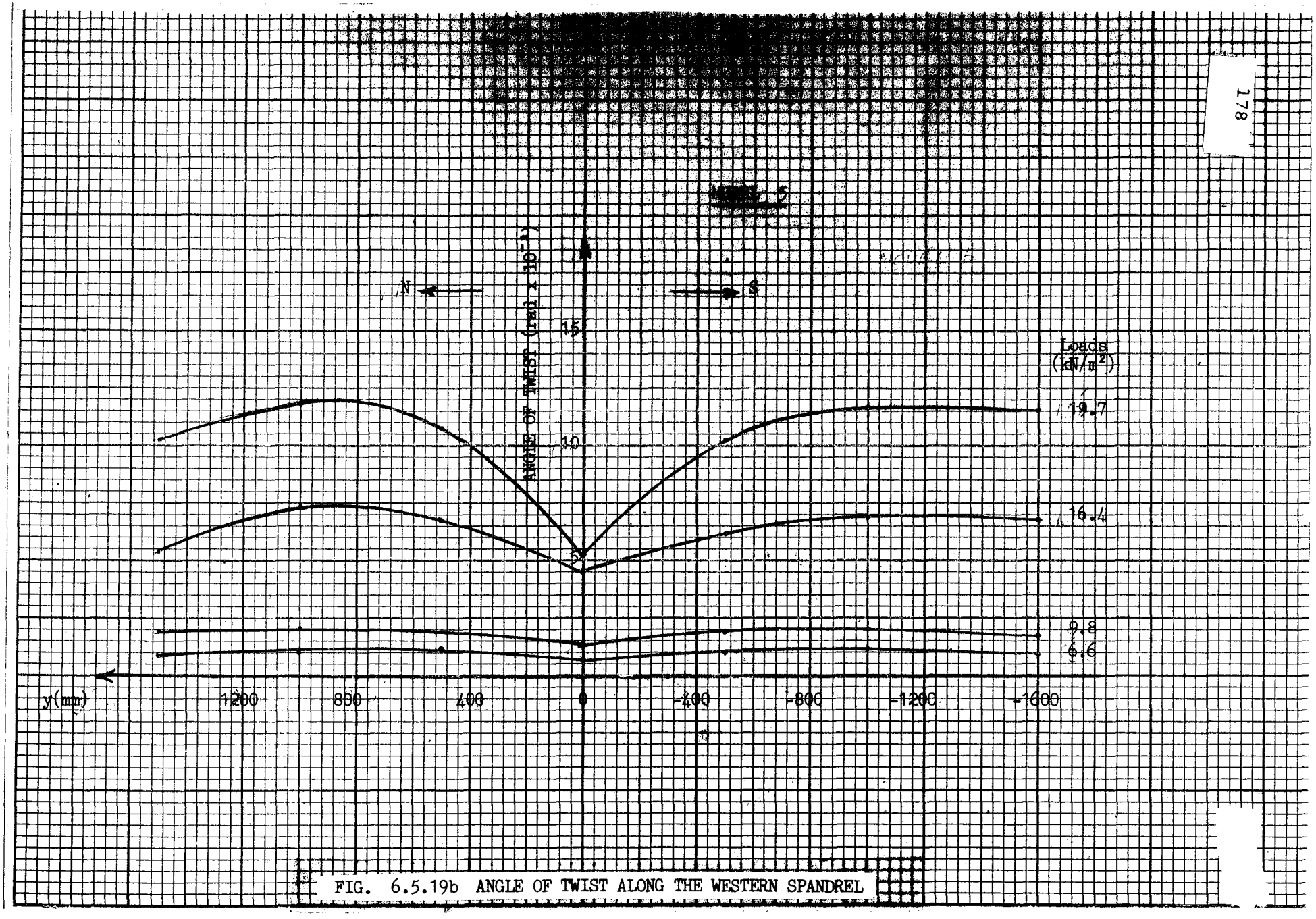

FIG. 6.5.19b ANGLE OF TWIST ALONG THE WESTERN SPANDREL

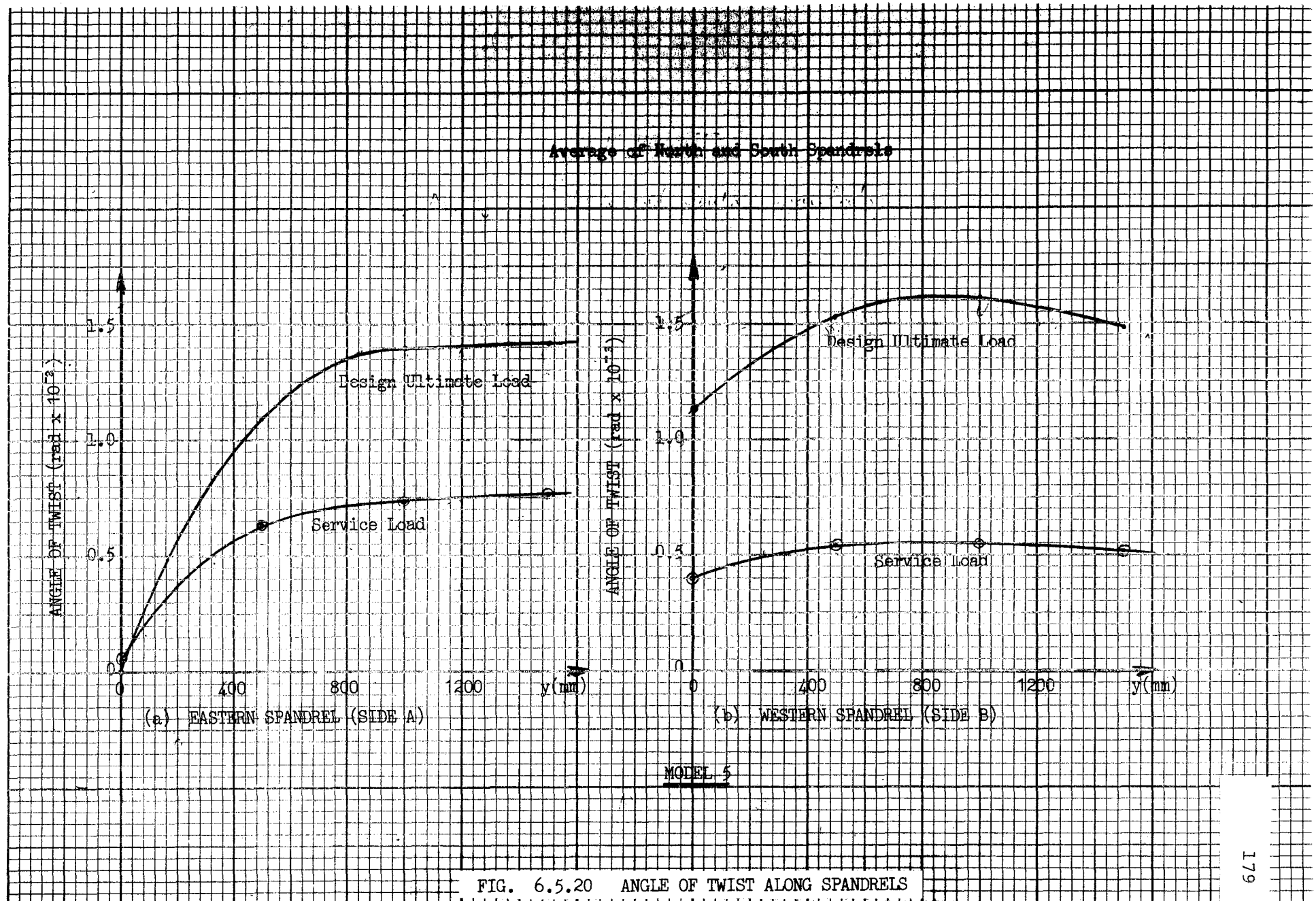

FIG. 6.5.20 ANGLE OF TWIST ALONG SPANDRELS

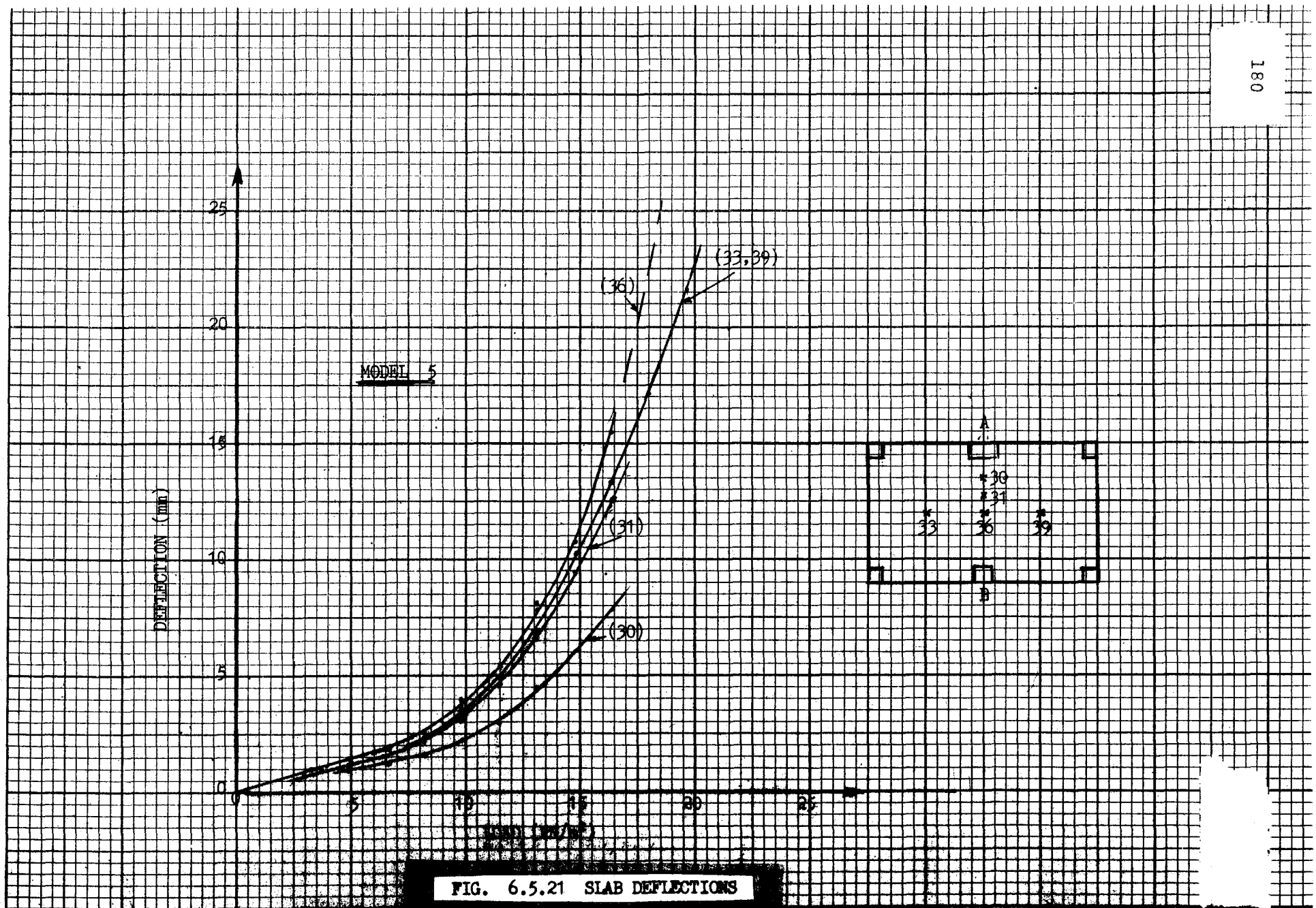

FIG. 6.5.21 SLAB DEFLECTIONS

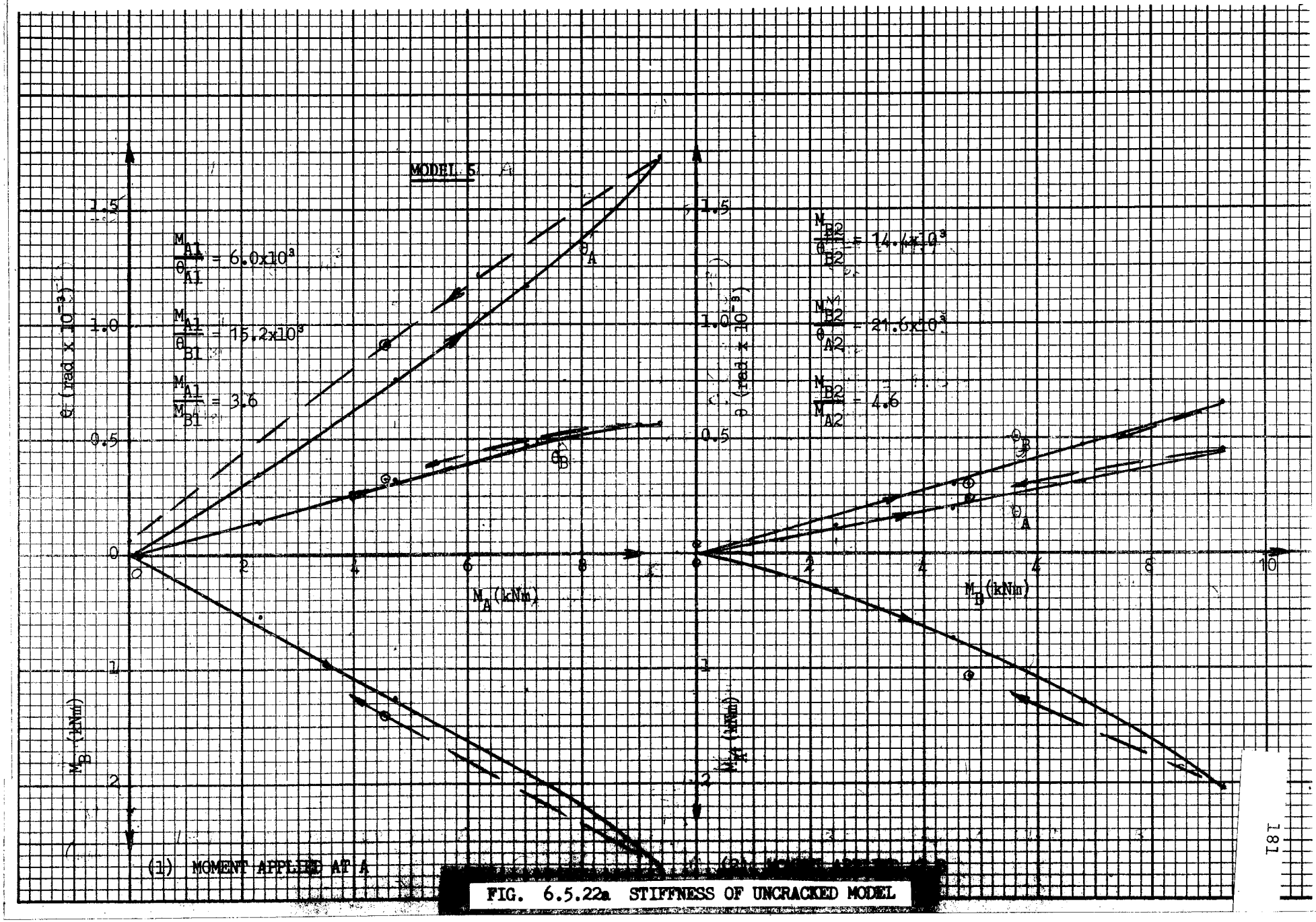

FIG. 6.5.22a STIFFNESS OF UNCRACKED MODEL

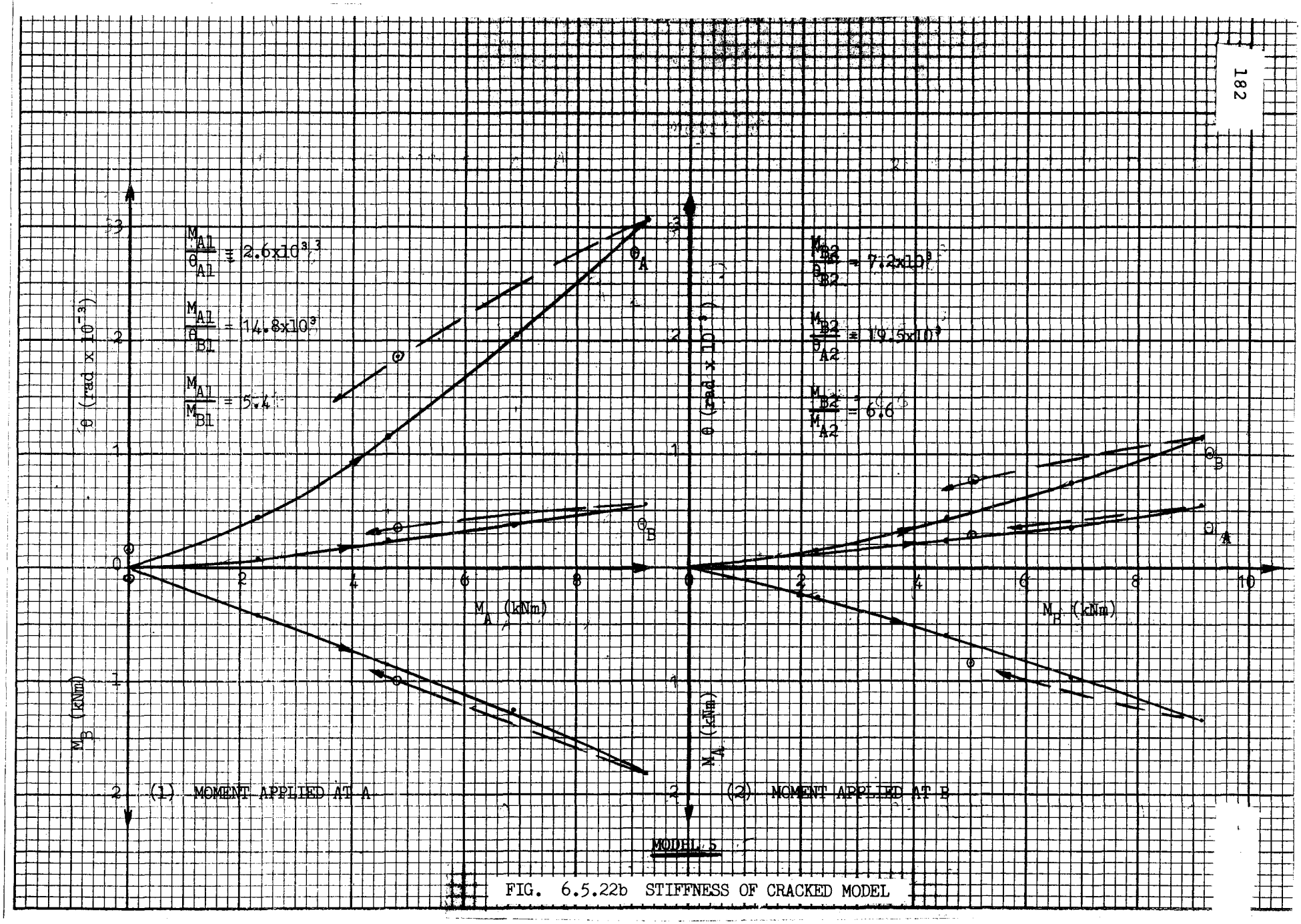

FIG. 6.5.22b STIFFNESS OF CRACKED MODEL

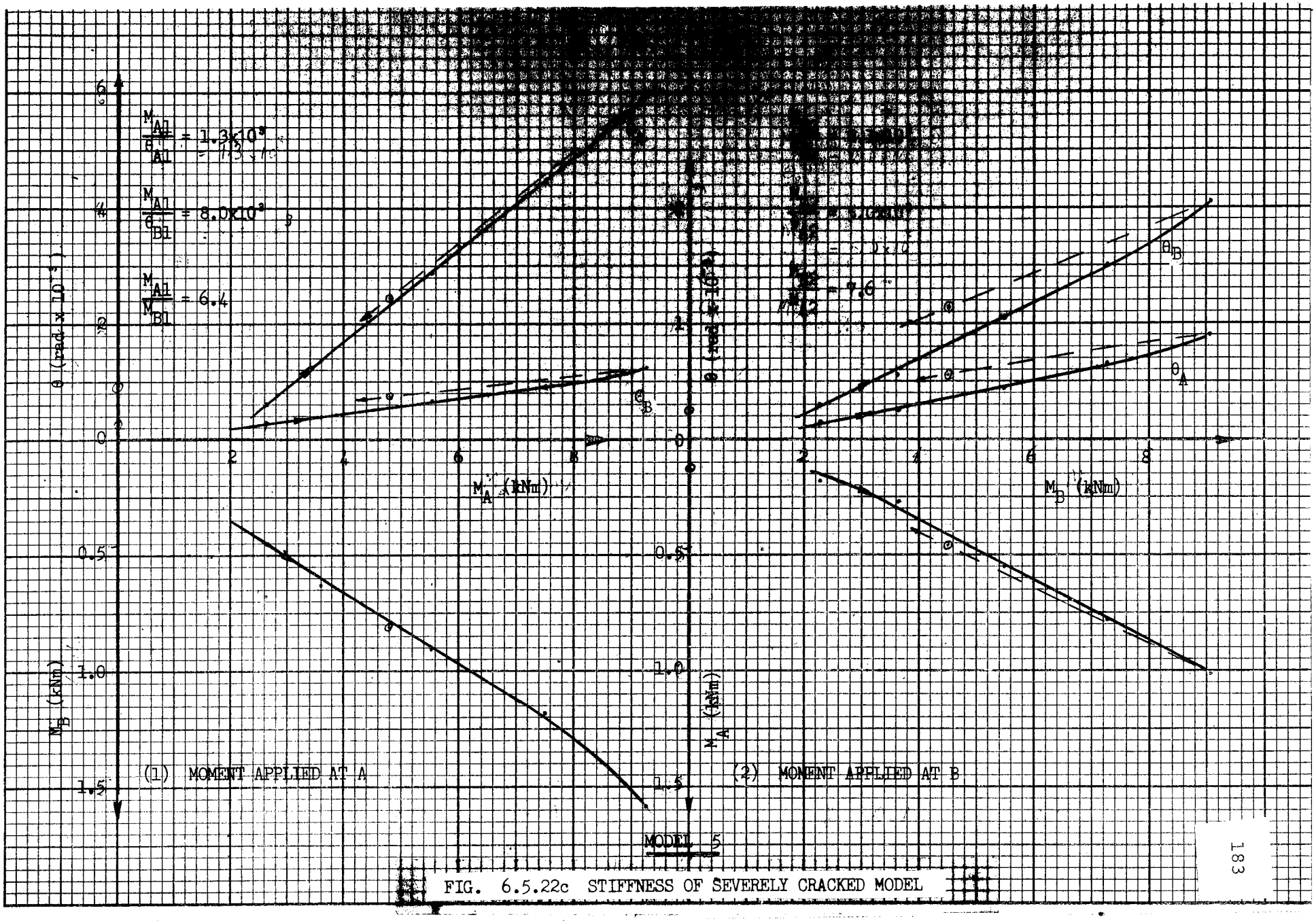

FIG. 6.5.22c STIFFNESS OF SEVERELY CRACKED MODEL

FIG. 6.5.23 VERTICAL REACTION, R_B, AND TOTAL SHEAR FORCE, V_B

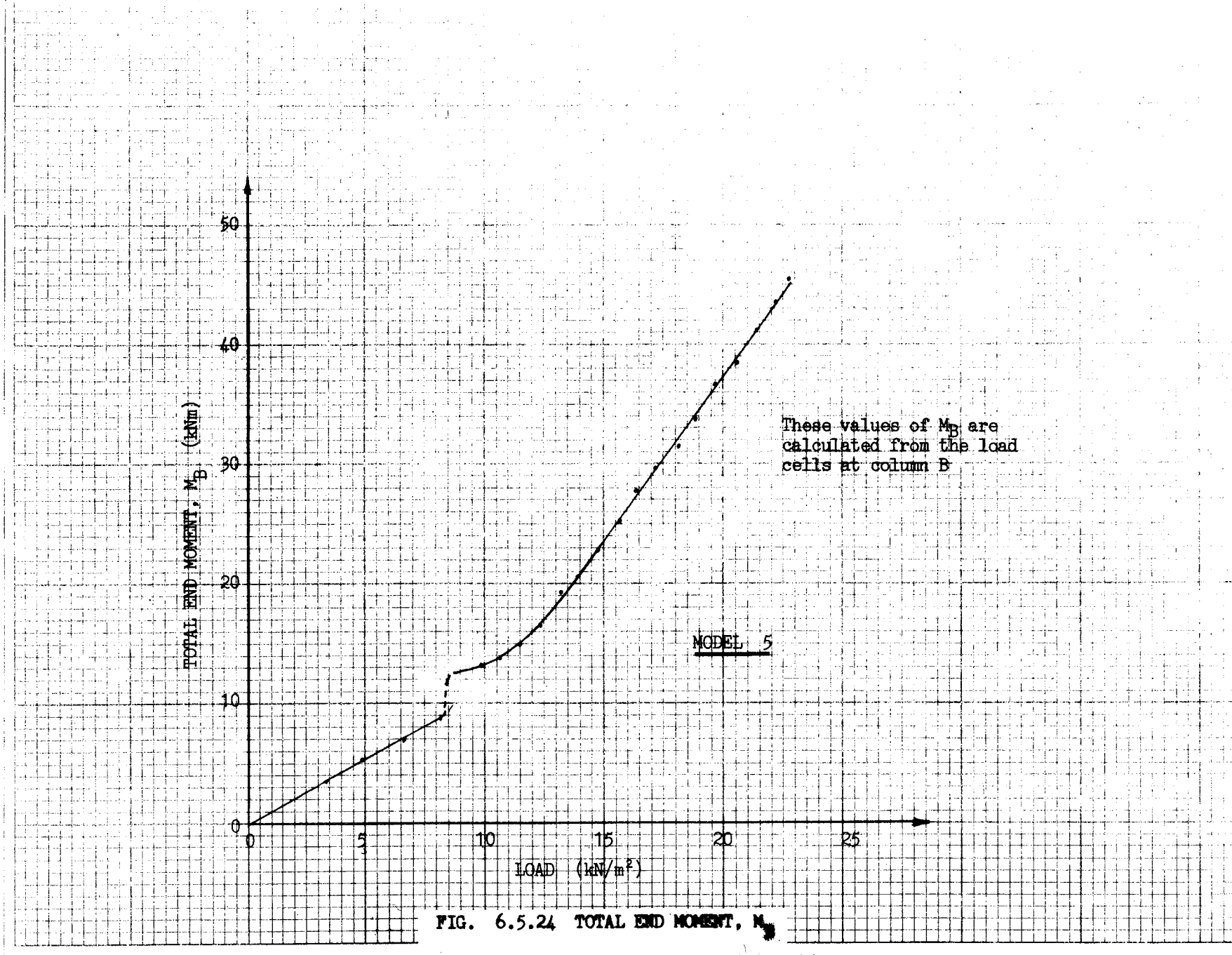

FIG. 6.5.24 TOTAL END MOMENT, M_B

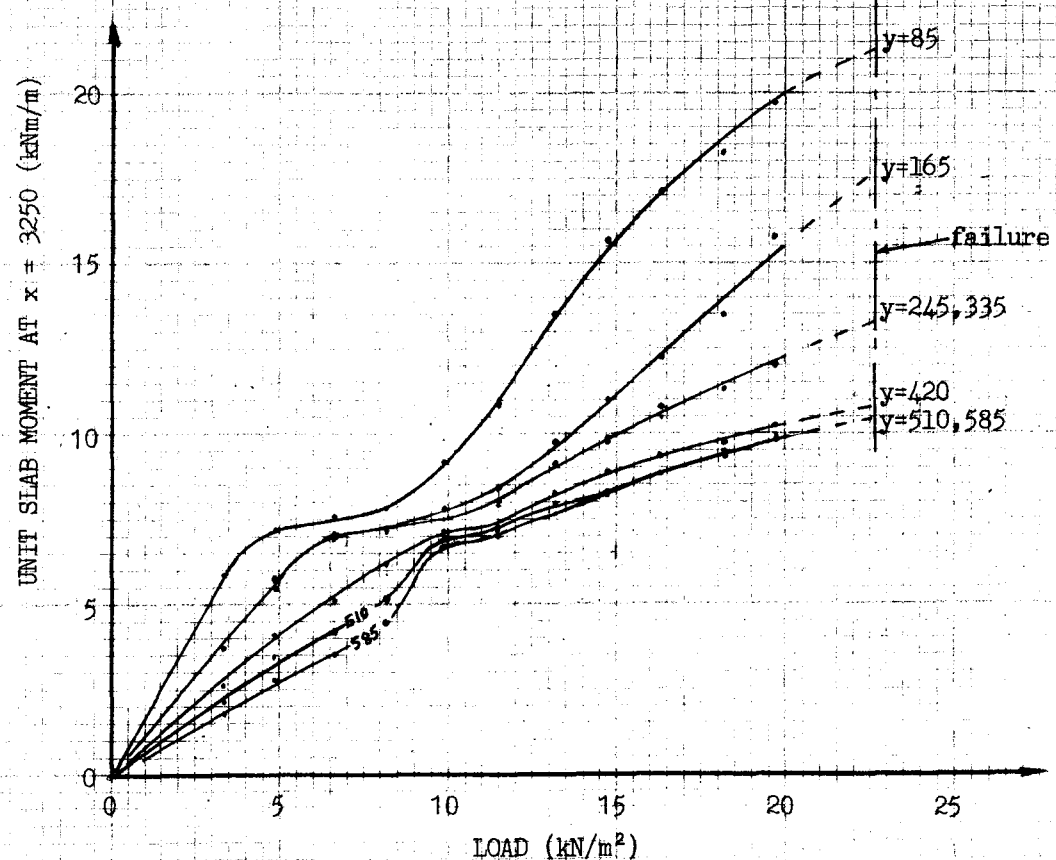

FIG. 6.5.25 UNIT SLAB MOMENTS ALONG THE WESTERN SPANDREL

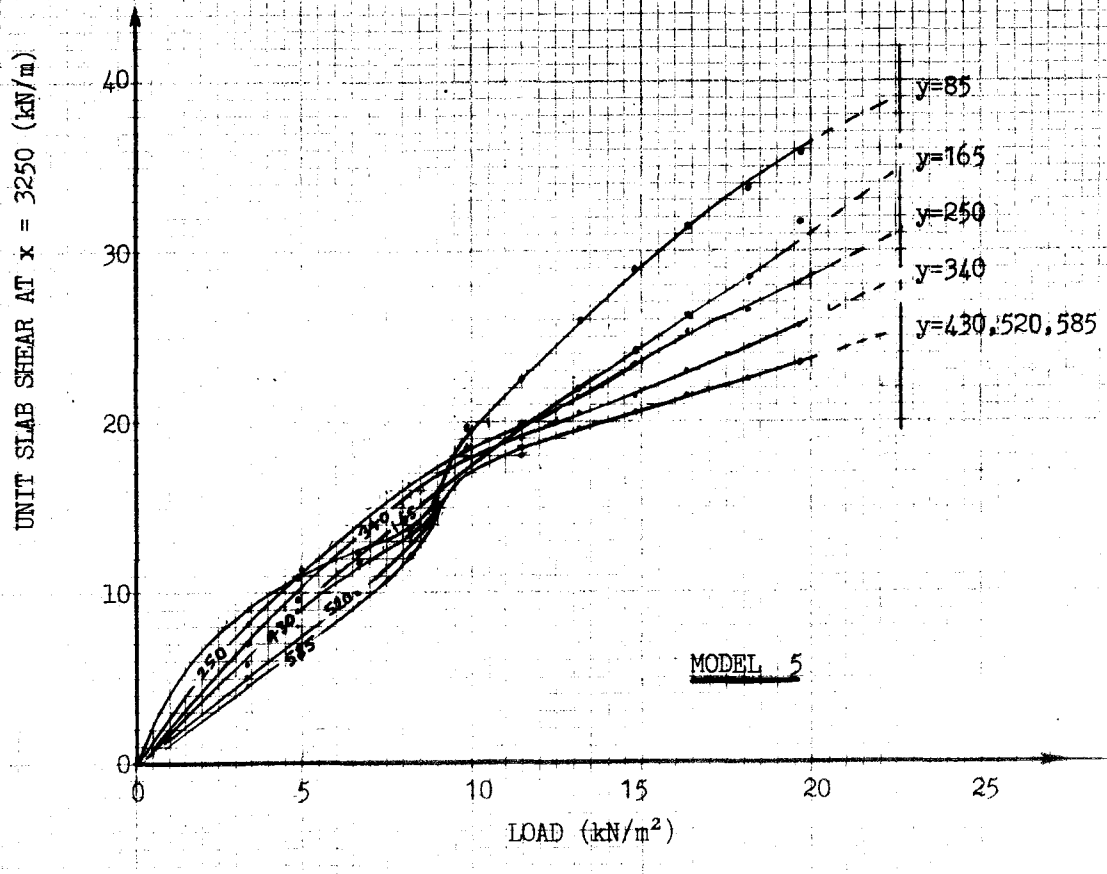

FIG. 6.5.26 UNIT SLAB SHEAR ALONG THE WESTERN SPANDREL

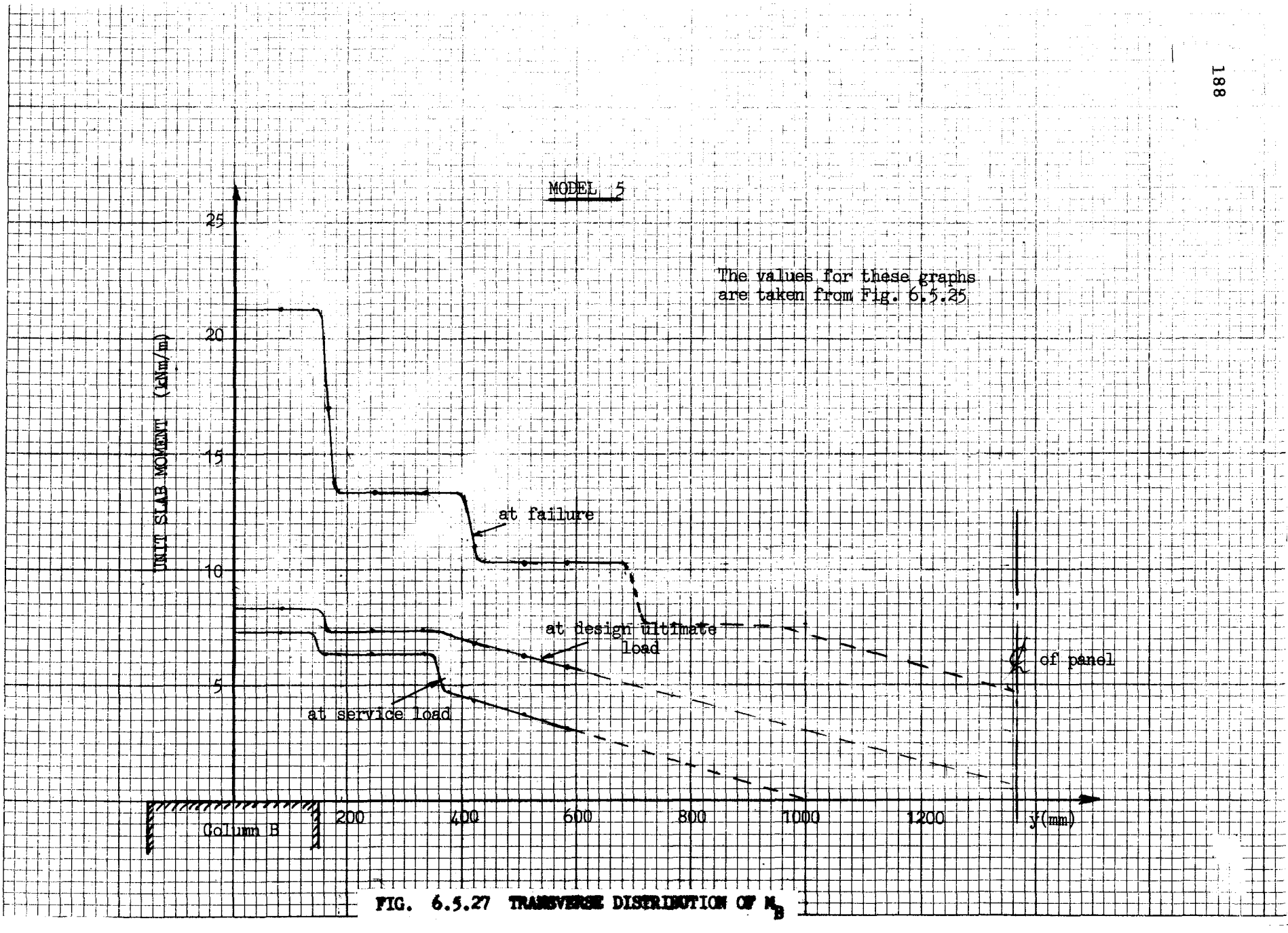

FIG. 6.5.27 TRANSVERSE DISTRIBUTION OF M_B

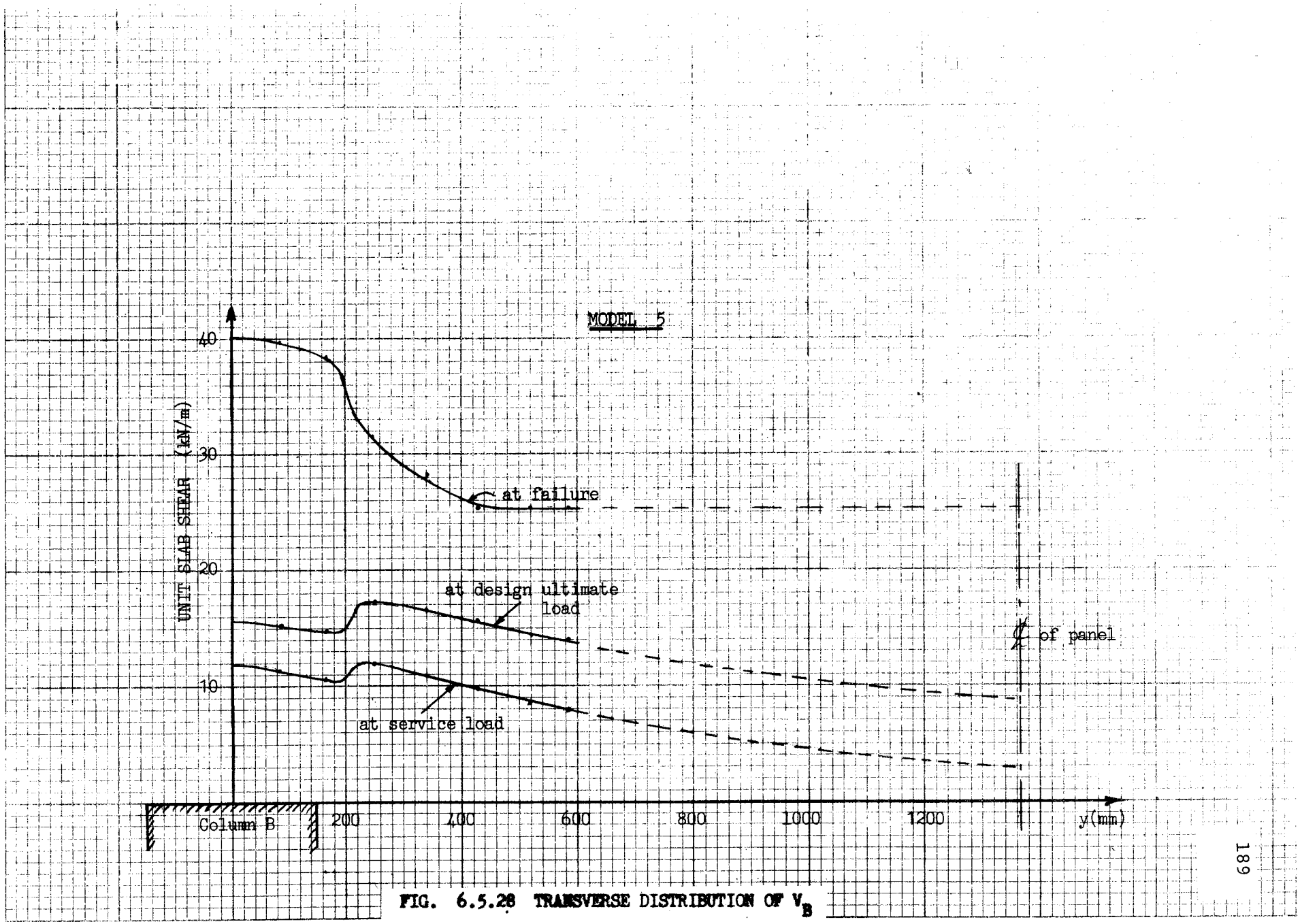

FIG. 6.5.28 TRANSVERSE DISTRIBUTION OF V_B

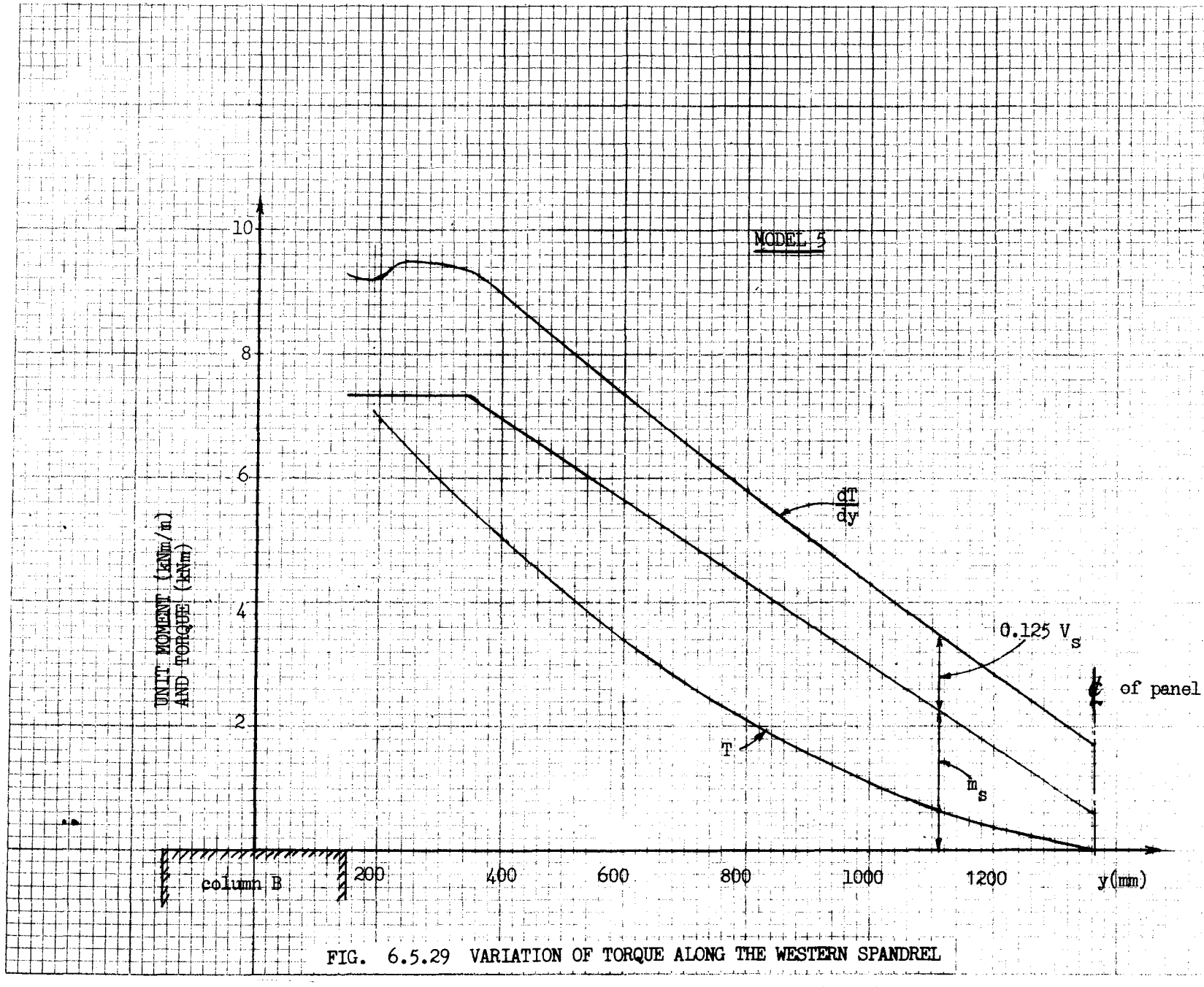

FIG. 6.5.29 VARIATION OF TORQUE ALONG THE WESTERN SPANDREL

MODEL No. 5.

TABLE 6.5.1 SUMMARY OF RESULTS OF VERTICAL LOAD TEST

Service Load = 5.4 kN/m^2
Design Ultimate Load = 9.0 kN/m^2
Failure Load = 22.8 kN/m^2

Item	Load Level (kN/m^2)	Test Value
1. Vertical Reaction at A = R_A (kN)	5.4 9.0 22.5	23.5 39.0 98
2. Vertical Reaction at B = R_B (kN)	5.4 9.0 22.5	25.5 42.0 103
3. Total Mid-Span Moment = M_M (kNm)	5.4 9.0 22.5	(10.3) (17.4) (23.2)
4. Total Moment at face of Spandrel A = M_A (kNm)	5.4 9.0 22.5	6.9 (7.4) 11.8 (11.9) 34.2 (27.7)
5. Total Shear Force at Face of Spandrel A = V_A (kN)	5.4 9.0 22.5	19.0 (19.3) 34.5 (33.9) 94 (71)
6. Total Moment at Face of Spandrel B = M_B (kNm)	5.4 9.0 22.5	5.8 (7.9) 12.8 (13.6) 45.5 (28.8)
7. Total Shear Force at Face of Spandrel B = V_B (kN)	5.4 9.0 22.5	22.0 (19.9) 38.6 (35.2) 100 (76)
8. Transverse Distribution of Mid-Span Moment M_M		See Fig. 6.5.17
9. Transverse Distribution of M_A		See Fig. 6.5.15
10. Transverse Distribution of M_B		See Fig. 6.5.27

* Values in brackets are obtained from strain gauge readings by integration. Other values are obtained from load cells.

MODEL No. 5

VERTICAL LOAD TEST (cont.)

Item	Load Level (kN/m^2)	Test Value
11. Distribution of Torque along Spandrel A	design ultimate load	See Fig. 6.5.18
12. Torque in Spandrel A at Face of Column A (kNm)	design ultimate load	
13. End Moment in Beam Strip at Face of Column A (kNm)	5.4 9.0 22.5	(4.1) (5.0) (12.3)
14. Shear Force in Beam Strip at Face of Column A (kN)	5.4 9.0 22.5	(6.7) (9.2) (21.1)
15. Shear Force in Spandrel at Face of Column A (kN)	5.4 9.0 22.5	6.9 (7.1) 13.4 (13.1) 37.2 (25.7)
16. Distribution of Torque along Spandrel B	design ultimate load	See Fig. 6.5.29
17. Torque in Spandrel B at Face of Column B (kNm)	design ultimate load	(7.1)
18. End Moment in Beam Strip at Face of Column B (kNm)	5.4 9.0 22.5	(2.7) (3.1) (7.8)
19. Shear Force in Beam Strip at Face of Column B (kN)	5.4 9.0 22.5	(4.3) (5.8) (15.2)
20. Shear Force in Spandrel at Face of Column B (kN)	5.4 9.0 22.5	10.1 (9.1) 17.6 (16.0) 47.5 (35.5)
21. Mid-span Moment in Beam Strip (kNm)	5.4 9.0 22.5	(1.3) (2.5) (5.4)

MODEL No. 5

TABLE 6.5.2 - SUMMARY OF RESULTS OF STIFFNESS TESTS

	Condition of Model		
	Uncracked	Cracked	Severely Cracked
Stiffness of Joint A = k_A (kNm/radian)	6.5×10^3	2.6×10^3	1.3×10^3
Carry-over factor from A to B = c_{BA}	0.83	0.3	0.12
Stiffness of Joint B = k_B (kNm/radian)	18.0×10^3	7.5×10^3	2.2×10^3
Carry-over factor from B to A = c_{AB}	0.08	0	0.13

Chapter 7

DISCUSSION OF RESULTS

7.1 RELIABILITY OF RESULTS

Before proceeding to the possible significance of the results presented in Chapter 6, it is perhaps desirable to discuss the general functioning of the models and the various measuring devices. Some estimate may then be made of the accuracy which can be ascribed to the results.

In regard to the models themselves, it must be recalled that the original purpose of the tests was to study the distribution of forces around the edge column A (at the middle of the eastern boundary). It would appear that the northern, western and southern boundaries of the model were in fact sufficiently far from the test area that the absence of the floor panels outside the model was of little significance. The cantilever tests applied to these artificial boundaries indicated that if further panels had been included in the model, then the loads on these panels would probably influence the forces around column A by less than 5%. From this point of view the adopted boundary conditions can be considered satisfactory.

In later models interest was also taken in the total moments M_A, M_B and M_M in the central panel, i.e. the panel centred on the column line AB. Here M_A is the total panel moment along the internal edge of spandrel A, M_B is the corresponding moment along spandrel B and M_M is the total mid-span moment in the panel. The tests were not originally designed for this purpose and, as might be expected, the chosen boundary conditions had rather more effect on these quantities. The small stiffening beams adopted on the three edges remote from A had the effect of attracting load away from the central panel. This is indicated partly by the fact the deflections at the panel centres were slightly less than that of the mid-point of the column line AB. This can be seen in Fig. 6.4.21 where the line 34-35-36-37-38 is virtually horizontal at any given load level whereas the panel centre-points 33 and 39 have a deflection about 16% less than this. Similar effects can

be seen in Figs. 6.3.21 and 6.5.21. In a true flat plate floor the deflection at the panel centre must be slightly greater than that of the column lines. The same effect is also observable when the test values of M_A, M_B and M_M are compared with the total static moment M_o.

The method of measuring the reaction components at the base of column A (by means of the rocker arms used as load cells as described in Section 4.4) proved to be very simple to operate and there is reason to believe that the results are very reliable.

About 5% of the strain gauges malfunctioned and these readings were disregarded. Since the gauges were fairly numerous, the malfunctioning of one here or there did not interrupt the interpretation. The reliability of the strain gauge readings is attested in two ways, (a) by the repeatability of certain features from one model to another, and (b) by correlation between certain values obtained independently by the strain gauges and by the load cells at the column bases. These will be discussed separately.

A comparison may be made of graphs 6.3.15, 6.4.15 and 6.5.15 which give the transverse distribution of M_A for models 3, 4 and 5 respectively. It will be noted that in each case there is a sharp fall-off in the unit moment just beyond the edge of the column. It can also be seen that in the case of models 4 and 5 there is a step in the curves for service load and design ultimate load at about y = 450 mm. Since these features recur from one model to another they clearly reflect a behavioural feature of the structure. However, when it is recalled how the graphs are derived from the raw gauge readings, a high degree of accuracy may be inferred from the appearance of these features in the graphs. A similar comparison may be made between graphs 6.4.12 and 6.5.12 which show the unit slab moments at various distances along the eastern spandrel for models 4 and 5 respectively. Here again the graphs are quite distinctive in appearance but much the same characteristics can be seen in each model.

In the case of all models, values for the total moment M_A at any load level can be obtained by integrating the unit slab moments along the spandrel between the centrelines of the panels on either side of line AB. The value of M_A obtained in this way is derived

entirely from the strain gauge readings. A value for the same quantity may be obtained quite independently from the load cells at the base of column A, and the two values may be compared. In the case of models 4 and 5 a similar comparison may be carried out for spandrel B. The values in question are shown in Table 7.1 where the first value is that obtained from the load cells and the number in brackets is obtained from the strain gauges by integration. (These values have been given previously in the Summary Tables in Chapter 6.)

Except for the final values in model 5, the agreement between these two independent sets of measurements is remarkably good. It is concluded on this basis that load cell readings and strain gauge readings are accurate at least to 5%. In model 5 a collapse of the load distribution system occurred between design ultimate load and failure. Although the apparatus was re-assembled and the test completed it is considered that readings for model 5 close to failure are unreliable.

For the last three models a similar comparison can be made for the values of the total shear force V_A (or V_B) derived from strain gauge readings with that obtained almost directly from the vertical load cell at A (or B). The values are summarized in Table 7.2.

Up to design ultimate load, the agreement is again quite good when it is considered that the slab shears were obtained as derivatives of the slab bending moments, a process which always enhances errors.

The method of measuring angles of twist along the spandrel was found to be quite simple and satisfactory. The angles of twist in models 1 and 2 were very small on account of the presence of beams. In model 3 there is some dissimilarity between the graphs for the northern and southern sides of column A (see Fig. 6.3.19). This was traced to the fact that the frame supporting the dial gauges had been inadvertently touched during the reading of the gauges. This problem was avoided for models 4 and 5 and then the similarity of the graphs for the northern and southern spandrels (see Figs. 6.4.19 and 6.5.19) suggests that these twist values are quite reliable.

TABLE 7.1 - Comparison of Values of Total Moments from Load Cells with Values Derived from Strain Gauges

Load Level (kN/m^2)	Model 1	Model 2	Model 3	Model 4		Model 5	
	M_A	M_A	M_A	M_A	M_B	M_A	M_B
5.4	4.5 (4.4)	5.3 (6.2)	6.4 (7.2)	4.7 (5.4)	5.4 (5.4)	6.9 (7.4)	5.8 (7.9)
9.0	7.7 (7.2)	9.0 (10.6)	11.0 (12.5)	8.7 (8.7)	10.2 (10.2)	11.8 (11.9)	12.8 (13.6)
22.5	31 (30.7)	22.9 (21.7)	30.3 (33.3)	26.0 (26.2)	29.4 (30.6)	34.2 (27.7)*	45.5 (28.8)*

* unreliable values

TABLE 7.2 - Comparison of Values of Total Shears from Load Cells with Values Derived from Strain Gauges

Load Level (kN/m^2)	Model 3	Model 4		Model 5	
	V_A	V_A	V_B	V_A	V_B
5.4	19.6 (18.0)	18.0 (17.5)	21.0 (17.6)	19.0 (19.3)	22.0 (19.9)
9.0	35.0 (31.0)	32.5 (32.3)	37.5 (34.8)	34.5 (33.9)	38.6 (35.2)
22.5	84.5 (69.1)	83 (76)	98 (85)	94 (71)*	100 (76)*

* unreliable values

Discussion of the reliability of the stiffness tests will be left until Section 7.8.

7.2 MODEL 1 - THE INFLUENCE OF THE FLOOR BEAM

Model 1 was the only model which contained a floor beam. This beam entirely changed the strength and behaviour of the model as compared with the other models.

As shown in Fig. 6.1.11, approximately 80% of the entire panel moment is confined to the beam. The floor slab takes very little part in the frame action. This also means that there is very little torsion in the spandrel beams. It may well be that the path of the load from the slab to the column via the beams is similar to that usually assumed in design, and often called 'trapezoidal loading' (see Fig. 7.6). This is very different from the load path which occurs when the floor beam is absent.

It is not possible to comment on the ultimate strength of the model since when the capacity of the testing frame was reached the model was clearly far from failure. The flat plate models, on the other hand, reached their capacity. All models were designed in accordance with the Code AS 1480. It would appear that with structures so designed, while the flat plate type more than meet the design strength the structures with beams are much stronger again.

Similar remarks may be made about cracking and deflection. Cracking was just commencing when the test was discontinued at twice the design strength. Deformation was also extremely small. The angle of twist of the spandrel beam was too small to be measured with any accuracy. Mid-span deflections at maximum load were about 5 mm compared with about 25 mm for the other models.

Although model 2 contained a spandrel beam while later models did not, the behaviour of this model was generally more similar to that of the flat plate models than to model 1. The presence of the spandrel beam did not influence mid-span deflections to any extent although it did spread the end moment along the spandrel.

Model 2 will therefore be discussed in with later models in the following sections.

7.3 LATERAL DISTRIBUTION OF END MOMENTS, END SHEARS, AND MID-SPAN MOMENTS

From the graphs and tables of Chapter 6 certain significant trends can be seen. Of these, we shall discuss first the lateral distribution of moments and shears along the inner face of the spandrel and also at mid-span.

(a) Distribution of End Moments

Models 3, 4 and 5, the flat plate models without spandrel beams, may be regarded as the main test specimens. They were more fully instrumented than the earlier models, and they will be discussed first.

Graphs 6.3.15, 6.4.15 and 6.5.15 show the distribution of the moment M_A along the spandrel face from the column centre to mid-panel. One characteristic is common to all three graphs and all load levels. The unit moment is very high opposite the column face and drops off dramatically just outside the column. It would not be in keeping with these results to divide the total moment M_A between a column strip moment and a middle strip moment as recommended by current Codes. The subdivision suggested by these graphs is between the high moment over the column width, and the considerably lower moment over the remainder of the panel. Accordingly, the strip of slab of width $c_2 + t$ will be called the *beam strip* and the remainder of the panel width will be called the *slab strip*.

Clearly the proportion of the total moment which occurs in the beam strip will be higher for wider columns. If a spandrel beam of infinite torsional stiffness were provided, it could be expected that M_A would be uniformly distributed across the panel width. As the torsional rigidity of the spandrel beam is diminished, then the slab strip will accept a lower proportion of the total moment. It might be expected therefore that the division of moment between beam strip and slab strip will depend on the relative stiffness of the beam strip in bending and the spandrel beam in torsion. Investigation showed the likelihood of such a relationship. However, there would be difficulties in practice in estimating the relative bending stiffness of the beam strip and torsional stiffness of the spandrel strip. In the uncracked state the

expressions EI and GJ might be used with I and J being based on the overall dimensions and J being assumed to be the St. Venant torsion constant. The calculation is cumbersome and would have no relevance at all after cracking.

It was found that the same trend could be obtained if the moments were related to the ratio of the *cross-sectional areas* of the beam strip and spandrel strips. Again for practical simplicity, the width of the beam strip was taken as $(c_2 + t)$ instead of $(c_2 + d)$ where c_2 is the width of the column parallel to the edge of the building. The width of the spandrel strip was taken as c_1, the column dimension at right-angles to the building edge. Thus a parameter $Z = \frac{(c_2 + t)t}{(c_2 + t)t + 2c_1 t}$ was defined.

In the original planning of the models side A was regarded as the exterior of the building and side B was regarded as an interior column line and a stiffening beam was added in an attempt to simulate the stiffness of the next interior panel. It was expected that this would have the effect of making the total moment M_B rather larger than M_A. As regards the lateral *distribution* of M_B it was now considered that the conditions at end A would have little effect. In other words side B might reasonably be taken as an exterior edge with a spandrel beam. This might not be correct in regard to the value of M_B but it should not seriously affect the distribution of M_B between the beam strip and the slab strip. In this case results would be available for three edges which contained spandrel beams, namely side A of model 2, and side B of models 4 and 5. Side B of models 2 and 3 were not instrumented.

The same analysis was extended to the edges with spandrel beams, the parameter Z being taken as $\frac{(c_2 + t)t}{(c_2 + t)t + 2bD}$ where b and D were the overall dimensions of the spandrel beam. In Table 7.3, model 3A refers to model 3 side A and so on; M refers to the total moment M_A or M_B as appropriate; M_{BS} refers to that part of M which occurs within the beam strip of width $(c_2 + t)$. Values of M and M_{BS} are extracted from the Summary Tables in Chapter 6. The values of M in Table 7.3 are the average of the values measured by the load cells and by the strain gauges, both of which values are given in the Summary Tables.

TABLE 7.3 - Distribution of End Moments

Model	Z	5.4 kN/m²			9.0 kN/m²			22.5 kN/m²		
		M	M_{BS}	M_{BS}/M	M	M_{BS}	M_{BS}/M	M	M_{BS}	M_{BS}/M
3A	0.375	6.8	1.9	0.28	11.75	3.4	0.29	31.8	8.7	0.27
4A	0.375	5.05	2.1	0.42	8.7	2.4	0.28	27.1	7.6	0.28
5A	0.524	7.15	4.1	0.57	11.85	5.0	0.42	32.5	12.3	0.38
2A	0.167	5.85	1.2	0.21	9.85	1.9	0.19	22.3	3.3	0.15
4B	0.267	5.4	2.0	0.37	10.2	2.3	0.23	32.45	6.6	0.20
5B	0.326	6.85	2.7	0.39	13.2	3.1	0.23	39.25	7.8	0.20

Values of M_{BS}/M are plotted against Z in Fig. 7.1. The load levels 5.4 and 9.0 kN/m² are the levels corresponding approximately to the service load and design ultimate load respectively. The load 22.5 kN/m² is the failure load for models 3 and 4, and the maximum load capacity of model 5. Models 2 and 5 did not fail in the sense of a punching shear failure.

A quite clear trend can be observed. The proportion of M taken by the beam strip is highest at service load and drops considerably by design ultimate load. There is no doubt that this change is due to cracking at the column face. This was where first cracking occurred in every case and it clearly results in the beam strip shedding some of its moment relative to the slab strip. A small additional drop occurs in most cases between design ultimate load and failure. It seems certain that the distribution of moments represented by the upper graph refers to the model in the uncracked state while the lower points refer to the cracked state. One may therefore suppose that the drop in the value of M_{BS}/M takes place suddenly at cracking. This would explain how two of the crosses fall approximately on the lower graph instead of the upper one. In these models cracking evidently occurred just before 5.4 kN/m² whereas in the other models it occurred above this load.

Ignoring the small change which takes place at very high loads, we can then obtain two expressions for M_{BS}/M, one applying to the uncracked state and one to the cracked state. The test results quite clearly indicate a curve and hence in this report a parabolic

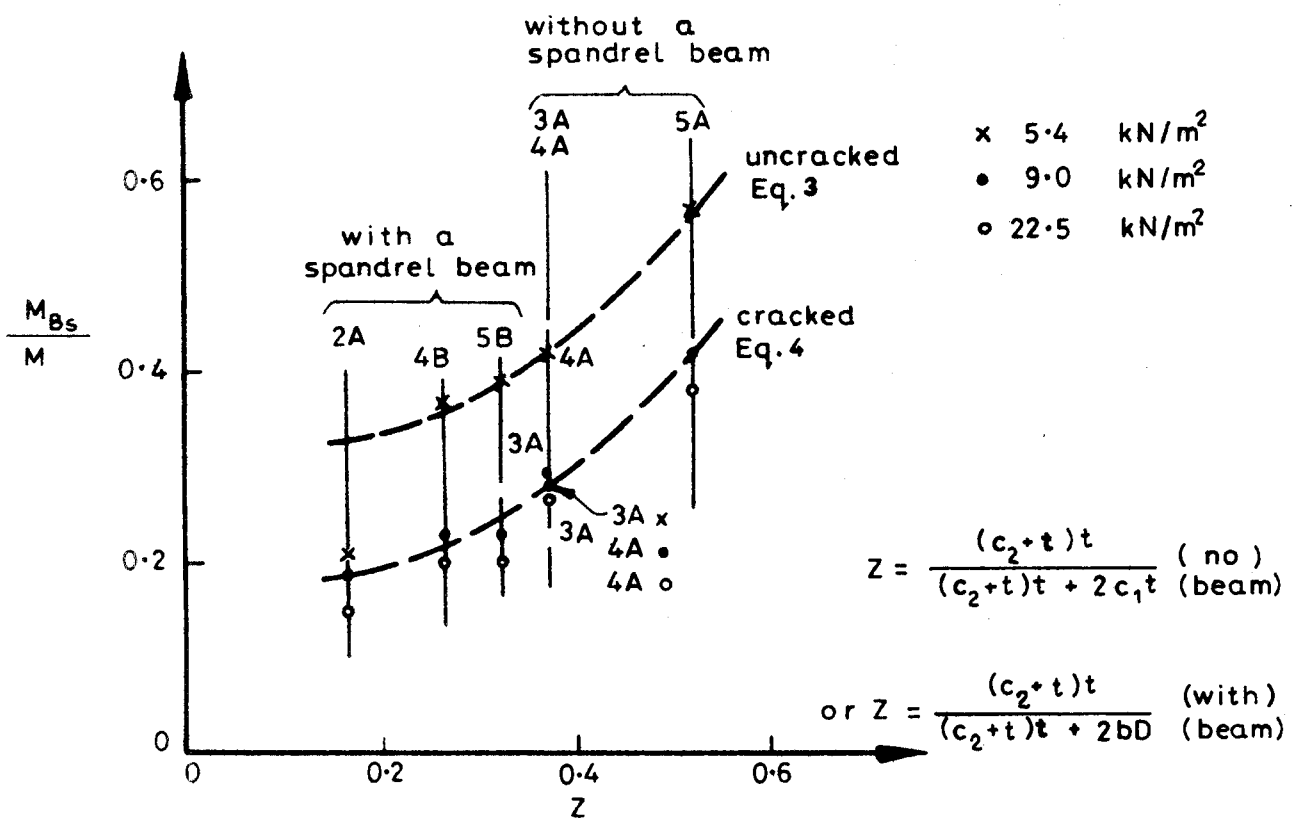

Fig.7.1 Variation of Beam Strip Moment.

relationship will be used. The following expressions are then obtained:

Before Cracking : $$\frac{M_{BS}}{M} = \alpha_{un} = 0.34 - 0.32Z + 1.42Z^2 \qquad (7.1)$$

After Cracking : $$\frac{M_{BS}}{M} = \alpha_{cr} = 0.20 - 0.32Z + 1.42Z^2 \qquad (7.2)$$

where $$Z = \frac{(c_2 + t)t}{(c_2 + t)t + 2c_1 t} \quad \text{(no spandrel beam)} \qquad (7.3a)$$

or $$Z = \frac{(c_2 + t)t}{(c_2 + t)t + 2bD} \quad \text{(with spandrel beam)} \qquad (7.3b)$$

The experimental work justifies the application of these equations only between the limits of $0.15 < Z < 0.6$. However, these limits probably embrace nearly all practical dimensions. For design purposes, straight line equations may be preferred and between the above limits, the following linear equations could be used:

Before Cracking : $$\frac{M_{BS}}{M} = \alpha_{un} = 0.16 + 0.65Z \qquad (7.1a)$$

After Cracking : $$\frac{M_{BS}}{M} = \alpha_{cr} = 0.04 + 0.65Z \qquad (7.2a)$$

The proportion of M_A which falls within the beam strip (M_{BS}) as given by equations (7.1) or (7.2) is of course based on the present series of tests and there is the possibility that this proportion is influenced to some extent by the distribution of steel actually employed in these tests. Thus small variations of α may be in order in design. There seems little doubt, however, that the intensity of moment in the beam strip will always be considerably greater than that in the slab strip.

Equations (7.1) and (7.2) give the proportions of M_{end} which fall within the beam strip and the slab strip respectively. The graphs of Chapter 6 suggest approximations to the distributions

within these two regions which could be of use in design. In all cases it is reasonable to assume that the beam strip moment (M_{BS}) is uniform across the width of the strip.

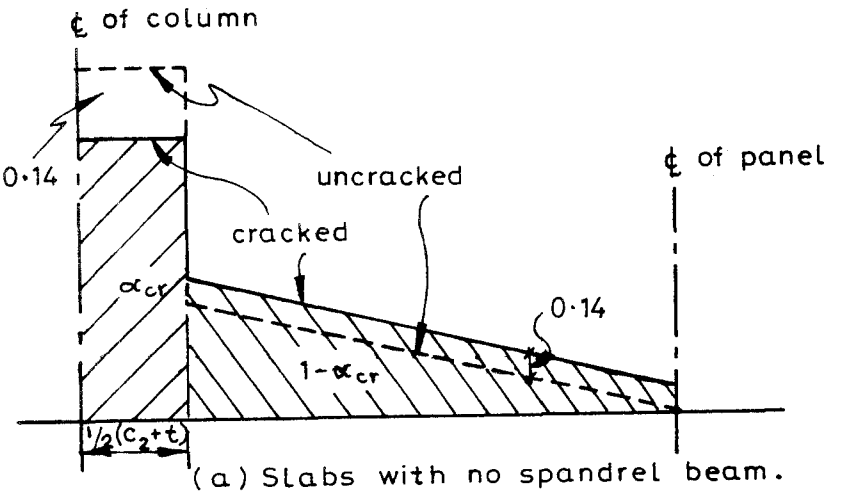

(a) Slabs with no spandrel beam.

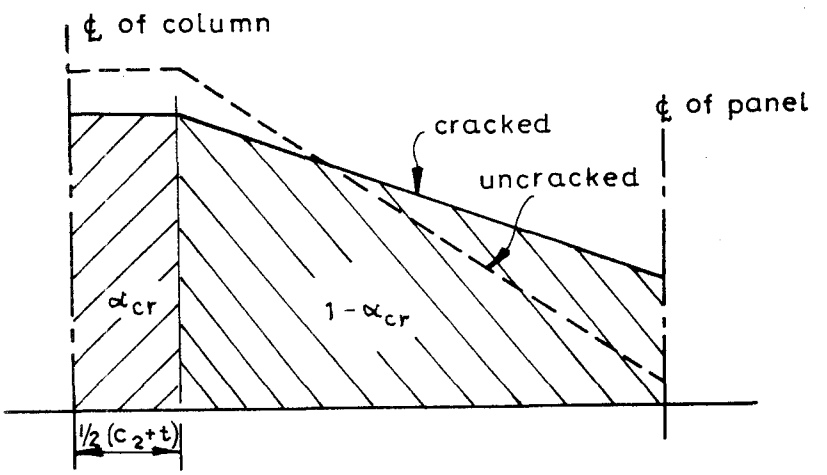

(b) Slabs with a spandrel beam.

Fig. 7·2 Approximations to the Distribution of End Moments.

In regard to the slab strip there is a noticeable difference according to whether a spandrel beam is provided or not. Graphs 6.3.15, 6.4.15 and 6.5.15 refer to tests in which there was no spandrel beam. In most cases, there is a very noticeable drop in moment just outside the edge of the beam strip. It also appears that the graphs at various load levels are approximately parallel over the slab strip. Based on these observations, approximations to the distributions are given in Fig. 7.2a. Values of α are

given by equations (7.1) or (7.2) and the various areas shown in Fig. 7.2a are obtained for any value of M_{end} by multiplying $\frac{1}{2}M_{end}$ by the factors shown.

Graphs 6.2.15, 6.4.27 and 6.5.27 refer to tests when a spandrel beam was present. Except at very advanced loads, the drop in moment at the edge of the beam strip is quite small and in the proposal shown in Fig. 7.2b it is neglected. In this case, and assuming a linear variation across the slab strip, the distribution of moments will be as shown in Fig. 7.2b.

If these distributions are accepted, then for a known end moment, the unit slab moment at any position along the spandrel face can be calculated from equations (7.1) or (7.2). An estimate must be made as to whether or not cracking at the column face has occurred at the particular end moment in question. This presents little problem. At service load or below it may be assumed that cracking has not occurred. For loads appreciably above the service load there will be cracking at the column face. More extensive cracking will not seriously alter the distribution.

(b) Distribution of End Shears

It was found that a very similar analysis could be applied to the distribution of an end shear V_{end}. Table 7.4 gives values of shears for the edges 3A, 4A, 5A (no spandrel beams) and 4B, 5B (with spandrel beams). The values of V, the total shear, and V_{BS}, the shear which occurred within the beam strip, were taken from the summary tables in Chapter 6. The same parameter Z was used as in the case of moments. In the case of shear, it was not possible to make use of results from model 2. Although the slab moment was measured at various positions along the spandrel, only at the column centre were enough moment values obtained to allow the shear to be estimated. As explained in Chapter 6, the distributions shown in Fig. 6.2.16 were assumed to be linear. The graphs were based only on the value at mid-column and the total area.

The values from Table 7.4 are plotted in Fig. 7.3. As with the moment values there is a sharp distinction between the values before and after cracking at the column face. By fitting second degree curves to these plotted points, the following expressions were obtained:

TABLE 7.4 - Distribution of End Shears

Model	Z	5.4 kN/m²			9.0 kN/m²			22.5 kN/m²		
		V	V_{BS}	V_{BS}/V	V	V_{BS}	V_{BS}/V	V	V_{BS}	V_{BS}/V
3A	0.375	18.8	3.4	0.18	33.0	5.8	0.18	76.8	14.5	0.19
4A	0.375	17.75	4.5	0.25	32.4	5.4	0.17	79.6	12.8	0.16
5A	0.524	19.15	6.7	0.35	34.2	9.2	0.27	82.5	21.1	0.26
4B	0.267	19.3	4.5	0.23	36.15	5.3	0.15	91.5	12.7	0.14
5B	0.326	20.95	4.3	0.21	36.8	5.8	0.16	88	15.2	0.17

Before Cracking : $$\frac{V_{BS}}{V} = \beta_{un} = 0.23 - 0.40Z + 1.19Z^2 \qquad (7.4)$$

After Cracking : $$\frac{V_{BS}}{V} = \beta_{cr} = 0.17 - 0.38Z + 1.10Z^2 \qquad (7.5)$$

As in the case of the moment values, limits of $0.15 < Z < 0.6$ are placed on equations (7.4) and (7.5) on account of the range of experimental values. Also, for design purposes, the following linear approximations are suggested:

Before Cracking : $$\frac{V_{BS}}{V} = \beta_{un} = 0.08 + 0.5Z \qquad (7.4a)$$

After Cracking : $$\frac{V_{BS}}{V} = \beta_{cr} = 0.5Z \qquad (7.5a)$$

When the overall distribution of V is considered, there is not the same marked fall-off of shear at the edge of the beam strip as there is in the case of moments. Certainly this characteristic is noticeable in model 3A (Fig. 6.3.16) but in the other tests the drop seems to occur only very close to failure and then only mildly. It is therefore suggested that in the case of shear, the distribution shown in Fig. 7.4 be used for all cases. In the event that this proposal predicts a negative ordinate at mid-panel the distribution over the slab strip should be taken as triangular with zero shear before mid-panel is reached. It should be pointed out that the experimentally derived shear distributions are less

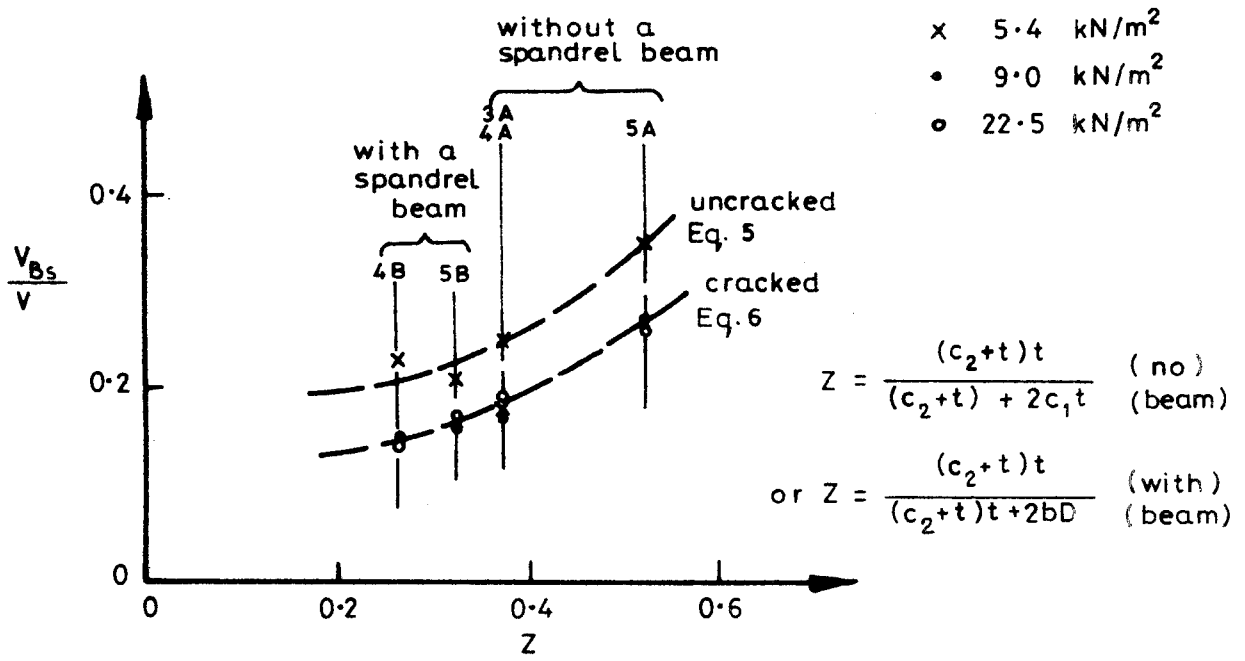

Fig. 7.3 Variation of Beam Strip Shear.

reliable than those for moment since the former have been obtained by the process of differentiation.

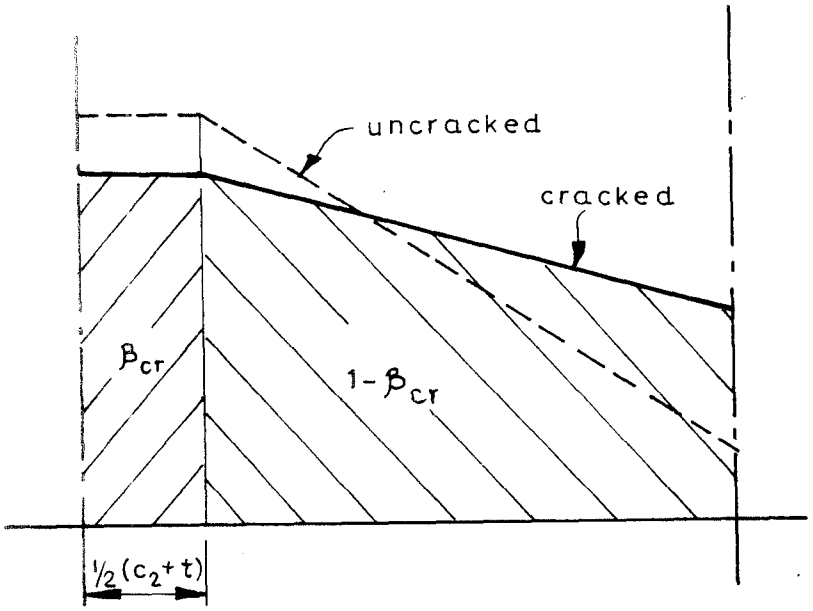

Fig. 7.4 Approximation to the Distribution of End Shears.

(c) Distribution of Mid-Span Moments

Mid-span moment distributions were measured only for models 3, 4 and 5. The distributions obtained for the three models are shown in Figs. 6.3.17, 6.4.17 and 6.5.17 respectively.

Each model shows some features not repeated in the other models. If we ignore the rather high beam strip moment in model 3 at service load only (and this is based on a single reading), then models 3 and 4 show quite similar trends. At service load there is a fairly uniform moment from the column centreline to about midway to the panel centre, then a rather lower moment for the remainder of the distance to the panel centre. At higher loads the same feature applies but the drop in moment becomes less pronounced. Before failure the moments in the column strip reach yield and in consequence the whole distribution migrates towards uniformity.

There is here no indication that the 'beam strip', as defined above for the end moments and shears, plays any special part in resisting the moments (except for the isolated reading on Fig. 6.3.17 mentioned above). The more customary division into column strip and middle strip seems more appropriate, with the column strip taking rather more than half of the moment at lower loads, but the difference between the two zones becoming progressively less marked as the load increases.

Model 5 on the other hand shows quite different features. Here a 'beam strip' is quite clearly defined and in this region the moments are considerably *lower* than in the remainder of the panel. This must be attributable to the substantially increased stiffness of columns A and B (and increased width in the case of column A as compared with the columns in models 3 and 4). It may be supposed that the stiffer columns increase the negative end moments in the beam strip and consequently decrease the mid-span moments. At very advanced loads the distribution tends to revert to that observed in the other models but this may be due largely to yielding in the more heavily stressed regions.

Current practice is to divide the slab into column strip and middle strip and to assign $0.6M_M$ to the column strip and $0.4M_M$ to the middle strip. In these three tests, only in Fig. 6.4.17 at service load is the column strip moment as much as 50% greater than the middle strip moment. At design ultimate load (9.0 kN/m^2) M_M is close to being uniformly distributed across the slab in all cases except for the dip in the beam strip in model 5.

In summary the tests appear to indicate that in the uncracked state, the column strip seems to attract slightly more than half M_M, but not $0.6M_M$. After cracking the distribution of moments becomes nearly uniform.

In these circumstances it would seem reasonable in practical design to take M_M as being uniformly distributed across the whole slab. This would in general agree more nearly with these test results than would the current practice.

7.4 DISTRIBUTION OF FORCES AROUND COLUMN PERIPHERY

The original objective of this research was to examine the distribution of forces in the vicinity of an edge column. Of the total moment transferred from the slab to the column, how much is transferred as bending moment at the 'front' or internal face of the column, and how much as torsion on the 'side' or spandrel faces? Of the total shear, how much acts on the front face and how much acts on the spandrel faces? These questions can now be answered in terms of the information developed in Section 7.3.

It is first necessary to know the total moment, M_A, and shear force, V_A, at the inner face of the spandrel beam or strip. This will be discussed in the next section. In terms of these quantities the forces on the various faces of the edge column can now be found by statics.

First, on the inner face of the column, which is taken as having a width $(c_2 + t)$, the bending moment is αM_A and the shear force is βV_A. According to whether the uncracked or cracked condition is being considered, α is obtained either from equation (7.1) or from equation (7.2). Similarly β is obtained from equation (7.4) or (7.5).

The balance of M_A and V_A of course acts on the slab strip and may be denoted by M_{SS} or V_{SS}.

Thus
$$M_{SS} = M_A (1 - \alpha) \tag{7.6}$$

and
$$V_{SS} = V_A (1 - \beta) \tag{7.7}$$

These slab strip forces are divided between the spandrels on either side of column A. By statics the twisting moment, T_{sp}, in the spandrel at t/2 from the column face is then

$$T_{sp} = \tfrac{1}{2}M_{SS} + \tfrac{1}{2}V_{SS} \left(\frac{c_1}{2}\right)$$

$$= M_A \left(\frac{1 - \alpha}{2}\right) + V_A \left(\frac{1 - \beta}{2}\right) \frac{c_1}{2} \tag{7.8}$$

The loading on the spandrel consists of:

(i) the self-weight of the spandrel plus any live load acting directly upon it. These together will be denoted by W_{sp}.

(ii) the slab shears acting on the face of the spandrel, V_{SS}.

(iii) the slab moments acting on the face of the spandrel, M_{SS}.

The moment M_{SS} contributes largely to the spandrel torque. However, the shear and bending moment in the spandrel depend only upon W_{sp} and V_{SS}. These produce a loading on the spandrel shown diagramatically in Fig. 7.5. The value of V_{SS} is given by equation (7.7) and an approximate guide to the distribution of this force was given previously in Fig. 7.4.

From Fig. 7.5 it can be seen that the shear force in the spandrel at the column face is given by

$$V_{sp} = V_A \left(\frac{1 - \beta}{2}\right) + \tfrac{1}{2}W_{sp} \qquad (7.9)$$

Moreover, Fig. 7.5 enables a reasonably accurate assessment to be made of the bending moments in the spandrel. It is noted first that the value of W_{sp} is nearly always small compared with $V(1 - \beta)$. When there is no spandrel beam, the load diagram closely

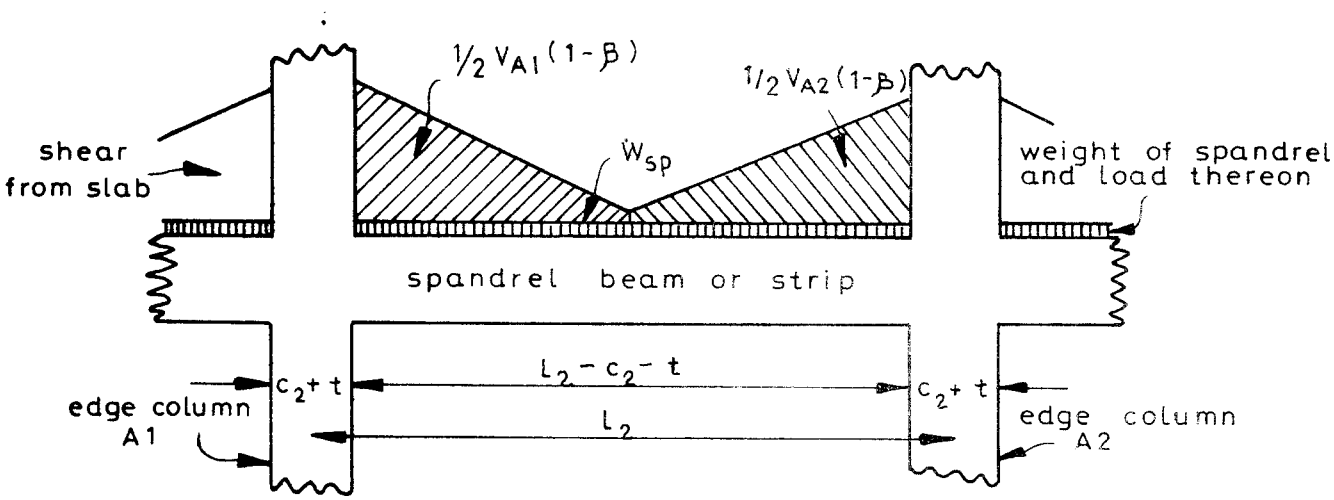

Fig. 7·5 Loading on the Spandrel Beam.

approximates to an inverted triangle with almost zero load at mid-span. This produces a static moment of WL/12. When there is a spandrel beam the distribution of load is rather more uniform and a static moment of WL/10 might be adopted. Allowing for a certain amount of re-distribution the support moment and span moment may be approximated by

$$M_{sp} = \frac{1}{\Omega}\left[W_{sp} + V_A(1 - \beta)\right](\ell_2 - c_2 - t) \qquad (7.10)$$

where Ω = 15 for the support moment with a beam
Ω = 30 " " span " " " "
Ω = 18 " " support " " no beam
Ω = 36 " " span " " " "

These support moments are fairly substantial and shortly after service load give rise to top cracking close to the column face. These cracks can be seen in the photograph of Fig. 6.3.4. However, it will be shown later that from an ultimate strength point of view there is no difficulty in designing for the moments, an accurate determination of which is not necessary.

It may be noted that the distribution of the load exerted by the slab on the spandrel is substantially different from one which is sometimes used in practice - often called 'trapezoidal' loading. This loading is illustrated in Fig. 7.6, and where both edge beams and floor beams are present this may well give a reasonable idea of the loading on the beams. However, when the floor beams are omitted as in model 2 (a flat plate floor with spandrel beam), the loading on the spandrel is very considerably altered. Instead of a triangular loading with a central peak, the loading is now greater near the columns, as shown in Fig. 7.5. If the spandrel beam is also omitted, the loading is even more concentrated towards the supports.

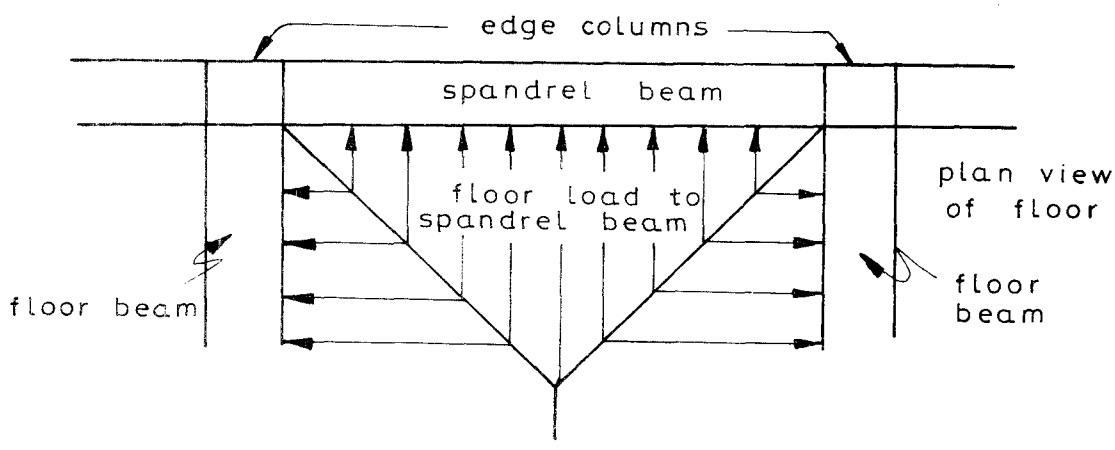

Fig. 7.6 Trapezoidal Loading.

Returning to the forces on the three faces of the edge column, reference to Fig. 7.3 indicates that for a fairly square column, the shear in the spandrels is roughly twice that on the front face - even more than this after cracking. That is to say, of the total load delivered to the column the greater part arrives as shear in the spandrels, and only a relatively small proportion as shear in the beam strip. Reference to Fig. 7.1 indicates that the same general trend is true of the moments. The spandrel torsion predominates over bending in the beam strip.

The predominance of the spandrel forces is of course greater when a spandrel beam is present. It is less when no beam is present and less again with a very wide column. However, even with the wide column of model 5 and no spandrel beam, after cracking the spandrel forces were still greater than those in the beam strip.

These observations will be of considerable importance in Section 7.6 where the question of failure in the vicinity of the column is considered.

7.5 DISTRIBUTION OF M_o BETWEEN M_A, M_M and M_B

In most design procedures, the value of the total end moment M_A is derived from the total static moment M_o where

$$M_o = \frac{(w\ell_2)\ \ell_n^2}{8}$$

and ℓ_n = clear span between columns A and B.

In most designs, M_o is determined and this is apportioned, either by arbitrary coefficients or by some analytical procedure, between M_A, M_M and M_B.

The ratios of these three moments as obtained in the tests are first discussed. In Table 7.4, the test values of M_A, M_M and M_B are shown. These are taken from the Summary Tables in Chapter 6.

The moments M_A, M_M and M_B have then been non-dimensionalized by expressing them as fractions of M_o ($= \frac{1}{2}(M_A + M_B) + M_M$). The resulting values are plotted in Fig. 7.7, where of course the total height of every parabola is unity. In order to obtain a value of M_o for model 3, an approximate value for M_B was obtained by analogy

with model 4 having regard to the fact that the overall dimensions of the two models were the same.

TABLE 7.4 - Total Panel Moments at Mid-Span and at the Supports

	Load Level	M_A	M_M	M_B	M_o	M_A/M_o	M_M/M_o	M_B/M_o
Model 3	5.4	6.8	8.8	—	15.6	0.43	0.56	—
	9.0	11.8	19.3	—	32.0	0.37	0.60	—
	22.5	31.8	25.2	—	59.4	0.53	0.42	—
Model 4	5.4	5.1	10.0	5.4	15.25	0.33	0.66	0.35
	9.0	8.7	19.5	10.2	29.0	0.30	0.67	0.35
	22.5	26.1	25.2	30.0	53.3	0.50	0.47	0.56
Model 5	5.4	7.2	10.3	6.9	17.4	0.41	0.59	0.40
	9.0	11.9	17.4	13.2	30.0	0.40	0.58	0.44
	22.5	31.4*	23.2	37.1*	57.5	0.55	0.40	0.65

* unreliable - load cell values considerably greater than strain gauge values

The behaviour pattern is similar in every case. For models 3 and 4, from service load (5.4) to design ultimate load the parabola moves slightly upward (i.e. the end moments decrease relative to M_M). In the case of model 5, the curves for 5.4 and 9.0 kN/m^2 the two curves are practically indistinguishable. From design ultimate load up to failure, there is in all models a marked downward shift of the parabola (i.e. a decided relative increase of the end moments).

The reasons for these re-distributions are also quite clear from the experiments. The first parabola (5.4) represents the distribution of moments in the uncracked state. In every model, cracking occurred first in the beam strip at the faces of columns A and B. As discussed in Section 7.3 this caused a change in the transverse distribution of M_A and M_B. The cracked beam strip accepted moment increase at a lower rate than did the uncracked slab strip (and also the uncracked mid-span section). This resulted in a smaller proportion of M_A (or M_B) being resisted by the beam strip (see Fig. 7.1). It also resulted in M_A and M_B being a smaller

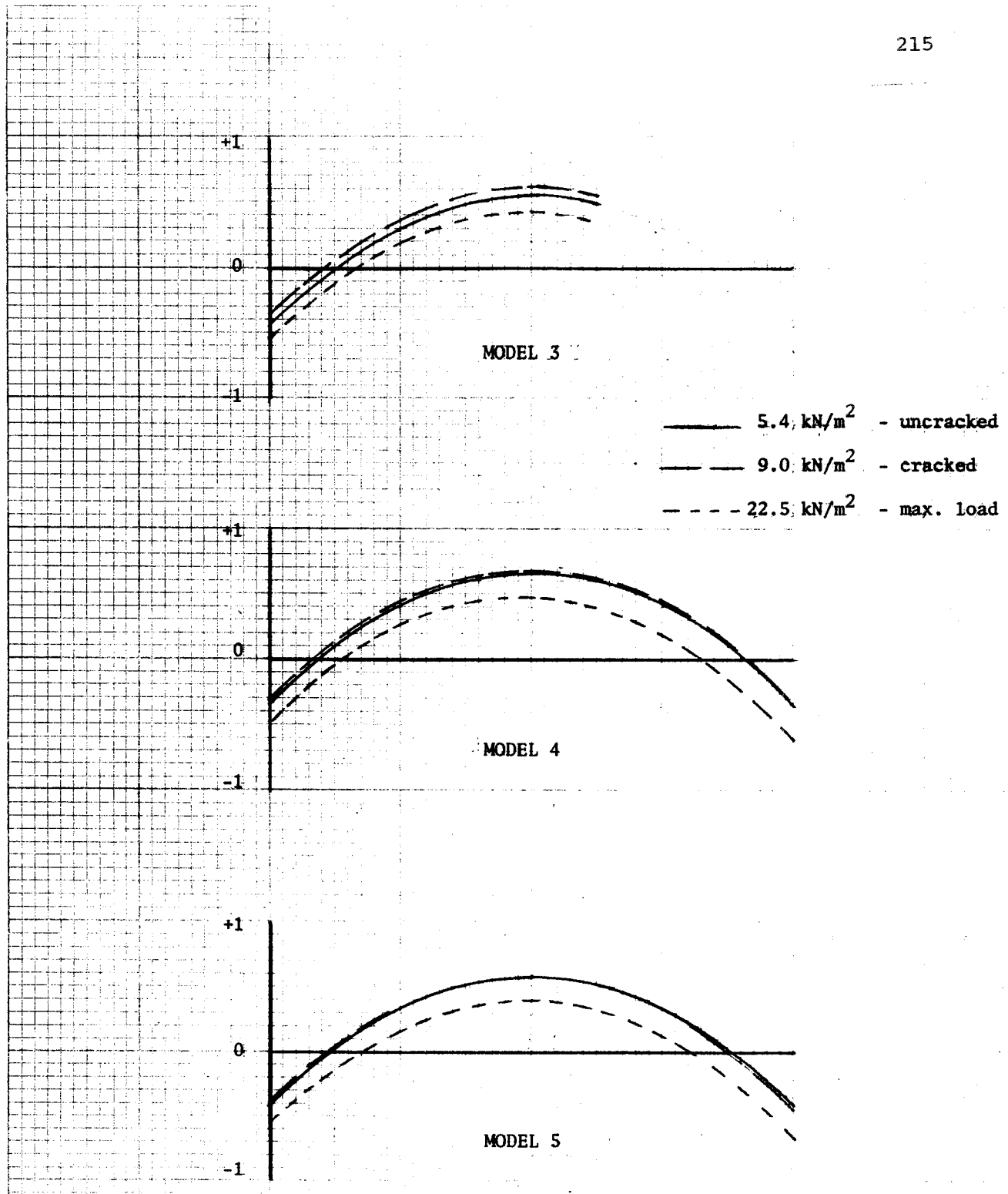

FIGURE 7.7 DISTRIBUTION OF M_o AT VARIOUS LOAD LEVELS

proportion of M_o than was the case in the uncracked state. Hence the upward shift of the parabolas.

Next occurred cracking at mid-span. On account of the relatively small reinforcement percentage provided at mid-span, yield occurred shortly after cracking. This then set an upper limit on the mid-span moment M_M, and any further increase of load was resisted by an increase of M_A and M_B.

At the ends A and B, cracking gradually extended from the column face (i.e. in the beam strip) along the face of the spandrel strip. However, as the end steel provided was greater than that at mid-span, cracking did not immediately lead to yield. Thus the end moments began to increase relative to the mid-span moment and the moment parabola moved downward. Eventually the whole of the negative steel at end B reached yield.

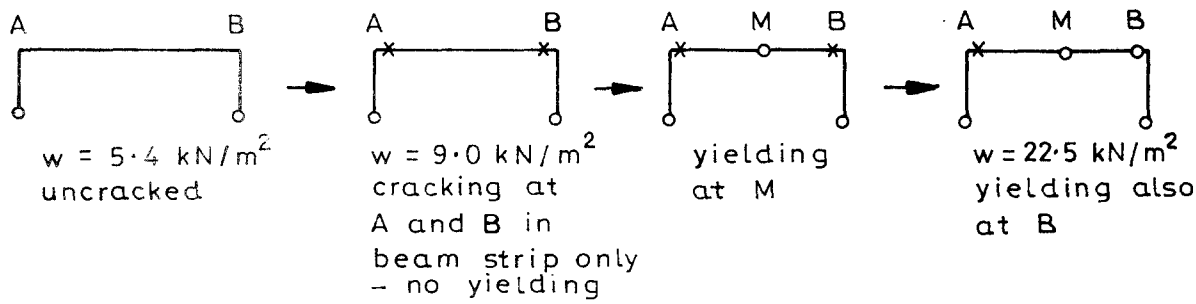

Fig. 7·8 Sequence of Cracking and Yielding.

If the models had continued indefinitely with similar panels to the North and South, then yield at A or B would have resulted in a mechanism collapse. Such a sequence of events is illustrated in Fig. 7.8. In the models, collapse of this sort was prevented since the adjacent panels to the North and South were considerably stronger than the central panel.

The behaviour of models 3, 4 and 5 all followed in general the sequence of events illustrated in Fig. 7.8. After maximum load had been reached, further deformation was imposed on models 3 and 4 and this led to a punching shear around column A. For reasons explained in Section 6.5 the test on model 5 was not continued to a punching shear at A. However, from the description of

the punching shear mechanism which will be described in the next section, it seems probable that a punching shear would have occurred in model 5 as in models 3 and 4 despite the wider column face in model 5.

The sequence of events in the three models is illustrated diagrammatically in Fig. 7.9. The numbers on the diagrams indicate the sequence in which the hinges or shear failures occurred.

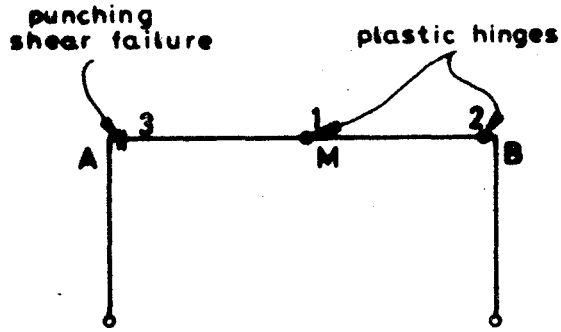

Fig.7·9 Failure Mechanism

TABLE 7.5 - Yield Moments and Moments at Failure

Model	M_A	M_M	M_B
3	40.8 (31.8)	25.2 (25.2)	40.8
4	29.3 (26.1)	25.2 (25.2)	29.3 (30.0)
5	32.1 (31.4)*	23.2 (23.2)	32.6 (37.1)*

* unreliable values

Table 7.5 shows the yield strengths of the sections A, M and B in each model. In each entry the first value is the yield moment calculated directly by assuming the yield stress (i.e. 0.2% proof stress) in every bar.

In brackets is shown the measured moment at failure. As regards M_M the measured value has been derived from the measured steel strains. Hence, if all bars reached or exceeded the yield strain, the value of M_M obtained in this way must agree with the value of M_M calculated directly.

As regards the end moments, these were not only obtained from the reinforcement strains, but also an independent value was available from the external load cells. Moreover, the bars in the beam strip at column B in model 3 reached a strain in excess of the 0.2% proof strain. The measured strain was used in conjunction with the stress-strain curve of the steel to calculate actual moments in the beam strip. The values shown in brackets in Table 7.5 are the averages of the values obtained from strain readings and those obtained from the load cells.

In the case of model 5, it was reported in Chapter 6 that difficulty was experienced with the loading system near failure. This seems to have resulted in unduly high values of M_A and M_B from the load cells, whereas the values calculated from strain readings agree well with the observed behaviour. Average values were still used in Table 7.5 but these averages are almost certainly higher than the true moments.

The behaviour of the models is typical of the collapse mechanism of statically indeterminate structures. The final distribution of moments was determined by the amount of steel provided at A and M.

Thus the tests did not and could not provide any confirmation of the distribution of moments suggested by the Code rules or by any analysis. Whatever system of analysis (or set of rules) is used, however spurious, it will indicate some set of values for M_A, M_M and M_B. If steel is provided in accordance with these values then the test results will migrate towards these values as collapse is approached, and will reach these values unless a shear failure supervenes. This will be discussed in the next section. Clearly such behaviour does not indicate that the analysis employed is *correct*, and in fact the term 'correct' has no inherent meaning.

It may be noted that a very considerable re-distribution of moments took place between the uncracked state and the maximum load

condition. This indicates that the distribution of M_o between M_A, M_M and M_B is arbitrary within quite wide limits. This in turn suggests that the accuracy implied in the present Code rules, and in the literature which supports these rules, is quite unjustified and that a much simpler set of design rules would be equally effective.

The present tests suggest that a set of coefficients 0.40, 0.50 and 0.60 for the exterior end moment, mid-span moment and interior end moment might be satisfactory. However, it must be taken into consideration that the determination of such coefficients was not one of the original aims of this research, and whether the modifications introduced into side B of the models properly simulated the effect of the next interior panel or not is a matter of conjecture.

7.6 THE MECHANISM OF PUNCHING SHEAR FAILURE

The mechanism of shear failure at column A can now be examined.

A shear failure did not occur in models 1 and 2 and this may be attributed the the fact that these models possessed a spandrel beam. This will be referred to again later.

A shear failure did not occur in model 5. However, this may have been due to the fact that at an advanced load, trouble was experienced with the loading system as reported in Chapter 6. The system was re-assembled and loading continued until the flexural capacity of the slab was reached, when the load distribution system once more collapsed. The test was then terminated but it is possible that if this had not occurred a shear failure may have been achieved.

In models 3 and 4 the flexural strength of the floor slab was reached, and then after further deformation, but without increased load, a punching shear occurred at column A. In these models cracking occurred at quite a low load in the top of the slab along the face of column A. At much higher loads 45^o cracks occurred in the spandrel strips at the upper face of the slab and coming from the corners of the column. These cracks were clearly the result of torsion in the spandrels. Towards the failure load, all cracks

became wider and the shear failure itself was of course sudden and violent.

The conclusions drawn in Sections 7.3 and 7.4 indicate clearly the probable sequence of events just before failure. Fig. 7.3 or equation (7.5) show that for these models and at high loads, the beam strip carried 0.18 of the total shear around the column. Each spandrel therefore carried 0.41 of the total shear, approximately twice the shear in the beam strip. In addition, the spandrels were subjected to considerable torsion. The total cross-sectional areas of the spandrels and the beam strip are approximately the same, hence there is no doubt that the spandrels were much more heavily stressed in shear and torsion than the beam strip. There is no doubt that failure occurred first in the spandrels followed immediately by total failure.

Even with the very wide column in model 5, the beam strip carried only 0.27 of the total shear. Each spandrel therefore sustained more shear than the beam strip, and torsion in addition. The beam strip was now much wider than the spandrels. Had a shear failure been achieved it would have originated in the spandrels.

A punching shear failure at an edge column is therefore essentially a shear-torsion failure in the spandrel. If a spandrel beam of normal proportions and reasonable reinforcement is provided (as in model 2) the shear-torsion strength will be well beyond the flexural capacity of the slab and a shear failure is not a problem. Where a spandrel beam is not provided, a satisfactory shear capacity depends on adequate reinforcement of the spandrel strip. It is of interest to note that it is not unusual in current design practice to find the spandrel strip quite devoid of hoop steel.

It remains now to discuss what punching shear strength may be expected from a given design. The test results showed that the measured torques in the spandrels at the face of the column were many times larger than the failure strength values calculated by the space-truss or skew bending theories of torsion. These theories yield quite similar failure values and are well substantiated by experiment. On the other hand it was shown in Section 7.1 that the values measured in these tests were certainly not in

error by more than 10%. The discrepancy can be fully explained by the fact that the spandrels were longitudinally restrained by the presence of the adjacent floor slab. Work carried out by Onsongo and Collins (1972) has shown that any longitudinal restraint increases the torsional capacity of a beam. The increased strength can be computed by expressing the restraint in terms of an equivalent area of additional longitudinal steel.

Any reinforced concrete beam subjected to torsion undergoes an increase of length in addition to twist. If the beam frames into columns at each end this will tend to cause the columns to move apart. In themselves, the columns have little resistance to such movement, but when the columns are integral with a floor slab, the latter will clearly provide a very considerable resistance to column movement and hence to spandrel expansion.

In effect, expansion of the spandrel will be resisted by a field of tensile stress in the floor slab. The total tensile force in the slab will be balanced by a corresponding compressive force in the spandrel.

The problem is similar to that of a beam (Fig. 7.10) being restrained by end blocks (the columns in the building) connected by steel bars (representing the floor slab). In this simplified case the steel bars can be considered as additional longitudinal reinforcement in the beam. In the real situation, we may replace the concrete slab by an equivalent area of steel. The problem is to determine the effective area of the restraining slab.

Fig. 7.11 shows the field of tensile stress which will be a maximum at the line of edge columns. Provided ℓ_{n1} is large compared with ℓ_{n2}, the total tensile force may be expressed as a function of ℓ_{n2}. If the effective area is denoted by $\lambda \ell_{n2}$ t then the equivalent area of longitudinal steel will be

$$A_{eq} = \lambda \ell_{n2} \, t \, \frac{E_c}{E_s} \qquad (7.11)$$

It is proposed now to investigate the value of λ which will increase the torsional strength of the spandrel up to the observed strength.

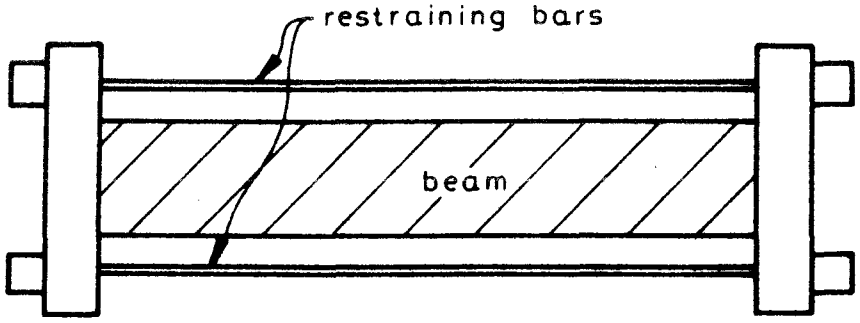

Fig.7.10 Restrained Beam

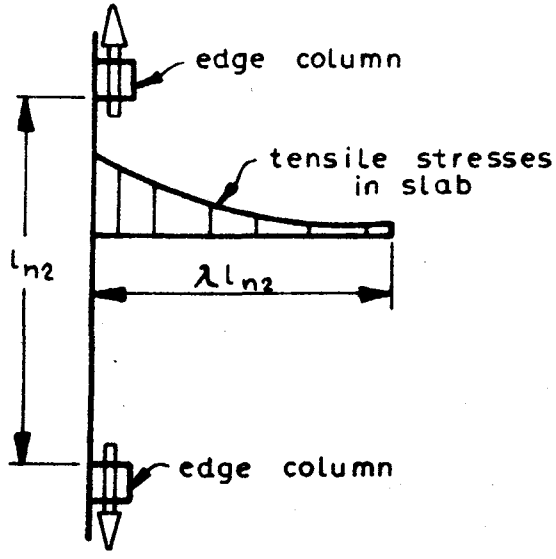

Fig.7.11 Effect of Longitudinal Restraint

According to the space-truss theory of torsion, the strength T_u of a beam subjected to combined torsion and shear is given by

$$T_u = \frac{1}{\left(1 + \frac{A_o V_u}{T_u y_o}\right)} 2A_o \sqrt{\frac{A_w}{s} f_{wy} \frac{A_\ell}{u_o} f_{\ell y}} \qquad (7.12)$$

where
- T_u = ultimate torque
- V_u = ultimate shear
- A_w = the cross-sectional area of the bar from which the hoops are made
- f_{wy} = the yield stress of the hoop steel
- s = the spacing of the hoops
- A_ℓ = the total area of longitudinal steel
- $f_{\ell y}$ = the yield stress of the longitudinal steel

A rectangle ABCD is defined by the centres of the bars in the corners of the hoops (Fig. 7.12). Then

- A_o = the area within this rectangle
- u_o = the perimeter of this rectangle
- y_o = the vertical dimension of this rectangle

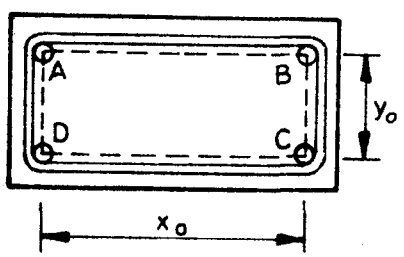

Fig. 7.12

Following the work of Onsongo and Collins, we must now replace A_ℓ by $(A_\ell + A_{eq})$, the latter term being given by equation (7.11) and representing the effect of the restraint. Then

$$T_u = \frac{1}{\left(1 + \frac{A_o V_u}{T_u y_o}\right)} 2A_o \sqrt{\frac{A_w}{s} f_{wy} \left(A_\ell + \lambda t \ell_{n2} \frac{E_c}{E_s}\right) \frac{f_{\ell y}}{u_o}} \qquad (7.13)$$

For any particular test, the measured values of T_u and V_u in the spandrel at punching failure can be substituted into

equation (7.13) in order to evaluate a value of λ which agrees with the test results.

The only failures which occurred were in models 3 and 4 at column A. These results yield $\lambda = 0.25$ and $\lambda = 0.24$ respectively. As explained before, it was considered that a shear failure was imminent in model 5 at the time the test was terminated. Using the final measured values of T_u and V_u a value of $\lambda = 0.24$ is obtained.

The average of these three values is approximately 0.25. Since the λ values are so consistent it appears reasonable to substitute the value $\lambda = 0.25$ into equation (7.13). The torsional strength of the spandrel strip (no beam) is then given by

$$T_u = \frac{1}{\left(1 + \frac{A_o V_u}{T_u y_o}\right)} 2A_o \sqrt{\frac{A_w}{s} f_{wy} \left(A_\ell + 0.25\, t\ell_n \frac{E_c}{E_s}\right) \frac{f_{\ell y}}{u_o}} \qquad (7.14)$$

In models 4 and 5, the spandrel forces were also measured at side B. Because small spandrel beams were present on this side the joint did not reach failure. Even so the final torque in the spandrels was considerably in excess of the failure torque which could be sustained by an unrestrained beam, and it was therefore evident that the slab was contributing to the behaviour of the spandrel beam. The determination of the extent of the slabs contribution (i.e. a value for λ) was difficult since equation (7.13) only applies to the failure condition. Despite this, the final measured values of T and V were substituted into equation (7.13) in place of T_u and V_u and in place of $f_{\ell y}$ the measured stress in the longitudinal steel was used. These stresses were 220 MPa and 305 MPa in models 4 and 5 respectively.

By this method values of 0.26 and 0.23 were obtained for λ. It would seem reasonable to use equation (7.14) for structures with a spandrel beam as well as those without a beam, although this has not been conclusively obtained from the present tests. The behavioural model suggested in Fig. 7.11 would also point in this direction. It is probable that as the torque increases towards failure, the tension both in the longitudinal bars of the spandrel and in the floor slab increases until the bars yield.

All the λ values are summarized in Table 7.6.

TABLE 7.6 - Values of λ

Model	Value of λ	
3 (A)	0.25	) beam failure reached
4 (A)	0.24	)
5 (A)	0.24	)
4 (B)	0.26	) beam failure not reached
5 (B)	0.23	)

When ℓ_{n1} is smaller than ℓ_{n2}, it is possible that the field of tensile stress in the slab may be curtailed by the proximity of the next interior row of columns, so that the effective width area is less than 0.25 ℓ_{n2}. In the absence of further information it is suggested that the effective width be taken as 0.25 ℓ_n where ℓ_n is the smaller of ℓ_{n1} and ℓ_{n2}.

It may be noted that in equation (7.14) the 'equivalent' area of steel provided by slab restraint (i.e. 0.25 tℓ_n E_c/E_s) is far greater than the actual steel in the spandrel, A_ℓ. This means that in design, the longitudinal steel provided in the spandrel is fairly arbitrary since it makes only a minor contribution to the total strength. For the same reason the strength of the spandrel is usually more than adequate in torsion and bending, and hence an accurate determination of the bending moments is not necessary.

Equation (7.14), taken in conjunction with the equations developed in Sections 7.3 and 7.4, governs what is usually called the punching shear strength of the slab around an edge column.

7.7 DESIGN OF EDGE COLUMN - SLAB CONNECTION

One of the primary objectives of this research was to develop a method for the design of the connection between a slab and an edge column. In this section it will be shown explicitly how such design follows from the equations developed earlier in this chapter. The design procedure will be followed by a numerical example.

Design Procedure

1. From the dimensions of the column, the slab thickness and the spandrel beam or strip, calculate the parameter Z (equation (7.3)) and hence the values of α_{cr} and β_{cr} (equations (7.2a) and (7.4a)).

2. From these values, and given the total panel moment M_A and shear V_A at design ultimate load, calculate the moment and shear (M_{BS} and V_{BS}) to be carried by the beam strip. Also calculate the torque, shear and moment (T_{sp}, V_{sp} and M_{sp}) in each spandrel (equations (7.8), (7.9) and (7.10)).

3. Assume the longitudinal reinforcement in the spandrel and design hoops to resist T_{sp} and V_{sp} simultaneously. The hoops are designed by means of equation (7.14).

For design purposes it is necessary to introduce a strength reduction factor ϕ into this equation. It is convenient to re-arrange equation (7.14) in the form

$$\frac{A_w}{s} = \frac{\left(\frac{T_u}{A_o} + \frac{V_u}{y_o}\right)^2}{\phi^2 4 f_{wy} \left(A_\ell + 0.25\, t\ell_n\, E_c/E_s\right) f_{\ell y}/u_o} \qquad (7.15)$$

4. Check that the spandrel is adequate to resist T_{sp} and M_{sp} in torsion and bending at the support.

5. Design suitable longitudinal reinforcement in the beam strip to carry the moment M_{BS}.

6. Check that the beam strip is adequate to resist the shear V_{BS}. The usual flexure and shear design rules given in codes of practice may be used for this purpose.

All reinforcement must be properly detailed to provide adequate anchorage.

Example

The above procedure will be illustrated by applying it to the design of an edge column-slab connection with no spandrel beams. The following data apply:

M_A = 330 kNm, V_A = 410 kN, c_1 = 400 mm,
c_2 = 500 mm, ℓ_1 = 8 m, ℓ_2 = 6 m,
ℓ_{n_1} = 7.6 m, ℓ_{n_2} = 5.5 m, t = 250 mm,
d = 217 mm, F'_c = 25 MPa, E_s/E_c = 8
$f_{\ell y}$ = 410 MPa, f_{wy} = 230 MPa, and clear cover = 25 mm.

(1) Calculate α_{cr} and β_{cr}:

Equation (7.3a): $$Z = \frac{(c_2 + t)t}{(c_2 + t)t + 2c_1 t}$$

$$= \frac{(500 + 250)250}{(500 + 250)250 + 2 \times 400 \times 250}$$

$$= 0.48$$

Equation (7.2a): $\alpha_{cr} = 0.04 + (0.65 \times 0.48) = 0.35$

Equation (7.4a): $\beta_{cr} = 0.5 \times 0.48 = 0.24$

(2) Calculate M_{BS}, V_{BS}, T_{sp}, V_{sp} and M_{sp}:

$$M_{BS} = \alpha_{cr} M_A = 0.35 \times 330 = 116 \text{ kNm}$$

$$V_{BS} = \beta_{cr} V_A = 0.24 \times 410 = 98 \text{ kN}$$

Equation (7.8): $$T_{sp} = 330\left(\frac{1 - 0.35}{2}\right) + 410\left(\frac{1 - 0.24}{2}\right)\frac{0.4}{2}$$

$$= 139 \text{ kNm}$$

Assuming that the only load acting directly on the spandrel strip is the self-weight, and using a load factor of 1.5 for this dead load, then the factored weight of one spandrel is

$$W_{sp} = 1.5 \times 0.25 \times 0.4 \times 5.25 \times 24$$

$$= 18.9 \text{ kN}$$

Equation (7.9): $$V_{sp} = 410\left(\frac{1 - 0.24}{2}\right) + 0.5 \times 18.9$$

$$= 165 \text{ kN}$$

Equation (7.10): $M_{sp} = \frac{1}{18}\left[18.9 + 410(1 - 0.24)\right] 5.25$

$= 96$ kNm

(3) Design Spandrel Reinforcement:

Assume 4 - Cl6 bars as longitudinal reinforcement. Then $A_\ell = 4 \times 200 = 800$ mm^2.

Try S12 bars for the hoops. Then

$x_o = 400 - 2 \times 25 - 2 \times 12 - 16 = 310$ mm

$y_o = 250 - 2 \times 25 - 2 \times 12 - 16 = 160$ mm

$u_o = 2(310 + 160) = 940$ mm

$A_o = 310 \times 160 = 49\ 600$ mm^2

Substituting these values into equation (7.15) and adopting a capacity reduction factor ϕ of 0.85,

$$\frac{A_w}{s} = \frac{\left(\frac{139 \times 10^6}{49\ 600} + \frac{165 \times 10^3}{160}\right)^2}{0.85^2 \times 4 \times 230(800 + 0.25 \times 250 \times 5500/8)\ 410/940}$$

$= 1.16$

Since $A_w = 110$ $s = 95$

Provide S12 hoops at 95 mm spacing

(4) Check Spandrel Strip for Torsion and Bending:

(see Warner, Rangan and Hall, p.147)

$$\frac{M}{T} = \frac{96}{139} = 0.69$$

$$T = 2 x_o y_o \frac{A_w}{s} f_{wy} \tan \beta$$

$$= 2 \times 160 \times 310 \times \frac{110}{95} \times 230 \tan \beta$$

$$\therefore \tan \beta = \frac{T}{26.4}$$

$$A_{st} = \frac{A_\ell + 0.25\, t\ell_n\, E_c/E_s}{2}$$

$$= \frac{800 + 0.25 \times 250 \times 5500/8}{2}$$

$$= 21\ 884\ mm^2$$

$$21\ 884 \times 410 = T\left(\frac{160 + 310}{2 \times 160 \times 310}\right) \frac{T}{26.4} + \frac{0.69T}{160}$$

Solution of this quadratic gives

$$T = 212\ kNm \quad (> 139 \quad \therefore\ O.K)$$

(5) Design the Beam Strip for M_{BS}:

$$M_{BS} = \phi (A_{st})_{BS}\, f_{\ell y} (0.9d)$$

$$116 \times 10^6 = 0.9\, A_{st} \times 410 \times 0.9 \times 217$$

$$\therefore \quad A_{st} \geq 1610\ mm^2$$

Provide 8 - C16 bars in the beam strip. As many as possible should be bent down into the column (about 4). The remainder must be adequately anchored in the spandrel strips.

(6) Check the Shear Strength of the Beam Strip:

The shear strength of the beam strip without shear reinforcement may be taken conservatively as $\phi\ 0.17\sqrt{F'_c}\ (c_2 + t)d$. Therefore, if no shear reinforcement is to be provided

$$V_{BS} \leq \phi\ 0.17\sqrt{F'_c}\ (c_2 + t)d$$

$$\leq 0.85 \times 0.17\sqrt{25}\ (500 + 250)217$$

$$\leq 118 \times 10^3\ N$$

The actual shear is

$$V_{BS} = 98\ kN \quad \therefore\ O.K.$$

concretes. In view of the number of independent variables involved, any analytical examination of these results is unwarranted.

Neither is any attempt made to compare the test results with stiffness values commonly used in the Equivalent Frame Method of analysis. In the first place, the tests did not correspond, in several respects, with conditions which might be expected to give the 4EI/L values usually used in this analysis. Secondly, in view of the doubtful validity of this method of analysis there seems little point in checking the accuracy or otherwise of the 4EI/L assumption.

7.9 DEFORMATIONS

Twists in the Spandrels

As mentioned earlier, model 1 was very stiff and the measured angles of twist in the spandrels were negligible.

For models 2, 3, 4 and 5 respectively the angles of twist at service load and at design ultimate load are summarized in Figs. 6.2.20, 6.3.20, 6.4.20 and 6.5.20. From these figures it can be seen that the angle of twist increases sharply from y = 0 to about y = 400 mm. Beyond this value the angle of twist remains practically constant. This behaviour is consistent with the values of torque which are larger near the column and approach zero at mid-span.

Although in two cases (eastern spandrel in model 4 and western spandrel in model 5) the maximum twist appears to occur at about y = 800 mm, and the twist at mid-span is less than the maximum, this behaviour cannot be accounted for. The angles of twist are of course quite small, and the decrease at mid-span is indicated by measurement at only one point (y = 1350 mm). It is possible that the apparent anomaly is due to experimental error.

Deflections of Slab

Figures 6.2.21, 6.3.21, 6.4.21 and 6.5.21 show deflections of slab. These load-deflection curves are all similar and are typical of the nature of behaviour observed in significantly under-reinforced concrete members. Maximum deflections occurred

at the centre of the column line AB due to the nature of the boundary conditions adopted in the tests. Even these deflections are small at service load and design ultimate load. For instance, the average maximum deflection at service load was less than span/2000 and at design ultimate load was less than span/1000.

The measured deflections could be predicted using any one of the standard deflection computation methods (e.g. Branson's method) available in the literature. However, no such calculations are given here because of the small order of magnitude of deflections measured at service load.

Chapter 8

SUMMARY AND CONCLUSIONS

At external columns of a building, considerable moment is transferred from the floor to the column in addition to shear. Code provisions are quite inadequate for predicting the amount of moment transfer and for the design of the region around such a column. The mechanism of transfer of both moment and shear has not been well explained.

Some previous research has been carried out and theories advanced. Of these, the 'beam analogy' theory is perhaps the most promising. However, there has been some doubt about the validity of the boundary conditions in previous tests. Hence in the present tests, a boundary was chosen rather more remote from the test area, i.e. a rather more extensive model was used. Tests indicated that forces applied to this boundary had minimal effect in the test region.

Five models were tested, each representing two adjacent edge panels of a floor. Model 1 contained a floor beam and a spandrel beam. Model 2 contained only a spandrel beam. Models 3, 4 and 5 had neither floor beam nor spandrel beam adjoining the test column (column A). At the pin-jointed base of column A, reactions in three orthogonal directions were measured directly by means of load cells. Strain gauges attached to the slab reinforcement permitted slab moments to be calculated and in some cases, by differentiation, slab shears.

In the first two models, the main aim was to measure the total panel moment M_A and shear V_A along the face of the spandrel beam adjacent to column A, and also the distribution of these forces along the spandrel. In model 3, the mid-span moment M_M was also measured. In models 4 and 5 the moment and shear, M_B and V_B, at side B were also measured.

Several of the parameters were measured both externally by the load cells and internally by the strain gauges. These independent measurements agreed quite well and the average of the two values would in nearly all cases be accurate to within 5%.

Model 1 (with a floor beam) was very stiff and strong. Little cracking had occurred at 2.2 x design ultimate load when the test was terminated. Of the total end moment M_A, about 80% was resisted by the floor beam and was transferred directly by bending into the column. This left only 10% to be transferred by torsion in each spandrel. The torsional design of the spandrels would seem to be not critical in this case.

In models 2, 3, 4 and 5 cracking occurred in the following sequence: (i) top cracking at the inner face of the test column; (ii) bottom cracking at mid-span; (iii) top radial cracking around column A, especially in a direction towards column B (i.e. at right-angles to the edge of the building); (iv) extension of the crack at the face of the column (see (i)) along the face of the spandrel beam or spandrel strip; (v) torsion cracking in the spandrel close to the column.

At mid-span, where the slab steel was light, the yield moment was only marginally higher than the cracking moment. At the ends, with heavier top steel, the yield moment was considerably higher than the cracking moment.

The progress of cracking was accompanied by redistribution of the slab moments. As far as total panel moments were concerned, in the uncracked condition the mid-span moment was about 60% of the total static moment M_o. Initial top cracking at the column faces increased slightly the magnitude of the mid-span moment relative to the end moments. Thereafter, mid-span cracking and steel yield gradually reduced the predominance of the mid-span moment, which at maximum load was around 50%. The main conclusion from this behaviour is that attempts to predict analytically the magnitudes of M_A, M_M and M_B are quite unnecessary. In view of the capacity of the structure for moment redistribution, these three moments may be expressed as simple proportions of M_o. The tests suggest values of $0.4M_o$, $0.5M_o$ and $0.6M_o$ for M_A, M_M and M_B respectively, but the limited range of the tests is pointed out.

In addition to changing the relative values of M_A, M_M and M_B, cracking also changed the lateral distribution of these quantities across the panel. In regard to M_A, which was the primary research

7.8 STIFFNESS TESTS

The joint stiffness tests were carried out mainly for the purpose of determining the degree of loss of stiffness due to cracking. It was considered that such information could be useful in connection with earthquake analysis.

In models 1 and 3, joint A was rotated while the other five joints were left unmetred. In fact very little rotation would have occurred at corner columns C, D, E and F while some minor rotation would have taken place at joint B. In models 4 and 5 joints A and B were separately rotated and in each case the moments M_A and M_B were both measured. By suitable analysis of the results (described in Section 6.4) values were obtained for the stiffness of joint A with B held fixed and similarly the stiffness of joint B with A held fixed.

TABLE 7.6 - Test Stiffness (kNm/radian) of Joint A with B Fixed

	Uncracked	Cracked	Severely Cracked
Model 4 joint A	5.2×10^3	1.6×10^3	0.55×10^3
Model 5 joint A	6.5×10^3	2.6×10^3	1.3×10^3

TABLE 7.7 - Test Stiffness (kNm/radian) of Joint B with A Fixed

	Uncracked	Cracked	Severely Cracked
Model 4 joint B	7.9×10^3	5.8×10^3	5.2×10^3
Model 5 joint B	18×10^3	7.5×10^3	2.2×10^3

In all cases, the stiffness of joint B is greater than that of joint A. This is due to the presence of a fairly shallow spandrel beam. This has two effects. In the first place it spreads the joint rotation further along the edge of the slab. The rotation at joint B is not so localized and in consequence the slab stiffness is increased.

The other two tests carried out concerned joint A in model 1, where there were both a spandrel beam and a floor beam, and joint

at the centre of the column line AB due to the nature of the boundary conditions adopted in the tests. Even these deflections are small at service load and design ultimate load. For instance, the average maximum deflection at service load was less than span/2000 and at design ultimate load was less than span/1000.

The measured deflections could be predicted using any one of the standard deflection computation methods (e.g. Branson's method) available in the literature. However, no such calculations are given here because of the small order of magnitude of deflections measured at service load.

Chapter 8

SUMMARY AND CONCLUSIONS

At external columns of a building, considerable moment is transferred from the floor to the column in addition to shear. Code provisions are quite inadequate for predicting the amount of moment transfer and for the design of the region around such a column. The mechanism of transfer of both moment and shear has not been well explained.

Some previous research has been carried out and theories advanced. Of these, the 'beam analogy' theory is perhaps the most promising. However, there has been some doubt about the validity of the boundary conditions in previous tests. Hence in the present tests, a boundary was chosen rather more remote from the test area, i.e. a rather more extensive model was used. Tests indicated that forces applied to this boundary had minimal effect in the test region.

Five models were tested, each representing two adjacent edge panels of a floor. Model 1 contained a floor beam and a spandrel beam. Model 2 contained only a spandrel beam. Models 3, 4 and 5 had neither floor beam nor spandrel beam adjoining the test column (column A). At the pin-jointed base of column A, reactions in three orthogonal directions were measured directly by means of load cells. Strain gauges attached to the slab reinforcement permitted slab moments to be calculated and in some cases, by differentiation, slab shears.

In the first two models, the main aim was to measure the total panel moment M_A and shear V_A along the face of the spandrel beam adjacent to column A, and also the distribution of these forces along the spandrel. In model 3, the mid-span moment M_M was also measured. In models 4 and 5 the moment and shear, M_B and V_B, at side B were also measured.

Several of the parameters were measured both externally by the load cells and internally by the strain gauges. These independent measurements agreed quite well and the average of the two values would in nearly all cases be accurate to within 5%.

Model 1 (with a floor beam) was very stiff and strong. Little cracking had occurred at 2.2 x design ultimate load when the test was terminated. Of the total end moment M_A, about 80% was resisted by the floor beam and was transferred directly by bending into the column. This left only 10% to be transferred by torsion in each spandrel. The torsional design of the spandrels would seem to be not critical in this case.

In models 2, 3, 4 and 5 cracking occurred in the following sequence: (i) top cracking at the inner face of the test column; (ii) bottom cracking at mid-span; (iii) top radial cracking around column A, especially in a direction towards column B (i.e. at right-angles to the edge of the building); (iv) extension of the crack at the face of the column (see (i)) along the face of the spandrel beam or spandrel strip; (v) torsion cracking in the spandrel close to the column.

At mid-span, where the slab steel was light, the yield moment was only marginally higher than the cracking moment. At the ends, with heavier top steel, the yield moment was considerably higher than the cracking moment.

The progress of cracking was accompanied by redistribution of the slab moments. As far as total panel moments were concerned, in the uncracked condition the mid-span moment was about 60% of the total static moment M_o. Initial top cracking at the column faces increased slightly the magnitude of the mid-span moment relative to the end moments. Thereafter, mid-span cracking and steel yield gradually reduced the predominance of the mid-span moment, which at maximum load was around 50%. The main conclusion from this behaviour is that attempts to predict analytically the magnitudes of M_A, M_M and M_B are quite unnecessary. In view of the capacity of the structure for moment redistribution, these three moments may be expressed as simple proportions of M_o. The tests suggest values of $0.4M_o$, $0.5M_o$ and $0.6M_o$ for M_A, M_M and M_B respectively, but the limited range of the tests is pointed out.

In addition to changing the relative values of M_A, M_M and M_B, cracking also changed the lateral distribution of these quantities across the panel. In regard to M_A, which was the primary research objective, the distribution of this moment across the panel is

given by equations (7.1) and (7.2) before and after cracking respectively. The peaking of the moment opposite the column face is, of course, more marked before cracking than after. After cracking, about 20% of the total moment M_A is resisted by bending in the beam strip when a spandrel beam is present. This increases to about 40% if there is no spandrel beam and if the column is very wide.

Similar remarks apply to the total end shear V_A, the distribution of which is given by equations (7.4) and (7.5) for the uncracked and cracked condition respectively. In the cracked condition, about 15% of the total shear is resisted in the beam strip when there is a spandrel beam, and about 25% when there is no beam and a wide column.

There is thus considerable torsion and shear in the spandrel even in the absence of a spandrel beam, and more when there is a beam. Values of the bending moment, shear force and torsion in the spandrel beam or strip are given by equations (7.8), (7.9) and (7.10) respectively.

In models 3 and 4, a punching shear occurred at column A, though only after the flexural capacity of the slab had been realized. The punching failure was initiated by a torsion-shear failure in the spandrel strips close to the column, followed immediately by shear failure in the beam strip. In model 5 a similar failure would probably have been reached if the test had been continued. In model 2 the presence of a spandrel beam precluded the possibility of shear failure.

The need for adequate shear-torsion design of the spandrels is emphasized by these results.

It was found that the floor slab, by restraining the spandrels against longitudinal expansion (during torsional deformation) considerably increased the torsional strength of the spandrels. Equation (7.14) indicates the extent of this effect, which should be taken into account in design.

The lateral distribution of the mid-span moment M_1 did not substantiate current Code proposals. In the uncracked state the column strip resisted slightly more that $0.5M_1$ but after cracking

the distribution of M_M was nearly uniform. In model 5, which had very wide columns, the mid-span moment on the column line AB was slightly *less* than elsewhere in the panel.

The findings of both mid-span and ends suggest modification of the current practice of dividing the panel into column strip and middle strip. These tests suggest that for end moments a division into 'beam strip' (width c_2 + t) and slab strip (the remainder) would be more meaningful, and for mid-span moments a uniform distribution across the whole panel would be sufficient.

Stiffness tests were carried out on some models by applying a moment to the slab-column junction at A and measuring the resulting rotation of the junction. In models 4 and 5 it was possible to perform the test also for junction B and to measure carry-over effects. It was found that after cracking the stiffness was only about 1/3 of that in the uncracked state. A shear failure at column A reduced the stiffness still further to about 0.1 of the uncracked value. Specific values are given in Table 7.9.

REFERENCES

ACI-ASCE Committee 326, "Shear and Diagonal Tension. Part 3 - Slabs and Footings", ACI Journal, Proc. Vol. 59, No. 3, March 1962, pp. 382-395.

ACI-ASCE Committee 426, "The Shear Strength of Reinforced Concrete Members - Slabs", Journal of the Structural Division, ASCE, Vol. 100, No. ST 8, August 1974.

Corley, W.G. and Jirsa, J.O., "Equivalent Frame Analysis for Slab Design", ACI Journal, Proc. Vol. 67, No. 11, Nov. 1970.

Comité Euro-International du Béton (CEB) (1978), "CEB-FIP Model Code for Concrete Structures", English Edition, Ca CA, London (3rd Edition of the International Recommendations).

Di Stasio, J. and Van Buren, M.P., "Transfer of Bending Moment Between Flat Plate Floors and Columns", ACI Journal, Proceedings Vol. 57, No. 3, Sept. 1960, pp. 299-314.

Faulkes, K.A., Smith, E.T. and Hall, A.S. (1973), "Correlation of Results from Flat Plate Model Tests and Analyses", UNICIV Report No. R-87, University of N.S.W., Kensington.

Fraser, D.J. (1974), "The Effective Section Properties of Beam-Slab Structures", Ph.D. Thesis, University of N.S.W., Kensington.

Fraser, D.J. (1976), "Effective Torsional Stiffness of Equivalent Beams", ACI Journal, Proc. Vol. 73, Oct., pp. 573-576.

French, S., Kabaila, A.P., Pulmano, V.A. (1975), "Single Element Panel for Multistorey Plate Structures", Journal of the Structural Division, ASCE, Vol. 101, No. ST 9, Sept., pp. 1801-1812.

Hanson, N.W. and Hanson, J.M., "Shear and Moment Transfer Between Concrete Slabs and Columns", Development Department Bulletin D 129, Portland Cement Association, Skokie, Jan. 1968.

Hatcher, D.S., Sozen, M.A. and Siess, C.P., "A Study of Tests on a Flat Plate and a Flat Slab", Structural Research Series No. 217, Civil Engineering Studies, University of Illinois, Urbana, Illinois, July 1961, 143 pp.

Hawkins, Neil M., "Lateral Load Design Consideration for Flat Plate Structures", Non-Linear Design of Concrete Structures, CSCE-ASCE-ACI-CEB, International Symposium, University of Waterloo, Ontario, Canada. Aug. 1979.

Hawkins, N.M., Corley, W.G., "Transfer of Unbalanced Moment and Shear from Flat-Plates to Columns", SP 30, Cracking, Deflection and Ultimate Load of Concrete Slab Systems, American Concrete Institute, Detroit, Michigan, 1971, pp. 147-176.

Hawkins, Neil M. and Mitchell, Denis, "Progressive Collapse of Flat Plate Structures", ACI Journal, Proc. Vol. 76, No. 34, July 1979, pp. 775-809.

Islam, Shafiqul and Park, Robert, "Tests on Slab - Column Connections with Shear and Unbalanced Flexure", Journal of Structural Division, ASCE, Vol. 102, No. ST 3, Proc. Paper 11972, March 1976, pp. 549-568.

Kanoh, Yoshikazu and Yoshizaki, Seiji, "Strength of Slab - Column Connections Transferring Shear and Moment", ACI Journal, Proc. Vol. 76, No. 22, March 1979, pp. 461-479.

Long, Adrian E., "Punching Failure of Slabs - Transfer of Moment and Shear", Journal of Structural Division ASCE, Vol. 99, No. ST 4, Proc. Paper 9654, April 1973, pp. 665-685.

Long, A.E. and Cleland, D.J., "An Equivalent Frame Method for Slab - Column Structures", The Structural Engineer, Vol. 59A, No. 5, May 1981, pp. 161-166.

Mast, Paul E., "Plate Stresses at Columns Near the Free Edge", ACI Journal, Proc. Vol. 67, No. 58, November 1970, pp. 898-902.

Moe, J., "Shearing Strength of Reinforced Concrete Slabs and Footings Under Concentrated Loads", Development Department Bulletin D 47, Portland Cement Association, Skokie, April 1961, 130 pp.

Nett, V.W., dePaiva, H.A.R. and Long, A.E., "Behaviour of Models of a Reinforced Concrete Flat Plate Edge Column Connection", ACI Journal Proceedings, Vol. 78, July-Aug. 1981, pp. 269-275.

Onsongo, W.M. and Collins, M.P., "Longitudinally Restrained Beams in Torsion", Publication 72-07, Department of Civil Engineering, University of Toronto, May 1972, 35 pp.

Regan, P.E., "Behaviour of Reinforced Concrete Flat Slabs", CIRIA Report No. 89, London, Feb. 1981, 90 pp.

Regan, P.E., "Design for Punching Shear", The Structural Engineer (GB), Vol. 52, No. 6, June 1974, pp. 513-531.

Stamenkovic, A., Chapman, J.C., "Local Strength at Columns Heads in Flat Slabs Subjected to a Combined Vertical and Horizontal Loading", Proc. Institution of Civil Engineers, Part 2 (GB), Vol. 57, June 1974, pp. 205-232.

Warner, R.F., Rangan, B.V. and Hall, A.S., "Reinforced Concrete", Pitman Australia, Second Edition, 1982.

Wiesinger, F.P., "Design of Flat Plates with Irregular Column Layout", ACI Journal, Proc. Vol. 70, No. 2, Feb. 1973, pp. 117-123.